



# **Region specific glia-to-neuron reprogramming: a step forward to neuronal repair**

*Doctoral Thesis presented by*

**Álvaro Herrero Navarro**

Thesis Director:

**Guillermina López-Bendito, PhD**

- 2021 -

*PhD Program in Neuroscience  
Instituto de Neurociencias de Alicante (UMH-CSIC)  
Universidad Miguel Hernández de Elche*







Sant Joan d'Alacant, 2<sup>nd</sup> of August 2021

To whom it may concern,

The doctoral thesis entitled “**Region specific glia-to-neuron reprogramming: a step forward to neuronal repair**” has been developed by myself, Álvaro Herrero Navarro. This thesis is presented in a compendium of publications format and includes the following publication in which I am the first author:

- **Astrocytes and neurons share region-specific transcriptional signatures that confer regional identity to neuronal reprogramming.**

**Álvaro Herrero-Navarro**, Lorenzo Puche-Aroca, Verónica Moreno-Juan, Alejandro Sempere-Ferrández, Ana Espinosa, Rafael Susín, Laia Torres-Masjoan, Eduardo Leyva-Díaz, Marisa Karow, María Figueres-Oñate, Laura López-Mascaraque, José P. López-Atalaya, Benedikt Berninger and Guillermina López-Bendito

**Science Advances** 07 Apr 2021; Vol 7, no. 15, eabe8978

DOI: 10.1126/sciadv.abe8978





Dr. Guillermina López-Bendito, director of the doctoral thesis entitled **“Region specific glia-to-neuron reprogramming: a step forward to neuronal repair”**

**CERTIFIES:**

That Álvaro Herrero Navarro has carried out under my supervisión the work entitled **“Region specific glia-to-neuron reprogramming: a step forward to neuronal repair”** in accordance with the terms and conditions defined in his Research Plan and in accordance with the Code of Good Practice of the University Miguel Hernández of Elche, satisfactorily fulfilling the objectives foreseen for its public defence as a doctoral thesis.

I sign for appropriate purposes, at Sant Joan d'Alacant, 2<sup>nd</sup> of August of 2021.

Thesis Director

Dra. Dña. Guillermina López Bendito





Sant Joan d'Alacant, 2<sup>nd</sup> of August 2021

Ms. Elvira de la Peña García, Coordinator of the Neurosciences PhD programme at the Institute of Neurosciences in Alicante, a joint centre of the Miguel Hernández University (UMH) and the Spanish National Research Council (CSIC),

INFORMS:

That D. Álvaro Herrero Navarro has carried out under the supervision of our PhD Programme the work entitled “**Region specific glia-to-neuron reprogramming: a step forward to neuronal repair**” in accordance with the terms and conditions defined in its Research Plan and in accordance with the Code of Good Practice of the University Miguel Hernández de Elche, fulfilling the objectives satisfactorily for its public defence as a doctoral thesis.

Which I sign for the appropriate purposes, in Sant Joan d'Alacant, 2<sup>nd</sup> of August, 2021.

Dr. Elvira de la Peña García  
Coordinator of the PhD Programme in Neurosciences

E-mail : [elvirap@umh.es](mailto:elvirap@umh.es)  
[www.in.umh.es](http://www.in.umh.es)

Tel: +34 965 919533  
Fax: +34 965 919549

Av Ramón y Cajal s/n  
CAMPUS DE SANT JOAN  
03550 SANT JOAN D'ALACANT- ESPAÑA





Sant Joan d'Alacant, 2<sup>nd</sup> of August 2021

To whom it may concern:

The present PhD thesis has been funded by the following research agencies:  
D. Álvaro Herrero Navarro is recipient of a FPI contract (BES-2016-076248) associated to the grants BFU2015-64432-R and PGC2018-096631-B-I00, from “Ministerio de Ciencia, Innovación y Universidades”.

Yours sincerely,

Álvaro Herrero Navarro



A mis padres y a mis hermanos,

A Kika,



# Index

<b>Abbreviations .....</b>	<b>3</b>
<b>Abstract/Resumen .....</b>	<b>9</b>
<b>Introduction and Objectives .....</b>	<b>15</b>
<b>1. Brain regionalization .....</b>	<b>16</b>
1.1 Early CNS formation. Gastrulation and neurulation.....	16
1.2 The formation of the cerebral cortex.....	19
1.3 The formation of the thalamus.....	24
<b>2. Astrocytes' diversity in the CNS .....</b>	<b>29</b>
2.1 Roles of astrocytes .....	30
2.2 Astrocytes' regional heterogeneity.....	32
2.3 Generation of astrocytes and emergence of their regional diversity.....	35
<b>3. Central Nervous system regeneration .....</b>	<b>37</b>
3.1 Adult neurogenesis .....	37
3.2 Cell transplantation.....	39
3.3 Cellular reprogramming .....	41
<b>Materials and methods .....</b>	<b>51</b>
<b>Discussion.....</b>	<b>67</b>
<b>Conclusions/Conclusiones .....</b>	<b>79</b>
<b>References .....</b>	<b>87</b>
<b>Annex.....</b>	<b>115</b>

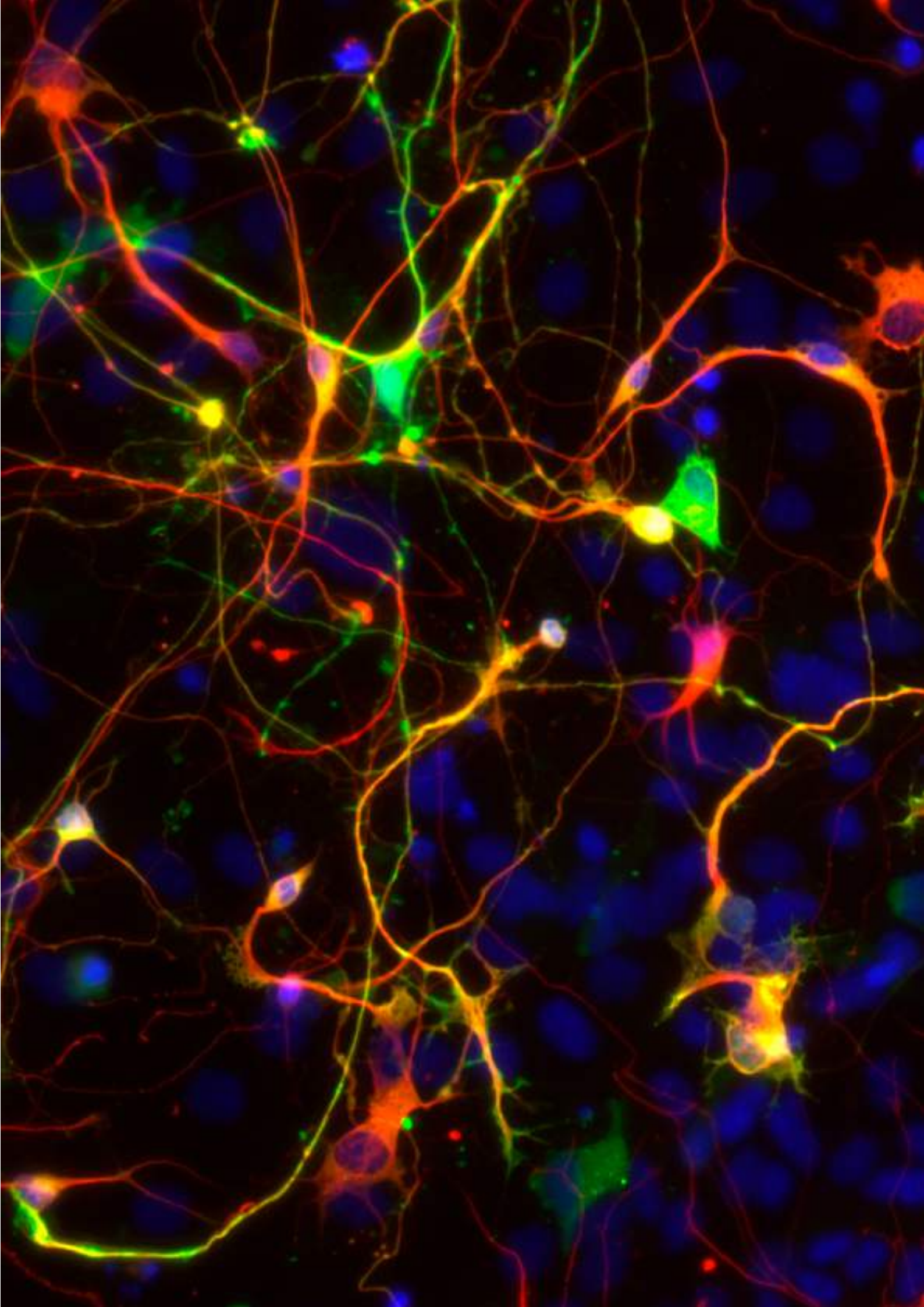


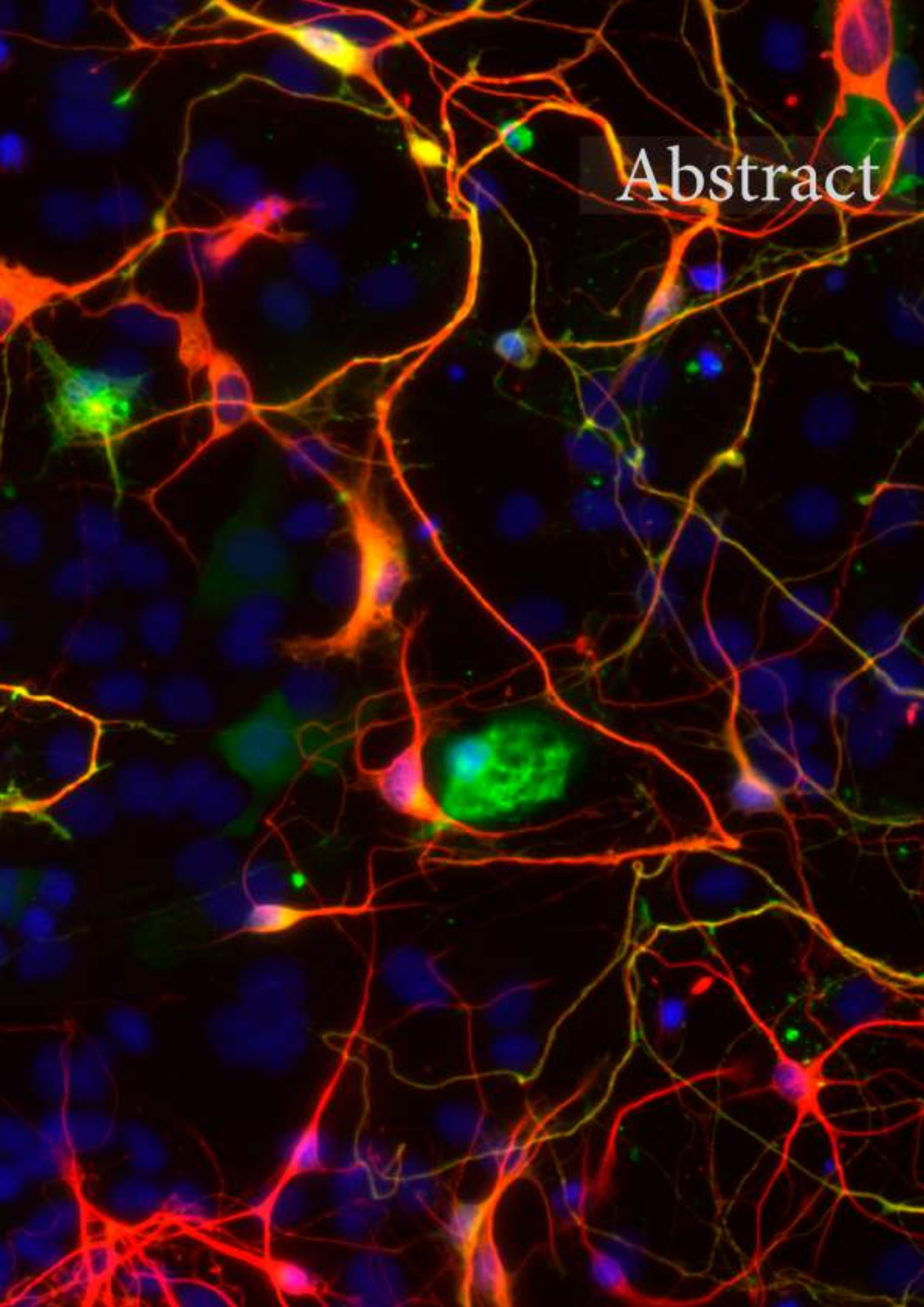
## Abbreviations

<b>A1</b>	Primary Auditory Cortex	<b>LP</b>	Lateral Posterior nucleus
<b>AAV</b>	Adeno-Associated Virus	<b>MADM</b>	Mosaic Analysis with Double Markers
<b>aCSF</b>	Artificial Cerebrospinal Fluid	<b>Mash1 or Ascl1</b>	Achaete-scute Family bHLH Transcription Factor 1
<b>AD</b>	Alzheimer's disease	<b>MGv</b>	Medial Geniculate Nucleus
<b>Aldh1l1</b>	Aldehyde Dehydrogenase 1 Family Member L1	<b>NeuN</b>	Neuronal Nuclei
<b>ANR</b>	Anterior Neural Ridge	<b>NeuroD</b>	Neuronal Differentiation
<b>APV</b>	D,L-2-amino-5-phosphonovaleric acid	<b>Neurog</b>	Neurogenin
<b>As</b>	Astrocytes	<b>Ns</b>	Neurons
<b>BMP</b>	Bone Morphogenetic Protein	<b>NSCs</b>	Neural Stem Cells
<b>Bcl2</b>	B-cell lymphoma 2	<b>Ntng1</b>	Netrin G1
<b>BDNF</b>	Brain Derived Neurotrophic Factor	<b>Olig3</b>	Oligodendrocyte Transcription Factor 3
<b>BrdU</b>	5-bromo-2'-deoxyuridine	<b>OPCs</b>	Oligodendrocyte Precursor Cells
<b>BSA</b>	Bovine Serum Albumin	<b>Otx2</b>	Orthodenticle Homeobox 2
<b>ChIP</b>	Chromatin Immunoprecipitation	<b>Pax6</b>	Paired Box 6
<b>CNS</b>	Central Nervous System	<b>PCA</b>	Principal Component Analysis
<b>CoupTF-1</b>	Nuclear Receptor Subfamily 2, Group F, Member 1	<b>PCR</b>	Polymerase Chain Reaction
<b>CreER</b>	Cre recombinase fused to Estrogen Receptor	<b>PD</b>	Parkinson's disease

<b>CTAs</b>	Corticothalamic Axons	<b>Ptbp1</b>	Polypyrimidine Tract Binding Protein 1
<b>Ctip</b>	COUP-TF-interacting protein	<b>pTH-C</b>	Caudal domain of the thalamus
<b>Ctx</b>	Cortex	<b>pTH-R</b>	Rostral domain of the thalamus
<b>DAPI</b>	4',6-diamidino-2-phenylindole	<b>PT</b>	Prethalamus
<b>DCX</b>	Doublecortin	<b>qPCR</b>	Quantitative PCR
<b>DEG</b>	Differentially Expressed Genes	<b>RA</b>	Retinoic Acid
<b>dLG</b>	Dorsal Lateral Geniculate Nucleus	<b>RGCs</b>	Retinal Ganglion Cells
<b>DG</b>	Dentate Gyrus	<b>Rlog</b>	Regularized logarithm
<b>EdU</b>	5-Ethynyl-2'-deoxyuridine	<b>RNA</b>	Ribonucleic Acid
<b>EGF</b>	Epidermal Growth Factor	<b>Rora</b>	RAR-Related Orphan Receptor A
<b>Emx</b>	Empty Spiracles Homeobox	<b>RT</b>	Room Temperature
<b>eNSCs</b>	Embryonic multipotent Neural Stem Cells	<b>S1</b>	Primary Somatosensory Cortex
<b>EYFP</b>	Enhanced Yellow Fluorescent Protein	<b>scRNAseq</b>	Single cell RNA sequencing
<b>Fezf2</b>	Fez Family Zinc Finger 2	<b>SGZ</b>	Subgranular Zone
<b>FISH</b>	Fluorescent <i>In Situ</i> Hybridization	<b>Shh</b>	Sonic hedgehog
<b>FO</b>	First Order	<b>Sox</b>	Sex Determining region Y-box
<b>GABA</b>	Gamma-Aminobutyric Acid	<b>Sp8</b>	Trans-Acting Transcription Factor 8
<b>Gapdh</b>	Glyceraldehyde-3-Phosphate Dehydrogenase	<b>SVZ</b>	Subventricular Zone

<b>Gbx2</b>	Gastrulation Brain Homeobox 2	<b>Tbr</b>	T-Box Brain Transcription Factor
<b>GFAP</b>	Glial Fibrillary Acidic Protein	<b>TCAs</b>	Thalamocortical Axons
<b>GO</b>	Gene Ontology	<b>Th</b>	Thalamus
<b>GFP</b>	Green Fluorescent Protein	<b>UbC</b>	polyubiquitin C gene
<b>H3K4me3</b>	Histone H3 lysine 4 trimethylation	<b>UMAP</b>	Uniform Manifold Approximation
<b>H3K27me3</b>	Histone H3 lysine 27 trimethylation	<b>V1</b>	Primary Visual Cortex
<b>hiPSCs</b>	human induced Pluripotent Stem Cells	<b>VZ</b>	Ventricular Zone
<b>huCNS-SC</b>	human Central Nervous System- Stem Cells	<b>vGlut</b>	Vesicular Glutamate Transporter
<b>iN</b>	induced Neuron	<b>VPM</b>	Ventral Posterior Medial Nucleus
<b>IRES</b>	Internal Ribosome Entry Site	<b>Wnt</b>	Wingless-type family
<b>IsO</b>	Isthmic Organizer	<b>ZLI</b>	zona limitans intrathalamica
<b>Lef1</b>	Lymphoid Enhancer Binding Factor 1		



A fluorescence microscopy image showing a dense network of neurons. The neurons are stained with multiple colors: bright orange/red for the cell bodies and processes, green for some specific cells or organelles, and blue for the nuclei. The background is dark, making the glowing structures stand out. The word "Abstract" is written in white, serif font on a semi-transparent dark rectangular background in the upper right quadrant.

# Abstract



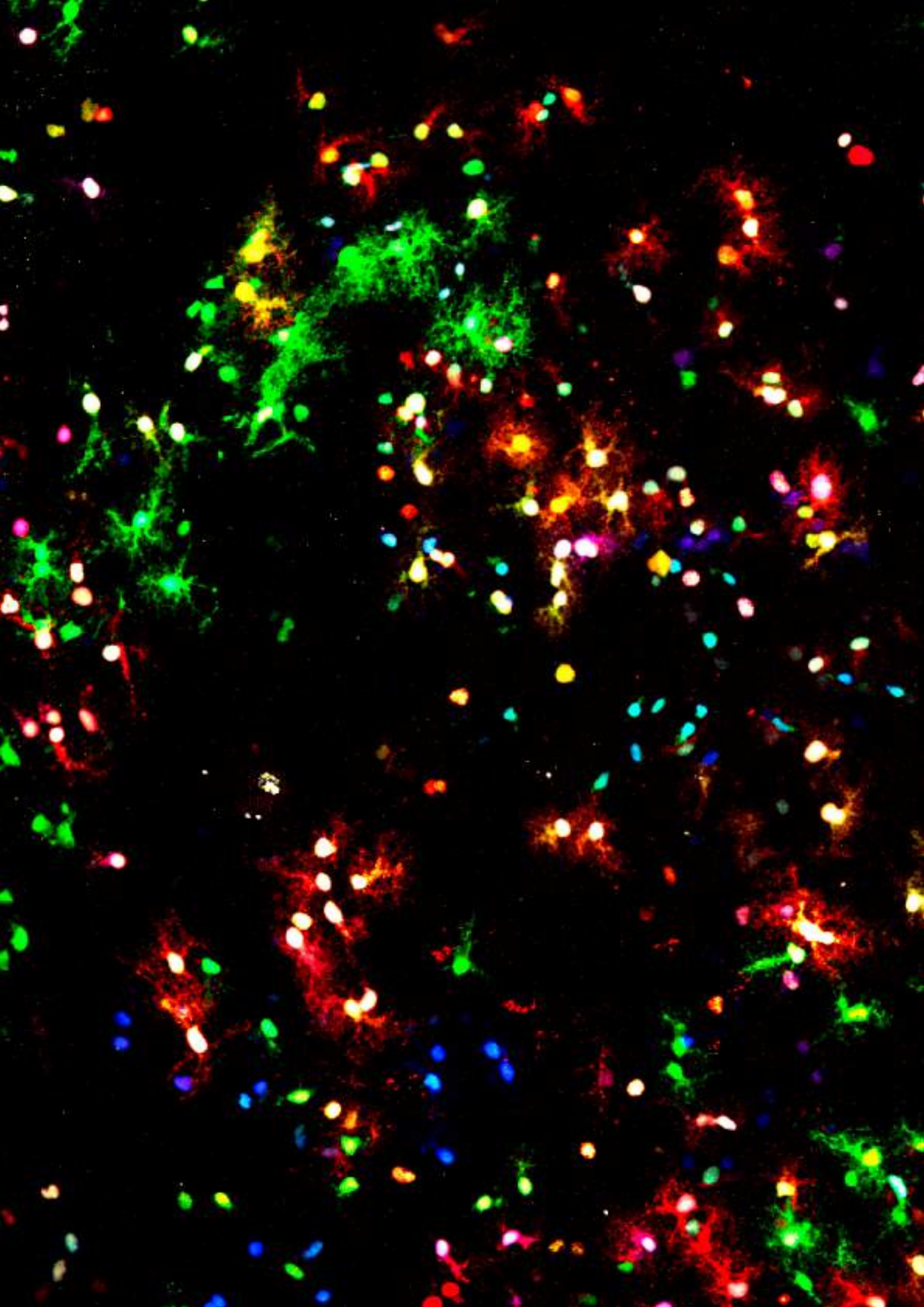
## Abstract

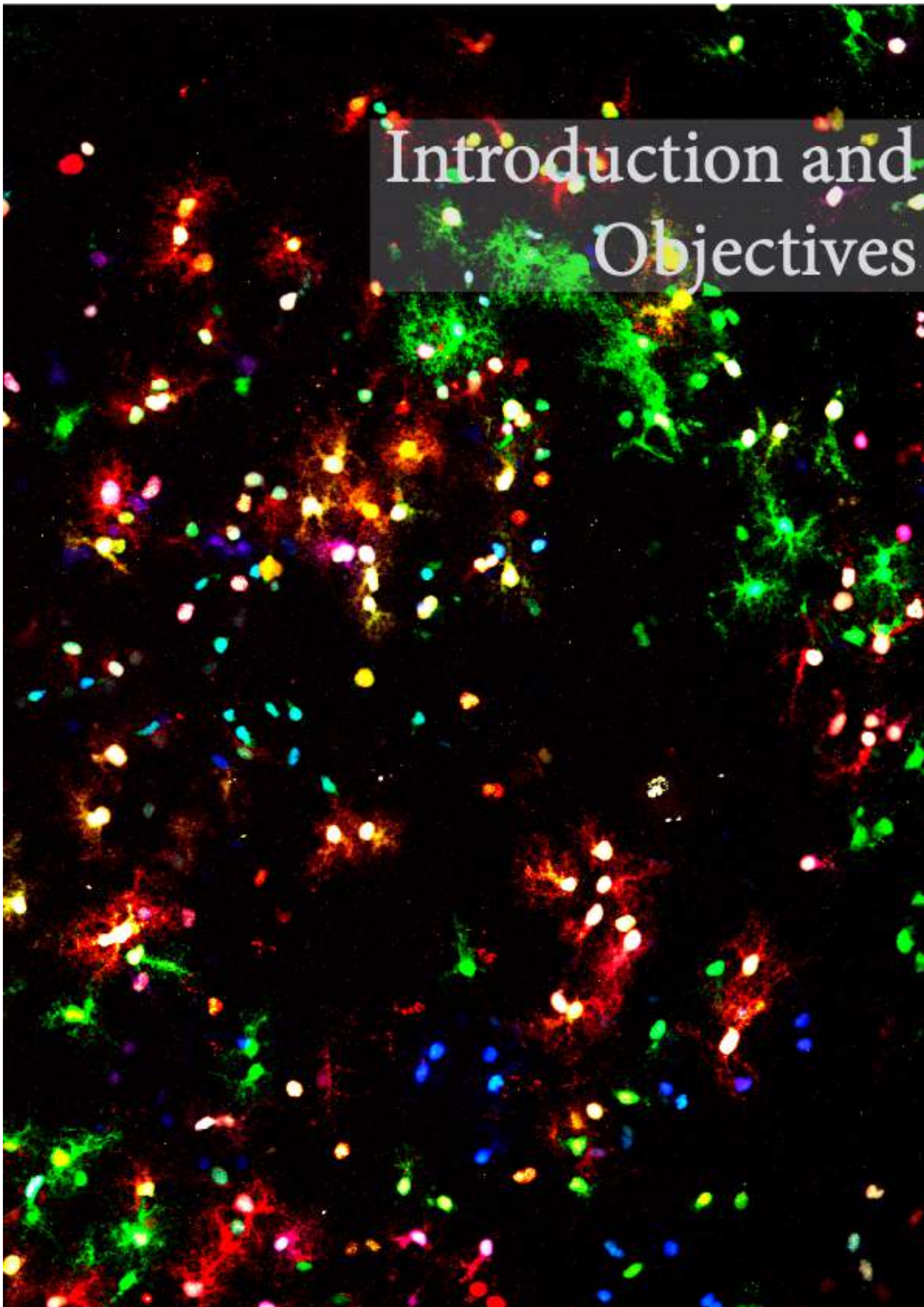
The reduced regenerative capacity of the brain represents a challenge when restoring neuronal circuits after a damage or in neurodegenerative diseases. During the last years, several studies aimed at trying to generate *de novo* neurons in the damaged regions of the brain in order to replace the affected ones. One of the most promising strategies is based on the conversion of resident glial cells, such as astrocytes, into neurons *in vivo* by the overexpression of neurogenic transcription factors. However, considering the vast neuronal heterogeneity in the brain, it is essential that those converted astrocytes acquire their appropriate neuronal identity when reprogrammed so that they properly replace the damaged neurons. In this thesis I demonstrate that astrocytes from different brain regions share transcriptional and molecular properties with neurons of the same territory. Moreover, this region-specific molecular signatures between astrocytes and neurons seem to emerge from their common origin, as our clonal analysis demonstrates that astrocytes and neurons that populate discrete brain regions such as thalamic sensory nuclei are generated from the same group of progenitors, that seem to transmit positional information to both cell types. Finally, we show that these transcriptional and epigenetic signatures conserved in both cell types are able to direct the reprogramming of astrocytes into neurons with regional specificity. Overall, the data presented in this thesis will represent an important advance for understanding how brain cell heterogeneity is achieved and to design future strategies for restoring specific neuronal circuits.



## Resumen

La reducida capacidad regenerativa del cerebro representa un importante desafío a la hora de tratar de regenerar circuitos neuronales afectados tras un daño cerebral o en enfermedades neurodegenerativas. En los últimos años, diferentes estudios se han centrado en intentar generar neuronas *de novo* en zonas dañadas del cerebro que reemplacen a las que se han perdido. Una de las estrategias más prometedoras en la actualidad se basa en la conversión de células gliales residentes del cerebro, como los astrocitos, en neuronas *in vivo* gracias a la sobreexpresión de factores de transcripción neurogénicos en dichos astrocitos. Sin embargo, teniendo en cuenta la gran heterogeneidad neuronal del cerebro, es esencial que estos astrocitos convertidos en neuronas adquieran la identidad del subtipo específico de neurona que se quiere reemplazar. En esta tesis, demostramos que los astrocitos de diferentes regiones del cerebro comparten propiedades transcripcionales y moleculares con las neuronas del mismo territorio. Además, estas marcas moleculares específicas de región compartidas parecen provenir de su origen común, puesto que nuestros experimentos de análisis clonal demuestran que los astrocitos y las neuronas que residen en una misma región cerebral, como los núcleos sensoriales talámicos, están generados por el mismo grupo de progenitores, que parecen ser los responsables de transmitir a ambos tipos celulares información posicional. Finalmente, demostramos que estas marcas transcripcionales y epigenéticas conservadas en ambos tipos celulares son capaces de dirigir la reprogramación de astrocitos a neuronas específicas de la misma región. En conclusión, los datos presentados en esta tesis representan un importante avance para entender el origen de la heterogeneidad celular del cerebro, y para diseñar futuras estrategias para la restauración de circuitos neuronales específicos.





# Introduction and Objectives



## Introduction

The mammalian brain is considered as one of the most complex organs due to its extraordinary cellular diversity and circuit organization. This complexity emerges since early stages of the development, through the tight control of sequential processes involving regionalization, neurogenesis, astrogenesis, cell migration, axon projection and synapse formation. Notably, such complex organization remains fixed during the entire life, with reduced possibilities for changes, thus hindering any possible restoration after a brain damage in the adult.

One of the most challenging questions for the neuroscience field is to find strategies for repairing the brain after disease or strokes. In addition to the aforementioned brain complexity that is restrictedly acquired during the development, the fact that neurons do not have the capacity for regenerating or self-renewing is a considerable challenge. Neurogenesis is almost entirely restricted to early developmental timepoints, and only few neurogenic niches remain active in the adulthood, albeit with low capacity for producing neurons (Bergmann et al., 2015; Gonçalves et al., 2016; Lim and Alvarez-Buylla, 2016). For that reason, during the last years several studies have focused on designing strategies aimed at replacing the damaged or dead neurons to keep their corresponding circuit and its associated functions working. Particularly, the majority of those strategies are based in a relatively new concept that claims that contrary to the classical dogma, a differentiated cell can be returned to a pluripotent state, or directly converted into a different cell type. Some of the already tested potential uses of this paradigm are: (I) the stimulation of adult neurogenesis in disease models, (II) the injection *in vivo* of induced neurons or pluripotent stem cells produced *in vitro* in the damaged area and (III) the conversion of endogenous non-neuronal cells into neurons in the affected area. This last scenario results particularly interesting and has been widely studied in the recent years, and currently it is feasible to reprogram cells like astrocytes, fibroblasts or pericytes into neurons *in vitro* and even *in vivo* in the case of astrocytes (reviewed in (Gascón et al., 2017; Götz and Bocchi, 2021)). However, these strategies, while promising, still have many challenges to face, such as the necessity of generating specific neurons in specific places, as it is essential to assure their proper integration into the circuit.

The aim of this Thesis work is to explore the potential of astrocytes to be converted into subtype specific neurons both *in vitro* and *in vivo*, especially in the thalamus and cortex, as a step forward in the design of strategies for neuronal circuit restoration.

## 1. Brain regionalization

### 1.1 Early CNS formation. Gastrulation and neurulation.

The mammalian brain is composed by several substructures that become specialized in particular functions thanks to their specific cellular populations and connectivity. In order to understand how the brain acquires this fine-tuned architecture that is essential for its correct function, it is crucial to understand its development and the processes that contribute to its compartmentalization. The formation and differentiation of these functional structures is a direct consequence of the processes of regionalization that take place at very early stages of the embryonic development (Metzis et al., 2018). The cells that will generate the nervous system (neuroepithelial cells in the neuroectoderm) become specialized during the process of gastrulation, concurrent with the midline and the basic body axes: anterior-posterior and medial-lateral. For the axes establishment, it is essential the graded influence of extracellular signals transmitted between neighboring cells, such as members of the bone morphogenetic protein (BMP) family, fibroblast growth factors (FGF) or *Hox* genes (Hooiveld et al., 1999; Linker et al., 2009; Pearson et al., 2005; Stern, 2006; Waddington, 1936; Wittler and Kessel, 2004). Those molecules will instruct the formation of the neural plate in the central area of the embryo from the neuroectoderm, which gives rise to the entire nervous system in a process called neurulation (**Figure 1A**).

Parallel to this process, the neural plate exhibits a thickening of the rostral part generating a progressive infolding and creating a neural groove that will close by fusing the endings of the lateral plates and thus forming the neural tube, in a process called neurulation. The aforementioned axes are also represented in the neural tube, but the medial-lateral axis is transformed into dorsal-ventral axis. The midline dorsal part derives from the fused cells that constituted before the lateral neural plate and is now called the roofplate. Meanwhile, the ventral midline of the neural tube, the cells immediately above the notochord, will be named the floorplate. Both structures (plates) contribute to the

specification of the different dorsal (alar plate) and ventral (basal plate) derivatives and territories of the nervous system by providing molecular cues that define structures along the dorso-ventral axis. For that reason, both populations (roofplate and floorplate) are called local organizers and the molecules that they secrete, morphogenes. Particularly, during for the dorso-ventral patterning of the brain, roofplate cells secrete BMPs and Wnts (wingless proteins) as dorsalizing factors, that will contribute to the specification of alar regions of the neural tube. On the other hand, the floorplate cells, together with the notochord, produce Shh (Sonic hedgehog) as ventralizing factor that will influence the basal plate regions (for review see (Jessell and Sanes, 2000)).

In addition to the dorso-ventral axis, the antero-posterior patterning in the neural tube will lead to the generation of the distinct transverse domains at different axial positions. This patterning begins during the gastrulation and starts with the induction of an anterior neural fate through the protein Cerberus and the transcription factors *Lim1* and *Otx2*. Then, graded second signals (retinoic acid, bFGF and Hox genes) posteriorize the neural plate regions that will become the hindbrain and the spinal cord (for review see (Stern, 2006; Vieira et al., 2010); **Figure 1A**).

Overall, the intersecting combination of those signals along the entire neural plate and neural tube are sufficient to induce specific gene expression profiles in the progenitors placed at different positions, thus drawing a grid-like Cartesian protomap of the future major brain substructures (Aroca and Puelles, 2005; Echevarria et al., 2003; Martínez, 2001) (**Figure 1B**). Traditionally, two different models have been used to interpret this regionalization, the columnar and the prosomeric models. However, it is the prosomeric model the most consistent with this protomap and the emergent regionalization of the neural tube, specially of the most rostral part, which will derive in the three main vesicles in which the early brain is initially divided: the forebrain (or prosencephalon), the midbrain (or mesencephalon) and the hindbrain (or rhombencephalon). This is particularly relevant for understanding the regionalization of the forebrain, as this model hypothesizes that it is subdivided in six prosomeres that will be divided later in the diencephalon (prosomeres 1-3) and the secondary prosencephalon (prosomeres 4-6). The basal plate of the secondary prosencephalon consists of the hypothalamus, and the telencephalic vesicles constitute the alar domain, from which the basal ganglia and striatum (ventral telencephalon) and the cortex (dorsal telencephalon)

develop. The diencephalon in turn, contains in their alar regions: the pretectum (p1), the thalamus plus the habenula or epithalamus (p2), and the prethalamus plus the eminentia thalamica (p3) ((Puelles et al., 2013); **Figure 1C**).

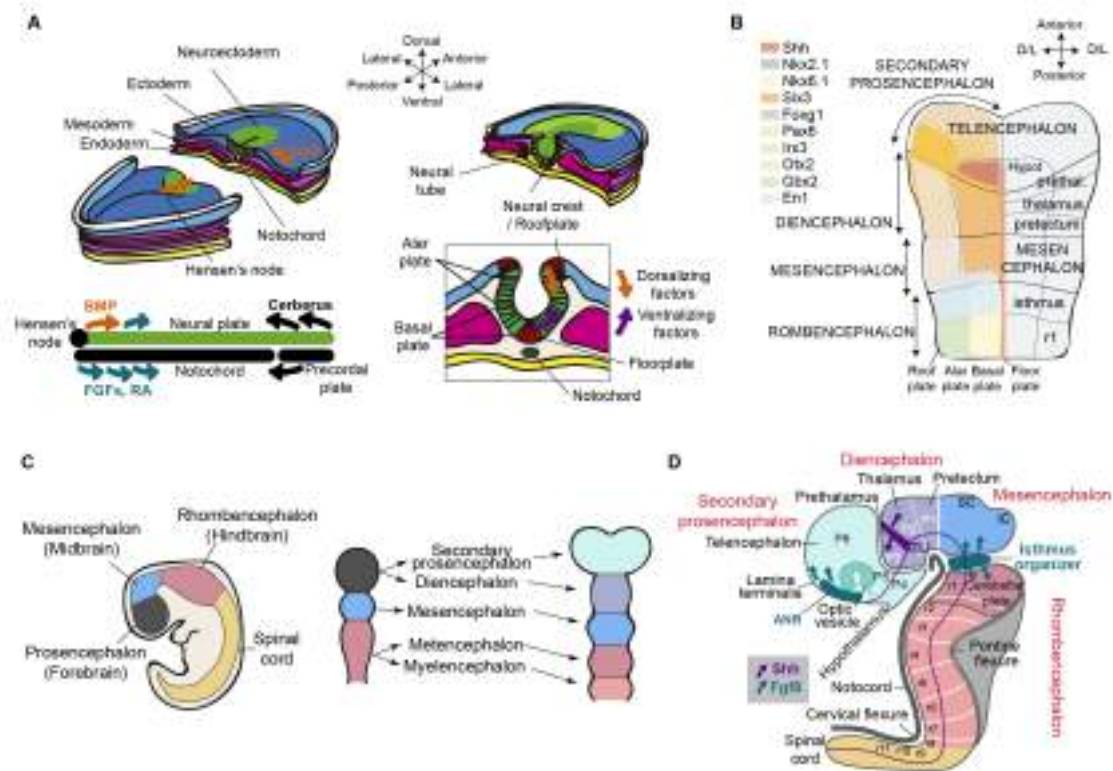


**Figure 1.** Early brain regionalization. (A) Schema of the early processes of regionalization that occur during gastrulation and neurulation processes, that induce the formation of dorso-ventral and medio-lateral axis in the neural plate and tube. (B) Cartesian protomap of the main brain subdivisions at early stages of development based on the combinatorial expression of different transcription factors in each region. (C) Formation of the main brain vesicles. (D) Schematic diagram of the sagittal brain from an E10.5 embryonic mouse brain following the prosomeric model. Main structures can be distinguished, together with the secondary organizers and their secreted morphogenes. Schemas adapted from (Purves et al., 1985; Vieira et al., 2010).

The appearance of the secondary organizers is crucial for the refining of the distinct territories and substructures. Those secondary organizers are specialized regions along the neural tube that secrete molecules that, in a graded fashion, influence the identity and polarity of their surrounding neuroepithelial regions. There are three secondary organizers, the anterior neural ridge (ANR), the zona limitans intrathalamica

(ZLI) and the isthmus organizer (IsO), which are placed at different positions along the antero-posterior axis of the neural tube.

The ANR cells, placed at the anterior end of the neural plate/tube express genes such as *Fgf8*, *Fgf15* or *Shh*, that regulate the expression of important genes for defining the telencephalic identity in the surrounding cells like *Foxg1*, *Gli3* and *Nkx2.1*. The ZLI, a narrow strip of cells that separates the thalamus and the prethalamus, functions as a local organizer of thalamic development, thanks to the diffusion of *Shh*. Finally, the IsO is localized at the mid-hindbrain transition and regulates midbrain and anterior hindbrain regionalization through the expression and secretion of *Fgf8* (for review see (Echevarria et al., 2003)).

For the purpose of this Thesis, I will focus on the formation and regionalization of the cerebral cortex and the thalamus (**Figure 1D**).

## 1.2 The formation of the cerebral cortex

The cerebral cortex is considered as the largest and most complex component of the mammalian brain, and more so than any other brain structure has been affected by evolutionary process. It emerges from the dorsal telencephalon (pallium) and is divided in archicortex (including entorhinal cortex, retrosplenial, subiculum, and hippocampus), paleocortex (olfactory piriform cortex), and neocortex, that is the largest region (**Figure 2D**). The neocortex (hereon referred to as “cortex”) is the responsible for the evolution of cognitive abilities in higher mammals, such as the human mental capacities. This structure possesses a very well-defined organization both at the radial and tangential levels (Rakic, 1995; Rakic et al., 2009) that is crucial for its correct function. Regarding the radial dimension, the neurons of the neocortex are distributed in six radially organized layers, each containing a heterogeneous population of neurons that are morphologically, connectionally, and functionally distinct from those of other layers. In its tangential dimension, it is functionally organized in areas, that were first described by Brodmann early in the 1900s. In general, we can find four primary areas: visual, auditory, somatosensory and motor. Those areas are functionally unique subdivisions distinguished from one another by differences in patterns of gene expression,

cytoarchitecture and chemoarchitecture, and input and output connections (O'Leary and Nakagawa, 2002; Rash and Grove, 2006; Sur and Rubenstein, 2005). These primary areas receive sensory inputs from the periphery and control motor output. Then, they connect to other areas specialized as integrating or processing centers called high or secondary order areas. Finally, those integrating areas transmit the information to multimodal associative cortical regions where is processed, combined, and integrated.

The unique architecture and connections specific for each area determine, in large part, the functional specializations that characterize areas in the adult and that are critical for processing all the information and producing a conscious thinking. Thus, it is essential to understand how these regions emerge and specialize during the development.

### **1.2.1 Arealization of the embryonic cerebral cortex**

The differentiation of those areas is a consequence of the combination of mechanisms intrinsic and extrinsic to the cortex. Among the extrinsic mechanisms, it is of special relevance the influence of the thalamocortical axons (TCAs). Those axons are the main source of the sensory information to the cortex (excepting the olfactory information), and several studies have demonstrated their importance for the specification and refinement of the sensory cortical areas (Antón-Bolaños et al., 2019; Chou et al., 2013; Martini et al., 2018; O'Leary, 1989; Rakic, 1988; Vue et al., 2013).

However, the correct coupling of the TCAs of a sensory modality with its target sensory cortical area also depends on intrinsic properties of the cortical plate cells. Indeed, it has been shown that both primary sensory thalamic nuclei and their target primary sensory areas show matching expression of cell adhesion molecules such as cadherin-6, -8 and -11, and ephrin ligands and receptors, even prior to TCAs arrival (Korematsu and Redies, 1997; Sestan et al., 2001; Suzuki et al., 1997; Vanderhaeghen et al., 2000). In experiments where TCAs were disrupted and failed to reach the cortex, it was observed that the graded and restricted expression of some of those genes was conserved at least at embryonic stages (Miyashita-Lin et al., 1999; Nakagawa et al., 1999). Overall, this suggests that even early in the development, progenitors and early born neurons in the cortex already possess a regional identity at the transcriptional level that facilitates the proper arealization of the cortex.

During the last years it has been demonstrated the presence of some patterning centers that secrete morphogenes or signaling molecules (such as Fgfs, Bmps, Wnts and Shh) which are the responsible of inducing the differential expression of transcription factors along the antero-posterior and latero-medial axis of the developing cortex. Among those graded expressed transcription factors, we can find COUP-TFI, Emx1, Emx2, Pax6 or Sp8 (O'Leary et al., 2007; Rakic, 1988), that contribute to the transcriptional specification of the progenitors from the different cortical areas together with their descendant cells, although these regions are better defined progressively during the development (**Figure 2A and 2B**).

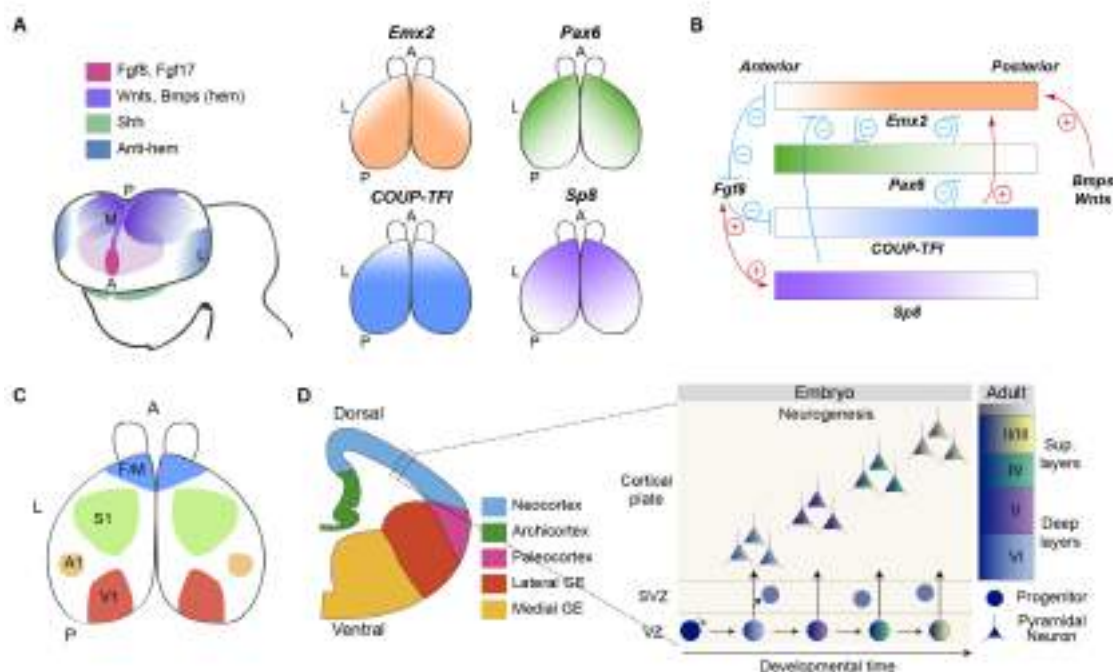


**Figure 2.** Arealization of the cerebral neocortex and neurogenesis. (A) Influence of different morphogenes across the main axis of the embryonic telencephalon, and consequential graded expression of four important transcription factors in different regions. (B) Genetic regulation of the mentioned transcription factors by secreted morphogenes Fgf8, Bmps and Wnts. (C) Schema of the main primary cortical areas related to motor (F/M), somatosensory (S1), auditory (A1) and visual (V1) functions. (D) Left: Main subdivisions of the dorsal telencephalon. Right: Schema of the neurogenic process in the neocortex, showing the generation of neurons from different cortical layers (II/III, IV, V and VI). Schemas adapted from (O'Leary et al., 2007; Oberst et al., 2019). A: Anterior, M: Medial, L: Lateral, P: Posterior.

### **1.2.2 Neurogenesis and neuronal diversity in the neocortex**

Excitatory neurons from the neocortex derive from a primitive neuroepithelium distributed lining the telencephalic vesicle, which is later transformed into the ventricular zone, whose cells (apical progenitors) will divide asymmetrically to produce at earlier stages more progenitors (intermediate progenitors) and neurons. These new cells migrate along basal radial processes of the progenitors and form a secondary germinal layer, the subventricular zone, composed of newly born neurons and basal or intermediate progenitors, which continue forming new neurons and progenitors that will populate the cortical plate (Borrell and Reillo, 2012; Smart et al., 2002).

However, cortical neurons are not a homogeneous population, and as previously mentioned, there are two levels of organization that rule the neuronal diversity across the neocortex. First, the tangential arealization that can be observed even from very early in cortical development, seem to be transmitted from the progenitors to their descendant neurons as suggested by the columnar model of neuronal generation (Elsen et al., 2013; Rakic, 1972; 1988; 1995; Rakic et al., 2009). Following this model, the neocortex is subdivided in columnar modules formed by cells that share the same birthplace, which follow the same migration pathway and populate the same ontogenetic cortical column. This hypothesis has been recently confirmed using viral or genetic tracing of single apical progenitors for tracing their progeny at different timepoints of the development (Guo et al., 2013; Luskin et al., 1988; Reid et al., 1995; Walsh and Cepko, 1988; Zong et al., 2005). Overall, those studies provide evidence for the capacity of radial glial progenitors for producing descendant cells that do not disperse across the cortex, thus maintaining the positional information (Gao et al., 2014; Llorca et al., 2019) (**Figure 2C**).

In addition to the tangential organization previously described, it exists an extra level of organization, where excitatory neurons of the neocortex are distributed in 6 horizontal layers, which are distinguished based on their connectivity, organization, cell population, function, and time of generation ((Mountcastle, 1997) and reviewed in (Lodato and Arlotta, 2015)).

As previously mentioned, apical progenitors have the capacity to generate neurons for all cortical layers, with rare exceptions that are a matter of controversy (Franco et al., 2012). However, the heterogeneity of these neurons emerges as early as they are generated, as neurons from each layer are born at a specific time point during the

embryonic development in an inside-out pattern, where neurons from lower layers are born first, and followed by upper layer neurons (Angevine and Sidman, 1961; Greig et al., 2013). As a result of this diversification, the cortical plate is finally populated by pyramidal neurons with different functions and connections which is essential for the proper functioning of the cortex. In a general view, neurons from upper layers (2-4) are more involved in associative intracortical connections, while lower layer neurons (5-6) consist of corticofugal neurons that project away from the neocortex to subcortical targets, such as brainstem, thalamus and spinal cord (Greig et al., 2013; Lodato and Arlotta, 2015).

The correct function and connectivity of every layer is dependent on the specific transcriptional programs encoded in their neuronal populations (Molyneaux et al., 2007; 2015). Indeed, several studies have shown that it is possible to alter the connectivity of layer-specific neurons by modifying the expression of key genes (Lodato et al., 2014; Molyneaux et al., 2005; Rouaux and Arlotta, 2013). Thus, understanding the mechanisms that control the distinct genetic programs acquired by excitatory neurons from each layer has been a crucial point for understanding brain development and function. Up to date, several studies have demonstrated that the identity of neurons born at a different timepoint are a consequence of the combination of extrinsic factors and intrinsic genetic programs transmitted from their progenitors (Oberst et al., 2019).

Among the extrinsic factors, it has been described the importance of the membrane potential of the apical progenitors through the regulation of Wnt signaling (Vitali et al., 2018), the influence of cerebrospinal fluid and the diffusible proteins that contains (Lehtinen et al., 2011), the thalamocortical axons invasion (Monko et al., 2021; Ohtaka-Maruyama et al., 2018; Pouchelon et al., 2012; Vue et al., 2013) or feedback cues from new-born neurons to apical progenitors (Toma et al., 2014). All these factors are key for providing apical progenitors with competence for generating distinct layer specific neurons, and to specify the identity of the new-born neurons. However, cell-intrinsic factors are also important for providing new-born neurons positional information and identity. Indeed, a recent work demonstrates that apical progenitors modify their transcriptional and epigenetic information before generating neurons for every layer, and that they can transmit such information to their daughter cells in order to instruct their positional identity (Telley et al., 2019) (**Figure 2D**).

### 1.3 The formation of the thalamus

Centrally located in the brain, the thalamus was traditionally considered as a mere relay station that transmitted the information from the peripheral receptors towards the cortex where it is integrated and processed. However, today we know that it also has other key functions such as being involved in processing higher-order information or regulating the states of sleep and wakefulness.

This structure is subdivided in several modality-specific nuclei, whose neurons have very specific functions and projection patterns. Although the specificity of every nucleus was typically defined by its connectivity, during the last years several studies have demonstrated that those nuclei are also diversified by specific transcriptional programs that emerge from early in development, even before the onset of sensory experience. This genetic patterning seems to be essential for the correct development and specification of all the neuronal connections that rely in the thalamus. Thus, for understanding the organizational principles behind the thalamic nuclei specification, it is mandatory to decipher the mechanisms regulating the emergence of neuronal heterogeneity during the early development of the thalamus.

#### 1.3.1 Development and regionalization of the thalamus

Following the prosomeric model, the thalamus emerges from the diencephalic vesicle, which is divided in three prosomeres in its alar region: the pretectum (p1), the thalamus plus the epithalamus or habenula (p2), and the prethalamus plus the eminentia thalami (p3) (Bulfone et al., 1993; Puelles and Rubenstein, 1993; 2003; Puelles et al., 2013). Between p2 and p3 there is the zona limitans intrathalamica (ZLI), that serves as a boundary between both prosomeres, but also as a secondary organizer important for diencephalic histogenesis. Cells placed in that area are characterized by expressing the morphogene *Shh*, which codifies for a diffusible molecule responsible for the determination of the transcriptional programs of the recipient cells (Scholpp and Lumsden, 2010). In addition, *Wnt1* is expressed dorsally and defines the roof plate regions, and *Fgf8* is expressed rostrally (Echevarria et al., 2003; Vue et al., 2009). Overall, those factors contribute to the regionalization of the diencephalon, and particularly of the

thalamus, as they induce the expression of important transcription factors that define the identity of the thalamic glutamatergic neurons in a graded fashion (Gezelius and López-Bendito, 2017) (**Figure 3A**). As a consequence of the graded presence of the aforementioned proteins, specially Shh, differential expression programs have been detected in the progenitor space, thus revealing the existence of different progenitor domains in the thalamus. *Olig3* was found to be present in the progenitors along the entire thalamus caudal to the ZLI (Vue et al., 2007). However, *Olig3*<sup>+</sup> progenitors can be divided in two different domains attending to the expression of key genes, and the type of cells that are produced. The rostral domain, called pTH-R, is immediately caudal to the ZLI, and their cells express *Nkx2.2* and *Ascl1* (*Mash1*). The most caudal domain to the ZLI, called pTH-C, contains most of thalamic progenitors and expresses the two bHLH transcription factors, *Neurog1* and *Neurog2*, that will give rise to the glutamatergic neurons of the thalamus. These regional differences depend directly on the graded concentration of Shh, which is more intense in rostral parts, and is progressively reduced along the caudal axis. Consequently, higher levels of *Gli1* and *Ptch*, the two major downstream targets of Shh signaling, have been detected in the cells placed closer to the ZLI, especially the ones of pTH-R, and the most rostral part of pTH-C (Vue et al., 2009) (**Figure 3B and 3C**). Furthermore, in addition to the gradual diffusion of Shh, distinct competence to respond to Shh has been detected in the progenitors at different positions and seem to be dependent on the Ikaros family transcription factor, *Irx3*, thus suggesting also a possible pre-specification in the diencephalic progenitors (Kiecker and Lumsden, 2004; Kobayashi et al., 2002). Finally, recent technical advances in the field of single-cell RNAseq have allowed to observe at a more accurate transcriptomic level the distinct trajectories of the progenitors and early-postmitotic neurons in the diencephalon (Guo and Li, 2019), confirming the early specification of those progenitors' domains.

### 1.3.2 Thalamic neurogenesis, neuronal diversity and nucleogenesis

The thalamic mantle is composed by several nuclei, that can be grouped in three main types: association, relay, and non-specific. Relay nuclei receive sensory and motor inputs from the periphery and project to primary sensory cortical areas. Association nuclei receive most of their input from primary and secondary cortical areas and project back to

the association areas of the cortex where they seem to regulate neural activity. Finally, non-specific nuclei project throughout the cerebral cortex, and are involved in general functions such as alerting.

The thalamic relay nuclei can be divided in two types. The first order (FO) nuclei receive sensory input from subcortical afferents. In this thesis, I will focus particularly in visual, somatosensory, and auditory FO nuclei of the thalamus. The visual thalamus, named dorsal lateral geniculate nucleus (dLG), receives direct input from the retina, specifically from the retinal ganglion cells (RGCs) (Godement et al., 1984; Reichova and Sherman, 2004; Valverde, 1968) and then, dLGN neurons send their axons towards the primary visual cortex (V1). The somatosensory thalamus, the ventral posterior medial nucleus (VPM), receives input from the trigeminal pathway (Ralston, 1969) and from this structure, neurons target the primary somatosensory cortex (S1). The auditory thalamus, the ventral medial geniculate nucleus (MGv), receives input from the inferior colliculus (IC) (Jones and Rockel, 1971; Lee and Sherman, 2010) and targets the primary auditory cortex (A1). These three modality-specific thalamic nuclei send their axons mainly to the Layer 4 of their corresponding cortical area (Clark, 1932; Sherman and Guillery, 2002), although they can also project to almost all the cortical layers (Frost and Caviness, 1980). The higher order (HO) nuclei also show modality-specific segregation of their axons but their main driver input is from the cortex instead from the periphery, and complete the cortico-thalamo-cortical loop of information (Guillery and Sherman, 2002; Sherman and Guillery, 2002) (**Figure 3D**).

Although there is an increasing knowledge about transcription factors that specify the fate of thalamic projection neurons (Nakagawa and Shimogori, 2012; Song et al., 2015), the identification of specific genes that influence the emergence of the distinct thalamic structures and regions has not been addressed systematically. In a study published by our laboratory, we unraveled key transcription factors and networks that likely underlie the specification of individual sensory-modality thalamocortical connections. In this study, several genes that had a restricted expression pattern in the principal thalamic nuclei were identified even prior to the arrival of peripheral information suggesting a possible role in specifying thalamocortical topographical targeting and organization (Gezelius and López-Bendito, 2017; Gezelius et al., 2017).

Overall, this suggests the existence of intrinsic mechanisms in the thalamus that contribute to the early nuclei-segregation that takes place even before the complete formation of the connectivity of the system. This idea is consistent with the previously described influence of diffusible proteins like Shh or Fgfs in the specification of progenitor domains early in the development of the thalamus. Thus, as proposed in the cortex (Telley et al., 2019), neuronal progenitors might transfer their specific transcriptomic and epigenetic profiles to their descendant neurons and might suppose a first step in the nuclei specification and generation of the thalamus, although more studies are needed to fully address this hypothesis.

In order to better understand this, it is also important to examine the neurogenic process of the thalamus. Neurons are generated in the thalamus between E10.5 and E14.5 from the progenitors placed in the walls of the third ventricle, that start dividing asymmetrically to generate another progenitor and a more differentiated cell, that can be a neuron or an intermediate progenitor. Pioneer studies with tritiated thymidine injections already demonstrated that neurons from different thalamic nuclei are generated at different timepoints following a rostro-caudal and dorso-ventral patterning (Altman and Bayer, 1988a; 1988b; 1988c; 1989a; 1989b; 1989c; Angevine, 1970). Although the results of such studies were interpreted following the past columnar model of the forebrain organization, a recent paper partially replicated those conclusions with EdU injections and confirmed the neurogenic gradients in the thalamus, describing also an outside-in temporal specification of the thalamic nuclei (Wong et al., 2018). Nevertheless, this temporal gradient was not enough to understand whether neurons populating every thalamic nucleus are generated from the same already specified progenitor, or if neurons are generated and migrate stochastically and are specified later. To shed some light into that question, two recent studies (Shi et al., 2017; Wong et al., 2018) took advantage of the MADM technique, which allows the labelling of a single progenitor and all its descendant cells (Hippenmeyer et al., 2010; Zong et al., 2005). Thus, they were able to follow the progeny of individual progenitors until they final position in the different thalamic nuclei and analyze the dispersion of those cells. By using different driver transgenic lines, both studies concluded that progenitors are partially pre-specified, as they found that most of the progeny of a progenitor, populated first-order or high-order nuclei, with very low dispersion. Those results are in coincidence with transcriptomic analysis done in the adult

thalamus, where an unbiased clustering reflected the distinction of nuclei based on the birth dating of their neurons, and also between high-order and first-order nuclei (Phillips et al., 2019). Finally, when targeting intermediate progenitors by using Neurog1-CreER driver, they found that their progeny was more restricted towards a single nucleus, although there remained some dispersion across nuclei, suggesting a progressive temporal specification during the neurogenic period (Wong et al., 2018).

Overall, those studies propose an early specification of progenitors and newborn neurons in the thalamus, that seem to be partially pre-fated to particular territories (Nakagawa, 2019), coincident with transcriptomic analysis done at early stages (Gezelius et al., 2017; Guo and Li, 2019; Nakagawa and O'Leary, 2001; Suzuki-Hirano et al., 2011), that might be fully refined as the embryo develops. However, considering the vast diversity of nuclei in the thalamus, there is still a gap in the understanding on how the final refinement and distinction between nuclei of the same order or date of birth is produced.

Finally, in addition to the intrinsic properties and genetic patterns of the thalamic cells, the afferent inputs have shown to also play a role for the final refinement of the nuclei. Bilateral enucleation or infraorbital nerve section in neonatal mice produced a partial conversion of the transcriptomic profile of the visual and somatosensory first order nuclei (dLG and VPM) into high order nuclei of the same modality, as they started to express genes of the LP and Pom respectively (Frangeul et al., 2016). Moreover, bilateral enucleation at e14.5, prior to the arrival of retinal axons to the thalamus, also induced transcriptomic alterations into the dLG and even VPM neurons (Moreno-Juan et al., 2017). However, those alterations of the afferent inputs did not trigger a dramatic change in the connectivity of the visual or somatosensory circuit, supporting the idea of a previous specification of the fate of those neurons, even prior to the influence of the peripheral axons. This might be explained because those afferents reach the thalamus when the nuclei have been already specified and their axons have arrived at the corresponding cortical area.

In sum, the current proposed hypothesis for the generation of neuronal diversity seem to coincide with a mixed model, where a pre-specification exists already in the progenitors, that is refined during the development thanks to external cues, as similarly proposed for the cortex (Nakagawa, 2019; Telley and Jabaudon, 2018) (**Figure 3E**).

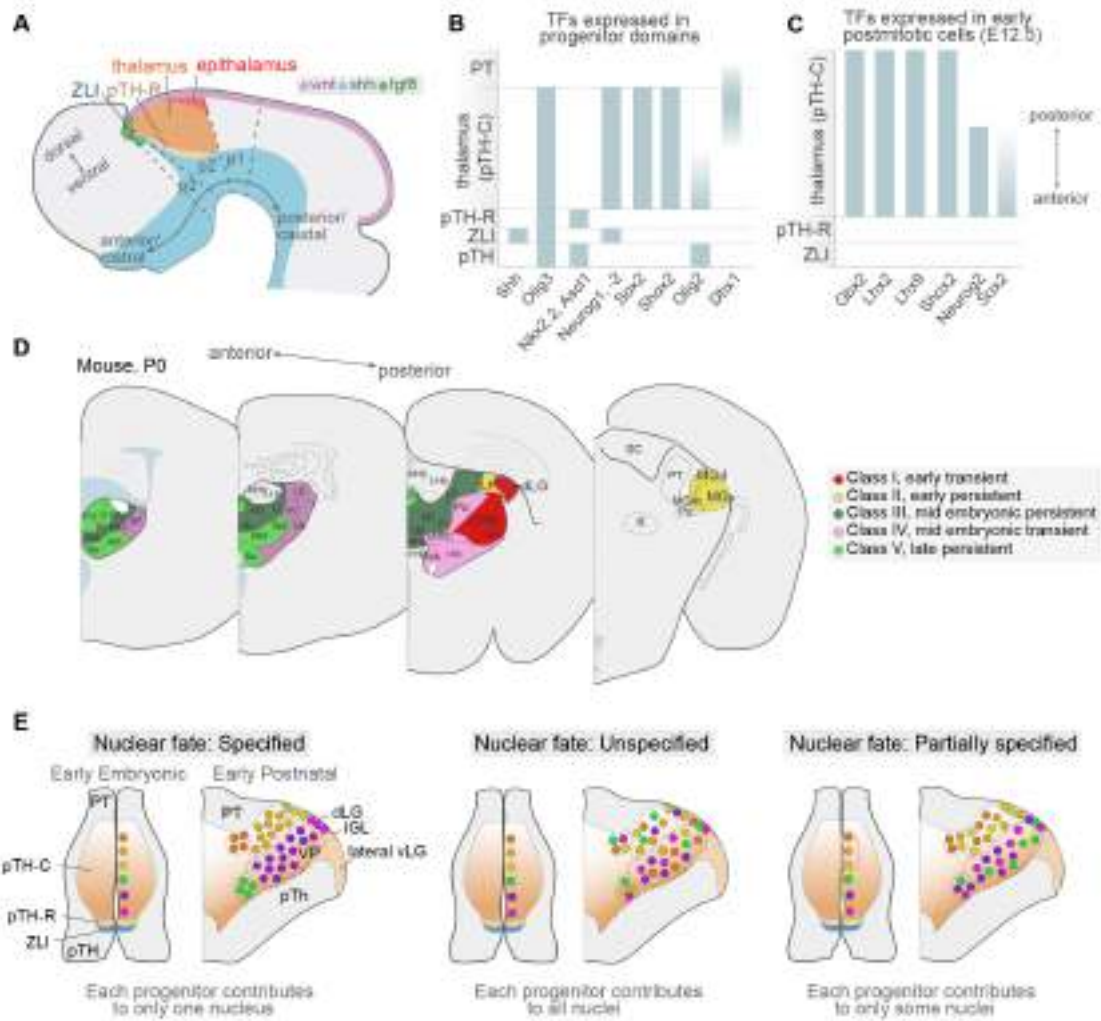


**Figure 3.** Thalamus formation and regionalization. (A) Schema of main secondary organizers and morphogenes that promote thalamic specification and regionalization. (B) Different transcription factors expressed at distinct progenitor domains in early stages of thalamic development. (C) Main transcription factors expressed by early postmitotic neurons in the developing thalamus. (D) Schema representing the main thalamic nuclei after nucleogenesis is completed. (E) Three proposed models for thalamic nuclei specification from early progenitors. Schemas adapted from (Gezelius and López-Bendito, 2017; Nakagawa, 2019).

## 2. Astrocytes' diversity in the CNS

Up to this point, the focus of the brain heterogeneity lay on the regionalization of the progenitor domains and in their descendant neurons, that inherit and refine this regional diversity. However, the processes of early parcellation and neurogenesis are immediately

followed by the gliogenic period. During this time, radial glial cells start producing more specialized glial cells, which include astrocytes and NG2-glia, also known as oligodendrocyte precursor cells (OPCs), although their role, heterogeneity and potential capacity for producing also astrocytes is a matter of controversy (see reviews in (Bernhardi and Dimou, 2016; Dimou and Gallo, 2015; Viganò and Dimou, 2016; Zhang et al.)). Overall, glial cells constitute nearly 50% of the cells in the human brain (Azevedo et al., 2009), being the astrocytes the largest population, and playing an essential role for the correct function of the brain circuits. For the purpose of this thesis, I will focus on the role, generation and heterogeneity only of the astrocytes.

## **2.1 Roles of astrocytes**

Despite that astrocytes have been traditionally considered a type of neural supporting cell (Rouach et al., 2008), since recently several investigations have unraveled additional roles (Barres, 2008; Verkhratsky and Nedergaard, 2018). Indeed, astrocyte dysfunction have been implicated in numerous diseases, including autism, Rett Syndrome and Fragile X Syndrome, as well as neurodegenerative disorders including Alzheimer's disease, multiple sclerosis, Huntington's Disease, and amyotrophic lateral sclerosis (reviewed in (Molofsky et al., 2012)).

Astrocytes are involved in the regulation of local neuronal circuits as they interact and communicate with their surrounding neurons and regulate their firing rates. They do so by taking part in the so called "tripartite synapse", where, contrary to the classical bipartite model, astrocytes are also able to interact with the pre- and post-synaptic neurons, responding to synaptic activity and modulating their responses (reviewed in (Araque et al., 2014; Hamilton and Attwell, 2010; Savtchouk and Volterra, 2018) and many others). Astrocytes sense the presence of synaptically-released neurotransmitters via G-protein-coupled receptors (GPCR) which trigger different intracellular signaling cascades, including calcium mobilization from internal stores and the release of gliotransmitters (Bazargani and Attwell, 2016; Dani et al., 1992). In addition, they can also uptake and release some of the synaptic-involved neurotransmitters (Bezzi and Volterra, 2001; Kinney and Spain, 2002). Indeed, distinct manipulations in the astrocytic calcium

signaling demonstrated their fundamental role for the correct function of specific neuronal circuits such as the thalamocortical, hippocampal or cerebellar circuits, as an impairment in their function is enough to induce even behavioral alterations (Haustein et al., 2014; Henneberger et al., 2010; Kwak et al., 2020; Paukert et al., 2014; Wang et al., 2006). In addition, the fact that astrocytes can specifically modulate neuronal circuits of brain regions, gives rise to the hypothesis that there exist circuit-specialized astrocytes in the brain (Nagai et al., 2021). How those astrocytes become circuit-specific is still a major question in neuroscience, and one of the main focuses of this thesis.

An additional role of astrocytes is their importance for synaptogenesis and synaptic plasticity. Establishment of the correct type and number of synapses is crucial for the proper development and function of the brain. This process coincides in time with gliogenesis, and glial maturation seem to mark the end of the synaptogenic and plastic periods (Fields, 2005; Müller and Best, 1989). Consequently, several studies have demonstrated that astrocytes can release signals to promote synapse formation and to eliminate incorrect synapses to modulate the process of axon pruning (reviewed in (Eroglu and Barres, 2010)). Moreover, a recent paper demonstrated that their influence is essential for closing the critical period for visual plasticity (Ribot et al., 2021).

Astrocytes have also important roles in responses to injury and disease, as described earlier by morphological analysis by Ramon y Cajal in the early 1900s. First, they take part in the formation of the glial scar that follows an injury (firstly observed by Del Rio-Hortega and Penfield in 1927, and recently reviewed in (Adams and Gallo, 2018)). They become activated or reactive as a response to a damage, thanks to extracellular signals of damage and to the recruitment mediated by microglia (Buffo et al., 2008; Liddel et al., 2017). This activation includes a change in the morphology (first observed by Achucarro in 1910), a change in their transcriptome, which includes an upregulation of genes like Glial-fibrillary acidic protein (GFAP), vimentin and nestin, which are progenitor markers in normal conditions (Sofroniew, 2005; Wu et al., 2017) and even the proliferation of some of them (Bardehle et al., 2013; Buffo et al., 2008; Escartin et al., 2021; Götz et al., 2015). Those reactive astrocytes populate the region of the injury, forming the glial scar in the case of strong and acute injuries, and exert functions aimed at restricting inflammation and protecting neurons and oligodendrocytes (Sofroniew, 2005). However, there is still controversy related to their

beneficial or harmful contribution for neuronal repair and axon regrowth (Anderson et al., 2016; Escartin et al., 2019; Liddel et al., 2017).

Those reactive astrocytes are an interesting field of study, as additionally to their role in the response to an injury, several studies have reported that reactive astrocytes might become immature, close to a progenitor-like state or to an adult neural stem cell as the ones present in hippocampus or in the subependymal zone. Pioneer *in vitro* studies demonstrated that astrocytes isolated from an injured brain region had a bigger capacity to form neurospheres than astrocytes from non-injured brain (Buffo et al., 2008). However, *in vivo*, adult progenitors or adult neural stem cells have bigger proliferative capacity than reactive astrocytes, and their lineage is committed to produce neurons, while reactive astrocytes are only able to divide once and produce another astrocyte (Sirko et al., 2013). Overall, although NSCs and reactive astrocytes share the expression of some genes, and even morphological similarities, they still conserve many differences related to their origin and functions (see review in (Götz et al., 2015)). Finally, in a recent publication it was revealed the transcriptomic and epigenetic modifications that take place in glial cells following an injury (in this case Müller cells in the retina). In that study the authors demonstrate how those Müller cells are able to produce neurons in zebrafish after a retinal injury, and which transcriptional and epigenetic factors prevent this *de novo* neurogenesis in murine Müller cells (Hoang et al., 2020). In sum, this and many other studies corroborate that in mice and superior mammals, reactive glia can acquire some immature properties, approaching them to a multipotent state, but it is not enough to induce spontaneous adult neurogenesis from those astrocytes following an injury.

## 2.2 Astrocytes' regional heterogeneity

Despite their wide diversity of functions, and their morphological diversity already documented by Ramon y Cajal and his contemporaries, astrocytes have been considered as a homogeneous population across the brain during many years. However, recently developed technical advances have facilitated a better description and characterization of the heterogeneity of astrocytes in the central and peripheral nervous system. In the CNS, we can find different types of astrocytes based on their morphology and localization,

including fibrous and protoplasmic astrocytes and specialized astrocytes such as radial glia, radial astrocytes (like Müller cells of the retina and Bergmann cells of the cerebellum), vellate astrocytes or surface-associated astrocytes (reviewed in (Verkhratsky and Nedergaard, 2018)). For the scope of this thesis, I will focus on grey matter's protoplasmic astrocytes, as they are present in most brain regions.

As discussed in the previous section, the implication of astrocytes in different new roles, including synapse and circuit regulation, suggests that astrocytes might be different depending on their location in the brain and in the neuronal circuits where they are integrated. Indeed, recent advances in microscopy, transcriptomic analysis, optogenetics, transgenic animals or electrophysiology have widely contributed to study and understand the heterogeneity of astrocytes. At the transcriptomic level, RNAseq of astrocytes from six different brain regions in the adult mice characterized the different transcriptomic profiles of their astrocytic populations and revealed that it exists a dorsoventral axis that distinguish the transcriptome of astrocytes from the brain regions analyzed (Morel et al., 2017) (**Figure 4A**). Advances in single cell transcriptomics also allowed a more accurate study of the regional differences between astrocytes from different brain areas (Gokce et al., 2016; Zeisel et al., 2018; 2015). In addition, this regionalization has been also observed within sub regions, such as in the cerebral cortex, where two recent studies demonstrated the existence of transcriptionally different groups of astrocytes after single cell transcriptomic analysis, that are distributed in layers (Batiuk et al., 2020; Bayraktar et al., 2020) (**Figure 4B**). Interestingly, although those reported astrocytic layers did not coincide with the neuronal layers, a previous paper demonstrated that astrocytes located in the six neuronal layers displayed differences between them at the transcriptomic, morphologic, and even functional level (Lanjakornsiripan et al., 2018). This suggests that additional features must be considered for understanding astrocytes' regionalization, such as their function and interaction with specific neuronal subtypes. Indeed, in other publication, hippocampal and striatal astrocytes were compared at molecular, morphological, and functional levels, providing a more refined way of classifying astrocytes based on the correlation between intrinsic differences and their interaction with the surrounding cells (Chai et al., 2017). Among the same line, a different publication reported differences in genes associated with synapse formation in astrocytes from different brain regions (John Lin et al., 2017). This was important as the same study

showed that, when coculturing astrocytes from one region with neurons from distinct regions, there were clear differences in the supporting of synapse formation, thus bridging the molecular and functional heterogeneity of regional subsets of astrocytes.

Finally, many more studies have provided extensive detail on the physiology of the astrocytes from different brain regions (see recent reviews and references in (Clarke et al., 2021; Durkee and Araque, 2019; Khakh and Deneen, 2019; Matias et al., 2019) and many others), however, for the scope of this thesis, I will focus on discussing how this diversity is achieved.

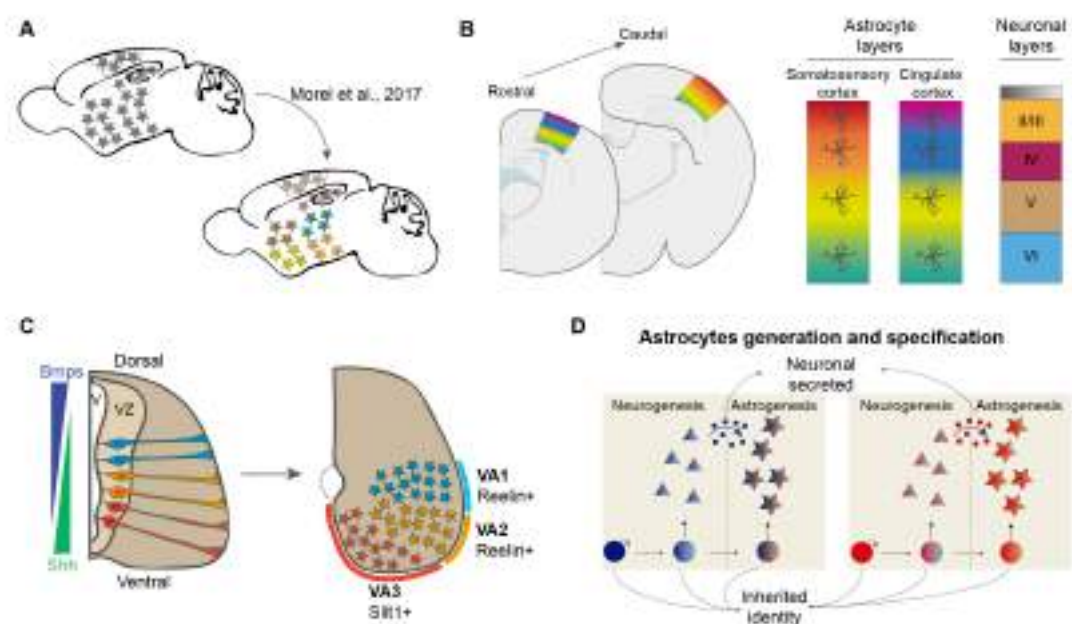


**Figure 4.** Astrocytes' heterogeneity and generation. (A) Schema of the main conclusions observed after transcriptomic analysis of astrocytes from different brain regions. (B) Astrocytes are organized in layers in the cortex based on their different transcriptomic landmarks, although those layers do not correspond with the neuronal layers. (C) Different progenitors and astrocytic domains in the developing spinal cord. Astrocytes seem to follow a radial dispersion from their progenitors, who seem to provide them with positional information. (D) Schema representing the generation of astrocytes from the same progenitors that produce neurons before. Astrocytic specification seems to be the consequence of a combination of intrinsic information inherited from progenitors and external cues. Schemas in (B) and (C) adapted from (Bayraktar et al., 2020; 2014).

### 2.3 Generation of astrocytes and emergence of their regional diversity.

The regional specification of astrocytes opens a novel view on astrocyte function and heterogeneity. The follow up question is, how is the heterogeneity of astrocytes acquired?

For answering this question, it is important to determine the origin and lineage of astrocytes. Although this has been a field of controversy, recent advances in clonal analysis and lineage tracing have allowed to decipher this. Currently it is widely accepted that the vast majority of protoplasmic astrocytes in the forebrain emerge from the same radial glia that in early stages of the development gave rise to neurons and intermediate progenitors, that are also a source of macroglia, including astrocytes. Those progenitors switch their fate to stop producing neurons when embryonic neurogenesis has been completed and start producing and differentiating into astrocytes and/or OPCs from E16.5-E17.5 onwards, although some of them remain present in the adulthood in particular niches (Eckler et al., 2015; Gao et al., 2014; Guo et al., 2013; Kriegstein and Alvarez-Buylla, 2009; Levison and Goldman, 1993; Magavi et al., 2012; Noctor et al., 2008; Zhang et al., 2020). Several studies have focused on unraveling the specific changes that take place at the transcriptomic and epigenetic level and the molecular processes that induce those changes, where we can find transcriptional changes regarding Nuclear Factor I-A, *Sox9* or Notch signaling (Deneen et al., 2006; Kang and Hébert, 2011; Stolt et al., 2003; Tiwari et al., 2018). Although this is the case for the majority of astrocytes, some studies have also reported the existence of clones that contain only glia or neurons, suggesting the existence of fate-specific progenitors, although it might also depend on the stage at which this progenitor was labelled (Gao et al., 2014; Zhang et al., 2020). Finally, contrary to what happens with neurons, newborn astrocytes proliferate locally during the first two postnatal weeks to increase their number up to the point that they become the main glial population in the brain (Ge et al., 2012).

Considering the shared origin between astrocytes and neurons, it seems plausible that both the gliogenic progenitors and the astrocytes are exposed to the same regionalizing cues as the neurons during the neurogenic period. Thus, a similar positional information that neural progenitors transmit to their neuronal progeny could be also transmitted to their descendant astrocytes to promote their regionalization and specification.

This patterning was first observed in spinal cord, where clear dorso-ventral domains can be identified based on the graded influence of Shh and BMP/Wnt morphogenes, giving rise to neuronal regional domains (Jessell, 2000; Ulloa and Briscoe, 2007). Interestingly the same regionalizing principles were observed for the generation of molecularly diverse astrocytes in the spinal cord, where patterning transcription factors Pax6 and Nkx2.2 are specifically expressed in subsets of white matter astrocytes, which are also defined by the differential expression of Reelin and Slit (Hochstim et al., 2008; Molofsky et al., 2014; Tsai et al., 2012) (**Figure 4C**). Regarding the brain, clonal analysis has revealed that in the cortex sibling astrocytes do not disperse or migrate far away after their generation and local proliferation, thus maintaining their original positional information and the columnar dispersion observed in neurons (Figueres-Oñate et al., 2016; Gao et al., 2014; García-Marqués and López-Mascaraque, 2013; Magavi et al., 2012; Zhang et al., 2020). This modular distribution might be one of the origins of the astrocytes' regionalization, which could explain their specificity for a particular neuronal circuit.

Despite the increasing number of studies about astrocyte heterogeneity in the cortex and spinal cord, less is known about this heterogeneity in other brain regions. For example, in the thalamus, one of the brain regions studied in this thesis, only the two studies with clonal analysis (Shi et al., 2017; Wong et al., 2018), showed data regarding the origin and dispersion of thalamic astrocytes. Essentially, they show that, as in the cortex, clonally related astrocytes seem to keep close to their sibling neurons, although more detail regarding their segregation across specific thalamic nuclei should be provided. Finally, although inherited cell-intrinsic signals from early development seem to be key for defining regional specificity, cell-extrinsic cues have been also reported that could be important for the final refinement of the astrocytes' regional identity. In the developing cortex, interaction of astrocytes and neurons mediated by neuroligins and neuronal neurexins is important for regulating astrocytic morphology (Stogsdill et al., 2017). In addition, in the cerebellum, it was shown that neuron derived Shh regulates Bergmann glia identity and function (Farmer et al., 2016).

Overall, regional identity of astrocytes seems to be developmentally controlled, as it emerges very early, although some external cues might contribute to the refinement of their heterogeneity and neural circuit specialized functions. However, it remains unclear

whether astrocytes, as share developmental origins with their surrounding neurons, and are exposed to the same regionalizing cues, might also share some characteristics with their neuronal counterparts because of that. Also, more experiments on manipulating the environment of astrocytes could reveal if their identity is fixed or plastic (**Figure 4D**).

### **3. Central Nervous System regeneration**

In the previous sections it has been discussed the extraordinary complexity of the central nervous system, based on the heterogeneity of their populating cells, especially neurons and glia, and in the intricate connectome that guarantees the correct processing of the information in the brain. However, as the correct assembly and function of the brain circuits is finely tuned during the development, and refined by the experience, it supposes a huge challenge for trying to repair a damaged neural circuit as a consequence of an injury or a neurodegenerative disease. It is widely known that postmitotic neurons do not regenerate and lack a proliferative capacity, so major efforts have done in trying to compensate a neuronal loss by using different strategies that will be discussed in the following sections. Moreover, apart from trying to generate new neurons that replace the damaged ones, it is important to consider that they should have similar properties that allow them to integrate properly in the circuit.

#### **3.1 Adult neurogenesis**

The first strategy is based on the existence of adult NSC that retain a proliferative and neurogenic capacity, which has been observed in adult mouse brain and even in humans mainly in the subventricular zone (SVZ) of the lateral ventricles (Lim and Alvarez-Buylla, 2016) and the subgranular zone (SGZ) of the hippocampal dentate gyrus (DG) (Bergmann et al., 2015; Gonçalves et al., 2016). In the murine healthy brain, SVZ produces neuroblasts that migrate to the olfactory bulb and integrate in the circuit as new granule and periglomerular interneurons, which are important for odor discrimination (Lazarini and Lledo, 2011). However, in human, SVZ supplies the striatum with new interneurons (Ernst et al., 2014). Regarding the SGZ, it is continuously generating granule neurons of

the hippocampal DG, which in rodents are known to be involved in memory, learning and pattern separation (Gonçalves et al., 2016).

Adult neurogenesis is quite restricted in the healthy brain to a couple of neuronal circuits, thus, in principle it should be not enough to compensate neuronal loss in other circuits. Interestingly, in several animal models and in humans, neuroblasts coming from SVZ have been observed in ectopic sites in response to stroke, trauma, epilepsy and Huntington's disease. Furthermore, it has been shown that neuroblast-derived newly generated neurons in some cases acquire the adequate identity when they differentiate in the place of the lesion (Arvidsson et al., 2002; Curtis et al., 2003; Jin et al., 2005; 2006; Kandasamy et al., 2015; Kohl et al., 2010; Kreuzberg et al., 2010; Macas et al., 2006; Magnusson et al., 2014; Martí-Fàbregas et al., 2010; Parent et al., 2002; Ramaswamy et al., 2005; Yamashita et al., 2006), while when they come from the SVZ niche they acquire different and not always adequate identities (Liu et al., 2010; Zhang et al., 2011). Anyway, even when the newborn neurons have the correct identity, they eventually succumb to cell death and fail to achieve long-term replacement of the degenerated neurons (Arvidsson et al., 2002; Thored et al., 2006).

Respect to the hippocampus, different pathologies can induce an increase or a reduction in the neurogenesis of the dentate gyrus, but in any of the cases those alterations reported any benefit and could even contribute to hyperexcitability of the neuronal network and epileptogenesis. Finally, other pathologies such as Alzheimers' disease or Parkinson disease also generate alterations in the neurogenesis of the neurogenic niches, but its benefits or effects are still a field of controversy (review on (Grade and Götz, 2017)). Apart from the migration from neurogenic niches, some studies have also proposed that spontaneous neurogenesis might occur from local progenitors in response to an injury (Chen et al., 2004; Magavi et al., 2000; Ohira et al., 2010). However, the origin of those new neurons is not clear, and there are studies showing the absence of this phenomenon (Diaz et al., 2013). Finally, due to the neural lineage of glial cells, and their plasticity upon injury, it has been hypothesized that they could be a potential source for neurogenesis after a damage. Indeed, although it is not the case for most injury conditions, it has been reported that after hypoxia in the postnatal mouse brain some astrocytes can undergo neurogenesis (Bi et al., 2011). Also, striatal astrocytes can undergo neurogenesis after ischemic stroke by downregulating Notch signaling (Magnusson et al., 2014), while their

connectivity remain to be determined. Those evidence suggest the potential of glia to be re differentiated into neurons *in vivo* by induction of extrinsic or intrinsic factors, which will be discussed in a following section.

Despite several advances in understanding or even trying to improve the responses of the adult neurogenesis to injury or disease (Belenguer et al., 2021; Llorens-Bobadilla et al., 2015; Maimon et al., 2021), there is still a gap as newborn neurons fail to survive for a long period, and also there are some concerns about their origin and capacity to integrate and recover the normal function of the circuit. Thus, more research among those lines is still required for improving and modulating this strategy for brain repair (see perspectives in (Grade and Götz, 2017)).

### **3.2 Cell transplantation**

While adult neurogenesis is quite restricted to specific brain regions, exogenous cells or neurons can be directly introduced in any damaged brain region, which is especially interesting for localized injuries or diseases, as the new neurons could replace the damaged ones. This has been recently done in mouse models of cortical damage, where notably the transplanted neurons were able to survive and extend their axons even in the context of a glial scar (Michelsen et al., 2015; Tornero et al., 2013). However, in non-focal diseases like AD, this strategy is not so suitable, and only transplantation of migratory cells like interneurons could be promising (Tong et al., 2014). One of the key factors at the time of designing this kind of therapies is the choice of the source of cells for the transplant. I will briefly describe the three main sources used including some examples where they have been applied:

#### Primary fetal neurons

One option is the use of primary neurons from fetal sources. They have the advantage that it is possible to specifically collect neurons from the specific region that wants to be repaired, thus the identity of the neurons will be the same. Some studies have used fetal midbrain dopaminergic neurons for reinnervating the striatum and improving behavior

in mice models of PD and even in patients (Barker et al., 2013; Grealish et al., 2010). This was also successfully carried on in the adult cortex after injury (Fricker-Gates et al., 2000; Hernit-Grant and Macklis, 1996; Shin et al., 2000)), where transplanted neurons were able to develop correct connections, which was later validated by team of Gaillard and Jaber in separated studies for assessing the connectivity and integration of transplanted neurons (Gaillard and Jaber, 2011; Gaillard et al., 2009; 2007). These promising studies highlighted the potential of this technique and later studies have confirmed the specificity and integrative capacity, such as for example in the visual circuit, where new neurons acquire similar properties to the ones of the visual cortex and even integrated properly in the visual circuit (Falkner et al., 2016). However, the limited availability of fetal neurons, especially from human, supposes an important problem for the use of this strategy, and hence efforts have been made towards the use of expandable cell sources.

#### eNSCs-derived neurons

As an alternative to the use of fetal neurons, it emerged the use of embryonic multipotent neural stem cells (eNSCs), that can be amplified and even immortalized for their posterior differentiation in specific neuronal types for later transplantation, which is their main challenge. As an example, cells from the immortalized C17.2 cell line were directly transplanted and successfully differentiated into neurons and glia and showed a protective role towards the host degenerating neurons (Ourednik et al., 2002; Park et al., 2002). In addition, human CNS-stem cells (huCNS-SC) were isolated (Uchida et al., 2000) and used for transplantation in rodent models of spinal cord injury, AD or hippocampal neuronal loss, where they induced behavioral recovery as assessed in locomotor or cognitive tasks (Ager et al., 2015; Cummings et al., 2005; Tamaki et al., 2002), although this has been discussed in recent studies (Anderson et al., 2017; Marsh et al., 2017). This controversy and the lack of enough evidence for their safety and efficacy promoted the search for more secure and controlled alternatives.

### ESCs-derived and iPSCs-derived neurons

Last, the development of a protocol for the conversion of somatic cells into induced pluripotent stem cells (hiPSCs) (Takahashi et al., 2007a; 2007b) supposed a big advance for the field, as it allowed to generate pluripotent cells from any somatic cell of a person with just a handful of genes. Its importance relied in the possibility of using cells from the same patient to generate other cell type, such as neurons, that can be transplanted back in the same patient avoiding possible problems of compatibility (Turner et al., 2013).

This approach allows to generate a pool of pluripotent stem cells that can then be redirected to the desired cell type, including distinct neuronal subtypes that match with the ones that want to be replaced after transplantation (reviewed on (Steinbeck and Studer, 2015)). In addition, other approaches focused on the direct conversion from somatic cells like fibroblasts in a neuron of interest, or in neural progenitors, thus skipping the pluripotent stem cell intermediate step, which makes this protocol faster and avoids the risk of tumor formation after transplantation (Lujan et al., 2012; Pang et al., 2011; Thier et al., 2012; Vierbuchen et al., 2010). For improving the specificity of those protocols, it has been essential the new technical approaches regarding single cell transcriptomics, as it is now easier to know the specific molecular patterning of every neuronal subtype, and which genes are key for instructing a particular neuronal identity (Tiklová et al., 2020).

Finally, several studies have demonstrated the therapeutic potential of this technique (see review in (Götz and Bocchi, 2021; Grade and Götz, 2017)), up to the point that at present, phase I/II trials have been initiated in patients with age-related macular degeneration and Stargardt macular dystrophy (Schwartz et al., 2012; 2015), and the next years will witness clinical translation also to Parkinson disease patients.

### **3.3 Cellular reprogramming**

A neuronal repair strategy that has gained more relevance during the last years is the direct conversion of resident non-neuronal cells, especially astrocytes, into neurons *in vivo*. This approach is based on the neural lineage of astroglial cells, and in the possibility

of converting them into neurons by overexpressing some neurogenic factors that are silent normally in astrocytes or repressing important genes for the maintenance of the astroglial identity.

Pioneer studies from Magdalena Gotz's laboratory demonstrated that repressing *Olig2* expression in astrocytes after an injury was sufficient to convert a significant number of them in immature neurons (Buffo et al., 2005). Later, it was also observed that the overexpression of a single neurogenic transcription factor, like *Neurog2* or *Ascl1* in cultured astrocytes was enough to reprogram them into functional and mature neurons, that were all glutamatergic when using *Neurog2*, while a mixed population of GABAergic and glutamatergic was achieved when using *Ascl1* (Berninger et al., 2007; Heinrich et al., 2010; 2011). Since then, two main objectives were established: improving the efficiency of the conversion by increasing the number of reprogrammed astrocytes and trying to extrapolate those optimized strategies to *in vivo*. First, *in vivo* approaches took advantage of the use of retrovirus to target specifically proliferating cells, which after an injury are mainly glial cells, and avoiding the infection of postmitotic neurons. In (Grande et al., 2013) authors managed to convert resident cells into new neurons by overexpressing *Neurog2* and adding a set of growth factors in the striatum and neocortex after a focal injury. Later, in (Guo et al., 2014) authors showed that it was possible to efficiently convert astrocytes and NG2 glia into glutamatergic or a mixture of glutamatergic and GABAergic neurons respectively, just by retrovirus-mediated overexpression of *NeuroD1* in the cerebral cortex after injury and in an Alzheimer's Disease mouse model. Interestingly, *NeuroD1* appeared to be also effective in non-reactive astrocytes (Bulet et al., 2017).

Despite the promising data from those and other studies, several questions remained to be assessed. First, it was important to increase the efficiency and the long-term survival and integration of the newly generated neurons. It was observed that the reprogramming process induced an oxidative-stress in the converting astrocytes, that caused ferroptosis-mediated cell death (Gascón et al., 2016). Interestingly, that study also showed that avoiding this process of ferroptosis by adding the overexpression of the anti-apoptotic gene *Bcl2* to the reprogramming cocktail highly increased the *in vivo* reprogramming efficiency, which was also improved by feeding animals with antioxidant compounds. In addition, other studies revealed the transcriptional changes that modulate the glia to neuron conversion, such as the involved transcription factors and checkpoints

for acquiring distinct neuronal identities, which opened new avenues for improving the efficiency and specificity of these strategies (Karow et al., 2018; Masserdotti et al., 2015; Russo et al., 2021; Smith et al., 2016; Treutlein et al., 2016; Xue et al., 2013). Also, adding small molecules that contribute to the remodeling of the chromatin in converting astrocytes improved the efficiency of the reprogramming and facilitated the neuronal maturation, although difficulted the generation of specific neuronal subtypes ((Ma et al., 2019; Rivetti di Val Cervo et al., 2017; Zhang et al., 2015), reviewed in (Qin et al., 2017)).

An alternative to the induction of a neurogenic program by overexpressing neuronal transcription factors, is the repression of key genes for maintaining the astrocytic identity. This strategy emerged during the last years and yielded a high efficiency *in vivo* by depleting the RNA-binding protein PTB, an important repressor for neuronal genes, in astrocytes from substantia nigra (Qian et al., 2020) and striatum (Zhou et al., 2020). This downregulation was triggered in mouse models of Alzheimer's disease, where converted neurons acquired a dopaminergic fate, and were able to partially reinnervate the striatum (Qian et al., 2020) and rescued the deficits in motor behavior in both studies. Interestingly, this strategy also worked for converting Müller glia into retinal ganglion cells *in vivo* after a retinal damage, that projected to the dLG in the thalamus and to the superior colliculus, also promoting an improvement of the visual responses (Zhou et al., 2020) (Figure 5).

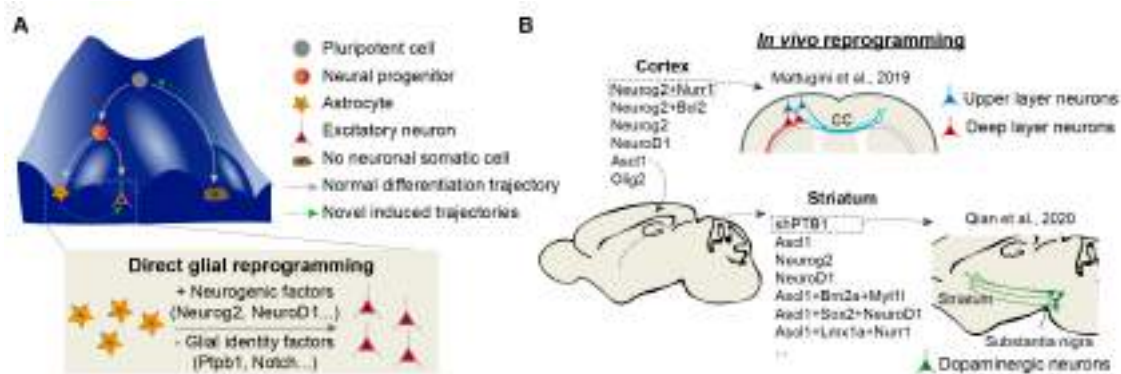


**Figure 5.** Recent advances for *in vivo* glia-to-neuron conversion. (A) Waddington's schema for illustrating the normal trajectories followed by pluripotent cells towards differentiated cell types. Also, new advances that challenge the classical dogma of the immutability of the cell identity, and that are the basis for novel therapies for neuronal repair, such as direct glia to neuron reprogramming. (B) Examples of the recent studies demonstrating the possibility of converting *in vivo* resident glia into neurons that in some cases can even connect with their brain targets.

The fact that in those studies the converted neurons were able to acquire a proper identity and to integrate correctly in the neural circuit where their original glia was placed, suggested an interesting concept. As in all the cases the targeted gene was the same, but the identity of the new neuron different, it proposes two scenarios:

- (i) That the neuronal environment influences the specification of the converted astrocyte, although in the adult brain the expression of regionalizing molecules is quite reduced compared to the developmental stages. However, as previously discussed, neurons seem to be able to specify astrocytes by secreting important signals like Shh (Farmer et al., 2016).
- (ii) The second scenario implies that astrocytes are different from their origin and are somehow regionalized in a similar way than their surrounding neurons. This scenario has been also proposed in a recent paper (Mattugini et al., 2019), where the same cocktail of transcription factors reprogrammed astrocytes towards different neuronal fates in the cortex. When infected astrocytes were placed in upper layers, converted neurons expressed markers and displayed connectivity typical of upper layer neurons, while similar data was obtained for deep layer astrocytes. This was in line with the layer heterogeneity of the cortical astrocytes proposed by recent studies (Batiuk et al., 2020; Bayraktar et al., 2020; Lanjakornsiripan et al., 2018). However, although their proved heterogeneity, a possible paralleling with the identity of their surrounding neuronal subtypes has not been proved.

Nevertheless, both scenarios are not mutually exclusives, as both components might play important roles for regulating the acquisition of a specific neuronal identity that facilitates the integration of reprogrammed astrocytes into a particular neuronal circuit. Thus, further research might focus on understanding the molecular mechanisms that govern such specification, as it could greatly improve the potential of those strategies for brain repair.

Finally, the strategy for gene activation or repression in astrocytes has also evolved in the recent years. The initial experiments took advantage of the use of retroviral vectors for targeting only proliferating cells, and thus avoiding the infection of endogenous

neurons (Buffo et al., 2005; Gascón et al., 2016; Guo et al., 2014). However, the use of AAV emerged as an interesting tool as they do not integrate their genome in the host cell and elicit a much less inflammatory and reactive gliosis response (Chen et al., 2020; Liu et al., 2020; Mattugini et al., 2019; Qian et al., 2020; Wu et al., 2020; Zhou et al., 2020). Notwithstanding, AAV vectors can infect also postmitotic neurons, so they require the use of specific promoters for the cell type that wants to be targeted, such as Gfap promoter in the case of astrocytes. Notably, aberrant activation of this gene in the infected neurons has been reported (Wang et al., 2020), thus highlighting the importance of stringent controls for the use of this strategies, as supposedly converted neurons can be confused with already present neurons, a concern that has been a matter of discussion in the last years.

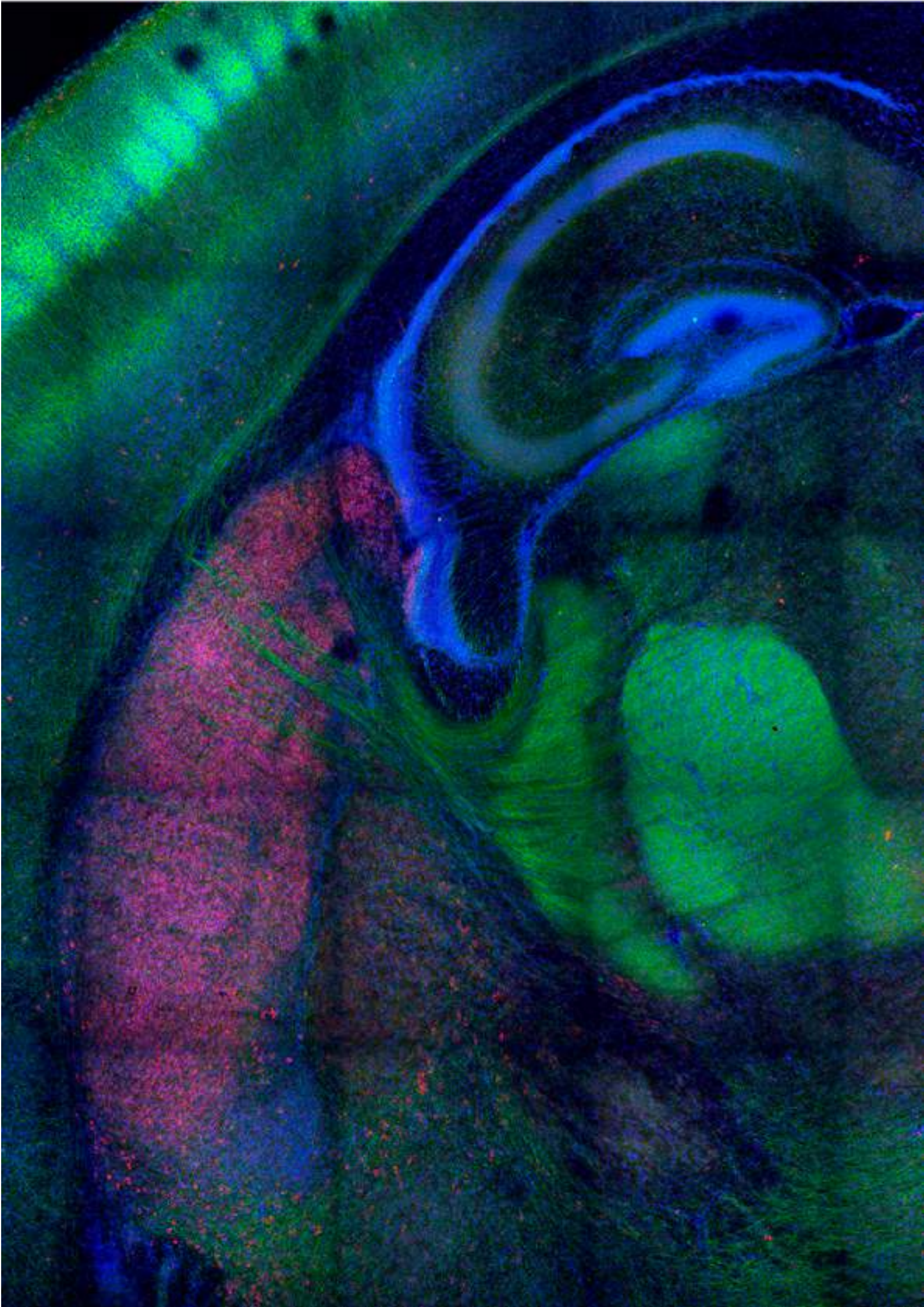
Overall, the field of neuronal replacement has approached a very exciting state thanks to the recent studies and the existence of different strategies could suppose an important advance for adapting treatments for every particular case. Nevertheless, there are still concerns and challenges that need to be addressed such as the specific targeting of a particular cell type for the conversion, the specification and circuit integration of the new neurons, the complete physiological rescue of the damaged function, and hopefully the extrapolation of those strategies to human patients.

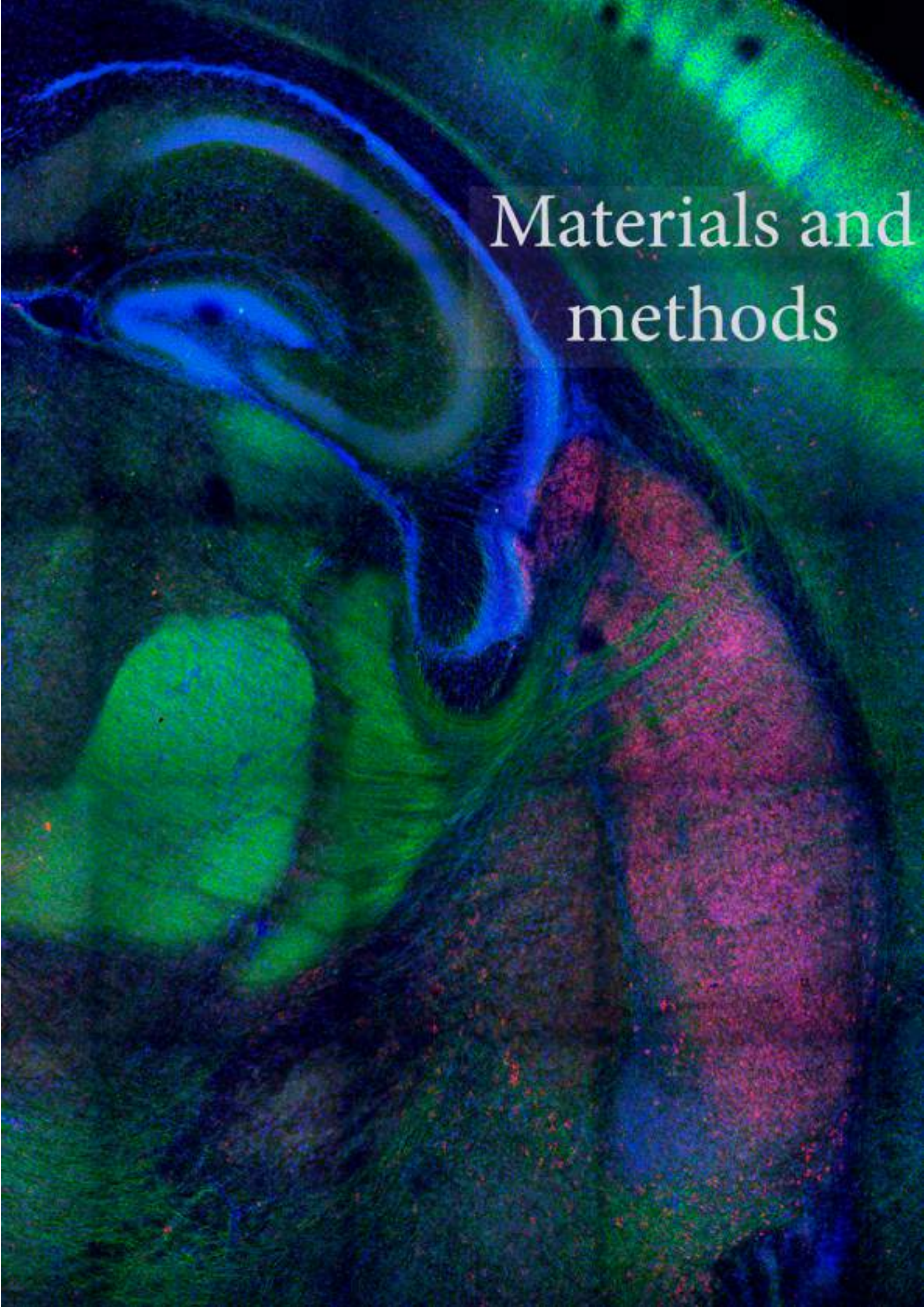


## **Objectives**

The main objective of this PhD thesis work was to understand the molecular mechanisms that facilitate the direct reprogramming of resident astrocytes into specific neuronal subtypes. The specific aims were the following:

- To decipher the region-specific molecular profiles of thalamic and cortical astrocytes.
- To determine if neurons and astrocytes from the same region share regional transcriptomes.
- To directly reprogram astrocytes from specific sensory thalamic nuclei into neurons and characterize their final neuronal fate.
- To unravel the molecular mechanisms that govern the acquisition of a specific regional identity of the converted astrocytes.





Materials and  
methods



## Materials and methods

### *Mouse strains*

All transgenic animals used in this study were maintained on ICR/CD-1, FVB/N-Tg, or C57BL/6J genetic backgrounds and genotyped by PCR. The day of the vaginal plug was stipulated as E0.5. The *Gfap::Gfp* line (Nolte et al., 2001) (the Jackson Laboratory, stock number 003257) was in an FVB/N-Tg genetic background, the *Gad67::Gfp* line (Tamamaki et al., 2003) was in C57BL/6J, and the *R26<sup>tdTomato</sup>* Cre-dependent line (the Jackson Laboratory, stock number 007908) and the *Gbx2<sup>CreERT2/+</sup>* mouse line (Chen et al., 2009) were in an ICR/CD-1 genetic background. Tamoxifen induction of Cre recombinase in the double-mutant embryos (*Gbx2<sup>CreERT2/+</sup>::R26<sup>tdTomato</sup>*) was performed as previously described (Antón-Bolaños et al., 2019). The Committee on Animal Research at the University Miguel Hernández approved all the animal procedures, which were carried out in compliance with Spanish and European Union regulations.

### *Isolation of astrocytes and neurons for RNA-seq*

The brains (four brains were pooled for each sample) were extracted in ice-cold KREBS solution and cut in the vibratome in 300- $\mu$ m slices, and cells were dissociated as in a previous publication (Gezelius et al., 2017). Thalamic nuclei (dLG, VPM, and MGv) and somatosensory cortex (S1) were dissected and pooled in cold dissociation medium [20 mM glucose, 0.8 mM kynurenic acid, 0.05 mM D,L-2-amino-5-phosphonovaleric acid (APV), penicillin (50 U/ml), streptomycin (0.05 mg/ml), 0.09 M Na<sub>2</sub>SO<sub>4</sub>, 0.03 M K<sub>2</sub>SO<sub>4</sub>, and 0.014 M MgCl<sub>2</sub>]. The tissue was transferred to sterile conditions and enzymatically digested in dissociation medium supplied with L-cysteine (0.16 mg/ml) and 70 U papain (Sigma-Aldrich) set to pH 7.35, at 37°C for 30 min with repeated shaking. The enzyme was then inhibited with dissociation medium containing ovomucoid (0.1 mg/ml) (Sigma-Aldrich) and bovine serum albumin (BSA) (0.1 mg/ml) set to pH 7.35, at room temperature. Tissue was transferred to iced Opti-MEM (Life Technologies) supplied with 20 mM glucose, 0.4 mM kynurenic acid, and 0.025 mM APV and mechanically dissociated until a single-cell suspension was obtained. Cells were concentrated by

centrifugation with 850 rpm for 5 min and filtered through a cell strainer (BD Falcon). The genetically labeled live cells were separated based on green or red fluorescence intensity using fluorescence-activated cell sorting (FACS Aria III, BD). FACS-purified cells were collected directly in lysis buffer of the RNeasy Micro Kit (Qiagen, no. 74004) that was used to recover total RNA according to the manufacturer's instructions. RNA quality for all samples was measured on an Agilent Bioanalyzer 2100 system. All samples with RNA Integrity Number (RIN) > 7 were used as input to library construction.

### ***Library preparation and RNA-seq***

Library construction and sequencing were performed at the CNAG-CRG (Centro Nacional de Análisis Genómico) genomics core facility (Barcelona, Spain). Briefly, cDNA multiplex libraries were prepared using SMARTer Ultra Low RNA Kit v4 (Takara, no. 634894) and NEBNext Ultra DNA Library Prep for Illumina according to the manufacturer's instructions (NEB, no. E7645). Libraries were sequenced together in a single flow cell on an Illumina HiSeq 2500 platform using v4 chemistry in 1 × 50 bp (base pair) single-end mode. A minimum of 25 million reads were generated from each library.

### ***Bioinformatic analysis of the RNA-seq***

RNA-seq analyses were performed as previously described (Scandaglia et al., 2017) with minor modifications: Quality control of the raw data was performed with FastQC (v0.11.7) and sequenced dataset adapters were trimmed using Cutadapt (v2.3) and Trim Galore (v0.6.1). RNA-seq reads were mapped to the mouse genome (GRCm.38.p6/mm10) using STAR (v2.7.0d), and SAM/BAM files were further processed using SAMtools (v1.9). Aligned reads were counted and assigned to genes using Ensembl release 95 gene annotation and FeatureCounts, Subread (v1.6.4) (Liao et al., 2014). Normalization of read counts and differential expression analyses were performed using DESeq2 (v1.22.2) and Bioconductor (v3.8) in the R statistical computing and graphics platform (v3.5.1 "Feather Spray").

In the analysis datasets of cortical astrocytes and thalamic astrocytes and neurons generated for this study, significantly DEGs were identified using statistical significance

threshold [Benjamini-Hochberg (BH)-adjusted  $P$  value  $< 0.1$ ] and absolute  $\log_2$  fold change ( $\log_2FC$ )  $> 0$  using shrunken  $\log_2FC$  using the adaptive  $t$  prior Bayesian shrinkage estimator “apeglm” (Zhu et al., 2019). To identify the top most differentially enriched genes between cortical and thalamic neurons, we used data generated in this study for thalamic neurons (P0) and publicly available dataset for cortical neurons (P1) from a previously published study (GSE63482) (Molyneaux et al., 2015). Datasets from (Molyneaux et al., 2015) consist of RNA-seq profiles of multiple classes of FACS-purified cortical neurons from ICR/CD-1 mice: callosal projecting neurons (CPN,  $n = 2$ ), corticothalamic projecting neurons (CThPN,  $n = 2$ ), and subcerebral projecting neurons (ScPN,  $n = 2$ ). Neuronal datasets from the cortex and thalamus were aligned from the raw sequence, and gene counts were generated using the same pipeline as indicated previously. Gene counts were normalized using the median of ratios method in DESeq2 R package, and the ratio between gene counts (regularized logarithm transformation of the normalized counts) were used to identify the top 400 most differentially enriched genes between cortical and thalamic neurons. Hypergeometric test (one-sided Fisher’s exact test) was performed to test independence between lists of enriched or significantly DEGs from neurons and astrocytes from different brain regions and to obtain estimated odds ratios. RNA-seq coverage tracks for selected genes were generated using Integrative Genomics Viewer (IGV) (v2.4.14) and plotted in a 5’ to 3’ direction. Hierarchical clustering analysis was performed using “Manhattan” distance and “Ward.2” clustering method metrics to visualize significantly up-regulated and down-regulated genes. In the functional enrichment analysis of the datasets from astrocytes, a more restrictive filtering criterion was used to detect high significantly DEG based on simultaneous threshold of BH-adjusted  $P$  value  $< 0.1$  and absolute  $\log_2FC > 0.322$ . This analysis revealed 508 versus 444 DEGs enriched in the thalamus and cortex, respectively. The GO overrepresentation analysis and GSEA were performed using clusterProfiler (v3.10.1) (Yu et al., 2012). All enriched terms were considered significant at adjusted  $P$  values by BH with  $P$  value cutoff  $< 0.01$  and  $0.1$ , in the GO overrepresentation analysis and GSEA, respectively. The reference gene set used to perform the analysis was C5 (GO Biological Process) collection from the Molecular Signatures Database (MSigDB) (v6.2).

### ***Bioinformatic analysis of the scRNA-seq***

We analyzed recent work from scRNA-seq to interrogate thalamic and cortical cellular heterogeneity (Zeisel et al., 2018). The sequence data are publicly available at the National Center for Biotechnology Information (NCBI) Sequence Read Archive (SRA) under accession SRP135960 (Zeisel et al., 2018). Briefly, scRNA-seq datasets (postfiltered count matrices) for the thalamus and cortex were downloaded from the associated wiki and processed with Seurat R package (v3.1.4) (Stuart et al., 2019). First, we performed quality control analysis that confirmed that the data were of high quality. All cells had more than 600 detected molecules (UMIs) and the proportion of mitochondrial reads was below 5% for the vast majority of cells. Next, data were preprocessed (log normalization and scaling) before performing linear dimensional reduction (PCA). Graph-based clustering approach using the top 30 principal components was used to identify cell populations (resolution was fixed to 0.8). FindAllMarkers function with default parameters was used to identify gene markers for each cluster and to assign cell-type identity to clusters).

Cortical and thalamic scRNA-seq datasets were subsequently integrated as previously described (Butler et al., 2018). The UMAP (Uniform Manifold Approximation and Projection) algorithm was used to nonlinear dimensionality reduction, visualization, and exploratory analysis of the datasets. Differential expression analyses between thalamic and cortical neurons and astrocytes were performed using the FindMarkers function based on the nonparametric Wilcoxon rank sum test with the following parameters (logFC.threshold = 0.1; min.pct = 0). Genes with BH-adjusted *P* value < 0.1 were considered significantly differentially expressed.

### ***In utero electroporation of StarTrack vectors***

For in utero electroporation, a procedure previously described was followed (Moreno-Juan et al., 2017). Pregnant females (E11.5) were deeply anesthetized with isoflurane to perform laparotomies. The embryos were exposed, and the third ventricles of the embryonic brains were visualized through the uterus with an optic fiber light source. The combination of the plasmids of the StarTrack method at a final concentration of 2 µg/µl was mixed with 0.1% Fast Green (Sigma-Aldrich), as previously described (Figueres-

Oñate et al., 2016; García-Marqués and López-Mascaraque, 2013). The plasmids used consisted of the coding sequence of six fluorescent proteins (EGFP, mCherry, mKusabian Orange, mTSapphire, mCerulean, and EYFP) subcloned under the regulation of the GFAP or UbC promoters for targeting specifically the astrocytes or all the cell types. Each reporter gene could be directed to the cytoplasm (PB-GFAP/UbC-XFP) or to the nucleus of the cell by fusing it with the H2B histone protein (PB-GFAP/UbC-H2B-XFP). Constructs were flanked by PiggyBac sequences to be inserted into the genome of the targeted cell by a PiggyBac transposase. The plasmids were injected into the third cerebral ventricle by an injector (Nanoliter 2010, WPI). For electroporation, five square electric pulses of 45 V and 50 ms were delivered through the uterus at 950-ms intervals using a square pulse electroporator (CUY21 Edit, NepaGene Co., Japan). The surgical incision was then closed, and embryos were allowed to develop until P8. In the electroporated animals with the UbC-StarTrack combination, tamoxifen was administered at P1 as previously described (Figueres-Oñate et al., 2016) for removing nonintegrated copies of the electroporated plasmids through the Cre recombinase system.

### ***Measurement of thalamic astrocytic clones***

Images were acquired with an Olympus FV1000 confocal IX81 microscope/FV10-ASW software following previously defined settings (García-Marqués and López-Mascaraque, 2013). All the pictures were acquired with a 20× oil immersion objective and analyzed with ImageJ software. Only electroporated animals with labeled cells in the three first order thalamic nuclei (dLG, VPM, and MGv) were used. Then, only clones with at least three cells and with the presence of more than one reporter were analyzed.

First, we assigned a binary code to every cell based on the presence or absence of each reporter protein in the cytoplasm and/or the cellular nuclei and the expression of the neuronal marker NeuN in order to distinguish neurons from glial cells. Once all the cells had been analyzed, they were grouped on the basis of their shared binary code, thereby identifying those cells that originated from the same progenitor. Then, we quantified the distribution (in %) of cells belonging to the same clone across the thalamic nuclei.

### ***Virus production***

For the production of the retrovirus, Lenti-X 293T cells (catalog no. 632180, Clontech) were plated on 5- to 10-cm dishes. Encapsulation plasmids containing gag-pol and vsv-g sequences (provided by V. Borrell) were cotransfected with the plasmid of interest using LipoD293 (catalog no. SL100668, SignaGen). The medium was changed after 5 hours, and the virus was collected after 72 hours using Lenti-X concentrator (catalog no. 631231, Clontech).

### ***In vivo viral and BrdU injections***

Pups at P3 were anesthetized on ice and placed in a digital stereotaxic. The virus was injected using an injector (Nanoliter 2010, WPI) in the thalamus or cortex through a small skull incision. BrdU was injected intraperitoneally at 50 mg/kg immediately after viral injections from stock solution (10 mg/ml).

### ***Astrocyte primary cultures***

Postnatal astroglia was cultured as previously described (Heinrich et al., 2011). Briefly, after removal of the meninges, the cortices (somatosensory and visual) and the thalamus from P4 to P6 mice were dissected and dissociated mechanically in cold KREBS 1×. Subsequently, cells were centrifuged for 10 min at 1000 rpm, resuspended, and plated in a medium consisting of DMEM/F12 (Gibco), 3.5 mM glucose (Sigma-Aldrich), 10% fetal calf serum (Gibco), 5% horse serum (Gibco), 1× GlutaMAX (Fisher), and antibiotic/antimycotic (100 U/μl) (Fisher) and supplemented with B27 2% (Gibco), epidermal growth factor (10 ng/ml) (EGF; Roche), and fibroblast growth factor 2 (10 ng/ml) (FGF2; Roche). Oligodendrocyte precursor cells were removed by brusquely shaking the culture flasks several times when changing the medium after 2 or 3 days. Cells were passaged after 1 week using trypsin/EDTA (Gibco) and plated on poly-D-lysine (Sigma-Aldrich) glass-coated coverslips at a density of 50,000 to 70,000 cells per coverslip (in 24-well plates; BD Biosciences) in the same medium. The vast majority of the cells (>90%) were positive for glial fibrillary acidic protein (Gfap). Nuclei-specific thalamic

astrocytic cultures were performed similarly but with a few modifications. Brains were dissected out and cut in a vibratome in 300µm slices in cold KREBS to dissect the three principal sensory thalamic nuclei: dLG nucleus, the somatosensory VPM nucleus, and the auditory MGv. Thalamic nuclei were then mechanically dissociated and plated on six-well plates and passed when confluent. Astrocytes were infected with CAG-*GFP*-IRES-*GFP*, CAG-(*Flag*)*Neurog2*-IRES-*DsRed*, CAG-(*Flag*)*Neurog2*-IRES-*TauGFP*, or CAG-*Gbx2*-IRES-*DsRed* retroviruses. After 24 hours, the medium was changed by a differentiation medium containing DMEM/F12 (Gibco), 3.5 mM glucose (Sigma-Aldrich), 1× GlutaMAX (Fisher), and antibiotic/antimycotic (100 U/µl) (Fisher) and supplemented with B27 2% (Gibco). BDNF (Sigma-Aldrich) was added at 20 ng/ml every fourth day during the differentiation process.

### ***Histology***

For immunofluorescence of reprogrammed neurons in vitro, cultures were fixed with 4% paraformaldehyde (PFA) in phosphate-buffered saline (PBS) (0.01 M) for 10 to 15 min at room temperature. Cultures were first incubated for 1 hour at room temperature in a blocking solution containing 2% BSA (Sigma-Aldrich) and 0.15% Triton X-100 (Sigma-Aldrich) in 0.01 M PBS. Subsequently, the cells were incubated overnight at 4°C with the corresponding primary antibodies. The cells were then rinsed in 0.01 M PBS and incubated for 2 hours at room temperature with adequate secondary. Counterstaining was performed by the fluorescent nuclear dye 4',6-diamidino-2-phenylindole (DAPI) (Sigma-Aldrich).

For histology in postnatal brains, mice were perfused transcardially first with 0.01 M PBS and 4% PFA. Brains were kept on 4% PFA overnight, embedded with 3% agarose in 0.01 M PBS, and cut into slices of 80 µm of thickness in a vibratome (Leica). For *Tbr1*, *Ctip2*, *Aldh1l1*, *Rora*, and *Lef1* antibodies, an antigen retrieval step with sodium citrate was performed. For BrdU detection, slices were first incubated with 2 N HCl and 0.5% Triton X-100 at 37°C for 30 min, followed by an incubation with borax buffer at room temperature. Slices were incubated for 1 hour at room temperature in a blocking solution containing 1% BSA, 2% donkey serum, 2% goat serum, and 0.4% Triton X-100 in 0.01 M PBS and subsequently incubated overnight at 4°C with primary antibodies. Slices were

incubated for 2 hours at room temperature with the appropriate secondary antibodies, washed, incubated with DAPI, and mounted. Images were acquired with a Leica DFC550 camera into a Leica DM5000B microscope, with an Olympus FV1000 confocal IX81 microscope/FV10-ASW software, or with a Zeiss confocal LSM880.

### ***Fluorescence in situ hybridization***

*Gfap::Gfp* brains were cut into slices of 100  $\mu\text{m}$  of thickness in a vibratome (Leica). Slices were dehydrated, incubated for 15 min with 2%  $\text{H}_2\text{O}_2$  in EtOH at room temperature for blocking endogenous peroxidase, and rehydrated. Then, slices were washed first with PBS and 0.1% Tween 20 (PBT), then with a detergent mix [1% NP-40, 1% SDS, 0.5% sodium deoxycholate, 50 mM tris-HCl (pH 8), 1 mM EDTA, and 150 mM NaCl] three times for 20 min and postfixed with 4% PFA. After three washes with PBT, slices were incubated with prehybridization solution [50% deionized formamide, 5 $\times$  SSC (pH 5.3), heparin (50  $\mu\text{g}/\text{ml}$ ), tRNA (50  $\mu\text{g}/\text{ml}$ ), single-stranded DNA (50  $\mu\text{g}/\text{ml}$ ), and 0.1% Tween 20] for 1 hour at 65°C in a humid chamber and then incubated overnight with the corresponding probe in prehybridization solution at 65°C.

The next day, slices were washed four times with prewarmed washing solution [50% formamide, 2 $\times$  SSC (pH 5.3), and 1% SDS] at 65°C and four times with MABT [100 mM maleic acid, 150 mM NaCl, 0.19 M NaOH (pH 7.5), and 0.1% Tween 20]. Slices were then incubated with blocking solution [2% Blocking Reagent (Sigma-Aldrich, no. 11096176001) in MABT] for 2 hours and then incubated overnight at 4°C with anti-digoxigenin-POD (Sigma-Aldrich, no. 11207733910) diluted 1/500 in blocking solution. Slices were washed four times with MABT and then revealed with TSA PLUS CYANINE 3 (Akoya, SKU NEL744001KT) diluted 1/500 in MABT. Once revealed, slices were washed with MABT and then immunofluorescence was performed as described above.

### ***Purification of total RNA and quantitative real-time PCR***

For specific isolation of reprogrammed astrocytes, a previously published method was followed (Molyneaux et al., 2015) but with some modifications for cultured cells. Astrocytes from the thalamus, cortex, dLG, VPM, and MGv were cultured and infected

with *Neurog2* retrovirus, and after 10 days in vitro, they were collected by applying trypsin/EDTA (Gibco) to the plate, resuspended with culture medium, and centrifuged. Reprogrammed astrocytes were fixed with PFA 1% for 10 min at 4°C, after which the PFA was quenched by adding 55  $\mu$ l of glycine, 1.25 M per 500  $\mu$ l of PFA solution. Immunocytochemistry against Tuj1 and RFP was performed, and cells were separated (Tuj1<sup>+</sup>/RFP<sup>+</sup> versus Tuj1<sup>-</sup>/RFP<sup>+</sup>) by a flow cytometer (BD FACSAria) based on their fluorescence. Once the cells were collected, they were centrifuged and incubated for 3 hours at 50°C with lysis buffer, their RNA was purified using TRIzol (Fisher), and cells were resuspended in RNase-free water.

cDNA was obtained from 1  $\mu$ g of total RNA using the specific protocol for first-strand cDNA synthesis in two-step reverse transcription (RT)-PCR using the High-Capacity cDNA Reverse Transcription Kit (Fisher) and stored at -20°C. qPCR was performed in a StepOnePlus real-time PCR system (Applied Biosystems, Foster City, CA, USA) using the MicroAmp fast 96-well reaction plate (Applied Biosystems) and the Power SYBR Green PCR Master Mix (Applied Biosystems). A master mix was prepared for each primer set containing the appropriate volume of SYBR Green, primers, and template cDNA. All reactions were performed in triplicate. The amplification efficiency for each primer pair and the cycle threshold (Ct) were determined automatically by the StepOne Software, v2.2.2 (Applied Biosystems). Transcript levels were represented relative to the *Gapdh* signal, adjusting for the variability in cDNA library preparation.

### ***Patch-clamp recordings of iNs***

For the electrophysiological analysis, astrocytes were infected with a retrovirus encoding CAG-*Neurog2*-ires-*TauGFP*. After 3 weeks, cultures were transferred to the recording chamber and were perfused with standard artificial cerebrospinal fluid (aCSF) containing the following: 119 mM NaCl, 5 mM KCl, 1.3 mM MgSO<sub>4</sub>, 2.4 mM CaCl<sub>2</sub>, 1 mM NaH<sub>2</sub>PO<sub>4</sub>, 26 mM Na<sub>2</sub>HCO<sub>3</sub>, and 11 mM glucose. The aCSF was perfused at a rate of 2.7 ml min<sup>-1</sup>, continuously bubbled with a gas mixture of 95% O<sub>2</sub> + 5% CO<sub>2</sub>, and warmed at 30° to 32°C.

Somatic whole-cell recordings were made under visual control using an upright microscope (Leica DM-LFSA) and a water immersion (20 or 40 $\times$ ) objective. The intracellular solution contained the following: 130 mM K-gluconate, 5 mM KCl, 5 mM

NaCl, 0.2 mM EGTA, 10 mM Hepes, 4 mM Mg-ATP, and 0.4 mM Na-GTP, pH 7.2 adjusted with KOH; 285 to 295 mOsm. Recordings were obtained in current-clamp and/or voltage-clamp mode with a patch-clamp amplifier (MultiClamp 700A, Molecular Devices, USA). No correction was made for the pipette junction potential. Voltage and current signals were filtered at 2 to 4 kHz and digitized at 20 kHz with a 16-bit resolution analog to digital converter (Digidata 1550B, Axon Instruments). The generation and acquisition of pulses were controlled by pClamp 10.6 software (Axon Instruments). Patch pipettes were made from borosilicate glass [1.5 mm OD (outer diameter), 0.86 mm ID (inner diameter), with inner filament] and had a resistance of 4 to 7 megohms when filled. Neurons in which series resistance was >30 megohms were discarded. Quantification of intrinsic membrane properties and spontaneous neuronal activity was performed on Clampfit 10.7 (Axon Instruments). The presence of putative spontaneous excitatory postsynaptic currents (sEPSCs) was assessed in voltage clamp recordings at  $-70$  mV.

### ***In silico Neurog2 binding sites determination***

In silico analysis was performed to find out Neurog2 binding sites across the whole genome using FIMO Motif Scanning from MEME Suite (v5.0.2) (Bailey et al., 2009). Neurog2 transcription factor motif (NGN2\_MOUSE.H11MO.0.C) from HOCOMOCO database (v11) and mouse genome (GRCm38.p6 GenCode M18) were used to carry out this analysis. Neurog2 binding sites were annotated to genes using ChIPseeker (v1.18) (Yu 2015) and Bioconductor (v3.8) in the R statistical computing and graphics platform (v3.5.1 Feather Spray). We retrieved genomic regions and selected binding sites [promoters, 5'UTR (5' untranslated region), first intron and first exon] whose location was  $\pm 3$  kb of GENCODE annotated TSSs (transcription start sites) of protein-coding genes. These criteria retrieved 180,611 putative Neurog2 binding sites belonging to 20,478 protein coding genes. Chromatin immunoprecipitation sequencing (ChIP-seq) coverage tracks for selected genes were generated using IGV (v2.4.14) and plotted in a 5' to 3' direction based on publicly available datasets from forebrain samples of H3K4me3 (ENCSR258YWW experiment) and H3K27me3 (ENCSR070MOK experiment) histone marks at P0 extracted from the ENCODE Project.

### ***ChIP for H3K4me3 and H3K27me3***

ChIP assays were performed following a previously published protocol (Gillot and Guillemot, 2016). Cultured astrocytes from the thalamus and cortex were collected after 1 week in vitro when confluence is reached, centrifuged, and resuspended to approximately 500,000 cells. Cells were fixed with 1% PFA in PBS for 10 min at room temperature and quenched with 55  $\mu$ l of glycine, 1.25 M per 500  $\mu$ l of PFA solution with orbital shaking. After that, cells were lysed in 300  $\mu$ l of SDS lysis buffer (0.5% SDS, 10 mM EDTA, and 50 mM Tris-HCl) supplemented with protease inhibitor cocktail (Roche, 11836153001), sonicated for 10 min in a Diagenode Bioruptor Pico, precleared with 30  $\mu$ l of washed Dynabeads (Invitrogen, 10003D), and diluted five times in ChIP IP buffer [20 mM HEPES, 0.2 M NaCl, 2 mM EDTA, 0.1% Na-DOC, 1% Triton X-100, and BSA (5 mg/ml)]. One percent of each sample was kept as input. Samples were divided into three tubes and incubated overnight at 4°C in a rotating wheel with 2.5  $\mu$ g per tube of the anti-H3K4me3 (Sigma-Aldrich, 07-473), anti-H3K27me3 (Abcam, ab6002), or control IgG antibody. The next day, washed and saturated Dynabeads were added and incubated with the samples for 2 hours at 4°C. Dynabeads were washed five times with LiCl buffer (50 mM HEPES, 1 mM EDTA, 1% NP-40, 1% Na-DOC, and 0.5 M LiCl) and once with TE buffer (10 mM Tris-HCl and 1 mM EDTA). Antibody/chromatin complexes together with the inputs were eluted by adding 100  $\mu$ l of elution buffer (50 mM NaHCO<sub>3</sub> and 1% SDS), 10  $\mu$ l of NaCl (5 M), and 1  $\mu$ l of proteinase K (Sigma-Aldrich, 3115836001) to each tube and put on a thermomixer, shaking at 1000 rpm at least 2 hours at 60°C. Samples and inputs were decross-linked by heating for 15 min at 95°C. Both samples and inputs were treated with RNase A (Roche, 10109142001) for 30 min at 65°C, and the DNA was purified with phenol/chloroform and ethanol precipitated.

### ***Primer design***

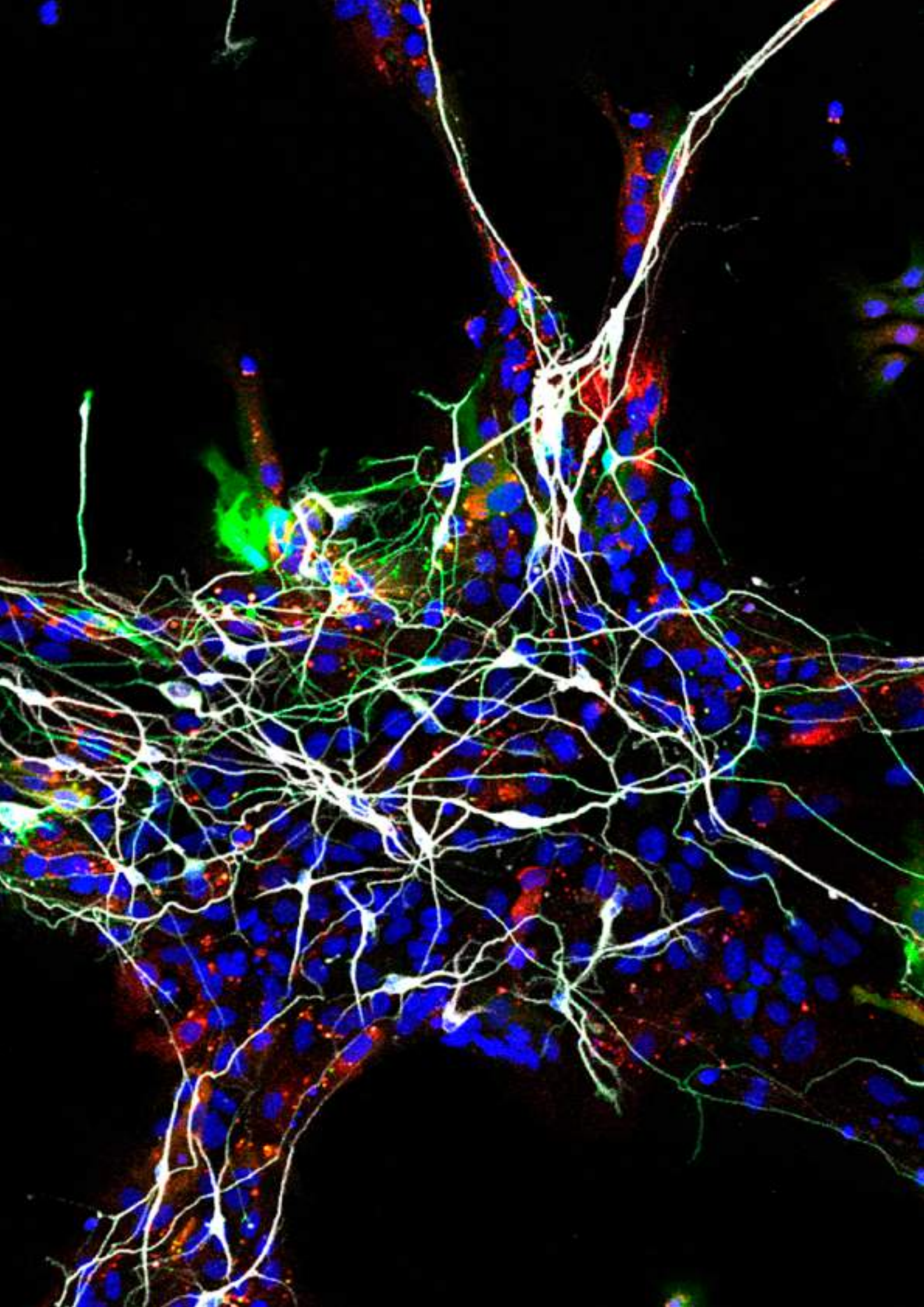
For RNA expression analysis, Primer3 and Blast tools from NCBI webpage were used, using the accession numbers of the coding sequences of the genes of interest. For ChIP experiments, we used the information obtained from the in silico *Neurog2* binding sites analysis and the open-source information of the ENCODE project. For primers design,

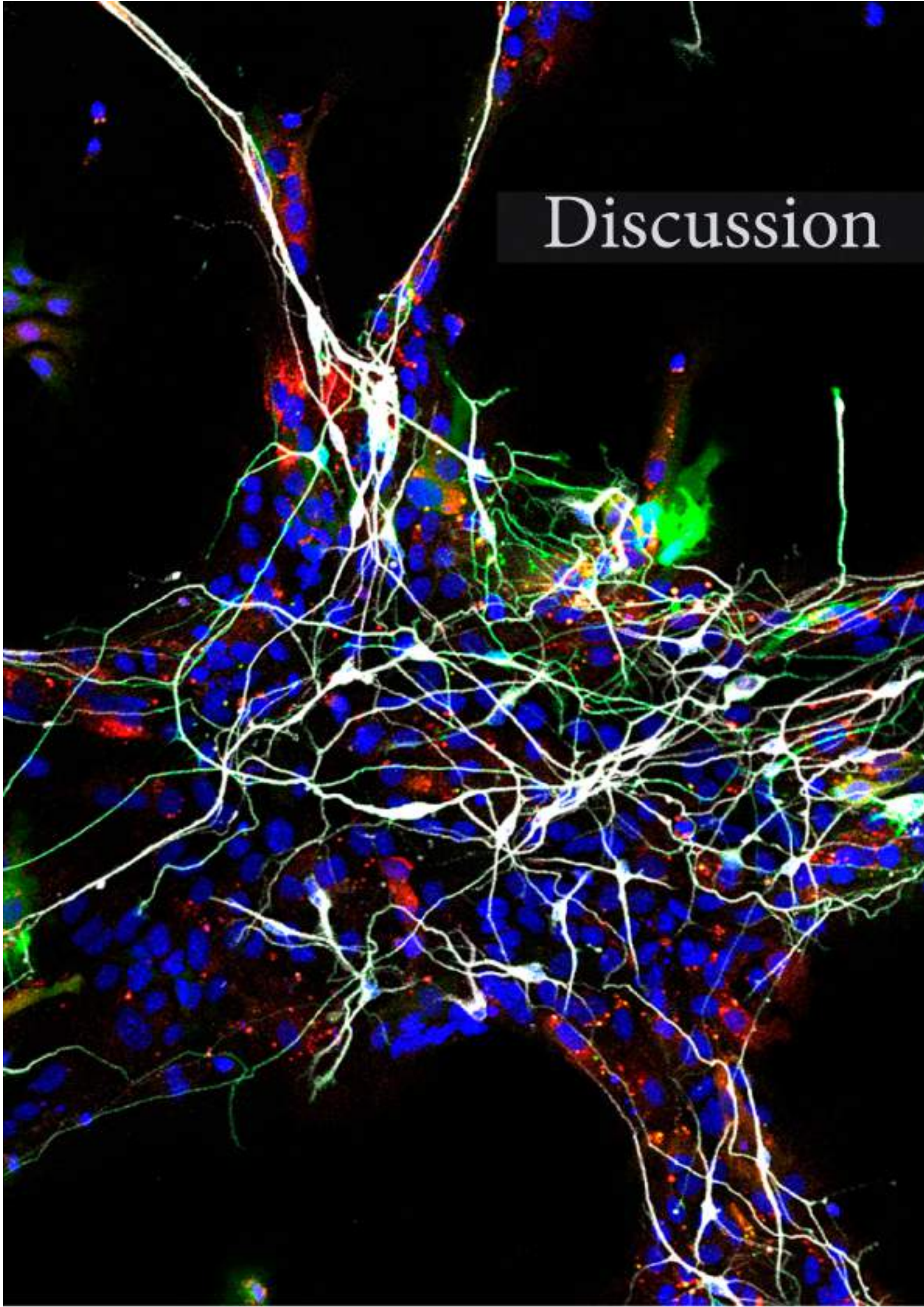
regions on the promoters of candidate genes that included a putative binding site for *Neurog2* and that were enriched in H3K4me3 and H3K27me3 signal were selected.

### ***Quantification and statistical analysis***

Statistical analysis was carried out in GraphPad Prism (v.6), Origin (v.8.0), and R (v3.5.1 Feather Spray) statistical computing and graphics platform. Data are presented as means  $\pm$  SEM or with box-and-whisker plots, which give the median, 25th and 75th percentiles, and range. Statistical comparison between groups was performed using paired or unpaired two-tailed Student's *t* test or Mann-Whitney *U* test nonparametric two-tailed test when data failed a Kolmogorov-Smirnov or a Shapiro-Wilk normality test. For multiple comparison analysis, a one-way analysis of variance (ANOVA) test with Holm-Sidak's multiple comparisons test was used, and Kruskal-Wallis test with Dunn's multiple comparisons test was used when data failed a Kolmogorov-Smirnov or a Shapiro-Wilk normality test. Simple effect analysis was performed when interaction was significant. *P* values  $< 0.05$  were considered statistically significant and set as follows: \**P*  $< 0.05$ , \*\**P*  $< 0.005$ , and \*\*\**P*  $< 0.0005$ . In the bioinformatical analysis, DEGs were identified using a statistical significance threshold (BH-adjusted *P* value  $< 0.1$ ) and set as follows: \*adj. *P*  $< 0.1$ , \*\*adj. *P*  $< 0.01$ , and \*\*\*adj. *P*  $< 0.001$ . No statistical methods were used to predetermine the sample size, but our sample sizes are considered adequate for the experiments and consistent with the literature. The mice were not randomized. The investigators were blinded to sample identity.





A fluorescence microscopy image showing a complex network of neurons. The neurons are stained with multiple colors: white, green, and blue. The white staining highlights the cell bodies and their extensive dendritic and axonal branching. The green staining appears to be localized in certain regions, possibly representing a specific marker or protein. The blue staining is distributed throughout the field, likely representing nuclei stained with DAPI. The overall structure is dense and interconnected, with many fine processes extending from the larger cell bodies.

# Discussion



## Discussion

Designing strategies for brain repair is one of the ultimate challenges in neuroscience. The reduced or even absent capacity of the brain for replacing damaged neurons implies that new neurons must be induced or grafted in the damaged areas of the brain to try to recover the function of the affected neuronal circuits. However, given the vast diversity and heterogeneity of brain neurons that makes them specific of brain circuits, supposes an important challenge for the design of adequate strategies. *In vivo* conversion of non-neuronal resident cells like astrocytes into neurons has emerged as a promising approach in the last few years. However, it remains unclear whether those new neurons will acquire a specific and adequate neuronal identity that facilitates their integration in the corresponding brain circuit, and if so, which molecular mechanisms drive this specification. In this Thesis work, it has been demonstrated that using the same transcription factor, Neurog2, it is possible to convert thalamic and cortical astrocytes in neurons *in vitro* and *in vivo*, which acquire a specific identity resembling the ones of the region of origin of the astrocytes. Using genome-wide analysis, we found that astrocytes of a particular region share the expression of a set of genes with their surrounding neurons, that provide both with regional identity. This shared transcriptional identity is conserved even at the level of substructures like thalamic sensory nuclei, where clonal analysis revealed that astrocytes and neurons of a particular nucleus emerge from a particular group of progenitors, that could provide them with the positional and transcriptional identity required for populating a sensory-modality specific nucleus.

Finally, apart from the regional transcriptional information already encoded in astrocytes, we also found differences in the epigenetic state of several genes, including some of them which only become differentially expressed in converted astrocytes, even up to the level of thalamic nuclei. Overall, the work presented here provides a logic for understanding the emergence of the regionalization of astrocytes, and how this can be extremely useful for the design of future therapies aiming at restoring damaged neuronal circuits.

### **Emergence and function of regional identity shared by astrocytes and neurons**

The early segmentation and regionalization of the neural plate and tube during embryonic development are essential for the formation of the final structures that form the brain, which are responsible of its correct function. These regions emerge as a consequence of the effect of morphogenes, which are expressed and diffused from primary and secondary organizers, and their graded and combined influence across the different axis induce particular identities of the territories placed at different positions in the neural tube (Metzis et al., 2018; Molofsky et al., 2014). This identity has been traditionally assigned to neuroepithelial cells and their descendant neural progenitors and finally to the neurons, which continue to refine their identity as brain development continues thanks also to the influence of different extrinsic factors. However, despite their common origin with neurons, astrocytes were traditionally considered as a homogeneous population independently of their brain region. In the recent years this view has changed especially thanks to the technical advances in microscopy and genome-wide analysis. Currently we know that astrocytes in spinal cord (Hochstim et al., 2008) and in some regions of the brain (Cahoy et al., 2008) can be differentiated based on their transcriptional profile. Nevertheless, it remained unclear whether they share some of the regional properties that characterize neurons from the same brain regions. In this work we show that astrocytes from the neocortex and the thalamus acquire different transcriptomic profiles, and that they share a significant percentage of differentially expressed genes with their surrounding neurons, that make both populations region-specific. Moreover, these shared signatures were observed also between neurons and astrocytes of the same sensory-modality thalamic nucleus, and when comparing different cortical areas along the rostro-caudal axis. These results make sense considering that in general, astrocytes are generated from the same progenitors than the neurons, and that clonal analysis in the cortex showed that sibling astrocytes also respect the columnar dispersion initially observed in clonally related neurons (Figueres-Oñate et al., 2016; García-Marqués and López-Mascaraque, 2013; Magavi et al., 2012). Thus, those results suggest that regionalizing cues might also influence the regional properties of astrocytes, as it has been shown for neurons and neural progenitors, that might provide them with positional information. Several studies have confirmed such hypothesis in the spinal cord

(Hochstim et al., 2008; Tsai et al., 2012), and future experiments should be done in order to decipher whether this is also the case in the brain, and which is the molecular logic governing such common specification. Recent studies with single-cell RNA-seq and spatial transcriptomics in the neocortex showed that astrocytes are clusterized in layers, that do not correspond with the ones observed in neurons (Batiuk et al., 2020; Bayraktar et al., 2020). However, regional identity in the neocortex is computed along the anteroposterior and mediolateral axes (Tasic et al., 2018), coincident with the results presented in this thesis from the reanalysis of (Zeisel et al., 2018) data. Indeed, in one of the abovementioned papers about astrocytic layering, authors even acknowledge that the clustering between astrocytes varies depending on the cortical region analyzed (Bayraktar et al., 2020). In addition, apart from the inherited intrinsic regional signatures, neurons might also influence the final identity of astrocytes by secreting signaling cues such as Shh (Farmer et al., 2016), which could also contribute to explain the observed functional coupling between neurons and astrocytes of specific cortical layers (Lanjakornsiripan et al., 2018) or other brain circuits (Chai et al., 2017; Huang et al., 2020; John Lin et al., 2017).

Overall, recent studies underpinning astrocytes heterogeneity, demonstrated its importance for regulating distinct neuronal circuits in the brain. Nevertheless, the shared expression of important sets of genes described in this thesis, open new avenues for understanding the importance of neuron-glia interactions and coupling. For the scope of this thesis, we focused on the presence of transcription factors among those shared genes (*Gbx2*, *Lef1*, *Fezf2* or *Tbr1*), which might play a role for providing astrocytes with a similar regional identity to the one observed in their neuronal counterparts (Bluske et al., 2012; Lodato et al., 2014; Mallika et al., 2015; Mihalas and Hevner, 2017). However, for understanding the biological function of this overlapping signatures, future experiments should focus on genes with more specific and known functions such as cell-cell communication. Among those genes we can find several examples both in thalamus and cortex, such as *Ntng1*, which have shown to be important for cell-cell communication and signaling (Fujita et al., 2020). Also, considering the role of astrocytes in the tripartite synapses, and that astrocytes can respond to similar neurotransmitters than the neurons, the co-expression of the receptors or channels for some of those signals, like genes of the solute carrier family (*Slc6a4*, *Slc6a13*, *Slc18a2*...), or voltage-dependent channels (*Kcnh1*,

*Kcnj4*, *Hcn1*...) could be also important for the correct regulation of the corresponding neuronal circuits.

More accurately, interesting genes were also found at the level of thalamic nuclei, which should be even more specific for a particular circuit, like the visual in the dLG astrocytes and neurons. Among the shared genes in this circuit, we found the expression of the gene encoding for connexin 36 (*Gjd2*), which is essential for the correct coupling of amacrine and ganglion cells (Roy et al., 2017) and rods and cones (Asteriti et al., 2017; Cowan et al., 2016) in the retina, and might exert also an important and similar function in the astrocyte-neuron coupling and interaction in the visual nucleus of the thalamus (dLG).

Overall, the data presented in this thesis open new avenues for better understanding astrocyte regionalization, and its importance for their coupling with surrounding neurons, and could contribute to better explain the mechanisms and the origin of their role for specific neuronal circuit regulation recently described (Chai et al., 2017; Huang et al., 2020; John Lin et al., 2017). Future experiments downregulating transcription factors or function-specific genes in astrocytic subpopulations might help to elucidate the role of those shared genes for the brain circuits physiology.

### **Clonal origin of neurons and astrocytes sharing region-specific genes**

The fact that astrocytes maintain the expression of some region-specific genes with their surrounding neurons even up to the level of sensory thalamic nuclei, rises the intriguing question of how this specificity is achieved in both cell types. In the majority of brain regions, astrocytes emerge from the same radial glial progenitors that initially generate all the neurons and intermediate progenitors (Kriegstein and Alvarez-Buylla, 2009). However, during the neurogenic period, neurons also migrate to their final location to form specialized sub-regions, such as the sensory cortical areas or the sensory thalamic nuclei. Thus, it remains unknown whether astrocytes follow the same organizing principles as their sibling neurons.

In this thesis, using clonal analysis with Startrack method (Figueres-Oñate et al., 2016; García-Marqués and López-Mascaraque, 2013), we have shown that in the thalamus astrocytes and neurons are generated from common apical progenitors, and that clonally

related cells populate the same thalamic sensory nucleus with very little dispersion. Our data goes in line with clonal analysis done in the cortex (Figueres-Oñate et al., 2016; Gao et al., 2014; García-Marqués and López-Mascaraque, 2013; Magavi et al., 2012; Zhang et al., 2020), and with two recent studies that took advantage of MADM technique for lineage tracing of single progenitors in the thalamus (Shi et al., 2017; Wong et al., 2018).

In the cortex, the fact that astrocytes maintain the columnar dispersion observed in their sibling neurons implies that they will remain in the same cortical area, which could explain the transcriptional overlapping described in this thesis between astrocytes and neurons of rostro-caudal regions of the cortex.

Regarding the thalamus, the two abovementioned studies showed that neuronal clones populate specifically only first order or high order nuclei and that astrocytes seem to keep close to their sibling neurons. However, in those studies authors do not quantify specifically the dispersion of a clone between different nuclei of the same order. In our study, we provide extensive data regarding the dispersion of clones among the first order nuclei dLG, VPM and MGv, and show that, albeit there is a minor dispersion especially when looking at neurons, there is always a clear tendency towards populating specifically one nucleus. Our data suggests that there might exist modules of pre-specified apical progenitors across the walls of the third ventricle, which generate cells of a particular sensory modality, and future experiments with single cell transcriptomics at different time points and time lapse of single progenitors labelled will help to elucidate how apical progenitors generate nucleus specific cells, and the transcriptional dynamics that they follow. Particularly, time lapse experiments could also help to understand how astrocytes, which are generated later in development, follow the same regionalizing guides than their sibling neurons. A possibility is that they emerge from intermediate progenitors that are generated after asymmetric divisions of the apical progenitors. If this is the case, intermediate progenitors might inherit the same epigenetic and transcriptional information than their sibling neurons, and migrate together towards their final position, while producing more neurons and finally astrocytes, that proliferate locally to increase their number (Ge et al., 2012). Although this is still a hypothesis, data from (Wong et al., 2018) shows that when performing lineage tracing of intermediate progenitors (Neurog1+) in the thalamus, their progeny is much more restricted to discrete territories, proposing that those progenitors are more specified than apical progenitors, and could

be the responsible of producing the majority of nucleus specific cells, and the cells that the apical progenitors keep producing at later stages could be the ones that disperse the most. If so, this model could also fit with the temporal variable, as in the thalamus there is also a gradient of nuclei formation, like the situation with cortical layers, as more lateral nuclei are formed before the medial ones.

Finally, our data, together with recent studies, shine light on the development and nucleogenesis of the thalamus and contribute to the understanding of the acquisition of regional shared properties between nucleus specific astrocytes and neurons.

### **Importance of glial region-specificity for the design of strategies for brain repair**

One of the main goals of this work has been to test the region-specific conversion of astrocytes into region or circuit specific neurons. Although we have shown that astrocytes express a significant number of genes that are shared with their surrounding neurons, it is important to consider that this does not represent the entire transcriptome of both cell types, and that many of the shared genes are expressed at lower levels in astrocytes than in neurons. Thus, for acquiring a full transcriptional identity of a specific neuronal subtype following reprogramming, several factors must contribute to modulate this switch of fate. We have shown that the basal expression of some transcription factors in the astrocytes is important for the Neurog2- mediated reprogramming. Particularly *Gbx2*, an essential transcription factor for defining thalamic neuronal identity (Mallika et al., 2015), is also expressed at lower levels in thalamic astrocytes, and when overexpressed in cortical astrocytes together with Neurog2, we found that the expression of some cortical neuronal genes is not increased as it happens in cortical astrocytes only transduced with Neurog2. However, genes that increase their expression in converted thalamic but not cortical astrocytes, show an upregulation in astrocytes from the cortex when transduced with *Neurog2* and *Gbx2*. These experiments demonstrate that the expression in astrocytes of important transcription factors like *Gbx2*, albeit at low levels, is functional and important for defining the fate of the converted astrocytes. Notwithstanding, the ectopic induction of *Gbx2* in cortical astrocytes was not enough to change the expression of other genes, whose expression seem to be fixed in astrocytes in a region-specific manner.

We found that the ability to respond to the effect of Neurog2 alone or together with Gbx2 was dependent on the epigenetic state of the promoter of the studied genes, based specially in the different presence of active (H3K4me3) or repressive (H3K27me3) histone marks (Voigt et al., 2013). These different epigenetic and transcriptomic configurations were observed even at the level of thalamic nucleus specific astrocytes, which also acquire an adequate and specific neuronal identity following reprogramming, as they express specific genes of neurons of a particular sensory modality (Gezelius et al., 2017). As discussed above, this similarity could be related to their common clonal origin, as several papers have demonstrated the capacity of neural progenitors to transmit epigenetic and transcriptomic information to their descendant cells, even after the switch from neurogenic to gliogenic fate (Hirabayashi et al., 2009; Kim and Rosenfeld, 2010; Telley et al., 2019).

Overall, our data shows that the transcriptional and epigenetic similarities between astrocytes and neurons of a particular region predispose astrocytes to acquire a very specific neuronal subtype identity following reprogramming. This is important as a unique reprogramming strategy could be used for converting astrocytes in different brain regions, as they will become specific based on their original regional properties. Indeed, recent studies also confirmed this hypothesis, as converted astrocytes of upper or lower cortical layers acquired properties similar to upper- or lower-layer neurons respectively (Mattugini et al., 2019). Also, two studies have recently demonstrated that it is possible to induce the reprogramming of astrocytes into neurons just by downregulating the expression of an important regulator of astrocytic identity, PTB (Qian et al., 2020; Zhou et al., 2020). Interestingly, when downregulating this gene in substantia nigra, striatum and retina, they showed that converted astrocytes into neurons are able to integrate in the corresponding circuit and even improving the function of the damaged circuit. This suggests that astrocytes seem to have a latent neurogenic program (Baser et al., 2019; Magnusson et al., 2014; 2020), that, as shown by the data presented in this thesis, corresponds with the regional identity of their surrounding neurons.

Finally, the remaining challenge will be to optimize methods for activating such specific neurogenic programs in astrocytes of a damaged brain area. Spontaneous neurogenesis from astrocytes does not occur in mammals even after becoming reactive in response to a damage (Buffo et al., 2008; Hoang et al., 2020). However, inducing their

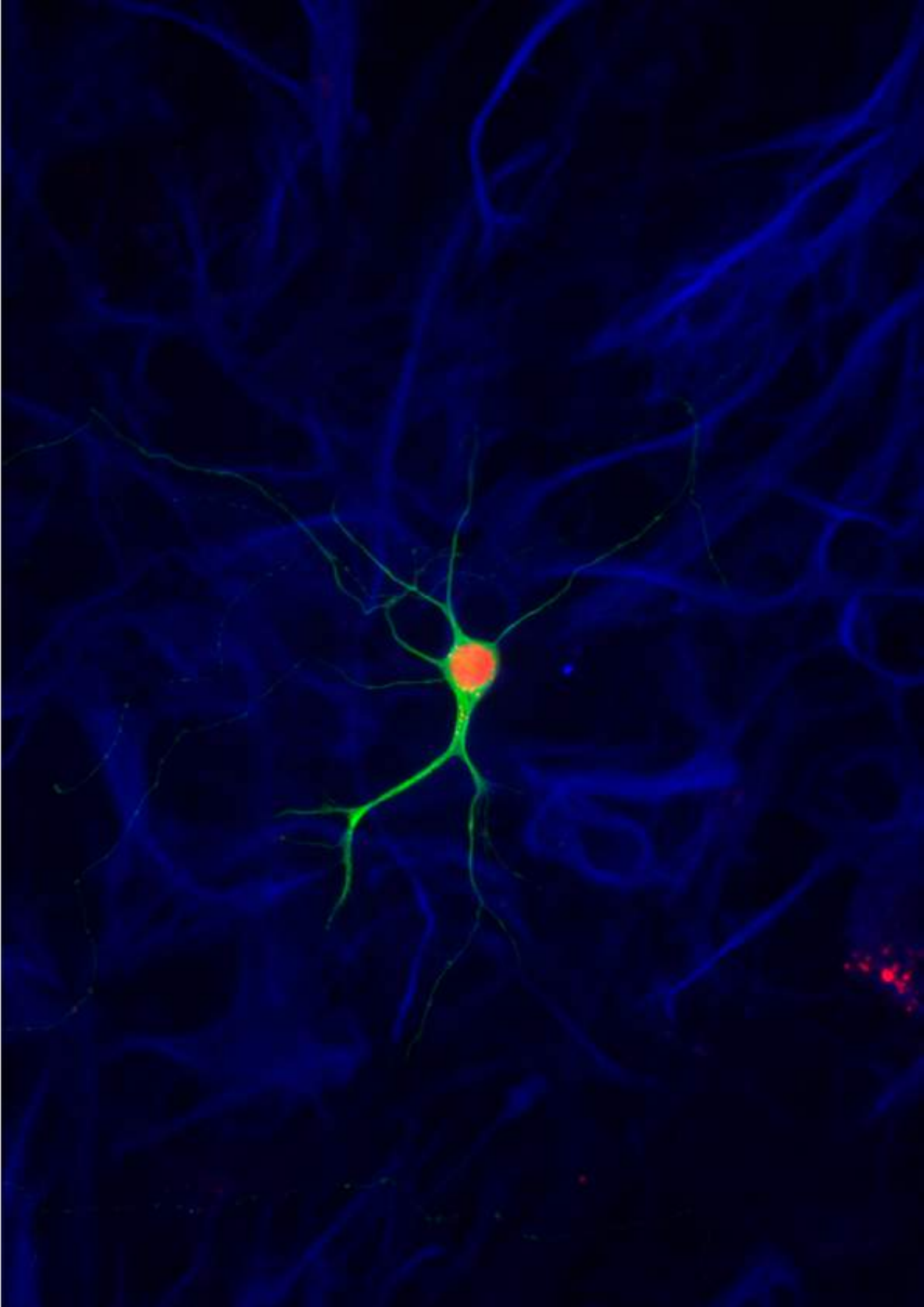
neurogenic programs by overexpressing neurogenic transcription factors, or repressing gliogenic genes like *Ptbp1* or *Notch* can facilitate their neurogenic switch, that, thanks to the regional identity that they seem to conserve even in a reactive state, would provide them with the ability to integrate in a specific circuit and replace damaged neurons.

### Concluding remarks

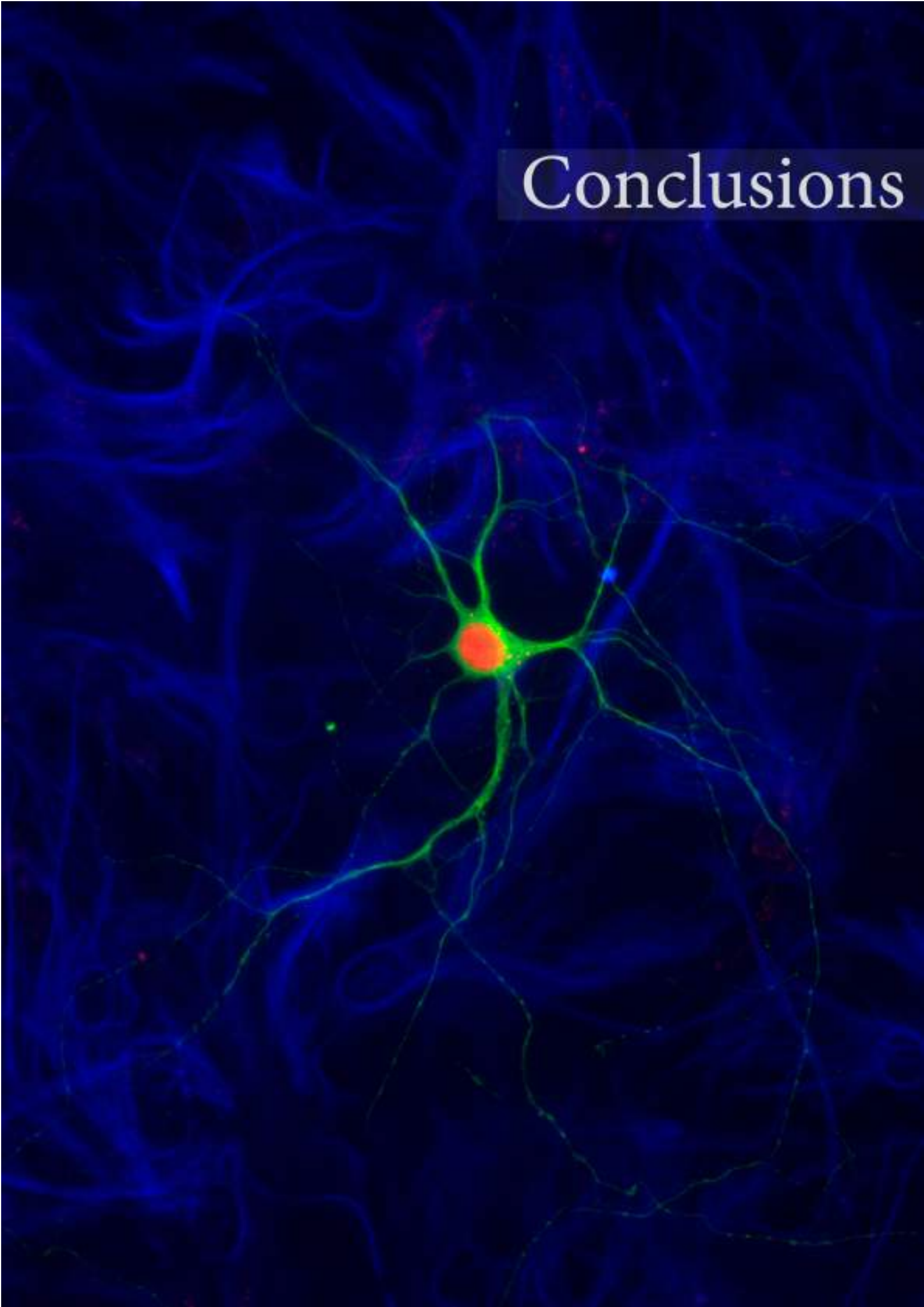
The extraordinary complexity of the brain supposes a huge challenge for designing strategies aimed at regenerating neurons after a brain damage or in neurodegenerative diseases. During the last years, increasing evidence has shown that it is possible to convert resident cells, like astrocytes, into neurons both *in vitro* and *in vivo*. However, these new neurons must be similar in terms of transcriptional profile and connectivity to the damaged ones. The data presented in this thesis shows that astrocytes are transcriptionally specific of brain regions such as the neocortex, the thalamus, and even up to the level of sensory thalamic nuclei, and that share the expression of some region-specific genes with their surrounding neurons. This transcriptional overlapping seems to emerge from their common clonal origin, as we show that in the thalamus, neurons and astrocytes generated from the same apical progenitor populate specifically one sensory thalamic nucleus with minor dispersion. Finally, our experiments reprogramming resident astrocytes from thalamus and cortex into neurons demonstrate that the newly generated neurons acquire specific properties of the surrounding resident neurons. Functional experiments altering the basal transcriptome of cortical astrocytes demonstrate that the basal transcriptome of astrocytes is important for providing regionalizing cues that will be transmitted to the neurons that emerge after reprogramming.

This molecular logic of regional specification common to astrocytes and neurons might suppose an important insight for improving the use of astrocyte reprogramming for regenerating damaged sensory circuits.





# Conclusions





## Conclusions

1. Thalamic and cortical astrocytes can be reprogrammed into neurons *in vitro* and *in vivo* by overexpressing *Neurog2* or *Neurog2* and *Bcl2* respectively.
2. Induced neurons acquire region-specific identity depending on the origin of the astrocytes.
3. The cellular environment does not affect to the final identity acquired by the converted astrocytes.
4. Astrocytes and neurons share the expression of a significant percentage of genes that defines the region-specificity of both cell types.
5. Shared transcriptional signatures are observed at the single-cell level (single-cell RNAseq) and conserved in later stages of development.
6. Distinct epigenetic profiles also regulate the regional specificity of astrocytes, even in genes which do not present differences in the expression levels.
7. Shared transcriptomic profiles between astrocytes and neurons from thalamus or cortex, together with the distinct epigenetic configurations of specific genes, regulate the regional specification of the reprogrammed astrocytes.
8. Astrocytes and neurons from discrete territories, such as a thalamic sensory nucleus, are generated from the same group of progenitors, that are responsible of transmitting positional information to both cell types.

## *Conclusions*

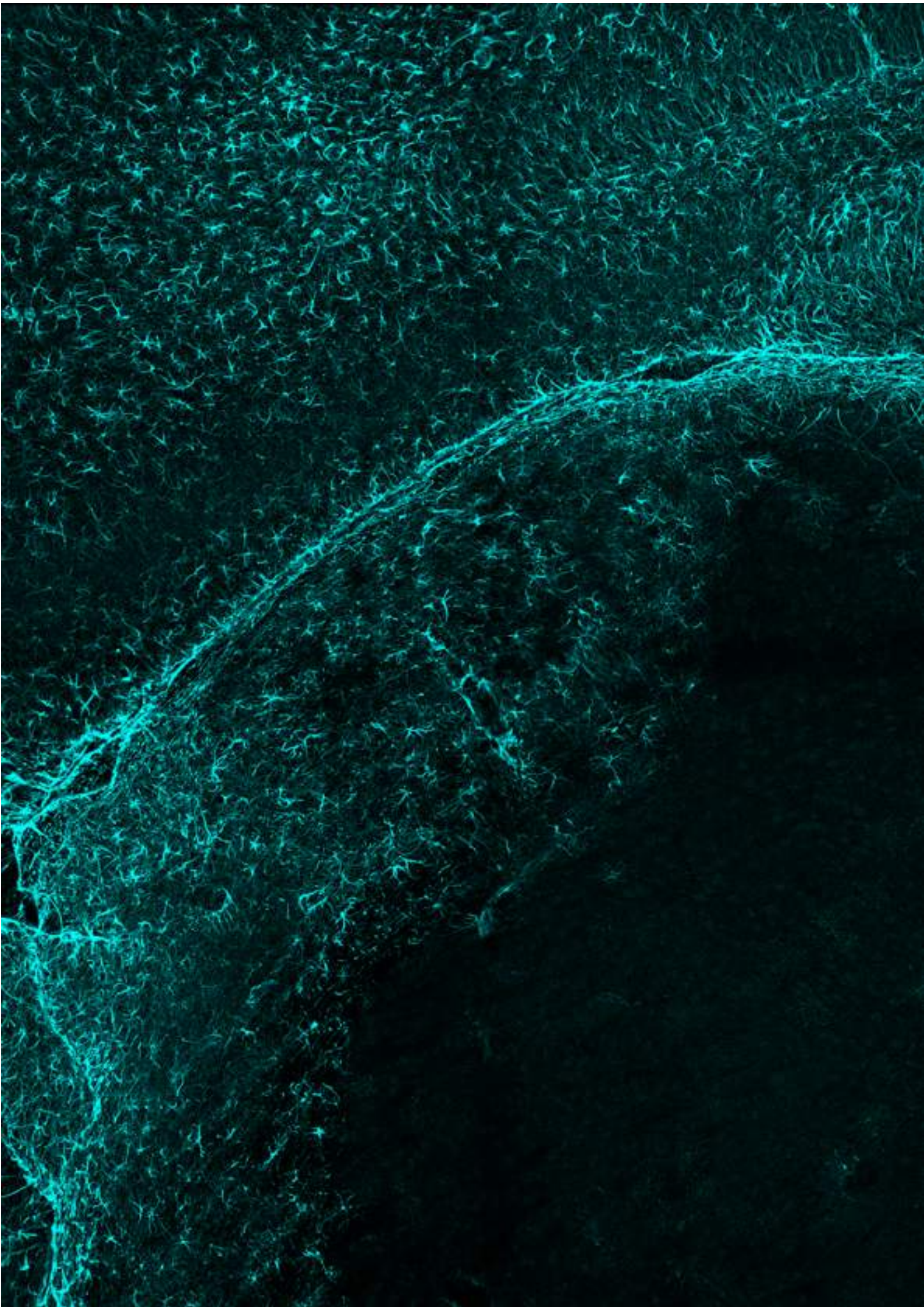
- 9.** Sibling astrocytes and neurons from a particular sensory thalamic nucleus, such as dLG (visual), VPM (somatosensory) or MGv (auditory), also share the expression of a core set of genes.
  
- 10.** Distinct epigenetic configurations of nucleus-specific genes also distinguish astrocytes from the three analyzed thalamic sensory nuclei.
  
- 11.** Astrocytes from the three sensory-modality thalamic nuclei studied (dLG, VPM and MGv) can be reprogrammed into neurons that express region-specific neuronal genes.

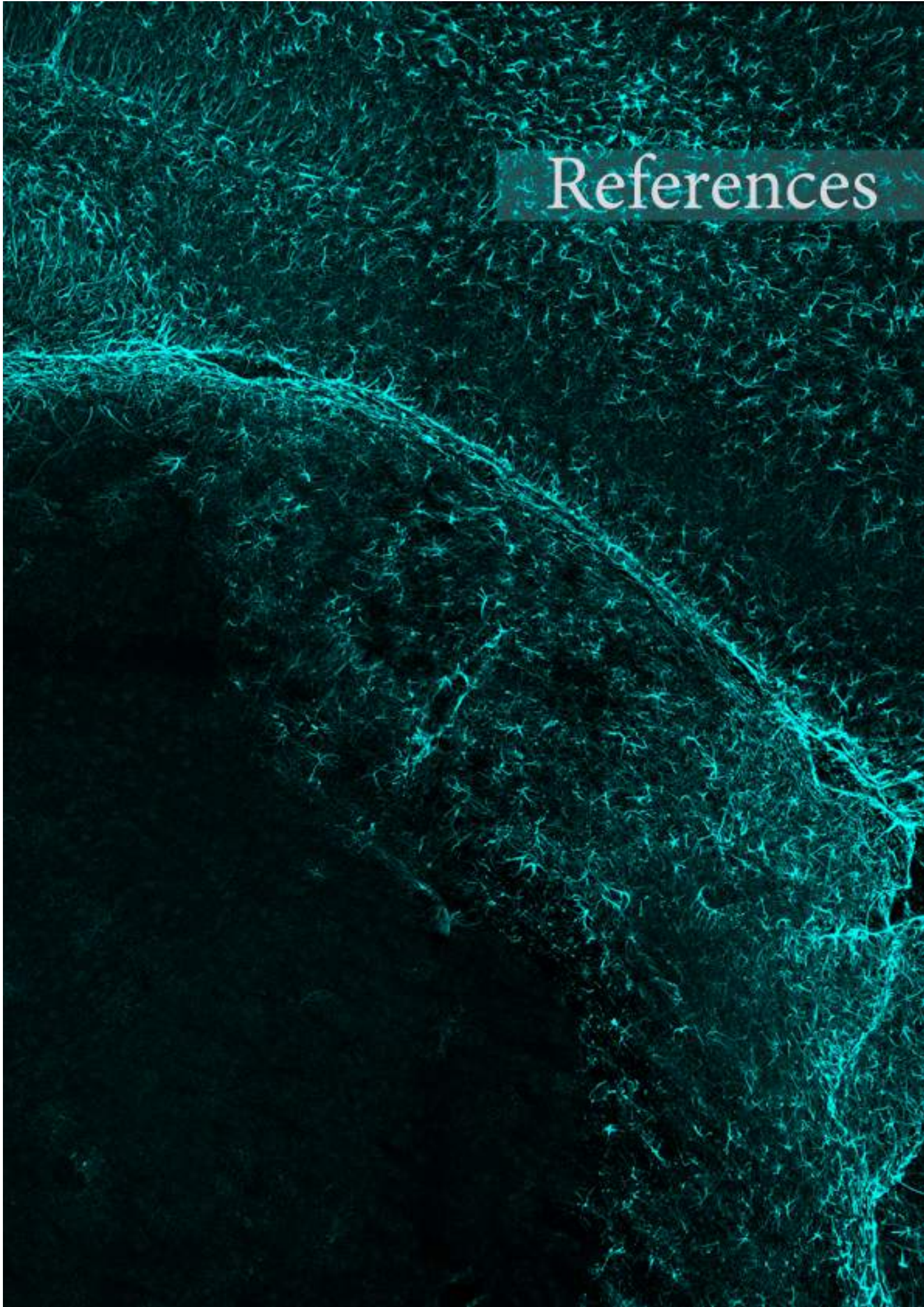
## Conclusiones

1. Los astrocitos del tálamo y la corteza se pueden reprogramar en neuronas in vitro e in vivo a través de la sobreexpresión de *Neurog2* o *Neurog2* y *Bcl2* respectivamente.
2. Las nuevas neuronas que se generan adquieren la identidad neuronal específica de la región cerebral en la que residen los astrocitos de origen.
3. El ambiente celular no afecta a la identidad final de las neuronas reprogramadas.
4. Los astrocitos y las neuronas de una misma región cerebral comparten la expresión de un porcentaje de genes significativo que proporciona a ambos tipos celulares la especificidad de dicha región.
5. Estas marcas transcripcionales compartidas también se observan a nivel de transcriptoma de célula única (*single-cell RNAseq*) y se mantienen en estadios más tardíos del desarrollo.
6. Diferentes perfiles epigenéticos también regulan la especificidad regional de los astrocitos, incluso en genes en los que no se observan diferencias en los niveles de expresión.
7. Los perfiles transcriptómicos compartidos por astrocitos y neuronas de tálamo o corteza, junto a las distintas configuraciones epigenéticas, regulan la especificación regional de los astrocitos reprogramados en neuronas.
8. Los astrocitos y las neuronas de territorios muy definidos, como los núcleos sensoriales talámicos, están generados a partir del mismo grupo de progenitores, que parecen ser responsables de transmitir información posicional a ambos tipos celulares.

- 9.** Los astrocitos y las neuronas generados a partir de un mismo progenitor, y que se sitúan específicamente en un núcleo sensorial talámico, como el dLG (visual), VPM (somatosensorial) o en el MGv (auditivo), también comparten la expresión de un grupo de genes específicos de dicha región.
  
- 10.** Las distintas configuraciones epigenéticas de genes específicos de un núcleo talámico también sirven para distinguir a los astrocitos de cada uno de los núcleos talámicos estudiados.
  
- 11.** Los astrocitos de cada uno de los tres núcleos talámicos específicos de una modalidad sensorial estudiados (dLG, VPM y MGv) pueden ser reprogramados en neuronas que expresan genes neuronales específicos de dichos núcleos, de forma similar a las neuronas endógenas.







# References



## References

Adams, K.L., and Gallo, V. (2018). The diversity and disparity of the glial scar. *Nat. Neurosci.* 21, 9–15.

Ager, R.R., Davis, J.L., Agazaryan, A., Benavente, F., Poon, W.W., LaFerla, F.M., and Blurton-Jones, M. (2015). Human neural stem cells improve cognition and promote synaptic growth in two complementary transgenic models of Alzheimer's disease and neuronal loss. *Hippocampus* 25, 813–826.

Altman, J., and Bayer, S.A. (1988a). Development of the rat thalamus: I. Mosaic organization of the thalamic neuroepithelium. *J. Comp. Neurol.* 275, 346–377.

Altman, J., and Bayer, S.A. (1988b). Development of the rat thalamus: II. Time and site of origin and settling pattern of neurons derived from the anterior lobule of the thalamic neuroepithelium. *J. Comp. Neurol.* 275, 378–405.

Altman, J., and Bayer, S.A. (1988c). Development of the rat thalamus: III. Time and site of origin and settling pattern of neurons of the reticular nucleus. *J. Comp. Neurol.* 275, 406–428.

Altman, J., and Bayer, S.A. (1989a). Development of the rat thalamus: IV. The intermediate lobule of the thalamic neuroepithelium, and the time and site of origin and settling pattern of neurons of the ventral nuclear complex. *J. Comp. Neurol.* 284, 534–566.

Altman, J., and Bayer, S.A. (1989b). Development of the rat thalamus: V. The posterior lobule of the thalamic neuroepithelium and the time and site of origin and settling pattern of neurons of the medial geniculate body. *J. Comp. Neurol.* 284, 567–580.

Altman, J., and Bayer, S.A. (1989c). Development of the rat thalamus: VI. The posterior lobule of the thalamic neuroepithelium and the time and site of origin and settling pattern of neurons of the lateral geniculate and lateral posterior nuclei. *J. Comp. Neurol.* 284, 581–601.

Anderson, A.J., Piltti, K.M., Hooshmand, M.J., Nishi, R.A., and Cummings, B.J. (2017). Preclinical Efficacy Failure of Human CNS-Derived Stem Cells for Use in the Pathway Study of Cervical Spinal Cord Injury. *Stem Cell Reports* 8, 249–263.

Anderson, M.A., Burda, J.E., Ren, Y., Ao, Y., O'Shea, T.M., Kawaguchi, R., Coppola, G., Khakh, B.S., Deming, T.J., and Sofroniew, M.V. (2016). Astrocyte scar formation aids central nervous system axon regeneration. *Nature* 532, 195–200.

## References

Angevine, J.B. (1970). Time of neuron origin in the diencephalon of the mouse. An autoradiographic study. *J. Comp. Neurol.* *139*, 129–187.

Angevine, J.B., and Sidman, R.L. (1961). Autoradiographic study of cell migration during histogenesis of cerebral cortex in the mouse. *Nature* *192*, 766–768.

Antón-Bolaños, N., Sempere-Ferrández, A., Guillamón-Vivancos, T., Martini, F.J., Pérez-Saiz, L., Gezelius, H., Filipchuk, A., Valdeolmillos, M., and López-Bendito, G. (2019). Prenatal activity from thalamic neurons governs the emergence of functional cortical maps in mice. *Science* *364*, 987–990.

Araque, A., Carmignoto, G., Haydon, P.G., Oliet, S.H.R., Robitaille, R., and Volterra, A. (2014). Gliotransmitters travel in time and space. *Neuron* *81*, 728–739.

Aroca, P., and Puelles, L. (2005). Postulated boundaries and differential fate in the developing rostral hindbrain. *Brain Res Brain Res Rev* *49*, 179–190.

Arvidsson, A., Collin, T., Kirik, D., Kokaia, Z., and Lindvall, O. (2002). Neuronal replacement from endogenous precursors in the adult brain after stroke. *Nat Med* *8*, 963–970.

Asteriti, S., Gargini, C., and Cangiano, L. (2017). Connexin 36 expression is required for electrical coupling between mouse rods and cones. *Vis Neurosci* *34*, E006.

Azevedo, F.A.C., Carvalho, L.R.B., Grinberg, L.T., Farfel, J.M., Ferretti, R.E.L., Leite, R.E.P., Jacob Filho, W., Lent, R., and Herculano-Houzel, S. (2009). Equal numbers of neuronal and nonneuronal cells make the human brain an isometrically scaled-up primate brain. *Journal of Comparative Neurology* *513*, 532–541.

Bailey, T.L., Boden, M., Buske, F.A., Frith, M., Grant, C.E., Clementi, L., Ren, J., Li, W.W., and Noble, W.S. (2009). MEME SUITE: tools for motif discovery and searching. *Nucleic Acids Res.* *37*, W202–W208.

Bardehle, S., Krüger, M., Buggenthin, F., Schwausch, J., Ninkovic, J., Clevers, H., Snippert, H.J., Theis, F.J., Meyer-Luehmann, M., Bechmann, I., et al. (2013). Live imaging of astrocyte responses to acute injury reveals selective juxtavascular proliferation. *Nat. Neurosci.* *16*, 580–586.

Barker, R.A., Barrett, J., Mason, S.L., and Björklund, A. (2013). Fetal dopaminergic transplantation trials and the future of neural grafting in Parkinson's disease. *Lancet Neurol* *12*, 84–91.

Barres, B.A. (2008). The mystery and magic of glia: a perspective on their roles in health and disease. *Neuron* *60*, 430–440.

- Baser, A., Skabkin, M., Kleber, S., Dang, Y., Gülcüler Balta, G.S., Kalamakis, G., Göpferich, M., Ibañez, D.C., Schefzik, R., Lopez, A.S., et al. (2019). Onset of differentiation is post-transcriptionally controlled in adult neural stem cells. *Nature* 566, 100–104.
- Batiuk, M.Y., Martirosyan, A., Wahis, J., de Vin, F., Marneffe, C., Kusserow, C., Koeppen, J., Viana, J.F., Oliveira, J.F., Voet, T., et al. (2020). Identification of region-specific astrocyte subtypes at single cell resolution. *Nat Commun* 11, 1220–15.
- Bayraktar, O.A., Bartels, T., Holmqvist, S., Kleshchevnikov, V., Martirosyan, A., Polioudakis, D., Ben Haim, L., Young, A.M.H., Batiuk, M.Y., Prakash, K., et al. (2020). Astrocyte layers in the mammalian cerebral cortex revealed by a single-cell in situ transcriptomic map. *Nat. Neurosci.* 8, 427.
- Bayraktar, O.A., Fuentealba, L.C., Alvarez-Buylla, A., and Rowitch, D.H. (2014). Astrocyte development and heterogeneity. *Cold Spring Harb Perspect Biol* 7, a020362.
- Bazargani, N., and Attwell, D. (2016). Astrocyte calcium signaling: the third wave. *Nat. Neurosci.* 19, 182–189.
- Belenguer, G., Duarte-Abadia, P., Jordán-Pla, A., Domingo-Muelas, A., Blasco-Chamarro, L., Ferrón, S.R., Morante-Redolat, J.M., and Fariñas, I. (2021). Adult Neural Stem Cells Are Alerted by Systemic Inflammation through TNF- $\alpha$  Receptor Signaling. *Cell Stem Cell* 28, 285–299.e289.
- Bergmann, O., Spalding, K.L., and Frisé, J. (2015). Adult Neurogenesis in Humans. *Cold Spring Harb Perspect Biol* 7, a018994.
- Bernhardi, J.E.-V., and Dimou, L. (2016). NG2-glia, More Than Progenitor Cells. In *Glial Cells in Health and Disease of the CNS*, (Springer, Cham), pp. 27–45.
- Berninger, B., Costa, M.R., Koch, U., Schroeder, T., Sutor, B., Grothe, B., and Götz, M. (2007). Functional properties of neurons derived from in vitro reprogrammed postnatal astroglia. *J. Neurosci.* 27, 8654–8664.
- Bezzi, P., and Volterra, A. (2001). A neuron-glia signalling network in the active brain. *Curr. Opin. Neurobiol.* 11, 387–394.
- Bi, B., Salmaso, N., Komitova, M., Simonini, M.V., Silbereis, J., Cheng, E., Kim, J., Luft, S., Ment, L.R., Horvath, T.L., et al. (2011). Cortical glial fibrillary acidic protein-positive cells generate neurons after perinatal hypoxic injury. *J. Neurosci.* 31, 9205–9221.
- Bluske, K.K., Vue, T.Y., Kawakami, Y., Taketo, M.M., Yoshikawa, K., Johnson, J.E., and Nakagawa, Y. (2012).  $\beta$ -Catenin signaling specifies progenitor cell identity in parallel with Shh signaling in the developing mammalian thalamus. *Development* 139, 2692–2702.

## References

- Borrell, V., and Reillo, I. (2012). Emerging roles of neural stem cells in cerebral cortex development and evolution. *Dev Neurobiol* 72, 955–971.
- Brulet, R., Matsuda, T., Zhang, L., Miranda, C., Giacca, M., Kaspar, B.K., Nakashima, K., and Hsieh, J. (2017). NEUROD1 Instructs Neuronal Conversion in Non-Reactive Astrocytes. *Stem Cell Reports* 8, 1506–1515.
- Buffo, A., Rite, I., Tripathi, P., Lepier, A., Colak, D., Horn, A.-P., Mori, T., and Götz, M. (2008). Origin and progeny of reactive gliosis: A source of multipotent cells in the injured brain. *Proc Natl Acad Sci U S A* 105, 3581–3586.
- Buffo, A., Vosko, M.R., Ertürk, D., Hamann, G.F., Jucker, M., Rowitch, D., and Götz, M. (2005). Expression pattern of the transcription factor Olig2 in response to brain injuries: implications for neuronal repair. *Proc Natl Acad Sci U S A* 102, 18183–18188.
- Bulfone, A., Puelles, L., Porteus, M.H., Frohman, M.A., Martin, G.R., and Rubenstein, J.L. (1993). Spatially restricted expression of *Dlx-1*, *Dlx-2* (*Tes-1*), *Gbx-2*, and *Wnt-3* in the embryonic day 12.5 mouse forebrain defines potential transverse and longitudinal segmental boundaries. *J. Neurosci.* 13, 3155–3172.
- Butler, A., Hoffman, P., Smibert, P., Papalexi, E., and Satija, R. (2018). Integrating single-cell transcriptomic data across different conditions, technologies, and species. *Nat. Biotechnol.* 36, 411–420.
- Cahoy, J.D., Emery, B., Kaushal, A., Foo, L.C., Zamanian, J.L., Christopherson, K.S., Xing, Y., Lubischer, J.L., Krieg, P.A., Krupenko, S.A., et al. (2008). A transcriptome database for astrocytes, neurons, and oligodendrocytes: a new resource for understanding brain development and function. *J. Neurosci.* 28, 264–278.
- Chai, H., Díaz-Castro, B., Shigetomi, E., Monte, E., Oceau, J.C., Yu, X., Cohn, W., Rajendran, P.S., Vondriska, T.M., Whitelegge, J.P., et al. (2017). Neural Circuit-Specialized Astrocytes: Transcriptomic, Proteomic, Morphological, and Functional Evidence. *Neuron* 95, 531–549.e539.
- Chen, J., Magavi, S.S.P., and Macklis, J.D. (2004). Neurogenesis of corticospinal motor neurons extending spinal projections in adult mice. *Proc Natl Acad Sci U S A* 101, 16357–16362.
- Chen, L., Guo, Q., and Li, J.Y.H. (2009). Transcription factor *Gbx2* acts cell-nonautonomously to regulate the formation of lineage-restriction boundaries of the thalamus. *Development* 136, 1317–1326.
- Chen, Y.-C., Ma, N.-X., Pei, Z.-F., Wu, Z., Do-Monte, F.H., Keefe, S., Yellin, E., Chen, M.S., Yin, J.-C., Lee, G., et al. (2020). A NeuroD1 AAV-Based Gene Therapy for

Functional Brain Repair after Ischemic Injury through In Vivo Astrocyte-to-Neuron Conversion. *Mol Ther* 28, 217–234.

Chou, S.-J., Babot, Z., Leingärtner, A., Studer, M., Nakagawa, Y., and O'Leary, D.D.M. (2013). Genuiculocortical input drives genetic distinctions between primary and higher-order visual areas. *Science* 340, 1239–1242.

Clark, W.E. (1932). A MORPHOLOGICAL STUDY OF THE LATERAL GENICULATE BODY. *Br J Ophthalmol* 16, 264–284.

Clarke, B.E., Taha, D.M., Tyzack, G.E., and Patani, R. (2021). Regionally encoded functional heterogeneity of astrocytes in health and disease: A perspective. *Glia* 69, 20–27.

Cowan, C.S., Abd-El-Barr, M., van der Heijden, M., Lo, E.M., Paul, D., Bramblett, D.E., Lem, J., Simons, D.L., and Wu, S.M. (2016). Connexin 36 and rod bipolar cell independent rod pathways drive retinal ganglion cells and optokinetic reflexes. *Vision Res* 119, 99–109.

Cummings, B.J., Uchida, N., Tamaki, S.J., Salazar, D.L., Hooshmand, M., Summers, R., Gage, F.H., and Anderson, A.J. (2005). Human neural stem cells differentiate and promote locomotor recovery in spinal cord-injured mice. *Proc Natl Acad Sci U S A* 102, 14069–14074.

Curtis, M.A., Penney, E.B., Pearson, A.G., van Roon-Mom, W.M.C., Butterworth, N.J., Dragunow, M., Connor, B., and Faull, R.L.M. (2003). Increased cell proliferation and neurogenesis in the adult human Huntington's disease brain. *Proc Natl Acad Sci U S A* 100, 9023–9027.

Dani, J.W., Chernjavsky, A., and Smith, S.J. (1992). Neuronal activity triggers calcium waves in hippocampal astrocyte networks. *Neuron* 8, 429–440.

Deneen, B., Ho, R., Lukaszewicz, A., Hochstim, C.J., Gronostajski, R.M., and Anderson, D.J. (2006). The transcription factor NFIA controls the onset of gliogenesis in the developing spinal cord. *Neuron* 52, 953–968.

Diaz, F., McKeehan, N., Kang, W., and Hébert, J.M. (2013). Apoptosis of glutamatergic neurons fails to trigger a neurogenic response in the adult neocortex. *J. Neurosci.* 33, 6278–6284.

Dimou, L., and Gallo, V. (2015). NG2-glia and their functions in the central nervous system. *Glia* 63, 1429–1451.

Durkee, C.A., and Araque, A. (2019). Diversity and Specificity of Astrocyte-neuron Communication. *Neuroscience* 396, 73–78.

## References

- Echevarria, D., Vieira, C., Gimeno, L., and Martínez, S. (2003). Neuroepithelial secondary organizers and cell fate specification in the developing brain. *Brain Res Brain Res Rev* 43, 179–191.
- Eckler, M.J., Nguyen, T.D., McKenna, W.L., Fastow, B.L., Guo, C., Rubenstein, J.L.R., and Chen, B. (2015). Cux2-positive radial glial cells generate diverse subtypes of neocortical projection neurons and macroglia. *Neuron* 86, 1100–1108.
- Elsen, G.E., Hodge, R.D., Bedogni, F., Daza, R.A.M., Nelson, B.R., Shiba, N., Reiner, S.L., and Hevner, R.F. (2013). The protomap is propagated to cortical plate neurons through an Eomes-dependent intermediate map. *Proc Natl Acad Sci U S A* 110, 4081–4086.
- Ernst, A., Alkass, K., Bernard, S., Salehpour, M., Perl, S., Tisdale, J., Possnert, G., Druid, H., and Frisén, J. (2014). Neurogenesis in the striatum of the adult human brain. *Cell* 156, 1072–1083.
- Eroglu, C., and Barres, B.A. (2010). Regulation of synaptic connectivity by glia. *Nature* 468, 223–231.
- Escartin, C., Galea, E., Lakatos, A., O'Callaghan, J.P., Petzold, G.C., Serrano-Pozo, A., Steinhäuser, C., Volterra, A., Carmignoto, G., Agarwal, A., et al. (2021). Reactive astrocyte nomenclature, definitions, and future directions. *Nat. Neurosci.* 24, 312–325.
- Escartin, C., Guillemaud, O., and Carrillo-de Sauvage, M.-A. (2019). Questions and (some) answers on reactive astrocytes. *Glia* 67, 2221–2247.
- Falkner, S., Grade, S., Dimou, L., Conzelmann, K.-K., Bonhoeffer, T., Götz, M., and Hübener, M. (2016). Transplanted embryonic neurons integrate into adult neocortical circuits. *Nature* 539, 248–253.
- Farmer, W.T., Abrahamsson, T., Chierzi, S., Lui, C., Zaelzer, C., Jones, E.V., Bally, B.P., Chen, G.G., Thérout, J.-F., Peng, J., et al. (2016). Neurons diversify astrocytes in the adult brain through sonic hedgehog signaling. *Science* 351, 849–854.
- Fields, R.D. (2005). Myelination: an overlooked mechanism of synaptic plasticity? *Neuroscientist* 11, 528–531.
- Figueres-Oñate, M., García-Marqués, J., and López-Mascaraque, L. (2016). UbC-StarTrack, a clonal method to target the entire progeny of individual progenitors. *Sci Rep* 6, 33896–13.
- Franco, S.J., Gil-Sanz, C., Martinez-Garay, I., Espinosa, A., Harkins-Perry, S.R., Ramos, C., and Müller, U. (2012). Fate-restricted neural progenitors in the mammalian cerebral cortex. *Science* 337, 746–749.

- Frangeul, L., Pouchelon, G., Telley, L., Lefort, S., Luscher, C., and Jabaudon, D. (2016). A cross-modal genetic framework for the development and plasticity of sensory pathways. *Nature* 538, 96–98.
- Fricker-Gates, R.A., Winkler, C., Kirik, D., Rosenblad, C., Carpenter, M.K., and Björklund, A. (2000). EGF infusion stimulates the proliferation and migration of embryonic progenitor cells transplanted in the adult rat striatum. *Exp Neurol* 165, 237–247.
- Frost, D.O., and Caviness, V.S. (1980). Radial organization of thalamic projections to the neocortex in the mouse. *J. Comp. Neurol.* 194, 369–393.
- Fujita, Y., Nakanishi, T., Ueno, M., Itohara, S., and Yamashita, T. (2020). Netrin-G1 Regulates Microglial Accumulation along Axons and Supports the Survival of Layer V Neurons in the Postnatal Mouse Brain. *Cell Rep* 31, 107580.
- Gaillard, A., and Jaber, M. (2011). Rewiring the brain with cell transplantation in Parkinson's disease. *Trends Neurosci.* 34, 124–133.
- Gaillard, A., Decressac, M., Frappé, I., Fernagut, P.O., Prestoz, L., Besnard, S., and Jaber, M. (2009). Anatomical and functional reconstruction of the nigrostriatal pathway by intranigral transplants. *Neurobiol Dis* 35, 477–488.
- Gaillard, A., Prestoz, L., Dumartin, B., Cantereau, A., Morel, F., Roger, M., and Jaber, M. (2007). Reestablishment of damaged adult motor pathways by grafted embryonic cortical neurons. *Nat. Neurosci.* 10, 1294–1299.
- Gao, P., Postiglione, M.P., Krieger, T.G., Hernandez, L., Wang, C., Han, Z., Streicher, C., Pappusheva, E., Insolera, R., Chugh, K., et al. (2014). Deterministic progenitor behavior and unitary production of neurons in the neocortex. *Cell* 159, 775–788.
- García-Marqués, J., and López-Mascaraque, L. (2013). Clonal identity determines astrocyte cortical heterogeneity. *Cereb. Cortex* 23, 1463–1472.
- Gascón, S., Masserdotti, G., Russo, G.L., and Götz, M. (2017). Direct Neuronal Reprogramming: Achievements, Hurdles, and New Roads to Success. *Cell Stem Cell* 21, 18–34.
- Gascón, S., Murenu, E., Masserdotti, G., Ortega, F., Russo, G.L., Petrik, D., Deshpande, A., Heinrich, C., Karow, M., Robertson, S.P., et al. (2016). Identification and Successful Negotiation of a Metabolic Checkpoint in Direct Neuronal Reprogramming. *Cell Stem Cell* 18, 396–409.
- Ge, W.-P., Miyawaki, A., Gage, F.H., Jan, Y.N., and Jan, L.Y. (2012). Local generation of glia is a major astrocyte source in postnatal cortex. *Nature* 484, 376–380.

## References

Gezelius, H., and López-Bendito, G. (2017). Thalamic neuronal specification and early circuit formation. *Dev Neurobiol* 77, 830–843.

Gezelius, H., Moreno-Juan, V., Mezzera, C., Thakurela, S., Rodríguez-Malmierca, L.M., Pistolic, J., Benes, V., Tiwari, V.K., and López-Bendito, G. (2017). Genetic Labeling of Nuclei-Specific Thalamocortical Neurons Reveals Putative Sensory-Modality Specific Genes. *Cereb. Cortex* 27, 5054–5069.

Gillotin, S., and Guillemot, F. (2016). Micro-chromatin Immunoprecipitation ( $\mu$ ChIP) Protocol for Real-time PCR Analysis of a Limited Amount of Cells. *Bio Protoc* 6.

Godement, P., Salaün, J., and Imbert, M. (1984). Prenatal and postnatal development of retinogeniculate and retinocollicular projections in the mouse. *J. Comp. Neurol.* 230, 552–575.

Gokce, O., Stanley, G.M., Treutlein, B., Neff, N.F., Camp, J.G., Malenka, R.C., Rothwell, P.E., Fuccillo, M.V., Südhof, T.C., and Quake, S.R. (2016). Cellular Taxonomy of the Mouse Striatum as Revealed by Single-Cell RNA-Seq. *Cell Rep* 16, 1126–1137.

Gonçalves, J.T., Schafer, S.T., and Gage, F.H. (2016). Adult Neurogenesis in the Hippocampus: From Stem Cells to Behavior. *Cell* 167, 897–914.

Götz, M., and Bocchi, R. (2021). Neuronal replacement: Concepts, achievements, and call for caution. *Curr. Opin. Neurobiol.* 69, 185–192.

Götz, M., Sirko, S., Beckers, J., and Irmeler, M. (2015). Reactive astrocytes as neural stem or progenitor cells: In vivo lineage, In vitro potential, and Genome-wide expression analysis. *Glia* 63, 1452–1468.

Grade, S., and Götz, M. (2017). Neuronal replacement therapy: previous achievements and challenges ahead. *NPJ Regen Med* 2, 29–11.

Grande, A., Sumiyoshi, K., López-Juárez, A., Howard, J., Sakhivel, B., Aronow, B., Campbell, K., and Nakafuku, M. (2013). Environmental impact on direct neuronal reprogramming in vivo in the adult brain. *Nat Commun* 4, 2373–12.

Grealish, S., Jönsson, M.E., Li, M., Kirik, D., Björklund, A., and Thompson, L.H. (2010). The A9 dopamine neuron component in grafts of ventral mesencephalon is an important determinant for recovery of motor function in a rat model of Parkinson's disease. *Brain* 133, 482–495.

Greig, L.C., Woodworth, M.B., Galazo, M.J., Padmanabhan, H., and Macklis, J.D. (2013). Molecular logic of neocortical projection neuron specification, development and diversity. *Nat. Rev. Neurosci.* 14, 755–769.

- Guillery, R.W., and Sherman, S.M. (2002). Thalamic relay functions and their role in corticocortical communication: generalizations from the visual system. *Neuron* 33, 163–175.
- Guo, C., Eckler, M.J., McKenna, W.L., McKinsey, G.L., Rubenstein, J.L.R., and Chen, B. (2013). *Fezf2* expression identifies a multipotent progenitor for neocortical projection neurons, astrocytes, and oligodendrocytes. *Neuron* 80, 1167–1174.
- Guo, Q., and Li, J.Y.H. (2019). Defining developmental diversification of diencephalon neurons through single cell gene expression profiling. *Development* 146, dev174284.
- Guo, Z., Zhang, L., Wu, Z., Chen, Y., Wang, F., and Chen, G. (2014). In vivo direct reprogramming of reactive glial cells into functional neurons after brain injury and in an Alzheimer's disease model. *Cell Stem Cell* 14, 188–202.
- Hamilton, N.B., and Attwell, D. (2010). Do astrocytes really exocytose neurotransmitters? *Nat. Rev. Neurosci.* 11, 227–238.
- Haustein, M.D., Kracun, S., Lu, X.-H., Shih, T., Jackson-Weaver, O., Tong, X., Xu, J., Yang, X.W., O'Dell, T.J., Marvin, J.S., et al. (2014). Conditions and constraints for astrocyte calcium signaling in the hippocampal mossy fiber pathway. *Neuron* 82, 413–429.
- Heinrich, C., Blum, R., Gascón, S., Masserdotti, G., Tripathi, P., Sanchez, R., Tiedt, S., Schroeder, T., Götz, M., and Berninger, B. (2010). Directing astroglia from the cerebral cortex into subtype specific functional neurons. *PLoS Biol.* 8, e1000373.
- Heinrich, C., Gascón, S., Masserdotti, G., Lepier, A., Sanchez, R., Simon-Ebert, T., Schroeder, T., Götz, M., and Berninger, B. (2011). Generation of subtype-specific neurons from postnatal astroglia of the mouse cerebral cortex. *Nat Protoc* 6, 214–228.
- Henneberger, C., Papouin, T., Oliet, S.H.R., and Rusakov, D.A. (2010). Long-term potentiation depends on release of D-serine from astrocytes. *Nature* 463, 232–236.
- Hernit-Grant, C.S., and Macklis, J.D. (1996). Embryonic neurons transplanted to regions of targeted photolytic cell death in adult mouse somatosensory cortex re-form specific callosal projections. *Exp Neurol* 139, 131–142.
- Hippenmeyer, S., Youn, Y.H., Moon, H.M., Miyamichi, K., Zong, H., Wynshaw-Boris, A., and Luo, L. (2010). Genetic mosaic dissection of *Lis1* and *Ndel1* in neuronal migration. *Neuron* 68, 695–709.
- Hirabayashi, Y., Suzuki, N., Tsuboi, M., Endo, T.A., Toyoda, T., Shinga, J., Koseki, H., Vidal, M., and Gotoh, Y. (2009). Polycomb limits the neurogenic competence of neural precursor cells to promote astrogenic fate transition. *Neuron* 63, 600–613.

## References

- Hoang, T., Wang, J., Boyd, P., Wang, F., Santiago, C., Jiang, L., Yoo, S., Lahne, M., Todd, L.J., Jia, M., et al. (2020). Gene regulatory networks controlling vertebrate retinal regeneration. *Science* 370.
- Hochstim, C., Deneen, B., Lukaszewicz, A., Zhou, Q., and Anderson, D.J. (2008). Identification of positionally distinct astrocyte subtypes whose identities are specified by a homeodomain code. *Cell* 133, 510–522.
- Hooiveld, M.H., Morgan, R., in der Rieden, P., Houtzager, E., Pannese, M., Damen, K., Boncinelli, E., and Durston, A.J. (1999). Novel interactions between vertebrate Hox genes. *Int J Dev Biol* 43, 665–674.
- Huang, A.Y.-S., Woo, J., Sardar, D., Lozzi, B., Bosquez Huerta, N.A., Lin, C.-C.J., Felice, D., Jain, A., Paulucci-Holthauzen, A., and Deneen, B. (2020). Region-Specific Transcriptional Control of Astrocyte Function Oversees Local Circuit Activities. *Neuron*.
- Jessell, T.M. (2000). Neuronal specification in the spinal cord: inductive signals and transcriptional codes. *Nat. Rev. Genet.* 1, 20–29.
- Jessell, T.M., and Sanes, J.R. (2000). Development. The decade of the developing brain. *Curr. Opin. Neurobiol.* 10, 599–611.
- Jin, K., LaFevre-Bernt, M., Sun, Y., Chen, S., Gafni, J., Crippen, D., Logvinova, A., Ross, C.A., Greenberg, D.A., and Ellerby, L.M. (2005). FGF-2 promotes neurogenesis and neuroprotection and prolongs survival in a transgenic mouse model of Huntington's disease. *Proc Natl Acad Sci U S A* 102, 18189–18194.
- Jin, K., Wang, X., Xie, L., Mao, X.O., Zhu, W., Wang, Y., Shen, J., Mao, Y., Banwait, S., and Greenberg, D.A. (2006). Evidence for stroke-induced neurogenesis in the human brain. *Proc Natl Acad Sci U S A* 103, 13198–13202.
- John Lin, C.-C., Yu, K., Hatcher, A., Huang, T.-W., Lee, H.K., Carlson, J., Weston, M.C., Chen, F., Zhang, Y., Zhu, W., et al. (2017). Identification of diverse astrocyte populations and their malignant analogs. *Nat. Neurosci.* 20, 396–405.
- Jones, E.G., and Rockel, A.J. (1971). The synaptic organization in the medial geniculate body of afferent fibres ascending from the inferior colliculus. *Z Zellforsch Mikrosk Anat* 113, 44–66.
- Kandasamy, M., Roskopf, M., Wagner, K., Klein, B., Couillard-Despres, S., Reitsamer, H.A., Stephan, M., Nguyen, H.P., Riess, O., Bogdahn, U., et al. (2015). Reduction in subventricular zone-derived olfactory bulb neurogenesis in a rat model of Huntington's disease is accompanied by striatal invasion of neuroblasts. *PLoS ONE* 10, e0116069.

- Kang, W., and Hébert, J.M. (2011). Signaling pathways in reactive astrocytes, a genetic perspective. *Mol Neurobiol* 43, 147–154.
- Karow, M., Camp, J.G., Falk, S., Gerber, T., Pataskar, A., Gac-Santel, M., Kageyama, J., Brazovskaja, A., Garding, A., Fan, W., et al. (2018). Direct pericyte-to-neuron reprogramming via unfolding of a neural stem cell-like program. *Nat. Neurosci.* 21, 932–940.
- Khakh, B.S., and Deneen, B. (2019). The Emerging Nature of Astrocyte Diversity. *Annu. Rev. Neurosci.* 42, 187–207.
- Kiecker, C., and Lumsden, A. (2004). Hedgehog signaling from the ZLI regulates diencephalic regional identity. *Nat. Neurosci.* 7, 1242–1249.
- Kim, H.-J., and Rosenfeld, M.G. (2010). Epigenetic control of stem cell fate to neurons and glia. *Arch Pharm Res* 33, 1467–1473.
- Kinney, G.A., and Spain, W.J. (2002). Synaptically evoked GABA transporter currents in neocortical glia. *J Neurophysiol* 88, 2899–2908.
- Kobayashi, D., Kobayashi, M., Matsumoto, K., Ogura, T., Nakafuku, M., and Shimamura, K. (2002). Early subdivisions in the neural plate define distinct competence for inductive signals. *Development* 129, 83–93.
- Kohl, Z., Regensburger, M., Aigner, R., Kandasamy, M., Winner, B., Aigner, L., and Winkler, J. (2010). Impaired adult olfactory bulb neurogenesis in the R6/2 mouse model of Huntington's disease. *BMC Neurosci* 11, 114–11.
- Korematsu, K., and Redies, C. (1997). Expression of cadherin-8 mRNA in the developing mouse central nervous system. *J. Comp. Neurol.* 387, 291–306.
- Kreuzberg, M., Kanov, E., Timofeev, O., Schwaninger, M., Monyer, H., and Khodosevich, K. (2010). Increased subventricular zone-derived cortical neurogenesis after ischemic lesion. *Exp Neurol* 226, 90–99.
- Kriegstein, A., and Alvarez-Buylla, A. (2009). The glial nature of embryonic and adult neural stem cells. *Annu. Rev. Neurosci.* 32, 149–184.
- Kwak, H., Koh, W., Kim, S., Song, K., Shin, J.-I., Lee, J.M., Lee, E.H., Bae, J.Y., Ha, G.E., Oh, J.-E., et al. (2020). Astrocytes Control Sensory Acuity via Tonic Inhibition in the Thalamus. *Neuron* 108, 691–706.e10.
- Lanjakornsiripan, D., Pior, B.-J., Kawaguchi, D., Furutachi, S., Tahara, T., Katsuyama, Y., Suzuki, Y., Fukazawa, Y., and Gotoh, Y. (2018). Layer-specific morphological and

molecular differences in neocortical astrocytes and their dependence on neuronal layers. *Nat Commun* 9, 1623–15.

Lazarini, F., and Lledo, P.-M. (2011). Is adult neurogenesis essential for olfaction? *Trends Neurosci.* 34, 20–30.

Lee, C.C., and Sherman, S.M. (2010). Topography and physiology of ascending streams in the auditory tectothalamic pathway. *Proc Natl Acad Sci U S A* 107, 372–377.

Lehtinen, M.K., Zappaterra, M.W., Chen, X., Yang, Y.J., Hill, A.D., Lun, M., Maynard, T., Gonzalez, D., Kim, S., Ye, P., et al. (2011). The cerebrospinal fluid provides a proliferative niche for neural progenitor cells. *Neuron* 69, 893–905.

Levison, S.W., and Goldman, J.E. (1993). Both oligodendrocytes and astrocytes develop from progenitors in the subventricular zone of postnatal rat forebrain. *Neuron* 10, 201–212.

Liao, Y., Smyth, G.K., and Shi, W. (2014). featureCounts: an efficient general purpose program for assigning sequence reads to genomic features. *Bioinformatics* 30, 923–930.

Liddel, S.A., Guttenplan, K.A., Clarke, L.E., Bennett, F.C., Bohlen, C.J., Schirmer, L., Bennett, M.L., Münch, A.E., Chung, W.-S., Peterson, T.C., et al. (2017). Neurotoxic reactive astrocytes are induced by activated microglia. *Nature* 541, 481–487.

Lim, D.A., and Alvarez-Buylla, A. (2016). The Adult Ventricular-Subventricular Zone (V-SVZ) and Olfactory Bulb (OB) Neurogenesis. *Cold Spring Harb Perspect Biol* 8, a018820.

Linker, C., De Almeida, I., Papanayotou, C., Stower, M., Sabado, V., Ghorani, E., Streit, A., Mayor, R., and Stern, C.D. (2009). Cell communication with the neural plate is required for induction of neural markers by BMP inhibition: evidence for homeogenetic induction and implications for *Xenopus* animal cap and chick explant assays. *Dev. Biol.* 327, 478–486.

Liu, M.-H., Li, W., Zheng, J.-J., Xu, Y.-G., He, Q., and Chen, G. (2020). Differential neuronal reprogramming induced by NeuroD1 from astrocytes in grey matter versus white matter. *Neural Regen Res* 15, 342–351.

Liu, Y., Namba, T., Liu, J., Suzuki, R., Shioda, S., and Seki, T. (2010). Glial fibrillary acidic protein-expressing neural progenitors give rise to immature neurons via early intermediate progenitors expressing both glial fibrillary acidic protein and neuronal markers in the adult hippocampus. *Neuroscience* 166, 241–251.

Llorca, A., Ciceri, G., Beattie, R., Wong, F.K., Diana, G., Serafeimidou-Pouliou, E., Fernández-Otero, M., Streicher, C., Arnold, S.J., Meyer, M., et al. (2019). A stochastic

framework of neurogenesis underlies the assembly of neocortical cytoarchitecture. *Elife* 8.

Llorens-Bobadilla, E., Zhao, S., Baser, A., Saiz-Castro, G., Zwadlo, K., and Martin-Villalba, A. (2015). Single-Cell Transcriptomics Reveals a Population of Dormant Neural Stem Cells that Become Activated upon Brain Injury. *Cell Stem Cell* 17, 329–340.

Lodato, S., and Arlotta, P. (2015). Generating neuronal diversity in the mammalian cerebral cortex. *Annu. Rev. Cell Dev. Biol.* 31, 699–720.

Lodato, S., Molyneaux, B.J., Zuccaro, E., Goff, L.A., Chen, H.-H., Yuan, W., Meleski, A., Takahashi, E., Mahony, S., Rinn, J.L., et al. (2014). Gene co-regulation by *Fezf2* selects neurotransmitter identity and connectivity of corticospinal neurons. *Nat. Neurosci.* 17, 1046–1054.

Lujan, E., Chanda, S., Ahlenius, H., Südhof, T.C., and Wernig, M. (2012). Direct conversion of mouse fibroblasts to self-renewing, tripotent neural precursor cells. *Proc Natl Acad Sci U S A* 109, 2527–2532.

Luskin, M.B., Pearlman, A.L., and Sanes, J.R. (1988). Cell lineage in the cerebral cortex of the mouse studied in vivo and in vitro with a recombinant retrovirus. *Neuron* 1, 635–647.

Ma, N.-X., Yin, J.-C., and Chen, G. (2019). Transcriptome Analysis of Small Molecule-Mediated Astrocyte-to-Neuron Reprogramming. *Front Cell Dev Biol* 7, 82.

Macas, J., Nern, C., Plate, K.H., and Momma, S. (2006). Increased generation of neuronal progenitors after ischemic injury in the aged adult human forebrain. *J. Neurosci.* 26, 13114–13119.

Magavi, S.S., Leavitt, B.R., and Macklis, J.D. (2000). Induction of neurogenesis in the neocortex of adult mice. *Nature* 405, 951–955.

Magavi, S., Friedmann, D., Banks, G., Stolfi, A., and Lois, C. (2012). Coincident generation of pyramidal neurons and protoplasmic astrocytes in neocortical columns. *J. Neurosci.* 32, 4762–4772.

Magnusson, J.P., Göritz, C., Tatarishvili, J., Dias, D.O., Smith, E.M.K., Lindvall, O., Kokaia, Z., and Frisén, J. (2014). A latent neurogenic program in astrocytes regulated by Notch signaling in the mouse. *Science* 346, 237–241.

Magnusson, J.P., Zamboni, M., Santopolo, G., Mold, J.E., Barrientos-Somarribas, M., Talavera-Lopez, C., Andersson, B., and Frisén, J. (2020). Activation of a neural stem cell transcriptional program in parenchymal astrocytes. *Elife* 9.

## References

- Maimon, R., Chillon-Marinas, C., Snethlage, C.E., Singhal, S.M., McAlonis-Downes, M., Ling, K., Rigo, F., Bennett, C.F., Da Cruz, S., Hnasko, T.S., et al. (2021). Therapeutically viable generation of neurons with antisense oligonucleotide suppression of PTB. *Nat. Neurosci.* 1–11.
- Mallika, C., Guo, Q., and Li, J.Y.H. (2015). Gbx2 is essential for maintaining thalamic neuron identity and repressing habenular characters in the developing thalamus. *Dev. Biol.* 407, 26–39.
- Marsh, S.E., Yeung, S.T., Torres, M., Lau, L., Davis, J.L., Monuki, E.S., Poon, W.W., and Blurton-Jones, M. (2017). HuCNS-SC Human NSCs Fail to Differentiate, Form Ectopic Clusters, and Provide No Cognitive Benefits in a Transgenic Model of Alzheimer's Disease. *Stem Cell Reports* 8, 235–248.
- Martini, F.J., Moreno-Juan, V., Filipchuk, A., Valdeolmillos, M., and López-Bendito, G. (2018). Impact of thalamocortical input on barrel cortex development. *Neuroscience* 368, 246–255.
- Martí-Fàbregas, J., Romaguera-Ros, M., Gómez-Pinedo, U., Martínez-Ramírez, S., Jiménez-Xarrié R Marín, E., J-L Martí-Vilalta, R., and Garcia-Verdugo, J.-M. (2010). Proliferation in the human ipsilateral subventricular zone after ischemic stroke: *Neurology* 2010;Vol.74:357-365. *Ann Neurosci* 17, 134–135.
- Martínez, S. (2001). The isthmic organizer and brain regionalization. *Int J Dev Biol* 45, 367–371.
- Masserdotti, G., Gillotin, S., Sutor, B., Drechsel, D., Irmeler, M., Jørgensen, H.F., Sass, S., Theis, F.J., Beckers, J., Berninger, B., et al. (2015). Transcriptional Mechanisms of Proneural Factors and REST in Regulating Neuronal Reprogramming of Astrocytes. *Cell Stem Cell* 17, 74–88.
- Matias, I., Morgado, J., and Gomes, F.C.A. (2019). Astrocyte Heterogeneity: Impact to Brain Aging and Disease. *Front Aging Neurosci* 11, 59.
- Mattugini, N., Bocchi, R., Scheuss, V., Russo, G.L., Torper, O., Lao, C.L., and Götz, M. (2019). Inducing Different Neuronal Subtypes from Astrocytes in the Injured Mouse Cerebral Cortex. *Neuron* 103, 1086–1095.e5.
- Metzis, V., Steinhauser, S., Pakanavicius, E., Gouti, M., Stamataki, D., Ivanovitch, K., Watson, T., Rayon, T., Mousavy Gharavy, S.N., Lovell-Badge, R., et al. (2018). Nervous System Regionalization Entails Axial Allocation before Neural Differentiation. *Cell* 175, 1105–1118.e1117.
- Michelsen, K.A., Acosta-Verdugo, S., Benoit-Marand, M., Espuny-Camacho, I., Gaspard, N., Saha, B., Gaillard, A., and Vanderhaeghen, P. (2015). Area-specific reestablishment of

damaged circuits in the adult cerebral cortex by cortical neurons derived from mouse embryonic stem cells. *Neuron* 85, 982–997.

Mihalas, A.B., and Hevner, R.F. (2017). Control of Neuronal Development by T-Box Genes in the Brain. *Curr. Top. Dev. Biol.* 122, 279–312.

Miyashita-Lin, E.M., Hevner, R., Wassarman, K.M., Martínez, S., and Rubenstein, J.L. (1999). Early neocortical regionalization in the absence of thalamic innervation. *Science* 285, 906–909.

Molofsky, A.V., Kelley, K.W., Tsai, H.-H., Redmond, S.A., Chang, S.M., Madireddy, L., Chan, J.R., Baranzini, S.E., Ullian, E.M., and Rowitch, D.H. (2014). Astrocyte-encoded positional cues maintain sensorimotor circuit integrity. *Nature* 509, 189–194.

Molofsky, A.V., Krencik, R., Krenick, R., Ullian, E.M., Ullian, E., Tsai, H.-H., Deneen, B., Richardson, W.D., Barres, B.A., and Rowitch, D.H. (2012). Astrocytes and disease: a neurodevelopmental perspective. *Genes Dev.* 26, 891–907.

Molyneaux, B.J., Arlotta, P., Hirata, T., Hibi, M., and Macklis, J.D. (2005). Fezl is required for the birth and specification of corticospinal motor neurons. *Neuron* 47, 817–831.

Molyneaux, B.J., Arlotta, P., Menezes, J.R.L., and Macklis, J.D. (2007). Neuronal subtype specification in the cerebral cortex. *Nat. Rev. Neurosci.* 8, 427–437.

Molyneaux, B.J., Goff, L.A., Brettler, A.C., Chen, H.-H., Brown, J.R., Hrvatin, S., Rinn, J.L., and Arlotta, P. (2015). DeCoN: genome-wide analysis of in vivo transcriptional dynamics during pyramidal neuron fate selection in neocortex. *Neuron* 85, 275–288.

Monko, T., Rebertus, J., Stolley, J., Salton, S.R., and Nakagawa, Y. (2021). Thalamocortical axons regulate neurogenesis and laminar fates in early sensory cortex. *bioRxiv* 2021.06.16.448668.

Morel, L., Chiang, M.S.R., Higashimori, H., Shoneye, T., Iyer, L.K., Yelick, J., Tai, A., and Yang, Y. (2017). Molecular and Functional Properties of Regional Astrocytes in the Adult Brain. *J. Neurosci.* 37, 8706–8717.

Moreno-Juan, V., Filipchuk, A., Antón-Bolaños, N., Mezzera, C., Gezelius, H., Andrés, B., Rodríguez-Malmierca, L., Susín, R., Schaad, O., Iwasato, T., et al. (2017). Prenatal thalamic waves regulate cortical area size prior to sensory processing. *Nat Commun* 8, 14172–14.

Mountcastle, V.B. (1997). The columnar organization of the neocortex. *Brain* 120 ( Pt 4), 701–722.

## References

- Müller, C.M., and Best, J. (1989). Ocular dominance plasticity in adult cat visual cortex after transplantation of cultured astrocytes. *Nature* 342, 427–430.
- Nagai, J., Yu, X., Papouin, T., Cheong, E., Freeman, M.R., Monk, K.R., Hastings, M.H., Haydon, P.G., Rowitch, D., Shaham, S., et al. (2021). Behaviorally consequential astrocytic regulation of neural circuits. *Neuron* 109, 576–596.
- Nakagawa, Y., and O'Leary, D.D. (2001). Combinatorial expression patterns of LIM-homeodomain and other regulatory genes parcellate developing thalamus. *J. Neurosci.* 21, 2711–2725.
- Nakagawa, Y., Johnson, J.E., and O'Leary, D.D. (1999). Graded and areal expression patterns of regulatory genes and cadherins in embryonic neocortex independent of thalamocortical input. *J. Neurosci.* 19, 10877–10885.
- Nakagawa, Y. (2019). Development of the thalamus: From early patterning to regulation of cortical functions. *Wiley Interdiscip Rev Dev Biol* 8, e345.
- Nakagawa, Y., and Shimogori, T. (2012). Diversity of thalamic progenitor cells and postmitotic neurons. *Eur J Neurosci* 35, 1554–1562.
- Noctor, S.C., Martínez-Cerdeño, V., and Kriegstein, A.R. (2008). Distinct behaviors of neural stem and progenitor cells underlie cortical neurogenesis. *Journal of Comparative Neurology* 508, 28–44.
- Nolte, C., Matyash, M., Pivneva, T., Schipke, C.G., Ohlemeyer, C., Hanisch, U.K., Kirchhoff, F., and Kettenmann, H. (2001). GFAP promoter-controlled EGFP-expressing transgenic mice: a tool to visualize astrocytes and astrogliosis in living brain tissue. *Glia* 33, 72–86.
- O'Leary, D.D. (1989). Do cortical areas emerge from a protocortex? *Trends Neurosci.* 12, 400–406.
- O'Leary, D.D.M., and Nakagawa, Y. (2002). Patterning centers, regulatory genes and extrinsic mechanisms controlling arealization of the neocortex. *Curr. Opin. Neurobiol.* 12, 14–25.
- O'Leary, D.D.M., Chou, S.-J., and Sahara, S. (2007). Area patterning of the mammalian cortex. *Neuron* 56, 252–269.
- Oberst, P., Agirman, G., and Jabaudon, D. (2019). Principles of progenitor temporal patterning in the developing invertebrate and vertebrate nervous system. *Curr. Opin. Neurobiol.* 56, 185–193.

- Ohira, K., Furuta, T., Hioki, H., Nakamura, K.C., Kuramoto, E., Tanaka, Y., Funatsu, N., Shimizu, K., Oishi, T., Hayashi, M., et al. (2010). Ischemia-induced neurogenesis of neocortical layer 1 progenitor cells. *Nat. Neurosci.* *13*, 173–179.
- Ohtaka-Maruyama, C., Okamoto, M., Endo, K., Oshima, M., Kaneko, N., Yura, K., Okado, H., Miyata, T., and Maeda, N. (2018). Synaptic transmission from subplate neurons controls radial migration of neocortical neurons. *Science* *360*, 313–317.
- Ourednik, J., Ourednik, V., Lynch, W.P., Schachner, M., and Snyder, E.Y. (2002). Neural stem cells display an inherent mechanism for rescuing dysfunctional neurons. *Nat. Biotechnol.* *20*, 1103–1110.
- Pang, Z.P., Yang, N., Vierbuchen, T., Ostermeier, A., Fuentes, D.R., Yang, T.Q., Citri, A., Sebastiano, V., Marro, S., Südhof, T.C., et al. (2011). Induction of human neuronal cells by defined transcription factors. *Nature* *476*, 220–223.
- Parent, J.M., Vexler, Z.S., Gong, C., Derugin, N., and Ferriero, D.M. (2002). Rat forebrain neurogenesis and striatal neuron replacement after focal stroke. *Ann Neurol* *52*, 802–813.
- Park, K.I., Teng, Y.D., and Snyder, E.Y. (2002). The injured brain interacts reciprocally with neural stem cells supported by scaffolds to reconstitute lost tissue. *Nat. Biotechnol.* *20*, 1111–1117.
- Paukert, M., Agarwal, A., Cha, J., Doze, V.A., Kang, J.U., and Bergles, D.E. (2014). Norepinephrine controls astroglial responsiveness to local circuit activity. *Neuron* *82*, 1263–1270.
- Pearson, J.C., Lemons, D., and McGinnis, W. (2005). Modulating Hox gene functions during animal body patterning. *Nat. Rev. Genet.* *6*, 893–904.
- Phillips, J.W., Schulmann, A., Hara, E., Winnubst, J., Liu, C., Valakh, V., Wang, L., Shields, B.C., Korff, W., Chandrashekar, J., et al. (2019). A repeated molecular architecture across thalamic pathways. *Nat. Neurosci.* *22*, 1925–1935.
- Pouchelon, G., Frangeul, L., Rijli, F.M., and Jabaudon, D. (2012). Patterning of pre-thalamic somatosensory pathways. *Eur J Neurosci* *35*, 1533–1539.
- Puelles, L., and Rubenstein, J.L. (1993). Expression patterns of homeobox and other putative regulatory genes in the embryonic mouse forebrain suggest a neuromeric organization. *Trends Neurosci.* *16*, 472–479.
- Puelles, L., and Rubenstein, J.L.R. (2003). Forebrain gene expression domains and the evolving prosomeric model. *Trends Neurosci.* *26*, 469–476.

## References

- Puelles, L., Harrison, M., Paxinos, G., and Watson, C. (2013). A developmental ontology for the mammalian brain based on the prosomeric model. *Trends Neurosci.* 36, 570–578.
- Purves, D., Purves, G.B.G.P.F.R.I.N.D., Lichtman, J.W., University William K Purves (1985). *Principles of Neural Development* (Sinauer Associates, Incorporated).
- Qian, H., Kang, X., Hu, J., Zhang, D., Liang, Z., Meng, F., Zhang, X., Xue, Y., Maimon, R., Dowdy, S.F., et al. (2020). Reversing a model of Parkinson's disease with in situ converted nigral neurons. *Nature* 582, 550–556.
- Qin, H., Zhao, A., and Fu, X. (2017). Small molecules for reprogramming and transdifferentiation. *Cell Mol Life Sci* 74, 3553–3575.
- Rakic, P. (1972). Mode of cell migration to the superficial layers of fetal monkey neocortex. *J. Comp. Neurol.* 145, 61–83.
- Rakic, P. (1988). Specification of cerebral cortical areas. *Science* 241, 170–176.
- Rakic, P. (1995). Radial versus tangential migration of neuronal clones in the developing cerebral cortex. *Proc Natl Acad Sci U S A* 92, 11323–11327.
- Rakic, P., Ayoub, A.E., Breunig, J.J., and Dominguez, M.H. (2009). Decision by division: making cortical maps. *Trends Neurosci.* 32, 291–301.
- Ralston, H.J. (1969). The synaptic organization of lemniscal projections to the ventrobasal thalamus of the cat. *Brain Res* 14, 99–115.
- Ramaswamy, S., Goings, G.E., Soderstrom, K.E., Szele, F.G., and Kozlowski, D.A. (2005). Cellular proliferation and migration following a controlled cortical impact in the mouse. *Brain Res* 1053, 38–53.
- Rash, B.G., and Grove, E.A. (2006). Area and layer patterning in the developing cerebral cortex. *Curr. Opin. Neurobiol.* 16, 25–34.
- Reichova, I., and Sherman, S.M. (2004). Somatosensory corticothalamic projections: distinguishing drivers from modulators. *J Neurophysiol* 92, 2185–2197.
- Reid, C.B., Liang, I., and Walsh, C. (1995). Systematic widespread clonal organization in cerebral cortex. *Neuron* 15, 299–310.
- Ribot, J., Breton, R., Calvo, C.-F., Moulard, J., Ezan, P., Zapata, J., Samama, K., Moreau, M., Bemelmans, A.-P., Sabatet, V., et al. (2021). Astrocytes close the mouse critical period for visual plasticity. *Science* 373, 77–81.
- Rivetti di Val Cervo, P., Romanov, R.A., Spigolon, G., Masini, D., Martín-Montañez, E., Toledo, E.M., La Manno, G., Feyder, M., Pifl, C., Ng, Y.-H., et al. (2017). Induction of

functional dopamine neurons from human astrocytes in vitro and mouse astrocytes in a Parkinson's disease model. *Nat. Biotechnol.* 35, 444–452.

Rouach, N., Koulakoff, A., Abudara, V., Willecke, K., and Giaume, C. (2008). Astroglial metabolic networks sustain hippocampal synaptic transmission. *Science* 322, 1551–1555.

Rouaux, C., and Arlotta, P. (2013). Direct lineage reprogramming of post-mitotic callosal neurons into corticofugal neurons in vivo. *Nat. Cell Biol.* 15, 214–221.

Roy, K., Kumar, S., and Bloomfield, S.A. (2017). Gap junctional coupling between retinal amacrine and ganglion cells underlies coherent activity integral to global object perception. *Proc Natl Acad Sci U S A* 114, E10484–E10493.

Russo, G.L., Sonsalla, G., Natarajan, P., Breunig, C.T., Bulli, G., Merl-Pham, J., Schmitt, S., Giehl-Schwab, J., Giesert, F., Jastroch, M., et al. (2021). CRISPR-Mediated Induction of Neuron-Enriched Mitochondrial Proteins Boosts Direct Glia-to-Neuron Conversion. *Cell Stem Cell* 28, 524–534.e527.

Savtchouk, I., and Volterra, A. (2018). Gliotransmission: Beyond Black-and-White. *J. Neurosci.* 38, 14–25.

Scandaglia, M., Lopez-Atalaya, J.P., Medrano-Fernandez, A., Lopez-Cascales, M.T., Del Blanco, B., Lipinski, M., Benito, E., Olivares, R., Iwase, S., Shi, Y., et al. (2017). Loss of Kdm5c Causes Spurious Transcription and Prevents the Fine-Tuning of Activity-Regulated Enhancers in Neurons. *Cell Rep* 21, 47–59.

Scholpp, S., and Lumsden, A. (2010). Building a bridal chamber: development of the thalamus. *Trends Neurosci.* 33, 373–380.

Schwartz, S.D., Hubschman, J.-P., Heilwell, G., Franco-Cardenas, V., Pan, C.K., Ostrick, R.M., Mickunas, E., Gay, R., Klimanskaya, I., and Lanza, R. (2012). Embryonic stem cell trials for macular degeneration: a preliminary report. *Lancet* 379, 713–720.

Schwartz, S.D., Regillo, C.D., Lam, B.L., Elliott, D., Rosenfeld, P.J., Gregori, N.Z., Hubschman, J.-P., Davis, J.L., Heilwell, G., Spirn, M., et al. (2015). Human embryonic stem cell-derived retinal pigment epithelium in patients with age-related macular degeneration and Stargardt's macular dystrophy: follow-up of two open-label phase 1/2 studies. *Lancet* 385, 509–516.

Sestan, N., Rakic, P., and Donoghue, M.J. (2001). Independent parcellation of the embryonic visual cortex and thalamus revealed by combinatorial Eph/ephrin gene expression. *Curr Biol* 11, 39–43.

Sherman, S.M., and Guillery, R.W. (2002). The role of the thalamus in the flow of information to the cortex. *Philos Trans R Soc Lond B Biol Sci* 357, 1695–1708.

## References

- Shi, W., Xianyu, A., Han, Z., Tang, X., Li, Z., Zhong, H., Mao, T., Huang, K., and Shi, S.-H. (2017). Ontogenetic establishment of order-specific nuclear organization in the mammalian thalamus. *Nat. Neurosci.* *20*, 516–528.
- Shin, J.J., Fricker-Gates, R.A., Perez, F.A., Leavitt, B.R., Zurakowski, D., and Macklis, J.D. (2000). Transplanted neuroblasts differentiate appropriately into projection neurons with correct neurotransmitter and receptor phenotype in neocortex undergoing targeted projection neuron degeneration. *J. Neurosci.* *20*, 7404–7416.
- Sirko, S., Behrendt, G., Johansson, P.A., Tripathi, P., Costa, M., Bek, S., Heinrich, C., Tiedt, S., Colak, D., Dichgans, M., et al. (2013). Reactive glia in the injured brain acquire stem cell properties in response to sonic hedgehog. [corrected]. *Cell Stem Cell* *12*, 426–439.
- Smart, I.H.M., Dehay, C., Giroud, P., Berland, M., and Kennedy, H. (2002). Unique morphological features of the proliferative zones and postmitotic compartments of the neural epithelium giving rise to striate and extrastriate cortex in the monkey. *Cereb. Cortex* *12*, 37–53.
- Smith, D.K., Yang, J., Liu, M.-L., and Zhang, C.-L. (2016). Small Molecules Modulate Chromatin Accessibility to Promote NEUROG2-Mediated Fibroblast-to-Neuron Reprogramming. *Stem Cell Reports* *7*, 955–969.
- Sofroniew, M.V. (2005). Reactive astrocytes in neural repair and protection. *Neuroscientist* *11*, 400–407.
- Song, H., Lee, B., Pyun, D., Guimera, J., Son, Y., Yoon, J., Baek, K., Wurst, W., and Jeong, Y. (2015). *Ascl1* and *Helt* act combinatorially to specify thalamic neuronal identity by repressing *Dlx5* activation. *Dev. Biol.* *398*, 280–291.
- Steinbeck, J.A., and Studer, L. (2015). Moving stem cells to the clinic: potential and limitations for brain repair. *Neuron* *86*, 187–206.
- Stern, C.D. (2006). Evolution of the mechanisms that establish the embryonic axes. *Curr Opin Genet Dev* *16*, 413–418.
- Stogsdill, J.A., Ramirez, J., Liu, D., Kim, Y.H., Baldwin, K.T., Enustun, E., Ejikeme, T., Ji, R.-R., and Eroglu, C. (2017). Astrocytic neuroligins control astrocyte morphogenesis and synaptogenesis. *Nature* *551*, 192–197.
- Stolt, C.C., Lommes, P., Sock, E., Chaboissier, M.-C., Schedl, A., and Wegner, M. (2003). The *Sox9* transcription factor determines glial fate choice in the developing spinal cord. *Genes Dev.* *17*, 1677–1689.

- Stuart, T., Butler, A., Hoffman, P., Hafemeister, C., Papalexi, E., Mauck, W.M., Hao, Y., Stoeckius, M., Smibert, P., and Satija, R. (2019). Comprehensive Integration of Single-Cell Data. *Cell* 177, 1888–1902.e21.
- Sur, M., and Rubenstein, J.L.R. (2005). Patterning and plasticity of the cerebral cortex. *Science* 310, 805–810.
- Suzuki, S.C., Inoue, T., Kimura, Y., Tanaka, T., and Takeichi, M. (1997). Neuronal circuits are subdivided by differential expression of type-II classic cadherins in postnatal mouse brains. *Mol Cell Neurosci* 9, 433–447.
- Suzuki-Hirano, A., Ogawa, M., Kataoka, A., Yoshida, A.C., Itoh, D., Ueno, M., Blackshaw, S., and Shimogori, T. (2011). Dynamic spatiotemporal gene expression in embryonic mouse thalamus. *Journal of Comparative Neurology* 519, 528–543.
- Takahashi, K., Okita, K., Nakagawa, M., and Yamanaka, S. (2007a). Induction of pluripotent stem cells from fibroblast cultures. *Nat Protoc* 2, 3081–3089.
- Takahashi, K., Tanabe, K., Ohnuki, M., Narita, M., Ichisaka, T., Tomoda, K., and Yamanaka, S. (2007b). Induction of pluripotent stem cells from adult human fibroblasts by defined factors. *Cell* 131, 861–872.
- Tamaki, S., Eckert, K., He, D., Sutton, R., Doshe, M., Jain, G., Tushinski, R., Reitsma, M., Harris, B., Tsukamoto, A., et al. (2002). Engraftment of sorted/expanded human central nervous system stem cells from fetal brain. *J Neurosci Res* 69, 976–986.
- Tamamaki, N., Yanagawa, Y., Tomioka, R., Miyazaki, J.-I., Obata, K., and Kaneko, T. (2003). Green fluorescent protein expression and colocalization with calretinin, parvalbumin, and somatostatin in the GAD67-GFP knock-in mouse. *J. Comp. Neurol.* 467, 60–79.
- Tasic, B., Yao, Z., Graybiuck, L.T., Smith, K.A., Nguyen, T.N., Bertagnolli, D., Goldy, J., Garren, E., Economo, M.N., Viswanathan, S., et al. (2018). Shared and distinct transcriptomic cell types across neocortical areas. *Nature* 563, 72–78.
- Telley, L., Agirman, G., Prados, J., Amberg, N., Fièvre, S., Oberst, P., Bartolini, G., Vitali, I., Cadilhac, C., Hippenmeyer, S., et al. (2019). Temporal patterning of apical progenitors and their daughter neurons in the developing neocortex. *Science* 364, eaav2522.
- Telley, L., and Jabaudon, D. (2018). A mixed model of neuronal diversity. *Nature* 555, 452–454.
- Thier, M., Wörsdörfer, P., Lakes, Y.B., Gorris, R., Herms, S., Opitz, T., Seiferling, D., Quandt, T., Hoffmann, P., Nöthen, M.M., et al. (2012). Direct conversion of fibroblasts into stably expandable neural stem cells. *Cell Stem Cell* 10, 473–479.

- Thored, P., Arvidsson, A., Cacci, E., Ahlenius, H., Kallur, T., Darsalia, V., Ekdahl, C.T., Kokaia, Z., and Lindvall, O. (2006). Persistent production of neurons from adult brain stem cells during recovery after stroke. *Stem Cells* 24, 739–747.
- Tiklová, K., Nolbrant, S., Fiorenzano, A., Björklund, Å.K., Sharma, Y., Heuer, A., Gillberg, L., Hoban, D.B., Cardoso, T., Adler, A.F., et al. (2020). Single cell transcriptomics identifies stem cell-derived graft composition in a model of Parkinson's disease. *Nat Commun* 11, 2434–11.
- Tiwari, N., Pataskar, A., Péron, S., Thakurela, S., Sahu, S.K., Figueres-Oñate, M., Marichal, N., López-Mascaraque, L., Tiwari, V.K., and Berninger, B. (2018). Stage-Specific Transcription Factors Drive Astroglialogenesis by Remodeling Gene Regulatory Landscapes. *Cell Stem Cell* 23, 557–571.e558.
- Toma, K., Kumamoto, T., and Hanashima, C. (2014). The timing of upper-layer neurogenesis is conferred by sequential derepression and negative feedback from deep-layer neurons. *J. Neurosci.* 34, 13259–13276.
- Tong, L.M., Djukic, B., Arnold, C., Gillespie, A.K., Yoon, S.Y., Wang, M.M., Zhang, O., Knoferle, J., Rubenstein, J.L.R., Alvarez-Buylla, A., et al. (2014). Inhibitory interneuron progenitor transplantation restores normal learning and memory in ApoE4 knock-in mice without or with A $\beta$  accumulation. *J. Neurosci.* 34, 9506–9515.
- Tornero, D., Wattananit, S., Grønning Madsen, M., Koch, P., Wood, J., Tatarishvili, J., Mine, Y., Ge, R., Monni, E., Devaraju, K., et al. (2013). Human induced pluripotent stem cell-derived cortical neurons integrate in stroke-injured cortex and improve functional recovery. *Brain* 136, 3561–3577.
- Treutlein, B., Lee, Q.Y., Camp, J.G., Mall, M., Koh, W., Shariati, S.A.M., Sim, S., Neff, N.F., Skotheim, J.M., Wernig, M., et al. (2016). Dissecting direct reprogramming from fibroblast to neuron using single-cell RNA-seq. *Nature* 534, 391–395.
- Tsai, H.-H., Li, H., Fuentealba, L.C., Molofsky, A.V., Taveira-Marques, R., Zhuang, H., Tenney, A., Murnen, A.T., Fancy, S.P.J., Merkle, F., et al. (2012). Regional astrocyte allocation regulates CNS synaptogenesis and repair. *Science* 337, 358–362.
- Turner, M., Leslie, S., Martin, N.G., Peschanski, M., Rao, M., Taylor, C.J., Trounson, A., Turner, D., Yamanaka, S., and Wilmut, I. (2013). Toward the development of a global induced pluripotent stem cell library. *Cell Stem Cell* 13, 382–384.
- Uchida, N., Buck, D.W., He, D., Reitsma, M.J., Masek, M., Phan, T.V., Tsukamoto, A.S., Gage, F.H., and Weissman, I.L. (2000). Direct isolation of human central nervous system stem cells. *Proc Natl Acad Sci U S A* 97, 14720–14725.

- Ulloa, F., and Briscoe, J. (2007). Morphogens and the control of cell proliferation and patterning in the spinal cord. *Cell Cycle* 6, 2640–2649.
- Valverde, F. (1968). Structural changes in the area striata of the mouse after enucleation. *Exp Brain Res* 5, 274–292.
- Vanderhaeghen, P., Lu, Q., Prakash, N., Frisé, J., Walsh, C.A., Frostig, R.D., and Flanagan, J.G. (2000). A mapping label required for normal scale of body representation in the cortex. *Nat. Neurosci.* 3, 358–365.
- Verkhratsky, A., and Nedergaard, M. (2018). Physiology of Astroglia. *Physiol Rev* 98, 239–389.
- Vieira, C., Pombero, A., García-Lopez, R., Gimeno, L., Echevarria, D., and Martínez, S. (2010). Molecular mechanisms controlling brain development: an overview of neuroepithelial secondary organizers. *Int J Dev Biol* 54, 7–20.
- Vierbuchen, T., Ostermeier, A., Pang, Z.P., Kokubu, Y., Südhof, T.C., and Wernig, M. (2010). Direct conversion of fibroblasts to functional neurons by defined factors. *Nature* 463, 1035–1041.
- Viganò, F., and Dimou, L. (2016). The heterogeneous nature of NG2-glia. *Brain Res* 1638, 129–137.
- Vitali, I., Fièvre, S., Telley, L., Oberst, P., Bariselli, S., Frangeul, L., Baumann, N., McMahon, J.J., Klingler, E., Bocchi, R., et al. (2018). Progenitor Hyperpolarization Regulates the Sequential Generation of Neuronal Subtypes in the Developing Neocortex. *Cell* 174, 1264–1276.e15.
- Voigt, P., Tee, W.-W., and Reinberg, D. (2013). A double take on bivalent promoters. *Genes Dev.* 27, 1318–1338.
- Vue, T.Y., Aaker, J., Taniguchi, A., Kazemzadeh, C., Skidmore, J.M., Martin, D.M., Martin, J.F., Treier, M., and Nakagawa, Y. (2007). Characterization of progenitor domains in the developing mouse thalamus. *J. Comp. Neurol.* 505, 73–91.
- Vue, T.Y., Bluske, K., Alishahi, A., Yang, L.L., Koyano-Nakagawa, N., Novitch, B., and Nakagawa, Y. (2009). Sonic hedgehog signaling controls thalamic progenitor identity and nuclei specification in mice. *J. Neurosci.* 29, 4484–4497.
- Vue, T.Y., Lee, M., Tan, Y.E., Werkhoven, Z., Wang, L., and Nakagawa, Y. (2013). Thalamic control of neocortical area formation in mice. *J. Neurosci.* 33, 8442–8453.
- Waddington, C.H. (1936). THE PROBLEMS OF EMBRYOLOGY. *Br Med J* 2, 862–864.

## References

- Walsh, C., and Cepko, C.L. (1988). Clonally related cortical cells show several migration patterns. *Science* *241*, 1342–1345.
- Wang, L.-L., Garcia, C.S., Zhong, X., Ma, S., and Zhang, C.-L. (2020). Rapid and efficient in vivo astrocyte-to-neuron conversion with regional identity and connectivity? *bioRxiv* 2020.08.16.253195.
- Wang, X., Lou, N., Xu, Q., Tian, G.-F., Peng, W.G., Han, X., Kang, J., Takano, T., and Nedergaard, M. (2006). Astrocytic Ca<sup>2+</sup> signaling evoked by sensory stimulation in vivo. *Nat. Neurosci.* *9*, 816–823.
- Wittler, L., and Kessel, M. (2004). The acquisition of neural fate in the chick. *Mech Dev* *121*, 1031–1042.
- Wong, S.Z.H., Scott, E.P., Mu, W., Guo, X., Borgenheimer, E., Freeman, M., Ming, G.-L., Wu, Q.-F., Song, H., and Nakagawa, Y. (2018). In vivo clonal analysis reveals spatiotemporal regulation of thalamic nucleogenesis. *PLoS Biol.* *16*, e2005211.
- Wu, Y.E., Pan, L., Zuo, Y., Li, X., and Hong, W. (2017). Detecting Activated Cell Populations Using Single-Cell RNA-Seq. *Neuron* *96*, 313–329.e316.
- Wu, Z., Parry, M., Hou, X.-Y., Liu, M.-H., Wang, H., Cain, R., Pei, Z.-F., Chen, Y.-C., Guo, Z.-Y., Abhijeet, S., et al. (2020). Gene therapy conversion of striatal astrocytes into GABAergic neurons in mouse models of Huntington's disease. *Nat Commun* *11*, 1105–1118.
- Xue, Y., Ouyang, K., Huang, J., Zhou, Y., Ouyang, H., Li, H., Wang, G., Wu, Q., Wei, C., Bi, Y., et al. (2013). Direct conversion of fibroblasts to neurons by reprogramming PTB-regulated microRNA circuits. *Cell* *152*, 82–96.
- Yamashita, T., Ninomiya, M., Hernández Acosta, P., García-Verdugo, J.M., Sunabori, T., Sakaguchi, M., Adachi, K., Kojima, T., Hirota, Y., Kawase, T., et al. (2006). Subventricular zone-derived neuroblasts migrate and differentiate into mature neurons in the post-stroke adult striatum. *J. Neurosci.* *26*, 6627–6636.
- Yu, G., Wang, L.-G., Han, Y., and He, Q.-Y. (2012). clusterProfiler: an R package for comparing biological themes among gene clusters. *Omics* *16*, 284–287.
- Zeisel, A., Hochgerner, H., Lönnerberg, P., Johnsson, A., Memic, F., van der Zwan, J., Häring, M., Braun, E., Borm, L.E., La Manno, G., et al. (2018). Molecular Architecture of the Mouse Nervous System. *Cell* *174*, 999–1014.e22.
- Zeisel, A., Muñoz-Manchado, A.B., Codeluppi, S., Lönnerberg, P., La Manno, G., Juréus, A., Marques, S., Munguba, H., He, L., Betsholtz, C., et al. (2015). Brain structure. *Cell*

types in the mouse cortex and hippocampus revealed by single-cell RNA-seq. *Science* 347, 1138–1142.

Zhang, L., Yin, J.-C., Yeh, H., Ma, N.-X., Lee, G., Chen, X.A., Wang, Y., Lin, L., Chen, L., Jin, P., et al. (2015). Small Molecules Efficiently Reprogram Human Astroglial Cells into Functional Neurons. *Cell Stem Cell* 17, 735–747.

Zhang, X., Jin, G., Li, W., Zou, L., Shi, J., Qin, J., Tian, M., and Li, H. (2011). Ectopic neurogenesis in the forebrain cholinergic system-related areas of a rat dementia model. *Stem Cells Dev* 20, 1627–1638.

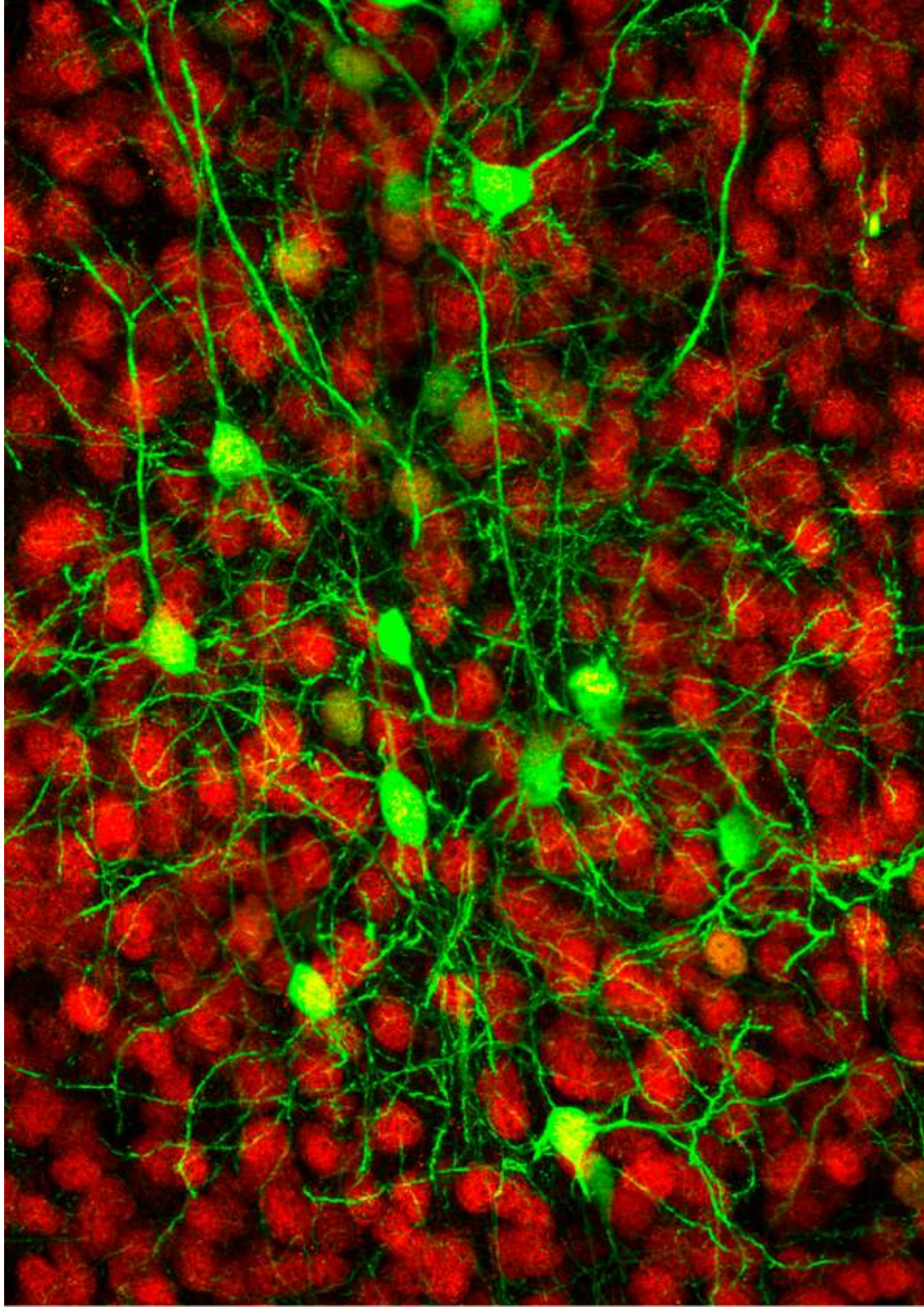
Zhang, X., Mennicke, C.V., Xiao, G., Beattie, R., Haider, M.A., Hippenmeyer, S., and Ghashghaei, H.T. (2020). Clonal Analysis of Gliogenesis in the Cerebral Cortex Reveals Stochastic Expansion of Glia and Cell Autonomous Responses to Egfr Dosage. *Cells* 9, 2662.

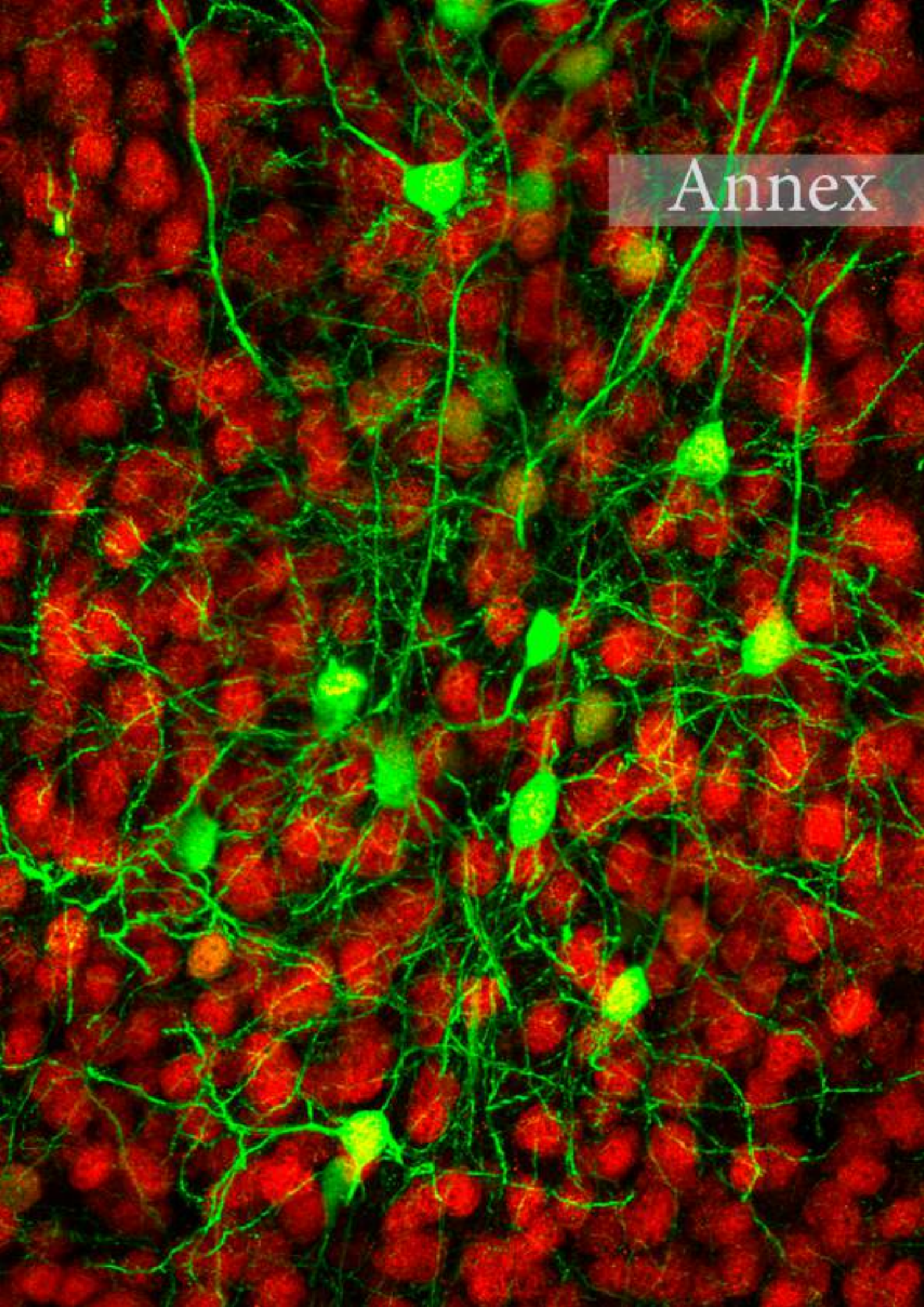
Zhang, Z., Zhou, H., and Zhou, J. Heterogeneity and Proliferative and Differential Regulators of NG2-glia in Physiological and Pathological States.

Zhou, H., Su, J., Hu, X., Zhou, C., Li, H., Chen, Z., Xiao, Q., Wang, B., Wu, W., Sun, Y., et al. (2020). Glia-to-Neuron Conversion by CRISPR-CasRx Alleviates Symptoms of Neurological Disease in Mice. *Cell* 181, 590–603.e16.

Zhu, A., Ibrahim, J.G., and Love, M.I. (2019). Heavy-tailed prior distributions for sequence count data: removing the noise and preserving large differences. *Bioinformatics* 35, 2084–2092.

Zong, H., Espinosa, J.S., Su, H.H., Muzumdar, M.D., and Luo, L. (2005). Mosaic analysis with double markers in mice. *Cell* 121, 479–492.



A fluorescence microscopy image showing a dense network of neurons. The neurons are stained with two different fluorescent dyes. One set of neurons, including their cell bodies and some branching processes, is stained in a bright green color. The other set of neurons, which appear more numerous and form a dense background, is stained in a bright red color. The overall appearance is a complex, interconnected web of neural structures. In the upper right corner, there is a semi-transparent grey rectangular box containing the word "Annex" in a white, serif font.

# Annex



## Annex

The results of this Thesis work have been published in Science Advances, in the annexed paper named “**Astrocytes and neurons share region-specific transcriptional signatures that confer regional identity to neuronal reprogramming**” in which I am the only first autor. However, this work has been done in collaboration with members of my laboratory and with researchers from other institutions. Here I describe the author contribution for each of the co-authors: Guillermina López-Bendito and Álvaro Herrero-Navarro designed the experiments. Álvaro Herrero-Navarro conducted the astrocyte reprogramming experiments *in vitro* and *in vivo* and the epigenetic analyses. Lorenzo Puche Aroca and Jose P. López-Atalaya conducted all bioinformatic analysis of massively parallel sequencing data. Verónica Moreno-Juan and Álvaro Herrero-Navarro conducted the *in vivo* clonal studies and performed the *in situ* hybridization validation of the RNA-seq. Alejandro Sempere-Ferrández performed the electrophysiological recordings. Álvaro Herrero-Navarro, Verónica Moreno-Juan and Ana Espinosa collected tissue for RNA-seq. Rafael Susín produced the viruses. Laia Torres-Masjoan cloned the Bcl2-Neurog2 plasmid for *in vivo* reprogramming. Eduardo Leyva-Díaz, Marisa Karow and Benedikt Berninger performed pioneer reprogramming experiments *in vitro* and provided the *Neurog2* reprogramming construct. María Figueres-Oñate and Laura López-Mascaraque provided the StarTrack constructs. Guillermina López-Bendito acquired funding. Álvaro Herrero-Navarro, Jose P. López-Atalaya, Benedikt Berninger and Guillermina López-Bendito wrote the paper.



# Astrocytes and neurons share region-specific transcriptional signatures that confer regional identity to neuronal reprogramming

Álvaro Herrero-Navarro<sup>1</sup>, Lorenzo Puche-Aroca<sup>1</sup>, Verónica Moreno-Juan<sup>1</sup>, Alejandro Sempere-Ferrández<sup>1,2</sup>, Ana Espinosa<sup>1</sup>, Rafael Susín<sup>1</sup>, Laia Torres-Masjoan<sup>4</sup>, Eduardo Leyva-Díaz<sup>1,3</sup>, Marisa Karow<sup>5,6</sup>, María Figueres-Oñate<sup>7,8</sup>, Laura López-Mascaraque<sup>7</sup>, José P. López-Atalaya<sup>1,†</sup>, Benedikt Berninger<sup>4,9,†</sup>, & Guillermina López-Bendito<sup>1,\*</sup>

<sup>1</sup>Instituto de Neurociencias de Alicante, Universidad Miguel Hernández-Consejo Superior de Investigaciones Científicas (UMH-CSIC), Sant Joan d'Alacant, Spain.

<sup>2</sup>Present address: Optical Approaches to Brain Function Laboratory, Istituto Italiano di Tecnologia, Via Morego 30, 16163 Genova, Italy.

<sup>3</sup>Present address: Department of Biological Sciences, Howard Hughes Medical Institute, Columbia University, New York, NY 10027, USA.

<sup>4</sup>Institute of Psychiatry, Psychology, and Neuroscience, Centre for Developmental Neurobiology, and MRC Centre for Neurodevelopmental Disorders, King's College London, SE1 1UL London, UK

<sup>5</sup>Institute of Biochemistry, Friedrich-Alexander-University Erlangen-Nürnberg, 91054 Erlangen, Germany.

<sup>6</sup>Physiological Genomics, Biomedical Center, Ludwig Maximilians University Munich, 82152 Planegg/Munich, Germany.

<sup>7</sup>Instituto Cajal, CSIC, Madrid, Spain.

<sup>8</sup>Present address: Max Planck Research Unit for Neurogenetics, Max von-Laue-Strasse 4, 60438 Frankfurt, Germany.

<sup>9</sup>Institute of Physiological Chemistry, University Medical Center Johannes Gutenberg University Mainz, 55128 Mainz, Germany.

<sup>†</sup>These authors contributed equally to this work

\*Correspondence: [g.lbendito@umh.es](mailto:g.lbendito@umh.es)

*Science Advances* 07 Apr 2021:Vol. 7, no. 15, eabe8978 DOI: 10.1126/sciadv.abe8978



## NEUROSCIENCE

## Astrocytes and neurons share region-specific transcriptional signatures that confer regional identity to neuronal reprogramming

Álvaro Herrero-Navarro<sup>1</sup>, Lorenzo Puche-Aroca<sup>1</sup>, Verónica Moreno-Juan<sup>1</sup>, Alejandro Sempere-Ferrández<sup>1†</sup>, Ana Espinosa<sup>1‡</sup>, Rafael Susín<sup>1</sup>, Laia Torres-Masjoan<sup>2</sup>, Eduardo Leyva-Díaz<sup>1§</sup>, Marisa Karow<sup>3,4</sup>, María Figueres-Oñate<sup>5||</sup>, Laura López-Mascaraque<sup>5</sup>, José P. López-Atalaya<sup>1¶</sup>, Benedikt Berninger<sup>2,6¶</sup>, Guillermina López-Bendito<sup>1\*</sup>

Neural cell diversity is essential to endow distinct brain regions with specific functions. During development, progenitors within these regions are characterized by specific gene expression programs, contributing to the generation of diversity in postmitotic neurons and astrocytes. While the region-specific molecular diversity of neurons and astrocytes is increasingly understood, whether these cells share region-specific programs remains unknown. Here, we show that in the neocortex and thalamus, neurons and astrocytes express shared region-specific transcriptional and epigenetic signatures. These signatures not only distinguish cells across these two brain regions but are also detected across substructures within regions, such as distinct thalamic nuclei, where clonal analysis reveals the existence of common nucleus-specific progenitors for neurons and astrocytes. Consistent with their shared molecular signature, regional specificity is maintained following astrocyte-to-neuron reprogramming. A detailed understanding of these regional-specific signatures may thus inform strategies for future cell-based brain repair.

## INTRODUCTION

The development of neuronal diversity is central for the organization and function of the central nervous system (CNS). This diversity is largely determined by specific transcriptional programs already expressed at the progenitor stage (1–7). These programs can undergo temporal regulation, allowing for sequential generation of different progeny from the same original progenitor (4, 8). The most drastic case of this temporal regulation occurs at the switch of progenitors from neurogenic to gliogenic competence (9). Moreover, transcriptional programs are also diversified across brain regions to reflect the positional identity of the progenitors. Pioneering work in the spinal cord suggests that the diversification of astrocytes might follow the same organizing principle of positional identity (10, 11). This notion has recently received further support by clonal analyses and single-cell transcriptomics that unveiled highly characteristic distributions of heterogeneous astroglia within and across brain regions

(12–15). However, given that neurons and astroglia are generated from the same germinal zones, they could share common molecular signatures, reflecting their origin and potentially acting to coordinate region-specific developmental features. Here, we address this possibility and report that thalamic and cortical astrocytes exhibit region-specific transcriptional and epigenetic signatures, which are shared with the neurons generated within the same thalamic or cortical progenitor domain but not beyond. These shared signatures confer a remarkable degree of regional specification for astrocyte-to-neuron reprogramming induced by the proneural factor Neurogenin 2. Last, manipulating the regional-specific code in defined astrocyte populations redirects reprogramming toward neurons of different, yet predictable, regional identity.

## RESULTS

## Shared gene expression signatures between astroglia and neurons

To test the hypothesis that astrocytes and neurons generated within the same brain region share molecular signatures unique to this region, we set out to identify differentially expressed genes (DEGs) between astrocytes of the thalamus and cortex, performed a similar analysis between thalamic and cortical neurons, and then searched for potential overlap among the two sets of DEGs. Toward this, we performed bulk RNA sequencing (RNA-seq) on astrocytes isolated from the thalamus [comprising dorsolateral geniculate (dLG), ventral posteromedial (VPM), and ventromedial geniculate (MGv) nuclei] and primary somatosensory cortex (S1) using astrocyte reporter mice (*Gfap::Gfp*) (16) at postnatal day 7 (P7) (Fig. 1A and fig. S1A) after the peak of astrogenesis (17). As for the analysis of neurons, we performed RNA-seq on neurons isolated from the thalamus at P0 using a *Gbx2-CreER::Tomato-floxed* thalamic reporter mouse, where early postmitotic thalamic neurons are labeled (fig. S1B) (18). By

<sup>1</sup>Instituto de Neurociencias, Universidad Miguel Hernández-Consejo Superior de Investigaciones Científicas (UMH-CSIC), Sant Joan d'Alacant, Spain. <sup>2</sup>Institute of Psychiatry, Psychology, and Neuroscience, Centre for Developmental Neurobiology, and MRC Centre for Neurodevelopmental Disorders, King's College London, SE1 1UL London, UK. <sup>3</sup>Institute of Biochemistry, Friedrich-Alexander-University Erlangen-Nürnberg, 91054 Erlangen, Germany. <sup>4</sup>Physiological Genomics, Biomedical Center, Ludwig Maximilians University Munich, 82152 Planegg/Munich, Germany. <sup>5</sup>Instituto Cajal, CSIC, Madrid, Spain. <sup>6</sup>Institute of Physiological Chemistry, University Medical Center Johannes Gutenberg University Mainz, 55128 Mainz, Germany. \*Corresponding author. Email: g.lbendito@umh.es

†Present address: Optical Approaches to Brain Function Laboratory, Istituto Italiano di Tecnologia, Via Morego 30, 16163 Genova, Italy.

‡Present address: AntalGenics, Quorum Building III, Scientific Park-UMH, Avda. de la Universidad s/n, 03202 Elche, Alicante, Spain.

§Present address: Department of Biological Sciences, Howard Hughes Medical Institute, Columbia University, New York, NY 10027, USA.

||Present address: Max Planck Research Unit for Neurogenetics, Max von-Laue-Strasse 4, 60438 Frankfurt, Germany.

¶These authors contributed equally to this work.

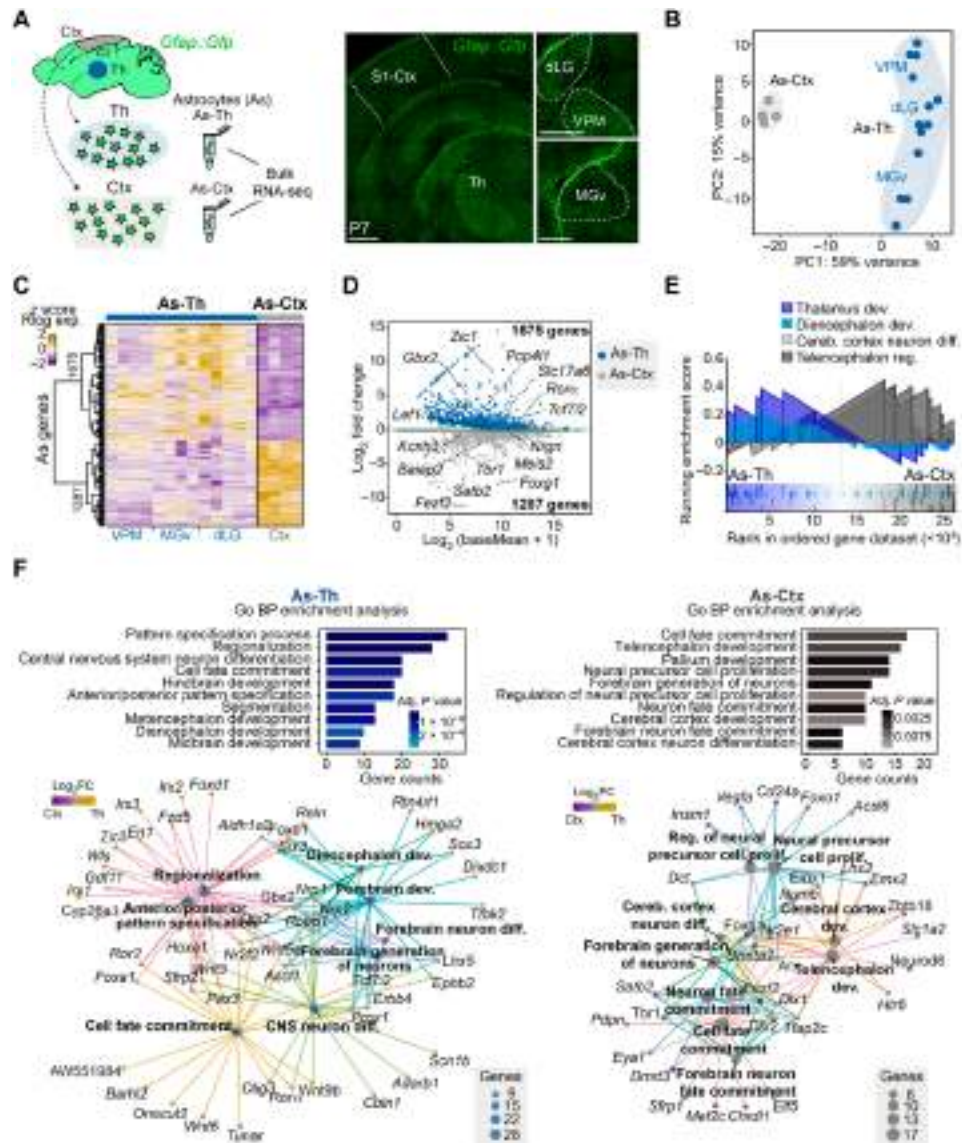


**Fig. 1. Astrocytes show region-specific transcriptomic profiles.** (A) Schematic of the RNA-seq experiments for cortical and thalamic astrocytes. Astrocytes from P7 *Gfap::Gfp* mice were fluorescence-activated cell sorting (FACS)-purified and sequenced. Right, images showing the thalamus and cortex of a *Gfap::Gfp* mouse at P7. (B) Principal components analysis (PCA) of the transcriptomes of astrocytes (As) from the thalamus (Th), including dLG ( $n = 5$  samples), VPM ( $n = 4$ ), and MGv ( $n = 4$ ), and cortex (Ctx,  $n = 4$ ) at P7. (C) Heatmap of z score normalized regularized logarithm (Rlog) expression and unbiased clustering of significantly DEGs between thalamic (As-Th) and cortical astrocytes (As-Ctx). Each row represents a gene, the columns are biological replicates, and the color code represents the normalized expression for up-regulated genes in yellow versus down-regulated genes in purple. (D) MA plot displaying DEGs. Blue and light gray dots represent thalamic and cortical DEGs with their mean normalized counts, respectively. Dark gray dots represent genes that failed to give a significant result. (E) Enrichment plots from the GSEA of two specific GO terms related to the thalamic and cortical formation. (F) GO biological process (BP) enrichment analysis of significantly DEGs in thalamic and cortical astrocytes and associated gene networks. The size of every node (enriched term) represents the number of genes enriched and the color code (yellow, high expression; purple, low expression) corresponds to the  $\log_2FC$  in DE analysis. In (A), scale bars, 400  $\mu\text{m}$ .

intersectional analysis within these astrocytic datasets, we first identified genes specifically expressed by astrocytes irrespective of their region of origin (e.g., *Aqp4* and *Aldh1l1*; fig. S1C). As for neurons, we used canonical genes conserved in all neuronal subtypes (e.g., *Rbfox3* or *Nefm*; fig. S1C) [see (19–21)]. The unambiguous expression pattern of these genes support the specificity of the *Gfap::Gfp* and *Gbx2-CreER::Tomato-floxed* mouse lines used for isolation of astrocytes and thalamic neurons, respectively (fig. S1, A to D). A principal components analysis (PCA) revealed that thalamic and

cortical astrocytes clustered according to their anatomical origins (Fig. 1B). Moreover, a differential expression analysis (DEA) revealed 1675 versus 1287 DEGs enriched in the thalamus and cortex, respectively (Fig. 1C). Among the DEGs enriched in each population, we identified several genes, including transcription factors, that are known to be highly expressed in neurons of the respective regions (Fig. 1D and table S1) (20, 22). This prompted us to perform Gene Ontology (GO) overrepresentation and gene set enrichment analyses (GSEA) of the DEGs between thalamic and cortical astrocytes,

which revealed marked differences in developmental programs and distinct region-specific molecular pathways that have been previously associated with neurons from these regions (Fig. 1, E and F). To unveil region-specific genes shared among astrocytes and neurons of the corresponding regions, we first identified the most highly DEGs enriched in thalamic and cortical neurons, by comparing RNA-seq data of neurons isolated at P0 from a thalamic reporter line (*Gbx2-CreER::Tomato-floxed*) (18) with a published dataset of P1 cortical neurons (Fig. 2A) (20). We found that genes specifically enriched in thalamic or cortical neurons were substantially overrepresented among DEGs in thalamic or cortical astrocytes, respectively. Among the 400 most DEGs in thalamic neurons, only 6% were shared with cortical astrocytes, whereas 32.75% of these genes were significantly expressed by thalamic astrocytes, albeit typically at a lower level (including *Gbx2*, *Rora*, or *Tcf7l2*; Fig. 2, B to D, and fig. S1, E to K). A

significant overlap in gene expression was also observed for cortical neurons and cortical astrocytes (17.5%), where genes such as *Fezf2* or *Foxg1* were identified in both populations. Overlap in gene expression was notably lower between cortical neurons and thalamic astrocytes (4.5%; Fig. 2, B to D).

Next, we interrogated the overlap in expression of region-specific genes between neurons and astrocytes at the single-cell level by analyzing an independent, published dataset containing single-cell transcriptomes of thalamic and cortical neurons and astrocytes from juvenile/young adult mice (fig. S2; fig. S3, A and B; and table S2) (23). The analysis of these single-cell data fully confirmed the existence of region-specific gene expression programs shared between astrocytes and neurons of thalamic and cortical origin, respectively (Fig. 2, E to G, and fig. S3, C to G). Notably, among the DEGs at the single-cell level shared between neurons and astrocytes (247 for the

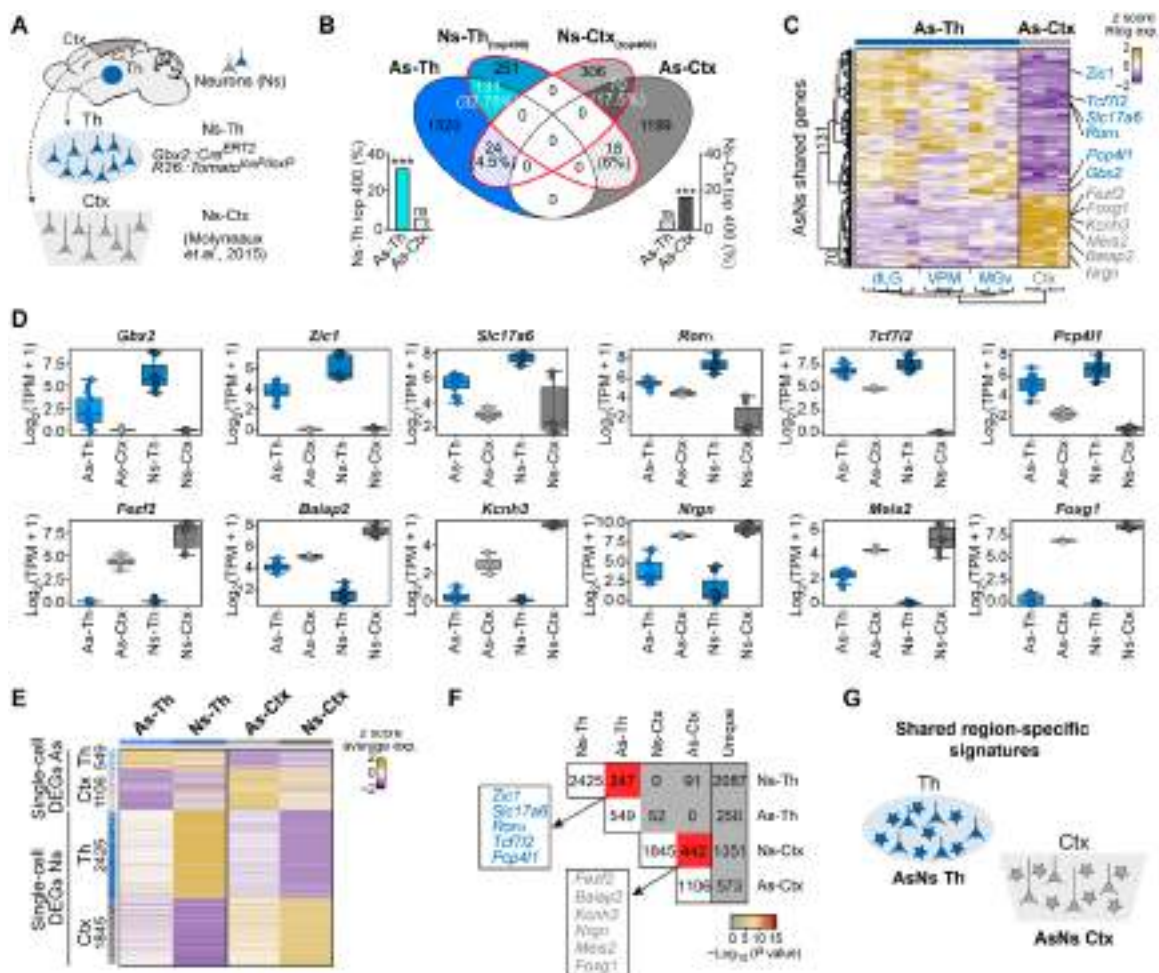


**Fig. 2. Astrocytes and neurons share region-specific transcriptome profiles.** (A) Schematic of the RNA-seq experiments for comparing thalamic and cortical neurons. Thalamic neurons were obtained from *Gbx2-Cre::Tomato-floxed* P0 mice and cortical neurons from publicly available datasets (20). Ns-Th included dLG ( $n = 4$ ), VPM ( $n = 4$ ), and MGv ( $n = 3$ ), and Ns-Ctx ( $n = 6$ ). (B) Venn diagram showing the genes that overlap between astrocytes (As) and neurons (Ns) in both the thalamus and cortex. Bar plots represent the percentage of the enriched genes shared between populations. (C) Heatmap showing overlapping genes between As and Ns in the thalamus and cortex. (D) Box plots showing expression levels of selected region-specific genes shared between neurons and astrocytes of the thalamus (top) or the cortex (bottom). TPM, transcripts per million. (E) Heatmap of the z score of average expression levels of DEGs at the single-cell level, identified by comparing cell types among different regions of origin (As-Th versus As-Ctx; Ns-Th versus Ns-Ctx) from publicly available data (23). (F) Comparison matrix of the number of shared specific gene lists between As and Ns datasets of every specific region. Color code according to significance of overlap. (G) Schematic of the main conclusion of the experiments. Data are plotted with box-and-whisker plots, which give the median, 25th and 75th percentiles, and range. Dots in (D) represent every single value.

thalamus and 442 for the cortex), we found numerous genes known to confer regional neuronal identity (e.g., *Rora*, *Tcf7l2*, *Fezf2*, or *Foxg1*), as observed in the bulk RNA-seq dataset. These single-cell data demonstrate that the shared region-specific transcriptional signature is not a transient developmental feature but maintained well beyond the first postnatal week.

Last, we conducted two additional experiments to validate the expression of region-specific “neuronal” genes in astrocytes. First, we performed fluorescence in situ hybridization (FISH) in fixed slices from *Gfap::Gfp* brains at P7 and confirmed the expression, in a region-specific manner, of shared genes in astrocytes (GFP<sup>+</sup> cells) (fig. S4, A and B). This expression was mainly found at the level of mRNA, as the corresponding proteins were only detected in a low percentage of the astrocytes, at least for the genes analyzed (fig. S4C), which suggests that posttranscriptional regulations might take place (24). Second, we isolated, purified, and cultured astrocytes from the thalamus or cortex and performed quantitative polymerase chain reaction (qPCR) for region-specific genes, confirming the expression of shared genes in astrocytes (fig. S4, D and E). Thus, single-cell RNA-seq (scRNA-seq), FISH, and qPCR provide strong support for the specificity of the detection of neuronal genes in astrocytes, arguing against neuronal contamination of the astrocyte datasets.

We next asked whether region-specific gene expression programs can be identified at the level of individual regional subdivisions such as those of sensory thalamic nuclei. Thus, we compared the transcriptomes of astrocytes and neurons from the three main sensory thalamic nuclei (dLG, VPM, and MGv; Fig. 3A). PCA identified three well-defined clusters corresponding to each nucleus in both astrocytes and neurons, supporting the notion that the identity of each thalamic nucleus is encoded transcriptionally in a cell type-independent manner (Fig. 3, B and C). Hence, the nucleus-specific DEGs of astrocytes exhibited a significant overlap with those of the neurons from the same nucleus (e.g., *Sp9* for dLG or *Crabp2* for MGv; Fig. 3, D and E, and tables S3 and S4), although the expression levels of these genes were notably lower in the astrocytic populations (Fig. 3F). Our single-cell data analysis also revealed a region-specific pattern of shared genes between astrocytes and neurons along the anteroposterior axis of the cerebral cortex (fig. S5 and table S5), supporting a generalization of the existence of region- and subregion-specific shared transcriptional programs between these two major cell types in the mouse brain.

### Thalamic progenitor clones are nucleus specific

Next, we investigated whether the significant gene expression overlap between postmitotic astrocytes and neurons from the same region reflects a common clonal origin during embryonic development. This would imply that within the thalamus, cells belonging to the same clone should not disperse beyond nuclear boundaries. To test this hypothesis, we first analyzed the distribution of astrocytes originating from single clones across thalamic sensory nuclei. We tracked astrocyte clones arising from embryonic day 11.5 (E11.5) progenitors by electroporating a battery of plasmids encoding distinct fluorophores under the control of the *Gfap* promoter, following transposase-mediated integration (“StarTrack”) (12), and analyzed the dispersion of each clone at P8 (Fig. 4, A and B, and fig. S6A). This revealed that clonally related astrocytes remain within the boundaries of a given nucleus with little dispersion to other nuclei, even in the case of larger clones (>10 cells) (Fig. 4C and fig. S6, B and C). Next, we addressed the question of whether thalamic progenitors that

generate astrocytes also produce neurons and, if so, whether these neurons stay within the same nuclear boundaries as their sibling astrocytes. Thalamic clones containing neuronal and/or nonneuronal cells were tracked by using the same set of fluorophores under the control of a ubiquitously expressed promoter (Fig. 4, D and E, and fig. S6, D and E) (25). While we found 39% of clones consisting only of neurons or glia, the majority (61%) were mixed, containing similar proportions of neurons and glia (Fig. 4F and fig. S6F). We found that mixed clones covered territories that largely respected nuclear boundaries, although neurons exhibited a wider range of dispersion (Fig. 4, G and H, and fig. S6G), extending and confirming previous studies (26, 27). Our data suggest that the overlap in region-specific gene expression between neurons and astrocytes of each sensory thalamic nucleus is the result of their common clonal origin together with the limited spatial dispersion of clonally related cells and may indicate that positional information is retained from an early progenitor stage onward.

### Astrocytes reprogram into region-specific neurons

Since forebrain astrocytes and neurons share region-specific gene expression, we hypothesized that such molecular signature could instruct transcription factor–induced reprogramming of astrocytes toward an identity akin to their sibling neurons. To test this hypothesis, we injected a retrovirus encoding the proneural gene *Neurogenin 2* (*Neurog2*) and the cell death regulator *Bcl2* (28) into the somatosensory cortex and thalamus of P3 mice (Fig. 5A). At this developmental stage, retroviruses only transduce proliferative glia (17). Transduction with a retrovirus encoding *Bcl2* and *Gfp* alone, as control, resulted in labeling of glial cells. In contrast, transduction with *Neurog2*- and *Bcl2*-encoding retrovirus resulted in the appearance of numerous induced neurons (fig. S7, A and B). Time course analysis of the transduced cells demonstrated the gradual reprogramming of glia into neurons via a doublecortin (DCX)–positive immature neuronal stage in vivo (fig. S7, C to H). At 3 days post infection (dpi), the vast majority of the transduced cells (GFP<sup>+</sup>) were positive for the astrocytic marker *Aldh1l1* and negative for the neuronal markers *NeuN* and *DCX*. Furthermore, we found that more than 90% of the transduced cells were also positive for 5-bromo-2'-deoxyuridine (BrdU), revealing that they are proliferating cells at the time of retroviral transduction (fig. S7D). After 7 and 14 dpi, the number of transduced cells positive for *DCX* or *NeuN* increased progressively. These *DCX*- or *NeuN*-positive cells were also BrdU positive, demonstrating again that they had been generated by the time of retroviral transduction and that *DCX* expression was not a result of reexpression in embryonically generated neurons (fig. S7, E to H). Consistent with our hypothesis, in vivo induced neurons expressed markers specific for a thalamic (*Lef1* and *Rora*) or cortical (*Tbr1* and *Ctip2*) neuronal identity despite the fact that they were induced with the same transcription factor (Fig. 5, B and C).

Our data suggest that reprogramming of astrocytes into region-specific neurons is a consequence of their shared gene expression through a common lineage. However, it does not exclude the possibility that region-specific reprogramming is influenced by environmental signals provided by other local cells. To test this, we cultured astrocytes from the thalamus and cortex and examined their newly acquired neuronal identity for region-specific gene expression following reprogramming by *Neurog2* (fig. S8, A and B). As observed in vivo, thalamic and cortical induced neurons exhibited signatures of the thalamus and cortex, respectively, as shown by the differential

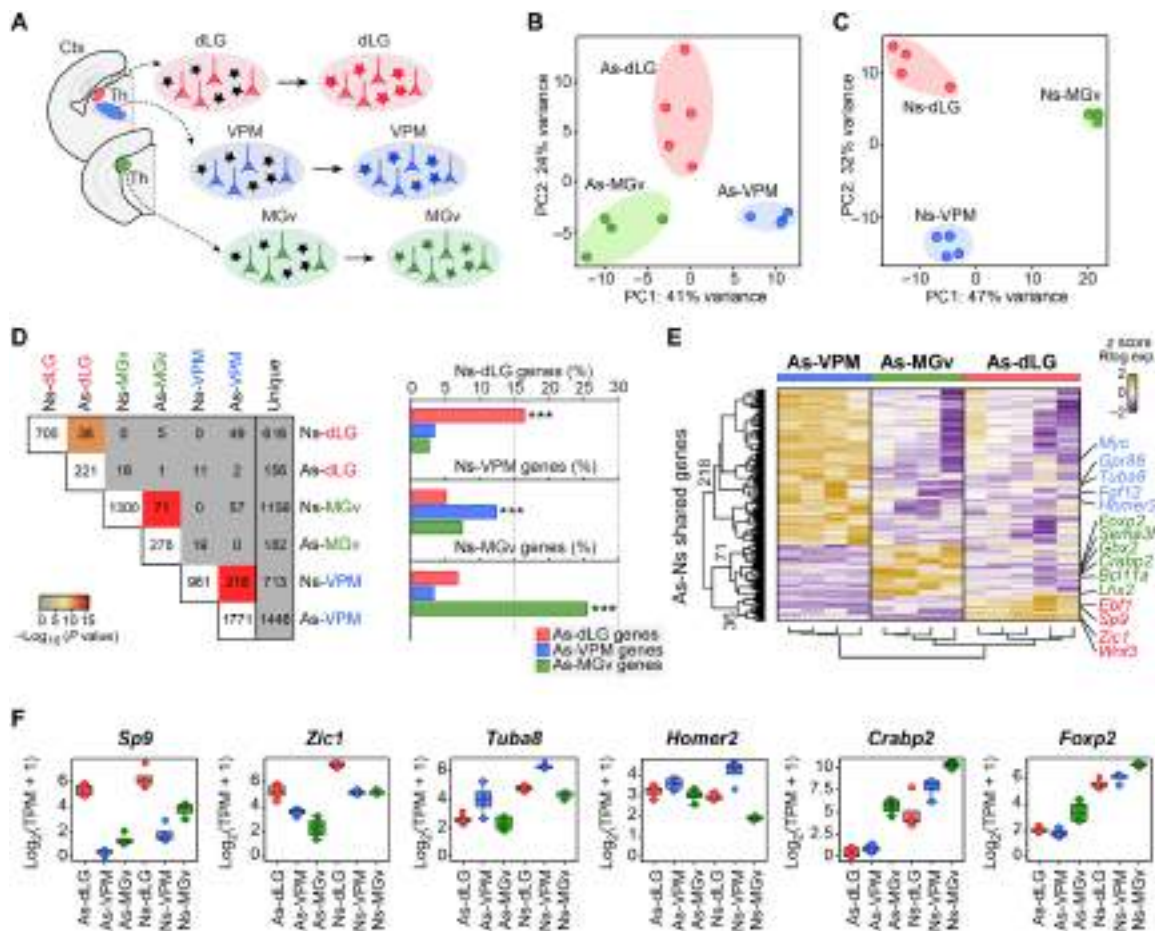


**Fig. 3. Sensory-modality thalamic astrocytes and neurons express common specific genes for every nucleus.** (A) Schematic of the RNA-seq experiments for comparing neurons and astrocytes from the sensory thalamic nuclei (dLG, VPM, and MGv) and main conclusion obtained. (B) PCA of transcriptomes from astrocytes (As) isolated from the distinct sensory-modality thalamic nuclei [dLG ( $n=5$ ), VPM ( $n=4$ ), and MGv ( $n=4$ )] at P7. (C) PCA of transcriptomes of neurons (Ns) from the distinct sensory-modality thalamic nuclei [dLG ( $n=4$ ), VPM ( $n=4$ ), and MGv ( $n=3$ )] at P0. (D) Left, comparison matrix of the number of shared specific gene lists between neurons and astrocytes datasets of every thalamic nuclei. Color code according to significance of overlap. Right, bar plots representing the percentage of gene overlap between As and Ns from each thalamic nucleus. (E) Heatmap showing the overlapping DEGs between As and Ns in each nucleus. Each column represents a biological replicate and the color code represents the z score normalized expression (up-regulated genes in yellow, down-regulated genes in purple). (F) Box plots showing expression levels of nuclei-specific shared genes between astrocytes and neurons in the distinct sensory-modality thalamic nuclei. TMP, transcripts per million. Data are plotted with box-and-whisker plots, which give the median, 25th and 75th percentiles, and range. Dots in (F) represent every single value. \*\*\* $P < 0.0005$ .

expression of thalamic markers such as *Slc17a6* (*vGlut2*), *Rora*, *Gbx2*, *Pou2f2*, or *Lef1* or cortical markers such as *Tbr1* or *Ctip2* (fig. S8, C to G). To exclude a prominent role of the environment in specifying the regional identity of induced neurons, we cocultured thalamic or cortical astrocytes undergoing reprogramming with neurons or astrocytes from the cortex or thalamus, respectively. Neurons induced from thalamic astrocytes expressed thalamic markers, irrespective of whether they had been cultured alone or with cortical cells. Conversely, cortical astrocytes gave rise to neurons expressing cortical markers irrespective of the culture conditions (Fig. 5, D to F). These experiments revealed that the regional identity of induced neurons is largely cell autonomous.

Last, as astrocytes and neurons from distinct thalamic sensory nuclei share expression of nucleus-specific genes, we hypothesized that reprogramming of thalamic astrocytes may yield neurons with nucleus-specific signatures. To this end, we isolated and reprogrammed astrocytes from dLG, VPM, and MGv in vitro with Neurog2 (Fig. 5G).

We found that induced neurons derived from dLG astrocytes expressed dLG-specific genes *Sp9* and *Hs6st2*, while those derived from MGv astrocytes expressed MGv-specific genes *Crabp2* and *Tshz1*. Last, induced neurons of VPM astrocyte origin expressed the VPM marker *Cck* (Fig. 5H) (22). Together, these results show that Neurog2 triggers specific neuronal gene expression in astrocytes that reflects their place of origin.

### Gbx2 respecifies cortical astrocytes toward thalamic fate

The aforementioned results strongly suggest that transcriptional signatures shared between neurons and astrocytes drive the regional specification of the latter during neuronal reprogramming. To directly test this, we examined whether coexpression of a thalamic fate determinant *Gbx2* (29), a factor being shared between astrocytes and neurons of the thalamus, could induce an early and fast redirection of neuronal reprogramming of cortical astrocytes toward a thalamic identity (Fig. 6A). Whereas in cortical astrocytes, expression

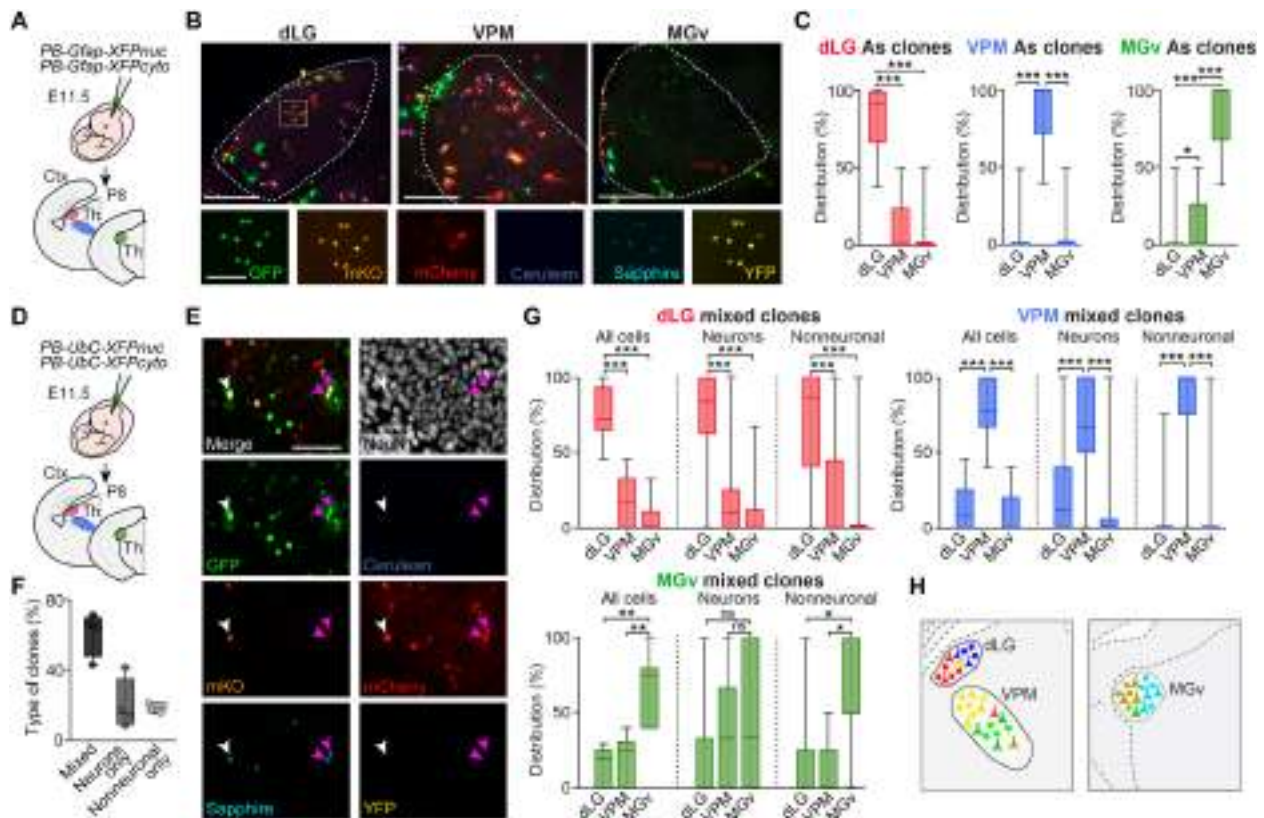


**Fig. 4. Clonally related astrocytes and neurons remain within the same nuclear boundaries.** (A) Experimental design for the analysis of astrocytic clones in the sensory nuclei (dLG, VPM, and MGv). A cocktail of integrative plasmids encoding six different fluorescent proteins under the *Gfap* promoter (*GFAP-StarTrack*) was electroporated in the third ventricle at E11.5. (B) Thalamic astrocytes labeled with the *GFAP-StarTrack* constructs at P8. Insets show the expression of each fluorescent reporter in a dLG astrocyte clone (white square). (C) Quantification of the dispersion of the clonally related astrocytes ( $n = 320$  clones from five electroporated animals). (D) Experimental design for the study of neuronal and nonneuronal clonal cells with the *UbC-StarTrack* constructs. (E) Example of a neuron (white arrows) and two astrocytes (purple arrows) from the VPM coming from the same progenitor, thus sharing the same color code. (F) Three types of clones were analyzed clones based on their cell-type composition: mixed clones (containing neurons and nonneuronal cells), clones with neurons only, or clones with nonneuronal cells only ( $n = 4$  electroporated animals). (G) Quantification of the dispersion of clonally related neuronal and nonneuronal cells from mixed clones, in the different thalamic sensory nuclei ( $n = 130$  clones from four electroporated animals). (H) Schema representing the specificity in the nuclei-dependent localization of clonal cells. Cells coming from the same progenitor are colored with the same color. Note that most clonally related cells respect the nuclei segregation and only few cells are dispersed. Data are plotted with box-and-whisker plots, which give the median, 25th and 75th percentiles, and range. Scale bars, 100  $\mu\text{m}$ . ns, not significant; \* $P < 0.05$ , \*\* $P < 0.005$ , and \*\*\* $P < 0.0005$ .

of *Neurog2* for 2 days induced the expression of the cortical neuron fate determinants *Tbr1* and *Ctip2*, coexpression of *Gbx2* strongly suppressed this. Moreover, combined expression of *Neurog2* and *Gbx2* increased thalamic signature genes such as *Pou2f2* and *Slc17a6* (*vGlut2*) in cortical astrocytes (Fig. 6B). These data provide strong support for the partial redirection of neuronal reprogramming toward a thalamic identity (Fig. 6C). In thalamic astrocytes, by contrast, *Neurog2* sufficed for inducing significant expression of *Pou2f2* and *Slc17a6* expression (Fig. 6B). Genes that displayed differential regulation by *Neurog2* with or without *Gbx2* (*Slc17a6*, *Pou2f2*, *Tbr1*, and *Ctip2*) exhibited an epigenetically poised state in cortical or thalamic astrocytes, as determined by the ratio of active (H3K4me3) and repressive (H3K27me3) histone marks in their proximal regulatory elements (Fig. 6D and figs. S9, A to C, and S10, A and B). In contrast, non-responsive genes (*Fzf2*, *Rora*, and *Lef1*) exhibited origin-dependent baseline expression both transcriptionally and epigenetically in thalamic and cortical astrocytes (Fig. 6, B to D; fig. S9, A to C; and fig. S10, A and B).

Last, we addressed the question of whether a similar epigenetically poised state might explain the differential induction of nuclei-specific neuronal genes in astrocytes of distinct thalamic territories. To this end, we first compared basal expression levels and presence of active (H3K4me3) and repressive (H3K27me3) epigenetic marks at proximal regulatory elements of these genes, known to be differentially expressed in dLG, VPM, and MGv neurons (Fig. 3) (22). Intriguingly, irrespective of the baseline expression level, these genes exhibited an active (*Sp9*, *Crabp2*, and *Tshz1*) or poised/less repressed (*Hs6st2* and *Cck*) epigenetic state of their proximal regulatory elements, consistent with their nuclear origin (Fig. 6E and figs. S9D and S10, C and D). Nucleus-specific epigenetic priming might explain the observed differential transcriptional responsiveness to *Neurog2* of genes whose levels of transcription are indistinguishable across nuclei before reprogramming. Future genome-wide analysis will be required to reveal the general importance of epigenetically poised states in dictating the region-specific gene expression following reprogramming.

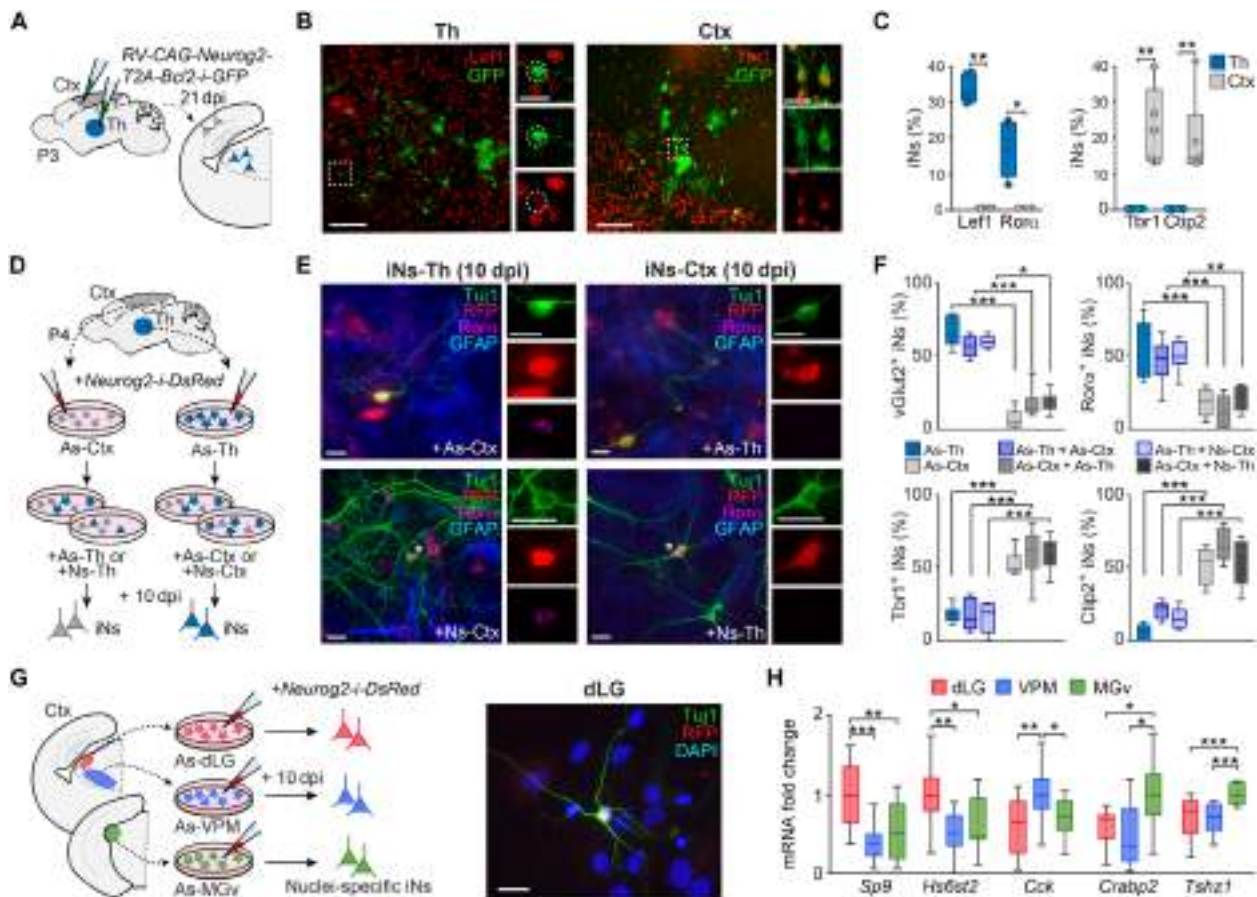


**Fig. 5. Astrocytes are reprogrammed into region-specific neurons.** (A) Experimental design for the in vivo reprogramming. Retrovirus encoding *Neurog2* and *Bcl2* or only *Bcl2* were injected in the thalamus and cortex of P3 animals. (B) Immunofluorescence for thalamic and cortical markers in iNs reprogrammed from cortical or thalamic astrocytes in vivo. (C) Percentage of iNs expressing thalamic or cortical markers after reprogramming in vivo ( $n = 4$  to 6 injected mice). (D) Experimental design for assessing the influence of the environment on the induced neurons identity. Isolated cortical or thalamic astrocytes were infected and then cocultured with thalamic or cortical astrocytes or neurons. (E) Immunostaining for the thalamic marker *Rora* in cortical or thalamic iNs ( $RFP^+/Tuj1^+$ ) in the different conditions. (F) Quantification of the percentage of iNs generated from cortical or thalamic astrocytes that express *vGlut2*, *Rora*, *Tbr1*, or *Ctbp2* in control conditions or when mixed with astrocytes or neurons from the thalamus or the cortex, respectively ( $n = 6$  to 14 independent cultures per condition). (G) Left, experimental design. Astrocytes from dLG, VPM, and MGv were isolated, cultured, and infected with *Neurog2* retrovirus. Right, image of an iN from dLG astrocytes at 10 days post infection (dpi). (H) Reverse transcription (RT)-qPCR showing the expression of specific neuronal genes in the iNs after 10 dpi ( $n = 10$  to 14 independent cultures per condition). Data are plotted with box-and-whisker plots, which give the median, 25th and 75th percentiles, and range. Dots in (C) represent every single value. Scale bars, 100  $\mu\text{m}$  in (B) (insets, 25  $\mu\text{m}$ ) and 25  $\mu\text{m}$  in (E) and (G). \* $P < 0.05$ , \*\* $P < 0.005$ , and \*\*\* $P < 0.0005$ .

## DISCUSSION

Using genome-wide analysis, we show that astrocytes of different brain regions actively transcribe genes that also correspond to regional genes in neurons. This remarkable relatedness between astrocytes and neurons from the same brain region correlates with their shared clonal origin, as shown for distinct sensory nuclei of the thalamus. Furthermore, region-specific molecular signatures create a strong bias intrinsic to astrocytes toward generating neurons of matching regional identity when reprogrammed by the proneural factor *Neurog2*. This latter finding is in line with reprogramming of cortical astrocytes into neurons with layer-specific properties in vivo (30), where a tight lineage relationship between starting and target cell is likely to exist. The transcriptional context of the starting cell might even account for acquisition of specific neuronal fates where region-specific determinants may be expressed more coincidentally, such as fibroblast conversion into retinal photoreceptors (31).

Despite their common developmental origin, neurons and astrocytes constitute cell types easily distinguishable by their morphological and electrophysiological properties. However, our study reveals that these two cell types show an unexpected overlap in the expression of genes that confer regional identity. Such overlap can be found at the single-cell level and extends into adulthood. Among the shared genes, there was a substantial amount of transcription factors, many of which play well-described roles in neuron subtype specification (e.g., *Gbx2*, *Lef1*, *Fefz2*, and *Tbr1*) (29, 32–34). The physiological function in astrocytes of the shared region-specific genes remains to be determined. Future experiments should decipher whether these genes may adopt different functions in astrocytes as compared to neurons or whether their shared expression might act as a code to facilitate region-specific interactions of astrocytes with their sibling neurons (35). While these scenarios are not mutually exclusive, the latter may provide an attractive mechanism by which

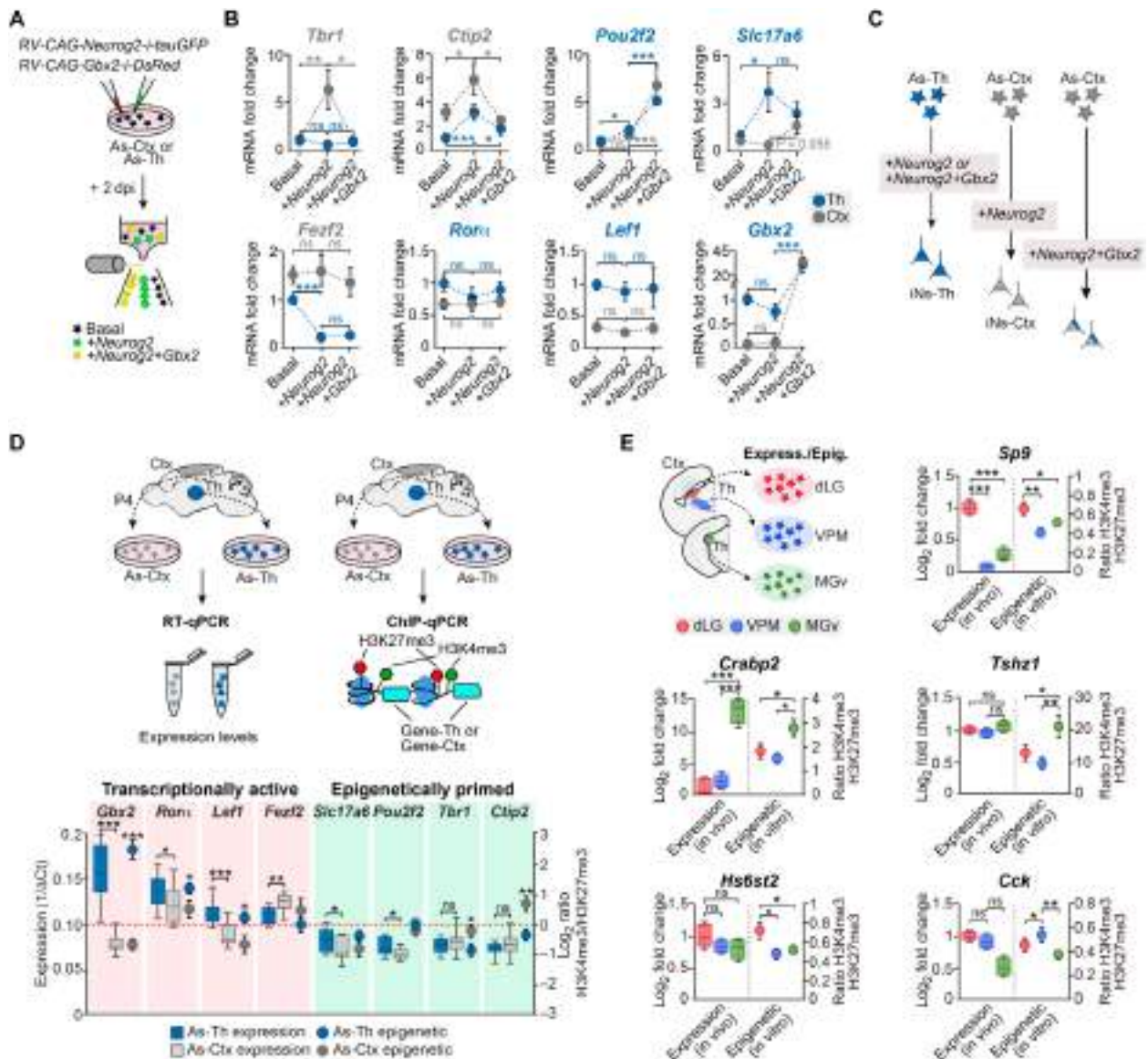


**Fig. 6. Poised epigenetic state of region-specific gene expression in astrocytes.** (A) Experimental design. Astrocytes from the thalamus and cortex were cultured and infected with either *Neurog2-i-Gfp* retrovirus alone or both *Neurog2-i-Gfp* and *Gbx2-i-DsRed*. After 2 days, astrocytes were FACS-purified based on the presence of the reporter protein in three groups (noninfected, infected only with *Neurog2*, or infected with *Neurog2* and *Gbx2*). (B) Quantification of specific gene expression by RT-qPCR in astrocytes in basal conditions and 2 days after the overexpression of *Neurog2* alone or with a thalamic-specific gene (*Gbx2*) ( $n = 6$  to 14 independent cultures per condition). Data are means  $\pm$  SEM. (C) Schematic conclusion of the experiment. (D) Astrocytes from the thalamus and cortex were isolated, and the expression levels of some region-specific genes were assessed by RT-qPCR or ChIP-qPCR. Box-and-whisker plots represent the basal expression levels of the studied genes in thalamic and cortical astrocytes (left axis), and dots show the means  $\pm$  SEM of the epigenetic state of the promoter of those genes, in terms of the presence of two histone marks, H3K4me3 and H3K27me3 (right axis) ( $n = 12$  to 23 independent ChIP samples per condition). The red dashed line indicates the point where H3K4me3 and H3K27me3 marks are present at the same level. (E) Box-and-whisker plots showing the H3K4me3 and H3K27me3 ratio in vitro (left axis) ( $n = 14$  to 18 independent ChIP samples per condition) and the basal in vivo expression of neuronal specific genes in thalamic astrocytes from each nucleus (right axis). ns, not significant;  $*P < 0.05$ ,  $**P < 0.005$ , and  $***P < 0.0005$ .

neurons could modulate the spatial distribution of astrocytes (13). Our clonal analyses reveal that neurons and sibling astrocytes originating from the same thalamic progenitor clone populate very similar territories, respecting boundaries among thalamic nuclei, extending earlier observations of the existence of nucleus-specific progenitor domains in the thalamus (26, 27, 36). Recent single-cell spatial transcriptomic mapping has revealed that in the cortex, astrocytes exhibit heterogeneity that does not follow neuronal layering (13).

However, it is not shown whether neurons and astrocytes populating the same neuronal layer are more likely to be clonally related than those of distinct layers. Nevertheless, cortical regional identity is clearly computed along the anteroposterior and mediolateral axes (19), and, indeed, our single-cell data analysis shows that gene expression profiles are shared by astrocytes and neurons along the anteroposterior and mediolateral axes and, thus, it may serve as a mechanism to impart cortical areal identity also to astrocytes, as

observed in the thalamus. Most likely, different dimensions of gene expression patterns underlie the unexpected molecular and spatial heterogeneity of astrocytes in the CNS.

It seems plausible that the shared region-specific gene expression is accounted for by epigenetic signatures inherited from a common progenitor and maintained throughout postmitotic development. Our data provide evidence for region-specific differences in the epigenetic state of regulatory elements of these genes in cortical and thalamic astrocytes, even up to the level of thalamic nuclear divisions. Conversely, these region-specific genes apparently escape the long-term epigenetic repression that occurs at neuronal gene loci at the developmental switch from neurogenesis to gliogenesis (37, 38). The epigenetic configuration at region-specific genes might function as a latent mechanism to keep some neuronal expressed genes in a “poised state” in astrocytes, which may become activated by reprogramming factors such as shown here. The fact that epigenetic configurations are heritable through cell divisions (4, 38, 39) might confer astrocytes with a specific and long-lasting regional differentiation potential as may occur during injury-induced neurogenesis (40, 41). Last, the fine-grained heterogeneity of astrocytes between and within brain regions [this study and (10, 13)] may provide a basis for reconstructing diseased brain circuits that require the generation of multiple neuron types (30, 42), with a minimal number of molecular manipulations.

## MATERIALS AND METHODS

### Mouse strains

All transgenic animals used in this study were maintained on ICR/CD-1, FVB/N-Tg, or C57BL/6J genetic backgrounds and genotyped by PCR. The day of the vaginal plug was stipulated as E0.5. The *Gfap::Gfp* line (16) (the Jackson Laboratory, stock number 003257) was in an FVB/N-Tg genetic background, the *Gad67::Gfp* line (43) was in C57BL/6J, and the  $R26^{tdTomato}$  Cre-dependent line (the Jackson Laboratory, stock number 007908) and the *Gbx2<sup>CreERT2/+</sup>* mouse line (18) were in an ICR/CD-1 genetic background. Tamoxifen induction of Cre recombinase in the double-mutant embryos (*Gbx2<sup>CreERT2/+</sup>::R26<sup>tdTomato</sup>*) was performed as previously described (44). The Committee on Animal Research at the University Miguel Hernández approved all the animal procedures, which were carried out in compliance with Spanish and European Union regulations.

### Isolation of astrocytes and neurons for RNA-seq

The brains (four brains were pooled for each sample) were extracted in ice-cold KREBS solution and cut in the vibratome in 300- $\mu$ m slices, and cells were dissociated as in a previous publication (22). Thalamic nuclei (dLG, VPM, and MGv) and somatosensory cortex (S1) were dissected and pooled in cold dissociation medium [20 mM glucose, 0.8 mM kynurenic acid, 0.05 mM D,L-2-amino-5-phosphonovaleric acid (APV), penicillin (50 U/ml), streptomycin (0.05 mg/ml), 0.09 M Na<sub>2</sub>SO<sub>4</sub>, 0.03 M K<sub>2</sub>SO<sub>4</sub>, and 0.014 M MgCl<sub>2</sub>]. The tissue was transferred to sterile conditions and enzymatically digested in dissociation medium supplied with L-cysteine (0.16 mg/ml) and 70 U papain (Sigma-Aldrich) set to pH 7.35, at 37°C for 30 min with repeated shaking. The enzyme was then inhibited with dissociation medium containing ovomucoid (0.1 mg/ml) (Sigma-Aldrich) and bovine serum albumin (BSA) (0.1 mg/ml) set to pH 7.35, at room temperature. Tissue was transferred to iced Opti-MEM (Life Technologies) supplied with 20 mM glucose, 0.4 mM kynurenic acid, and 0.025 mM

APV and mechanically dissociated until a single-cell suspension was obtained. Cells were concentrated by centrifugation with 850 rpm for 5 min and filtered through a cell strainer (BD Falcon). The genetically labeled live cells were separated based on green or red fluorescence intensity using fluorescence-activated cell sorting (FACSARIA III, BD). FACS-purified cells were collected directly in lysis buffer of the RNeasy Micro Kit (Qiagen, no. 74004) that was used to recover total RNA according to the manufacturer’s instructions. RNA quality for all samples was measured on an Agilent Bioanalyzer 2100 system. All samples with RNA Integrity Number (RIN) > 7 were used as input to library construction.

### Library preparation and RNA-seq

Library construction and sequencing were performed at the CNAG-CRG (Centro Nacional de Análisis Genómico) genomics core facility (Barcelona, Spain). Briefly, cDNA multiplex libraries were prepared using SMARTer Ultra Low RNA Kit v4 (Takara, no. 634894) and NEBNext Ultra DNA Library Prep for Illumina according to the manufacturer’s instructions (NEB, no. E7645). Libraries were sequenced together in a single flow cell on an Illumina HiSeq 2500 platform using v4 chemistry in 1 × 50 bp (base pair) single-end mode. A minimum of 25 million reads were generated from each library.

### Bioinformatic analysis of the RNA-seq

RNA-seq analyses were performed as previously described (45) with minor modifications: Quality control of the raw data was performed with FastQC (v0.11.7) and sequenced dataset adapters were trimmed using Cutadapt (v2.3) and Trim Galore (v0.6.1). RNA-seq reads were mapped to the mouse genome (GRCm.38.p6/mm10) using STAR (v2.7.0d), and SAM/BAM files were further processed using SAMtools (v1.9). Aligned reads were counted and assigned to genes using Ensembl release 95 gene annotation and FeatureCounts, Subread (v1.6.4) (46). Normalization of read counts and differential expression analyses were performed using DESeq2 (v1.22.2) and Bioconductor (v3.8) in the R statistical computing and graphics platform (v3.5.1 “Feather Spray”).

In the analysis datasets of cortical astrocytes and thalamic astrocytes and neurons generated for this study, significantly DEGs were identified using statistical significance threshold [Benjamini-Hochberg (BH)-adjusted  $P$  value < 0.1] and absolute log<sub>2</sub> fold change (log<sub>2</sub>FC) > 0 using shrunken log<sub>2</sub>FC using the adaptive  $t$  prior Bayesian shrinkage estimator “apeglm” (tables S1, S3, and S4) (47). To identify the top most differentially enriched genes between cortical and thalamic neurons, we used data generated in this study for thalamic neurons (P0) and publicly available dataset for cortical neurons (P1) from a previously published study (GSE63482) (20). Datasets from (20) consist of RNA-seq profiles of multiple classes of FACS-purified cortical neurons from ICR/CD-1 mice: callosal projecting neurons (CPN,  $n = 2$ ), corticothalamic projecting neurons (CThPN,  $n = 2$ ), and subcerebral projecting neurons (ScPN,  $n = 2$ ) (20). Neuronal datasets from the cortex and thalamus were aligned from the raw sequence, and gene counts were generated using the same pipeline as indicated previously. Gene counts were normalized using the median of ratios method in DESeq2 R package, and the ratio between gene counts (regularized logarithm transformation of the normalized counts) were used to identify the top 400 most differentially enriched genes between cortical and thalamic neurons. Hypergeometric test (one-sided Fisher’s exact test) was performed to test independence between lists of enriched or significantly DEGs from

neurons and astrocytes from different brain regions and to obtain estimated odds ratios. RNA-seq coverage tracks for selected genes were generated using Integrative Genomics Viewer (IGV) (v2.4.14) and plotted in a 5' to 3' direction. Hierarchical clustering analysis was performed using “Manhattan” distance and “Ward.2” clustering method metrics to visualize significantly up-regulated and down-regulated genes. In the functional enrichment analysis of the datasets from astrocytes, a more restrictive filtering criterion was used to detect high significantly DEG based on simultaneous threshold of BH-adjusted  $P$  value  $< 0.1$  and absolute  $\log_2FC > 0.322$ . This analysis revealed 508 versus 444 DEGs enriched in the thalamus and cortex, respectively. The GO overrepresentation analysis and GSEA were performed using clusterProfiler (v3.10.1) (48). All enriched terms were considered significant at adjusted  $P$  values by BH with  $P$  value cutoff  $< 0.01$  and  $0.1$ , in the GO overrepresentation analysis and GSEA, respectively. The reference gene set used to perform the analysis was C5 (GO Biological Process) collection from the Molecular Signatures Database (MSigDB) (v6.2).

### Bioinformatic analysis of the scRNA-seq

We analyzed recent work from scRNA-seq to interrogate thalamic and cortical cellular heterogeneity (23). The sequence data are publicly available at the National Center for Biotechnology Information (NCBI) Sequence Read Archive (SRA) under accession SRP135960 (23). Briefly, scRNA-seq datasets (postfiltered count matrices) for the thalamus and cortex were downloaded from the associated wiki and processed with Seurat R package (v3.1.4) (49). First, we performed quality control analysis that confirmed that the data were of high quality. All cells had more than 600 detected molecules (UMIs) and the proportion of mitochondrial reads was below 5% for the vast majority of cells (see fig. S2, A and B). Next, data were preprocessed (log normalization and scaling) before performing linear dimensional reduction (PCA). Graph-based clustering approach using the top 30 principal components was used to identify cell populations (resolution was fixed to 0.8). FindAllMarkers function with default parameters was used to identify gene markers for each cluster and to assign cell-type identity to clusters (see fig. S2, C and D).

Cortical and thalamic scRNA-seq datasets were subsequently integrated as previously described (50). The UMAP (Uniform Manifold Approximation and Projection) algorithm was used to nonlinear dimensionality reduction, visualization, and exploratory analysis of the datasets. Differential expression analyses between thalamic and cortical neurons and astrocytes were performed using the FindMarkers function based on the nonparametric Wilcoxon rank sum test with the following parameters ( $\logFC.threshold = 0.1$ ;  $min.pct = 0$ ). Genes with BH-adjusted  $P$  value  $< 0.1$  were considered significantly differentially expressed (tables S2 and S5).

### In utero electroporation of StarTrack vectors

For in utero electroporation, a procedure previously described was followed (51). Pregnant females (E11.5) were deeply anesthetized with isoflurane to perform laparotomies. The embryos were exposed, and the third ventricles of the embryonic brains were visualized through the uterus with an optic fiber light source. The combination of the plasmids of the StarTrack method at a final concentration of  $2 \mu\text{g}/\mu\text{l}$  was mixed with 0.1% Fast Green (Sigma-Aldrich), as previously described (12, 25). The plasmids used consisted of the coding sequence of six fluorescent proteins (EGFP, mCherry, mKusabian Orange, mTSapphire, mCerulean, and EYFP) subcloned under the

regulation of the GFAP or UbC promoters for targeting specifically the astrocytes or all the cell types. Each reporter gene could be directed to the cytoplasm (PB-GFAP/UbC-XFP) or to the nucleus of the cell by fusing it with the H2B histone protein (PB-GFAP/UbC-H2B-XFP). Constructs were flanked by PiggyBac sequences to be inserted into the genome of the targeted cell by a PiggyBac transposase. The plasmids were injected into the third cerebral ventricle by an injector (Nanoliter 2010, WPI). For electroporation, five square electric pulses of 45 V and 50 ms were delivered through the uterus at 950-ms intervals using a square pulse electroporator (CUY21 Edit, NepaGene Co., Japan). The surgical incision was then closed, and embryos were allowed to develop until P8. In the electroporated animals with the UbC-StarTrack combination, tamoxifen was administered at P1 as previously described (25) for removing nonintegrated copies of the electroporated plasmids through the Cre recombinase system.

### Measurement of thalamic astrocytic clones

Images were acquired with an Olympus FV1000 confocal IX81 microscope/FV10-ASW software following previously defined settings (12). All the pictures were acquired with a  $20\times$  oil immersion objective and analyzed with ImageJ software. Only electroporated animals with labeled cells in the three first order thalamic nuclei (dLG, VPM, and MGv) were used. Then, only clones with at least three cells and with the presence of more than one reporter were analyzed.

First, we assigned a binary code to every cell based on the presence or absence of each reporter protein in the cytoplasm and/or the cellular nuclei and the expression of the neuronal marker NeuN in order to distinguish neurons from glial cells. Once all the cells had been analyzed, they were grouped on the basis of their shared binary code, thereby identifying those cells that originated from the same progenitor. Then, we quantified the distribution (in %) of cells belonging to the same clone across the thalamic nuclei.

### Virus production

For the production of the retrovirus, Lenti-X 293T cells (catalog no. 632180, Clontech) were plated on 5- to 10-cm dishes. Encapsulation plasmids containing gag-pol and vsv-g sequences (provided by V. Borrell) were cotransfected with the plasmid of interest using LipoD293 (catalog no. SL100668, SigmaGen). The medium was changed after 5 hours, and the virus was collected after 72 hours using Lenti-X concentrator (catalog no. 631231, Clontech).

### In vivo viral and BrdU injections

Pups at P3 were anesthetized on ice and placed in a digital stereotaxic. The virus was injected using an injector (Nanoliter 2010, WPI) in the thalamus or cortex through a small skull incision. BrdU was injected intraperitoneally at 50 mg/kg immediately after viral injections from stock solution (10 mg/ml).

### Astrocyte primary cultures

Postnatal astroglia was cultured as previously described (52). Briefly, after removal of the meninges, the cortices (somatosensory and visual) and the thalamus from P4 to P6 mice were dissected and dissociated mechanically in cold KREBS  $1\times$ . Subsequently, cells were centrifuged for 10 min at 1000 rpm, resuspended, and plated in a medium consisting of DMEM/F12 (Gibco), 3.5 mM glucose (Sigma-Aldrich), 10% fetal calf serum (Gibco), 5% horse serum (Gibco),  $1\times$  GlutaMAX (Fisher), and antibiotic/antimycotic (100 U/ $\mu\text{l}$ ) (Fisher)

and supplemented with B27 2% (Gibco), epidermal growth factor (10 ng/ml) (EGF; Roche), and fibroblast growth factor 2 (10 ng/ml) (FGF2; Roche). Oligodendrocyte precursor cells were removed by brusquely shaking the culture flasks several times when changing the medium after 2 or 3 days. Cells were passaged after 1 week using trypsin/EDTA (Gibco) and plated on poly-D-lysine (Sigma-Aldrich) glass-coated coverslips at a density of 50,000 to 70,000 cells per coverslip (in 24-well plates; BD Biosciences) in the same medium. The vast majority of the cells (>90%) were positive for glial fibrillary acidic protein (Gfap). Nuclei-specific thalamic astrocytic cultures were performed similarly but with a few modifications. Brains were dissected out and cut in a vibratome in 300- $\mu$ m slices in cold KREBS to dissect the three principal sensory thalamic nuclei: dLG nucleus, the somatosensory VPM nucleus, and the auditory MGv. Thalamic nuclei were then mechanically dissociated and plated on six-well plates and passed when confluent. Astrocytes were infected with CAG-*GFP-IRES-GFP*, CAG-(*Flag*)*Neurog2-IRES-DsRed*, CAG-(*Flag*)*Neurog2-IRES-TauGFP*, or CAG-*Gbx2-IRES-DsRed* retroviruses. After 24 hours, the medium was changed by a differentiation medium containing DMEM/F12 (Gibco), 3.5 mM glucose (Sigma-Aldrich), 1 $\times$  GlutaMAX (Fisher), and antibiotic/antimycotic (100 U/ $\mu$ l) (Fisher) and supplemented with B27 2% (Gibco). BDNF (Sigma-Aldrich) was added at 20 ng/ml every fourth day during the differentiation process.

### Histology

For immunofluorescence of reprogrammed neurons in vitro, cultures were fixed with 4% paraformaldehyde (PFA) in phosphate-buffered saline (PBS) (0.01 M) for 10 to 15 min at room temperature. Cultures were first incubated for 1 hour at room temperature in a blocking solution containing 2% BSA (Sigma-Aldrich) and 0.15% Triton X-100 (Sigma-Aldrich) in 0.01 M PBS. Subsequently, the cells were incubated overnight at 4°C with the primary antibodies listed in table S6. The cells were then rinsed in 0.01 M PBS and incubated for 2 hours at room temperature with adequate secondary antibodies listed in table S6. Counterstaining was performed by the fluorescent nuclear dye 4',6-diamidino-2-phenylindole (DAPI) (Sigma-Aldrich).

For histology in postnatal brains, mice were perfused transcardially first with 0.01 M PBS and 4% PFA. Brains were kept on 4% PFA overnight, embedded with 3% agarose in 0.01 M PBS, and cut into slices of 80  $\mu$ m of thickness in a vibratome (Leica). For *Tbr1*, *Ctip2*, *Aldh1l1*, *Rora*, and *Lef1* antibodies, an antigen retrieval step with sodium citrate was performed. For BrdU detection, slices were first incubated with 2 N HCl and 0.5% Triton X-100 at 37°C for 30 min, followed by an incubation with borax buffer at room temperature. Slices were incubated for 1 hour at room temperature in a blocking solution containing 1% BSA, 2% donkey serum, 2% goat serum, and 0.4% Triton X-100 in 0.01 M PBS and subsequently incubated overnight at 4°C with primary antibodies. Slices were incubated for 2 hours at room temperature with the appropriate secondary antibodies, washed, incubated with DAPI, and mounted. Images were acquired with a Leica DFC550 camera into a Leica DM5000B microscope, with an Olympus FV1000 confocal IX81 microscope/FV10-ASW software, or with a Zeiss confocal LSM880.

### Fluorescence in situ hybridization

*Gfap::Gfp* brains were cut into slices of 100  $\mu$ m of thickness in a vibratome (Leica). Slices were dehydrated, incubated for 15 min with 2% H<sub>2</sub>O<sub>2</sub> in EtOH at room temperature for blocking endogenous peroxidase, and rehydrated. Then, slices were washed first with PBS

and 0.1% Tween 20 (PBT), then with a detergent mix [1% NP-40, 1% SDS, 0.5% sodium deoxycholate, 50 mM tris-HCl (pH 8), 1 mM EDTA, and 150 mM NaCl] three times for 20 min, and postfixed with 4% PFA. After three washes with PBT, slices were incubated with prehybridization solution [50% deionized formamide, 5 $\times$  SSC (pH 5.3), heparin (50  $\mu$ g/ml), tRNA (50  $\mu$ g/ml), single-stranded DNA (50  $\mu$ g/ml), and 0.1% Tween 20] for 1 hour at 65°C in a humid chamber and then incubated overnight with the corresponding probe in prehybridization solution at 65°C.

The next day, slices were washed four times with prewarmed washing solution [50% formamide, 2 $\times$  SSC (pH 5.3), and 1% SDS] at 65°C and four times with MABT [100 mM maleic acid, 150 mM NaCl, 0.19 M NaOH (pH 7.5), and 0.1% Tween 20]. Slices were then incubated with blocking solution [2% Blocking Reagent (Sigma-Aldrich, no. 11096176001) in MABT] for 2 hours and then incubated overnight at 4°C with anti-digoxigenin-POD (Sigma-Aldrich, no. 11207733910) diluted 1/500 in blocking solution.

Slices were washed four times with MABT and then revealed with TSA PLUS CYANINE 3 (Akoya, SKU NEL744001KT) diluted 1/500 in MABT. Once revealed, slices were washed with MABT and then immunofluorescence was performed as described above.

### Purification of total RNA and quantitative real-time PCR

For specific isolation of reprogrammed astrocytes, a previously published method was followed (20) but with some modifications for cultured cells. Astrocytes from the thalamus, cortex, dLG, VPM, and MGv were cultured and infected with *Neurog2* retrovirus, and after 10 days in vitro, they were collected by applying trypsin/EDTA (Gibco) to the plate, resuspended with culture medium, and centrifuged. Reprogrammed astrocytes were fixed with PFA 1% for 10 min at 4°C, after which the PFA was quenched by adding 55  $\mu$ l of glycine, 1.25 M per 500  $\mu$ l of PFA solution. Immunocytochemistry against *Tuj1* and RFP was performed, and cells were separated (*Tuj1*<sup>+</sup>/*RFP*<sup>+</sup> versus *Tuj1*<sup>-</sup>/*RFP*<sup>+</sup>) by a flow cytometer (BD FACSAria) based on their fluorescence (see schema on fig. S8, C to E). Once the cells were collected, they were centrifuged and incubated for 3 hours at 50°C with lysis buffer, their RNA was purified using TRIzol (Fisher), and cells were resuspended in RNase-free water.

cDNA was obtained from 1  $\mu$ g of total RNA using the specific protocol for first-strand cDNA synthesis in two-step reverse transcription (RT)-PCR using the High-Capacity cDNA Reverse Transcription Kit (Fisher) and stored at -20°C. qPCR was performed in a StepOnePlus real-time PCR system (Applied Biosystems, Foster City, CA, USA) using the MicroAmp fast 96-well reaction plate (Applied Biosystems) and the Power SYBR Green PCR Master Mix (Applied Biosystems). The primers used for detecting the expression of the different genes are listed in table S7. A master mix was prepared for each primer set containing the appropriate volume of SYBR Green, primers, and template cDNA. All reactions were performed in triplicate. The amplification efficiency for each primer pair and the cycle threshold (Ct) were determined automatically by the StepOne Software, v2.2.2 (Applied Biosystems). Transcript levels were represented relative to the *Gapdh* signal, adjusting for the variability in cDNA library preparation.

### Patch-clamp recordings of iNs

For the electrophysiological analysis, astrocytes were infected with a retrovirus encoding CAG-*Neurog2-ires-TauGFP*. After 3 weeks, cultures were transferred to the recording chamber and were perfused

with standard artificial cerebrospinal fluid (aCSF) containing the following: 119 mM NaCl, 5 mM KCl, 1.3 mM MgSO<sub>4</sub>, 2.4 mM CaCl<sub>2</sub>, 1 mM NaH<sub>2</sub>PO<sub>4</sub>, 26 mM Na<sub>2</sub>HCO<sub>3</sub>, and 11 mM glucose. The aCSF was perfused at a rate of 2.7 ml min<sup>-1</sup>, continuously bubbled with a gas mixture of 95% O<sub>2</sub> + 5% CO<sub>2</sub>, and warmed at 30° to 32°C.

Somatic whole-cell recordings were made under visual control using an upright microscope (Leica DM-LFSA) and a water immersion (20 or 40×) objective. The intracellular solution contained the following: 130 mM K-gluconate, 5 mM KCl, 5 mM NaCl, 0.2 mM EGTA, 10 mM Hepes, 4 mM Mg-ATP, and 0.4 mM Na-GTP, pH 7.2 adjusted with KOH; 285 to 295 mOsm. Recordings were obtained in current-clamp and/or voltage-clamp mode with a patch-clamp amplifier (MultiClamp 700A, Molecular Devices, USA). No correction was made for the pipette junction potential. Voltage and current signals were filtered at 2 to 4 kHz and digitized at 20 kHz with a 16-bit resolution analog to digital converter (Digidata 1550B, Axon Instruments). The generation and acquisition of pulses were controlled by pClamp 10.6 software (Axon Instruments). Patch pipettes were made from borosilicate glass [1.5 mm OD (outer diameter), 0.86 mm ID (inner diameter), with inner filament] and had a resistance of 4 to 7 megohms when filled. Neurons in which series resistance was >30 megohms were discarded. Quantification of intrinsic membrane properties and spontaneous neuronal activity was performed on Clampfit 10.7 (Axon Instruments). The presence of putative spontaneous excitatory postsynaptic currents (sEPSCs) was assessed in voltage clamp recordings at -70 mV.

### In silico *Neurog2* binding sites determination

In silico analysis was performed to find out *Neurog2* binding sites across the whole genome using FIMO Motif Scanning from MEME Suite (v5.0.2) (53). *Neurog2* transcription factor motif (NGN2\_MOUSE.H11MO.0.C) from HOCOMOCO database (v11) and mouse genome (GRCm38.p6 GenCode M18) were used to carry out this analysis. *Neurog2* binding sites were annotated to genes using ChIPseeker (v1.18) (54) and Bioconductor (v3.8) in the R statistical computing and graphics platform (v3.5.1 Feather Spray). We retrieved genomic regions and selected binding sites [promoters, 5'UTR (5' untranslated region), first intron and first exon] whose location was ±3 kb of GENCODE annotated TSSs (transcription start sites) of protein-coding genes. These criteria retrieved 180,611 putative *Neurog2* binding sites belonging to 20,478 protein coding genes. Chromatin immunoprecipitation sequencing (ChIP-seq) coverage tracks for selected genes were generated using IGV (v2.4.14) and plotted in a 5' to 3' direction based on publicly available datasets from forebrain samples of H3K4me3 (ENCSR258YWW experiment) and H3K27me3 (ENCSR070MOK experiment) histone marks at P0 extracted from the ENCODE Project (see fig. S9).

### ChIP for H3K4me3 and H3K27me3

ChIP assays were performed following a previously published protocol (55). Cultured astrocytes from the thalamus and cortex were collected after 1 week in vitro when confluence is reached, centrifuged, and resuspended to approximately 500,000 cells. Cells were fixed with 1% PFA in PBS for 10 min at room temperature and quenched with 55 μl of glycine, 1.25 M per 500 μl of PFA solution with orbital shaking. After that, cells were lysed in 300 μl of SDS lysis buffer (0.5% SDS, 10 mM EDTA, and 50 mM Tris-HCl) supplemented with protease inhibitor cocktail (Roche, 11836153001), sonicated for 10 min in a Diagenode Bioruptor Pico, precleared with 30 μl

of washed Dynabeads (Invitrogen, 10003D), and diluted five times in ChIP IP buffer [20 mM Hepes, 0.2 M NaCl, 2 mM EDTA, 0.1% Na-DOC, 1% Triton X-100, and BSA (5 mg/ml)]. One percent of each sample was kept as input. Samples were divided into three tubes and incubated overnight at 4°C in a rotating wheel with 2.5 μg per tube of the anti-H3K4me3 (Sigma-Aldrich, 07-473), anti-H3K27me3 (Abcam, ab6002), or control IgG antibody. The next day, washed and saturated Dynabeads were added and incubated with the samples for 2 hours at 4°C. Dynabeads were washed five times with LiCl buffer (50 mM Hepes, 1 mM EDTA, 1% NP-40, 1% Na-DOC, and 0.5 M LiCl) and once with TE buffer (10 mM Tris-HCl and 1 mM EDTA). Antibody/chromatin complexes together with the inputs were eluted by adding 100 μl of elution buffer (50 mM NaHCO<sub>3</sub> and 1% SDS), 10 μl of NaCl (5 M), and 1 μl of proteinase K (Sigma-Aldrich, 3115836001) to each tube and put on a thermomixer, shaking at 1000 rpm at least 2 hours at 60°C. Samples and inputs were decross-linked by heating for 15 min at 95°C. Both samples and inputs were treated with RNase A (Roche, 10109142001) for 30 min at 65°C, and the DNA was purified with phenol/chloroform and ethanol-precipitated. Primers used for detecting the immunoprecipitated genomic regions are listed in table S7.

### Primer design

For RNA expression analysis, Primer3 and Blast tools from NCBI webpage were used, using the accession numbers of the coding sequences of the genes of interest. For ChIP experiments, we used the information obtained from the in silico *Neurog2* binding sites analysis and the open-source information of the ENCODE project. For primers design, regions on the promoters of candidate genes that included a putative binding site for *Neurog2* and that were enriched in H3K4me3 and H3K27me3 signal were selected.

### Quantification and statistical analysis

Statistical analysis was carried out in GraphPad Prism (v.6), Origin (v.8.0), and R (v3.5.1 Feather Spray) statistical computing and graphics platform. Data are presented as means ± SEM or with box-and-whisker plots, which give the median, 25th and 75th percentiles, and range. Statistical comparison between groups was performed using paired or unpaired two-tailed Student's *t* test or Mann-Whitney *U* test nonparametric two-tailed test when data failed a Kolmogorov-Smirnov or a Shapiro-Wilk normality test. For multiple comparison analysis, a one-way analysis of variance (ANOVA) test with Holm-Sidak's multiple comparisons test was used, and Kruskal-Wallis test with Dunn's multiple comparisons test was used when data failed a Kolmogorov-Smirnov or a Shapiro-Wilk normality test. Simple effect analysis was performed when interaction was significant. *P* values < 0.05 were considered statistically significant and set as follows: \**P* < 0.05, \*\**P* < 0.005, and \*\*\**P* < 0.0005. In the bioinformatical analysis, DEGs were identified using a statistical significance threshold (BH-adjusted *P* value < 0.1) and set as follows: \*adj. *P* < 0.1, \*\*adj. *P* < 0.01, and \*\*\*adj. *P* < 0.001. No statistical methods were used to predetermine the sample size, but our sample sizes are considered adequate for the experiments and consistent with the literature. The mice were not randomized. The investigators were blinded to sample identity.

For Fig. 1B, PCA of astrocytes shows only the first two principal components, PC1 represents 59% variance and PC2 represents 15% variance (*n* = 4 Ctx, *n* = 4 to 5 each Th nucleus). For Fig. 1C, DE analysis (adj. *P* < 0.1, log<sub>2</sub>FC > 0; 1675 DEG As-Th versus 1287 DEG

As-Ctx). For Fig. 1D, DE analysis (adj.  $P < 0.1$ ,  $\log_2FC > 0$ ; 1675 DEG As-Th versus 1287 DEG As-Ctx) (table S1). For Fig. 1E, GSEA: thalamus development (GO:0021794) (NES = 1.666;  $P = 0.028$ ; adj.  $P = 0.074$ ), diencephalon development (GO:00221536) (NES = 1.889;  $P = 0.018$ ; adj.  $P = 0.052$ ), cerebral cortex neuron differentiation (GO:0021895) (NES = -2.119;  $P = 0.002$ ; adj.  $P = 0.011$ ), and telencephalon regionalization (GO:0021978) (NES = -1.879;  $P = 0.008$ ; adj.  $P = 0.029$ ) produced with a more restrictive DE analysis (adj.  $P < 0.1$ ,  $\log_2FC > 0.322$ , As-Th: 508 DEGs, As-Ctx: 444 DEGs). Figure 1F used a more restrictive DE analysis (adj.  $P < 0.1$ ,  $\log_2FC > 0.322$ , As-Th: 508 DEGs, As-Ctx: 444 DEGs).

For Fig. 2B, hypergeometric test (one-sided Fisher's exact test). As-Th enriched in Ns-Th  $***P = 3.649224 \times 10^{-37}$ , OD = 4.7272; As-Th enriched in Ns-Ctx ns  $P = 0.9981097$ , OD = 0.5754116; As-Ctx enriched in Ns-Ctx  $***P = 3.304775 \times 10^{-11}$ , OD = 2.669471, As-Ctx enriched in Ns-Th ns  $P = 0.9957097$ , OD = 0.5668416. Quantification was recovered from data of RNA-seq analysis of astrocytic DEGs (adj.  $P < 0.1$ ,  $\log_2FC > 0$ ; 1675 DEG As-Th versus 1287 DEG As-Ctx) and top 400 neuronal genes. For Fig. 2E, DE analysis of astrocytes, Wilcoxon rank sum test (adj.  $P < 0.1$ ,  $\log_2FC > 0.1$ , As-Th: 549 DEGs, As-Ctx: 1106 DEGs). For the DE analysis of neurons, Wilcoxon rank sum test (adj.  $P < 0.1$ ,  $\log_2FC > 0.1$ , Ns-Th: 2425 DEGs, Ns-Ctx: 1845 DEGs) (table S2). For Fig. 2F, hypergeometric test (one-sided Fisher's exact test). As-Th enriched in Ns-Th  $***P = 4.001415 \times 10^{-73}$ , OD = 5.57147; As-Th enriched in Ns-Ctx ns  $P = 0.9992975$ , OD = 0.6456831; As-Ctx enriched in Ns-Ctx  $***P = 2.066775 \times 10^{-159}$ , OD = 7.142444; and As-Ctx enriched in Ns-Th ns  $P = 0.9962708$ , OD = 0.7517044. Quantification was recovered from the data of scRNA-seq analysis of astrocytic DEGs (adj.  $P < 0.1$ ,  $\log_2FC > 0.1$ , As-Th: 549 DEGs, As-Ctx: 1106 DEGs) and neuronal DEGs (adj.  $P < 0.1$ ,  $\log_2FC > 0.1$ , Ns-Th: 2425 DEGs, Ns-Ctx: 1845 DEGs) (table S2).

For Fig. 3B, PCA shows only the first two principal components in astrocytes of the three thalamic nuclei, PC1 represents 41% variance and PC2 represents 24% variance ( $n = 4$  to 5 replicates each; table S3). For Fig. 3C, PCA shows only the first two principal components, PC1 represents 47% variance and PC2 represents 32% variance ( $n = 3$  to 4 replicates each; table S4). For Fig. 3D, hypergeometric test (one-sided Fisher's exact test) from intersect between the populations of genes for the comparison of significant overexpression in As-dLG and enriched in Ns-dLG  $***P = 1.750051 \times 10^{-11}$ , OD = 4.4.292546; significant overexpression in As-MGv and enriched in Ns-dLG ns  $P = 0.9956851$ , OD = 0.3838985; significant overexpression in As-VPM and enriched in Ns-dLG ns  $P = 0.9999685$ , OD = 0.5766173; significant overexpression in As-dLG and enriched in Ns-MGv ns  $P = 0.7531583$ , OD = 0.8598092; significant overexpression in As-MGv and enriched in Ns-MGv  $***P = 3.358423 \times 10^{-18}$ , OD = 3.946944; significant overexpression in As-VPM and enriched in Ns-MGv ns  $P = 1$ , OD = 0.3334283; significant overexpression in As-dLG and enriched in Ns-VPM ns  $P = 0.8043838$ , OD = 0.7983417; significant overexpression in As-MGv and enriched in Ns-VPM ns  $P = 0.3478912$ , OD = 1.123736; significant overexpression in As-VPM and enriched in Ns-VPM  $***P = 1.256227 \times 10^{-25}$ , OD = 2.495969. Quantification was recovered from the data of RNA-seq analysis of astrocytic DEGs (adj.  $P < 0.1$ ,  $\log_2FC > 0$ ; 221 DEG As-dLG, 1771 DEG As-VPM, and 278 DEG As-MGv) (table S3) and neuronal DEGs (adj.  $P < 0.1$ ,  $\log_2FC > 0$ ; 705 DEG Ns-dLG, 961 DEG Ns-VPM, 1330 DEG Ns-MGv) between distinct sensory-modality thalamic nuclei (table S4).

For Fig. 4C, Kruskal-Wallis test, with Dunn's multiple comparisons test.  $n = 5$  electroporated mice. For dLG clones,  $n = 59$  clones:  $***P < 0.0001$ ; dLG [confidence interval (CI): 77.24 to 87.74%] versus VPM (CI: 6.932 to 15.36%),  $***P < 0.0001$ ; dLG versus MGv (CI: 2.909 to 9.824%),  $***P < 0.0001$ ; VPM versus MGv, ns  $P = 0.7795$ . For VPM clones,  $n = 179$  clones:  $***P < 0.0001$ ; dLG (CI: 3.65 to 7.266%) versus VPM (CI: 84.69 to 90.01%),  $***P < 0.0001$ ; VPM versus MGv (CI: 5.131 to 9.401%),  $***P < 0.0001$ ; dLG versus MGv, ns  $P > 0.9999$ . For MGv clones,  $n = 82$  clones:  $***P < 0.0001$ ; dLG (CI: 0.7806 to 4.859%) versus MGv (CI: 78.39 to 88.03%),  $***P < 0.0001$ ; VPM (CI: 8.903 to 16.60%) versus MGv,  $***P < 0.0001$ ; dLG versus VPM,  $*P = 0.0253$ . For Fig. 4G, Kruskal-Wallis test, with Dunn's multiple comparisons test.  $n = 4$  electroporated animals. For dLG mixed clones,  $n = 52$  clones. For all cells,  $***P < 0.0001$ ; dLG (CI: 72.52 to 81.64%) versus VPM (CI: 13.12 to 21.29%),  $***P < 0.0001$ ; dLG versus MGv (CI: 3.346 to 7.865%),  $***P < 0.0001$ . For neurons,  $***P < 0.0001$ ; dLG (CI: 64.72 to 82.4%) versus VPM (CI: 11.40 to 27.25%),  $***P < 0.0001$ ; dLG versus MGv (CI: 3.305 to 10.61%),  $***P < 0.0001$ . For no neurons,  $***P < 0.0001$ ; dLG (CI: 57.50 to 78.95%) versus VPM (CI: 14.45 to 33.54%),  $***P < 0.0001$ ; dLG versus MGv (CI: 1.136 to 14.42%),  $***P < 0.0001$ . For VPM clones,  $n = 71$  clones. For all cells,  $***P < 0.0001$ ; dLG (CI: 9.353 to 16.29%) versus VPM (CI: 74.28 to 82.26%),  $***P < 0.0001$ ; VPM versus MGv (CI: 5.639 to 11.73%),  $***P < 0.0001$ . For neurons,  $***P < 0.0001$ ; dLG (CI: 17.88 to 33.37%) versus VPM (CI: 54.55 to 71.69%),  $***P < 0.0001$ ; VPM versus MGv (CI: 4.817 to 17.69%),  $***P < 0.0001$ . For no neurons,  $***P < 0.0001$ ; dLG (CI: 0.7925 to 7.465%) versus VPM (CI: 74.88 to 90.40%),  $***P < 0.0001$ ; VPM versus MGv (CI: 5.491 to 19.11%),  $***P < 0.0001$ . For MGv clones,  $n = 7$  clones. For all cells,  $***P < 0.0001$ ; VPM (CI: 6.127 to 33.87%) versus MGv (CI: 44.95 to 87.91%),  $**P = 0.0099$ ; dLG (CI: 1.42 to 25.72%) versus MGv,  $**P = 0.0011$ . For neurons, ns  $P = 0.7463$ ; VPM (CI: -2.264 to 68.93%) versus MGv (CI: 0.3102 to 85.40%), ns  $P > 0.9999$ ; dLG (CI: -10.49 to 58.11%) versus MGv, ns  $P = 0.8395$ . For no neurons,  $*P = 0.0167$ ; VPM (CI: -7.477 to 28.91%) versus MGv (CI: 35.05 to 107.8%),  $*P = 0.0209$ ; dLG (CI: -16.73 to 52.45%) versus MGv,  $*P = 0.0354$ .

For Fig. 5C, Mann-Whitney  $U$  test nonparametric two-tailed test. For *Lef1*,  $**P = 0.0065$ ,  $n = 6$  mice (265 iNs in Th and 103 iNs in Ctx); for *Rora*,  $*P = 0.0286$ ,  $n = 4$  mice (69 iNs in Th and 176 iNs in Ctx); for *Tbr1*,  $**P = 0.0022$ ,  $n = 5$  to 6 mice (202 iNs in Th and 109 iNs in Ctx); and for *Ctip2*,  $**P = 0.0022$ ,  $n = 6$  mice (202 iNs in Th and 109 iNs in Ctx). For Fig. 5F, ordinary one-way ANOVA and Holm-Sidak's multiple comparisons test for *Rora* [ $F = 13.00$ , degrees of freedom (df) = 29,  $***P < 0.0001$ ], *Tbr1* ( $F = 23.56$ , df = 31,  $***P < 0.0001$ ), and *Ctip2* ( $F = 30.70$ , df = 28,  $***P < 0.0001$ ), and Kruskal-Wallis test with Dunn's multiple comparisons test for *vGlut2* ( $***P < 0.0001$ ). For *Rora*, Inf. As-Th versus Inf. As-Ctx,  $***P < 0.0001$ ,  $n = 6$  independent cultures; Inf. As-Th + As-Ctx versus Inf. As-Ctx + As-Th,  $***P = 0.0008$ ,  $n = 6$ ; Inf. As-Th + Ns-Ctx versus Inf. As-Ctx + Ns-Th,  $**P = 0.0022$ ,  $n = 6$ . For *Tbr1*, Inf. As-Th versus Inf. As-Ctx,  $***P < 0.0001$ ,  $n = 6$ ; Inf. As-Th + As-Ctx versus Inf. As-Ctx + As-Th,  $***P < 0.0001$ ,  $n = 6$ ; Inf. As-Th + Ns-Ctx versus Inf. As-Ctx + Ns-Th,  $***P < 0.0001$ ,  $n = 6$ . For *Ctip2*, Inf. As-Th versus Inf. As-Ctx,  $***P < 0.0001$ ,  $n = 6$ ; Inf. As-Th + As-Ctx versus Inf. As-Ctx + As-Th,  $***P < 0.0001$ ,  $n = 6$ ; Inf. As-Th + Ns-Ctx versus Inf. As-Ctx + Ns-Th,  $***P < 0.0001$ ,  $n = 6$ . For *vGlut2*, Inf. As-Th versus Inf. As-Ctx,  $***P = 0.0003$ ,  $n = 6$ ; Inf. As-Th + As-Ctx versus Inf. As-Ctx + As-Th,  $*P = 0.0437$ ,  $n = 7$ ; Inf. As-Th + Ns-Ctx versus Inf. As-Ctx + Ns-Th,  $*P = 0.0239$ ,  $n = 5$ . For Fig. 5H, ordinary one-way

ANOVA test with Holm-Sidak's multiple comparisons test. *Sp9*,  $F = 8.924$ ,  $df = 32$ ,  $***P = 0.0008$ ; dLG versus VPM,  $***P = 0.0007$ ,  $n = 12$  independent cultures; dLG versus MGv,  $**P = 0.0034$ ,  $n = 12$ . *Hs6st2*,  $F = 5.128$ ,  $df = 25$ ,  $*P = 0.0136$ ; dLG versus VPM,  $**P = 0.0093$ ,  $n = 10$ ; dLG versus MGv,  $*P = 0.0331$ ,  $n = 10$ . *Crabp2*,  $F = 4.702$ ,  $df = 24$ ,  $*P = 0.0189$ ; MGv versus dLG,  $*P = 0.0341$ ,  $n = 10$ ; MGv versus VPM,  $*P = 0.0147$ ,  $n = 10$ . *Tshz1*,  $F = 10.97$ ,  $df = 37$ ,  $***P = 0.0002$ ; MGv versus dLG,  $***P = 0.0006$ ,  $n = 14$ ; MGv versus VPM,  $***P = 0.0003$ ,  $n = 14$ . *Cck*,  $F = 5.409$ ,  $df = 30$ ,  $**P = 0.0099$ ; VPM versus dLG,  $**P = 0.0064$ ,  $n = 12$ ; VPM versus MGv,  $*P = 0.0393$ ,  $n = 12$ .

For Fig. 6B, ordinary one-way ANOVA test with Holm-Sidak's multiple comparisons test; for *Gbx2* in Th,  $F = 39.71$ ,  $***P < 0.0001$ ; Th basal ( $n = 19$ ) versus Th + Neurog2 ( $n = 14$ ),  $ns P = 0.9579$ ,  $t = 0.05318$ ,  $df = 36$ ; Th basal versus Th + Neurog2 + *Gbx2* ( $n = 6$ ),  $***P < 0.0001$ ,  $t = 8.429$ ,  $df = 36$ ; Th + Neurog2 versus Th + Neurog2 + *Gbx2*,  $***P < 0.0001$ ,  $t = 8.128$ ,  $df = 36$ . For Ctx,  $F = 167.4$ ,  $***P < 0.0001$ ; Ctx basal ( $n = 14$ ) versus Ctx + Neurog2 ( $n = 14$ ),  $ns P = 0.9831$ ,  $t = 0.02134$ ,  $df = 31$ ; Ctx basal versus Ctx + Neurog2 + *Gbx2* ( $n = 6$ ),  $***P < 0.0001$ ,  $t = 16.88$ ,  $df = 31$ ; Ctx + Neurog2 versus Ctx + Neurog2 + *Gbx2*,  $***P < 0.0001$ ,  $t = 16.86$ ,  $df = 31$ . *Pou2f2*, for Th,  $F = 20.15$ ,  $***P < 0.0001$ ; Th basal ( $n = 12$ ) versus Th + Neurog2 ( $n = 14$ ),  $*P = 0.0386$ ,  $t = 2.163$ ,  $df = 30$ ; Th basal versus Th + Neurog2 + *Gbx2* ( $n = 7$ ),  $***P < 0.0001$ ,  $t = 6.307$ ,  $df = 30$ ; Th + Neurog2 versus Th + Neurog2 + *Gbx2*,  $***P = 0.0001$ ,  $t = 4.642$ ,  $df = 30$ . For Ctx,  $F = 11.79$ ,  $***P = 0.0001$ ; Ctx basal ( $n = 14$ ) versus Ctx + Neurog2 ( $n = 12$ ),  $ns P = 0.6091$ ,  $t = 0.5164$ ,  $df = 32$ ; Ctx basal versus Ctx + Neurog2 + *Gbx2* ( $n = 9$ ),  $***P = 0.0002$ ,  $t = 4.589$ ,  $df = 32$ ; Ctx + Neurog2 versus Ctx + Neurog2 + *Gbx2*,  $***P = 0.0007$ ,  $t = 3.986$ ,  $df = 32$ . *Tbr1*, for Th,  $F = 0.2125$ ,  $ns P = 0.8095$ ; Th basal ( $n = 20$ ) versus Th + Neurog2 ( $n = 14$ ),  $ns P = 0.8900$ ,  $t = 0.6478$ ,  $df = 39$ ; Th basal versus Th + Neurog2 + *Gbx2* ( $n = 8$ ),  $ns P = 0.9203$ ,  $t = 0.1537$ ,  $df = 39$ ; Th + Neurog2 versus Th + Neurog2 + *Gbx2*,  $ns P = 0.9023$ ,  $t = 0.3642$ ,  $df = 39$ . For Ctx,  $F = 5.79$ ,  $**P = 0.0062$ ; Ctx basal ( $n = 20$ ) versus Ctx + Neurog2 ( $n = 15$ ),  $**P = 0.0076$ ,  $t = 3.222$ ,  $df = 40$ ; Ctx basal versus Ctx + Neurog2 + *Gbx2* ( $n = 8$ ),  $ns P = 0.9186$ ,  $t = 0.1029$ ,  $df = 40$ ; Ctx + Neurog2 versus Ctx + Neurog2 + *Gbx2*,  $*P = 0.0403$ ,  $t = 2.416$ ,  $df = 40$ . *Ctip2*, for Th,  $F = 15.57$ ,  $***P < 0.0001$ ; Th basal ( $n = 19$ ) versus Th + Neurog2 ( $n = 14$ ),  $***P < 0.0001$ ,  $t = 5.452$ ,  $df = 37$ ; Th basal versus Th + Neurog2 + *Gbx2* ( $n = 7$ ),  $ns P = 0.4738$ ,  $t = 0.7238$ ,  $df = 37$ ; Th + Neurog2 versus Th + Neurog2 + *Gbx2*,  $**P = 0.0028$ ,  $t = 3.457$ ,  $df = 37$ . For Ctx,  $F = 4.681$ ,  $*P = 0.0154$ ; Ctx basal ( $n = 20$ ) versus Ctx + Neurog2 ( $n = 12$ ),  $*P = 0.018$ ,  $t = 2.913$ ,  $df = 37$ ; Ctx basal versus Ctx + Neurog2 + *Gbx2* ( $n = 8$ ),  $ns P = 0.9460$ ,  $t = 0.06815$ ,  $df = 37$ ; Ctx + Neurog2 versus Ctx + Neurog2 + *Gbx2*,  $*P = 0.05$ ,  $t = 2.268$ ,  $df = 37$ . *Rora*, for Th,  $F = 0.7022$ ,  $ns P = 0.5015$ ; Th basal ( $n = 22$ ) versus Th + Neurog2 ( $n = 14$ ),  $ns P = 0.5676$ ,  $t = 1.183$ ,  $df = 40$ ; Th basal versus Th + Neurog2 + *Gbx2* ( $n = 7$ ),  $ns P = 0.8707$ ,  $t = 0.4299$ ,  $df = 40$ ; Th + Neurog2 versus Th + Neurog2 + *Gbx2*,  $ns P = 0.8707$ ,  $t = 0.4707$ ,  $df = 40$ . For Ctx,  $F = 0.05697$ ,  $ns P = 0.9447$ ; Ctx basal ( $n = 22$ ) versus Ctx + Neurog2 ( $n = 14$ ),  $ns P = 0.9827$ ,  $t = 0.1035$ ,  $df = 41$ ; Ctx basal versus Ctx + Neurog2 + *Gbx2* ( $n = 8$ ),  $ns P = 0.9827$ ,  $t = 0.2709$ ,  $df = 41$ ; Ctx + Neurog2 versus Ctx + Neurog2 + *Gbx2*,  $ns P = 0.9827$ ,  $t = 0.3321$ ,  $df = 41$ . *Lef1*, for Th,  $F = 0.2178$ ,  $ns P = 0.8053$ ; Th basal ( $n = 21$ ) versus Th + Neurog2 ( $n = 14$ ),  $ns P = 0.8893$ ,  $t = 0.6494$ ,  $df = 40$ ; Th basal versus Th + Neurog2 + *Gbx2* ( $n = 8$ ),  $ns P = 0.9353$ ,  $t = 0.3267$ ,  $df = 40$ ; Th + Neurog2 versus Th + Neurog2 + *Gbx2*,  $ns P = 0.9353$ ,  $t = 0.1993$ ,  $df = 40$ . For Ctx,  $F = 0.4896$ ,  $ns P = 0.6164$ ; Ctx basal ( $n = 22$ ) versus Ctx + Neurog2 ( $n = 14$ ),  $ns P = 0.7079$ ,

$t = 0.9725$ ,  $df = 41$ ; Ctx basal versus Ctx + Neurog2 + *Gbx2* ( $n = 8$ ),  $ns P = 0.8896$ ,  $t = 0.1396$ ,  $df = 41$ ; Ctx + Neurog2 versus Ctx + Neurog2 + *Gbx2*,  $ns P = 0.7871$ ,  $t = 0.6201$ ,  $df = 41$ . *Fezf2*, for Th,  $F = 21.11$ ,  $***P < 0.0001$ ; Th basal ( $n = 17$ ) versus Th + Neurog2 ( $n = 10$ ),  $***P < 0.0001$ ,  $t = 5.764$ ,  $df = 32$ ; Th basal versus Th + Neurog2 + *Gbx2* ( $n = 8$ ),  $***P < 0.0001$ ,  $t = 4.800$ ,  $df = 32$ ; Th + Neurog2 versus Th + Neurog2 + *Gbx2*,  $ns P = 0.6177$ ,  $t = 0.5040$ ,  $df = 32$ . For Ctx,  $F = 0.2050$ ,  $ns P = 0.8157$ ; Ctx basal ( $n = 18$ ) versus Ctx + Neurog2 ( $n = 10$ ),  $ns P = 0.9051$ ,  $t = 0.3393$ ,  $df = 33$ ; Ctx basal versus Ctx + Neurog2 + *Gbx2* ( $n = 8$ ),  $ns P = 0.9051$ ,  $t = 0.3998$ ,  $df = 33$ ; Ctx + Neurog2 versus Ctx + Neurog2 + *Gbx2*,  $ns P = 0.8938$ ,  $t = 0.6402$ ,  $df = 33$ . *Slc17a6*, for Th,  $F = 4.011$ ,  $*P = 0.0261$ ; Th basal ( $n = 21$ ) versus Th + Neurog2 ( $n = 13$ ),  $*P = 0.0228$ ,  $t = 2.813$ ,  $df = 39$ ; Th basal versus Th + Neurog2 + *Gbx2* ( $n = 8$ ),  $ns P = 0.4043$ ,  $t = 1.224$ ,  $df = 39$ ; Th + Neurog2 versus Th + Neurog2 + *Gbx2*,  $ns P = 0.4043$ ,  $t = 1.077$ ,  $df = 39$ . For Ctx,  $F = 3.454$ ,  $*P = 0.0427$ ; Ctx basal ( $n = 20$ ) versus Ctx + Neurog2 ( $n = 9$ ),  $ns P = 0.4808$ ,  $t = 0.7127$ ,  $df = 35$ ; Ctx basal versus Ctx + Neurog2 + *Gbx2* ( $n = 9$ ),  $ns P = 0.0702$ ,  $t = 2.184$ ,  $df = 35$ ; Ctx + Neurog2 versus Ctx + Neurog2 + *Gbx2*,  $ns P = 0.0550$ ,  $t = 2.466$ ,  $df = 35$ .

In Fig. 6D, for the  $\log_2$  of the ratio of H3K4me3/HeK27me3, unpaired Student's  $t$  test two-tailed test; *Gbx2*, Th ( $n = 14$ ) versus Ctx ( $n = 12$ ),  $***P < 0.0001$ ,  $t = 8.037$ ,  $df = 24$ ; *Rora*, Th ( $n = 23$ ) versus Ctx ( $n = 22$ ),  $*P = 0.0450$ ,  $t = 2.065$ ,  $df = 43$ ; *Lef1*, Th ( $n = 20$ ) versus Ctx ( $n = 21$ ),  $*P = 0.0126$ ,  $t = 2.616$ ,  $df = 39$ ; *Fezf2*, Th ( $n = 10$ ) versus Ctx ( $n = 10$ ),  $ns P = 0.3111$ ,  $t = 1.042$ ,  $df = 18$ ; *Slc17a6*, Th ( $n = 16$ ) versus Ctx ( $n = 16$ ),  $ns P = 0.2250$ ,  $t = 1.239$ ,  $df = 30$ ; *Pou2f2*, Th ( $n = 16$ ) versus Ctx ( $n = 18$ ),  $ns P = 0.5076$ ,  $t = 0.6700$ ,  $df = 32$ ; *Tbr1*, Th ( $n = 19$ ) versus Ctx ( $n = 21$ ),  $*P = 0.0152$ ,  $t = 2.542$ ,  $df = 38$ ; *Ctip2*, Th ( $n = 17$ ) versus Ctx ( $n = 18$ ),  $**P = 0.0013$ ,  $t = 3.524$ ,  $df = 33$ . For the expression levels (1/ $\Delta$ Ct), unpaired Student's  $t$  test two-tailed test; *Gbx2*, Th ( $n = 19$ ) versus Ctx ( $n = 14$ ),  $***P < 0.0001$ ,  $t = 9.066$ ,  $df = 31$ ; *Rora*, Th ( $n = 22$ ) versus Ctx ( $n = 14$ ),  $*P = 0.0216$ ,  $t = 2.409$ ,  $df = 34$ ; *Lef1*, Th ( $n = 22$ ) versus Ctx ( $n = 22$ ),  $***P < 0.0001$ ,  $t = 6.388$ ,  $df = 42$ ; *Fezf2*, Th ( $n = 10$ ) versus Ctx ( $n = 10$ ),  $***P = 0.0028$ ,  $t = 3.458$ ,  $df = 18$ ; *Slc17a6*, Th ( $n = 21$ ) versus Ctx ( $n = 14$ ),  $*P = 0.0298$ ,  $t = 2.271$ ,  $df = 33$ ; *Pou2f2*, Th ( $n = 17$ ) versus Ctx ( $n = 11$ ),  $*P = 0.0118$ ,  $t = 2.708$ ,  $df = 26$ ; *Tbr1*, Th ( $n = 13$ ) versus Ctx ( $n = 20$ ),  $ns P = 0.3033$ ,  $t = 1.047$ ,  $df = 31$ ; *Ctip2*, Th ( $n = 14$ ) versus Ctx ( $n = 14$ ),  $ns P = 0.1874$ ,  $t = 3.524$ ,  $df = 26$ .

In Fig. 6E, for the epigenetics, ordinary one-way ANOVA test with Holm-Sidak's multiple comparisons test. For *Sp9*,  $F = 6.486$ ,  $**P = 0.0036$ ; dLG versus VPM,  $**P = 0.0018$ ,  $n = 14$ ,  $t = 3.587$ ,  $df = 41$ ; dLG versus MGv,  $*P = 0.0394$ ,  $n = 14$  to 16,  $t = 2.128$ ,  $df = 41$ . *Hs6st2*,  $F = 4.188$ ,  $*P = 0.0215$ ; dLG versus VPM,  $*P = 0.0164$ ,  $n = 13$  to 18,  $t = 2.764$ ,  $df = 45$ ; dLG versus MGv,  $*P = 0.0268$ ,  $n = 13$  to 17,  $t = 2.289$ ,  $df = 45$ . *Crabp2*,  $F = 4.794$ ,  $*P = 0.0132$ ; MGv versus dLG,  $*P = 0.0409$ ,  $n = 18$  to 12,  $t = 2.108$ ,  $df = 43$ ; MGv versus VPM,  $*P = 0.01$ ,  $n = 16$  to 18,  $t = 2.958$ ,  $df = 43$ . *Tshz1*,  $F = 5.125$ ,  $*P = 0.0106$ ; MGv versus dLG,  $*P = 0.0355$ ,  $n = 13$  to 15,  $t = 2.178$ ,  $df = 39$ ; MGv versus VPM,  $**P = 0.0072$ ,  $n = 14$  to 15,  $t = 3.098$ ,  $df = 39$ . *Cck*,  $F = 5.489$ ,  $**P = 0.0076$ ; VPM versus dLG,  $*P = 0.0227$ ,  $n = 13$  to 16,  $t = 2.365$ ,  $df = 42$ ; VPM versus MGv,  $**P = 0.0058$ ,  $n = 16$ ,  $t = 3.164$ ,  $df = 42$ . For in vivo basal expression, data from the RNA-seq analysis of the astrocytes (adjusted  $P < 0.1$ ,  $\log_2FC > 0.322$ ) from the three thalamic nuclei were used.

For fig. S1H, Pearson correlation coefficient,  $R = 0.9750593$  ( $T = 121.83$ ,  $df = 769$ ,  $***P < 2.2 \times 10^{-16}$ ). For fig. S3C, for the differential expression of astrocytes, Wilcoxon rank sum test (adj.  $P < 0.1$ ,

$\log_2FC > 0.1$ , As-Th: 549 DEGs, As-Ctx: 1106 DEGs). For the differential expression of neurons, Wilcoxon rank sum test (adj.  $P < 0.1$ ,  $\log_2FC > 0.1$ , Ns-Th: 2425 DEGs, Ns-Ctx: 1845 DEGs) (table S2). For fig. S3D, hypergeometric test (one-sided Fisher's exact test). As-Th enriched in Ns-Th,  $***P = 4.001415 \times 10^{-73}$ , OD = 5.57147; As-Th enriched in Ns-Ctx, ns  $P = 0.9992975$ , OD = 0.6456831; As-Ctx enriched in Ns-Th,  $***P = 2.066775 \times 10^{-159}$ , OD = 7.142444; As-Ctx enriched in Ns-Th, ns  $P = 0.9962708$ , OD = 0.7517044. Quantification was recovered from data of scRNA-seq analysis of astrocytic DEGs (adj.  $P < 0.1$ ,  $\log_2FC > 0.1$ , As-Th: 549 DEGs, As-Ctx: 1106 DEGs), neuronal DEGs (adj.  $P < 0.1$ ,  $\log_2FC > 0.1$ , Ns-Th: 2425 DEGs, Ns-Ctx: 1845 DEGs), and among both cell types in thalamic DEGs (adj.  $P < 0.1$ ,  $\log_2FC > 0.1$ , Ns-Th: 3991 DEGs, As-Th: 1642 DEGs) and cortical DEGs (adj.  $P < 0.1$ ,  $\log_2FC > 0.1$ , Ns-Ctx: 4142 DEGs, As-Th: 1562 DEGs) (table S2). For fig. S3 (F and G), significance values according to DE analysis performed in Fig. 2E and fig. S3C (table S2). For fig. S4E, Student's unpaired two-tailed  $t$  test; *Slc17a6*,  $**P = 0.0018$ ,  $n = 14$ ; *Rora*,  $*P = 0.0124$ ,  $n = 14$ ; *Lef1*,  $***P < 0.0001$ ,  $n = 11$  to 14; *Gbx2*,  $***P < 0.0001$ ,  $n = 11$  to 14; *Pou2f2*,  $*P = 0.0382$ ,  $n = 12$  to 14; *Tcf7l2*,  $***P = 0.0003$ ,  $n = 8$ ; *Zic1*,  $*P = 0.0342$ ,  $n = 8$ ; *Foxg1*,  $***P < 0.0001$ ,  $n = 8$ ; *Meis2*,  $***P < 0.0001$ ,  $n = 8$ ; *Fezf2*,  $***P = 0.0007$ ,  $n = 9$ .

For fig. S5D, for the differential expression of astrocytes, Wilcoxon rank sum test (adj.  $P < 0.1$ ,  $\log_2FC > 0.1$ ; 426-DEG As-Ctx1, 258-DEG As-Ctx2, 325-DEG As-Ctx3) and neuronal DEGs (adj.  $P < 0.1$ ,  $\log_2FC > 0.1$ ; 567-DEG Ns-Ctx1, 335-DEG Ns-Ctx2, 980-DEG Ns-Ctx3) between distinct cortical regions (table S5). For fig. S5E, hypergeometric test (one-sided Fisher's exact test) from intersect between the populations of genes for the comparison of significant overexpression in As-Ctx1 and enriched in Ns-Ctx1,  $***P = 7.82738 \times 10^{-213}$ , OD = 47.36863; significant overexpression in As-Ctx2 and enriched in Ns-Ctx1,  $***P = 1.633766 \times 10^{-33}$ , OD = 9.798625; significant overexpression in As-Ctx3 and enriched in Ns-Ctx1, ns  $P = 0.1058762$ , OD = 1.462861; significant overexpression in As-Ctx1 and enriched in Ns-Ctx2,  $***P = 7.232017 \times 10^{-63}$ , OD = 16.83166; significant overexpression in As-Ctx2 and enriched in Ns-Ctx2,  $***P = 1.007917 \times 10^{-95}$ , OD = 39.70291; significant overexpression in As-Ctx3 and enriched in Ns-Ctx2, ns  $P = 70.9493607$ , OD = 0.4745243; significant overexpression in As-Ctx1 and enriched in Ns-Ctx3, ns  $P = 0.9978754$ , OD = 0.4842368; significant overexpression in As-Ctx2 and enriched in Ns-Ctx3, ns  $P = 0.9966557$ , OD = 0.3993004; significant overexpression in As-Ctx3 and enriched in Ns-Ctx3,  $***P = 7.169234 \times 10^{-93}$ , OD = 15.39014.

For fig. S6B, left graph, ordinary one-way ANOVA and Holm-Sidak's multiple comparisons test,  $F = 0.07668$ , ns  $P = 0.9266$ ; dLG versus VPM, ns  $P = 0.9737$ ; dLG versus MGv, ns  $P = 0.9737$ ; MGv versus VPM, ns  $P = 0.9737$ ,  $n = 5$ . Right graph, ordinary one-way ANOVA and Holm-Sidak's multiple comparisons test,  $F = 0.3985$ , ns  $P = 0.6799$ ; dLG versus VPM, ns  $P = 0.8286$ ; dLG versus MGv, ns  $P = 0.7913$ ; MGv versus VPM, ns  $P = 0.7913$ ,  $n = 5$  electroporated animals. In fig. S6C, left graph,  $n = 59$  dLG clones,  $n = 179$  VPM clones, and  $n = 82$  MGv clones. In the right graph, Kruskal-Wallis test with Dunn's multiple comparisons test. For dLG clones,  $P > 0.9999$  in dLG,  $P > 0.9999$  in VPM, and  $P = 0.6773$  in MGv,  $n = 43$  clones with 3 to 10 cells and  $n = 16$  clones with >10 cells. For VPM clones,  $P = 0.6386$  in dLG,  $P > 0.9999$  in VPM, and  $P = 0.0976$  in MGv,  $n = 137$  clones with 3 to 10 cells and  $n = 44$  clones with >10 cells. For MGv clones,  $P = 0.4436$  in dLG,  $P > 0.9999$  in VPM, and  $P > 0.9999$  in MGv,  $n = 66$  clones with 3 to 10 cells and  $n = 15$  clones with >10

cells. In fig. S6F, Mann-Whitney  $U$  test nonparametric two-tailed test ( $n = 128$  clones); neurons versus nonneurons, ns  $P = 0.3112$ . In fig. S6G, Kruskal-Wallis test, with Dunn's multiple comparisons test.  $n = 4$  electroporated animals. For dLG neuronal clones,  $n = 61$  clones,  $***P < 0.0001$ ; dLG (CI: 80.53 to 88.87%) versus VPM (CI: 5.962 to 13.56%),  $***P < 0.0001$ ; dLG versus MGv (CI: 3.069 to 8.002%),  $***P < 0.0001$ . For dLG nonneuronal clones,  $n = 14$  clones,  $***P < 0.0001$ ; dLG (CI: 100 to 100%) versus VPM (CI: 0 to 0%),  $***P < 0.0001$ ; dLG versus MGv (CI: 0 to 0%),  $***P < 0.0001$ . For VPM neuronal clones,  $n = 7$  clones,  $***P = 0.0007$ ; dLG (CI: 0.856 to 37.24%) versus VPM (CI: 45.53 to 82.08%),  $**P = 0.0081$ ; dLG versus MGv (CI: -0.13 to 34.42%),  $***P = 0.0039$ . For VPM nonneuronal clones,  $n = 25$  clones,  $***P < 0.0001$ ; dLG (CI: -0.7909 to 7.458%) versus VPM (CI: 92.54 to 100.8%),  $***P < 0.0081$ ; dLG versus MGv (CI: 0 to 0%),  $***P < 0.0001$ . For MGv neuronal clones,  $n = 4$  clones,  $**P = 0.0052$ ; VPM (CI: -18.95 to 60.61%) versus MGv (CI: 39.39 to 118.9%), ns  $P = 0.0917$ ; dLG (CI: 0 to 0%) versus MGv,  $**P = 0.0077$ . For MGv nonneuronal clones,  $n = 3$  clones,  $*P = 0.0357$ ; VPM (CI: 0 to 0%) versus MGv (CI: 100 to 100%),  $*P = 0.0286$ ; dLG (CI: 0 to 0%) versus MGv,  $**P = 0.0286$ . For fig. S7B, in Th,  $**P = 0.0079$ ,  $n = 5$  injected mice (427 cells with control and 572 cells with *Neurog2* virus), and in Cx,  $**P = 0.0043$ ,  $n = 5$  injected mice (362 cells with control and 292 cells with *Neurog2* virus).

For fig. S8F, for *Gfap*, two-tailed unpaired Student's  $t$  test,  $**P = 0.0014$ ,  $n = 8$ ; for *Neurog2*, ordinary one-way ANOVA test,  $F = 23.41$ ,  $***P < 0.0001$ ; Holm-Sidak's multiple comparisons test,  $Tuj1^+/RFP^+$  versus  $RFP^+$ ,  $***P = 0.0006$ ;  $Tuj1^+/RFP^+$  versus  $Tuj1^-/RFP^-$ ,  $***P < 0.0001$ ;  $RFP^+$  versus  $Tuj1^-/RFP^-$ ,  $*P = 0.0116$ ;  $n = 12$  cultures. For fig. S8G, Student's  $t$  test or Mann-Whitney  $U$  test nonparametric two-tailed test; *Slc17a6*,  $**P = 0.0058$ ,  $n = 16$ ; *Rora*,  $**P = 0.0027$ ,  $n = 17$ ; *Gbx2*,  $**P = 0.0065$ ,  $n = 7$ ; *Pou2f2*,  $*P = 0.0181$ ,  $n = 5$ ; *Lef1*,  $**P = 0.0016$ ,  $n = 7$ ; *Tbr1*,  $**P = 0.0078$ ,  $n = 11$ ; *Ctip2*,  $**P = 0.0079$ ,  $n = 5$ .

For fig. S10B, for *Gapdh* and *Cdx2* upper graphs, two-tailed unpaired Student's  $t$  test; for *Gapdh*,  $**P = 0.0065$ ,  $n = 9$ ; and for *Cdx2*, ns  $P = 0.3406$ ,  $n = 9$ . In the lower graph, *Gapdh* versus *Cdx2*, Mann-Whitney  $U$  test nonparametric two-tailed test,  $***P < 0.0001$ ,  $n = 8$ . For *Gbx2*, two-tailed paired Student's  $t$  test: Th,  $***P < 0.0001$ ,  $n = 14$ ; Ctx,  $**P = 0.0049$ ,  $n = 12$ . For *Rora*, two-tailed Wilcoxon matched pairs test: Th,  $***P < 0.0001$ ,  $n = 23$ ; Ctx,  $*P = 0.019$ ,  $n = 22$ . For *Lef1*, two-tailed paired Student's  $t$  test: Th, ns  $P = 0.0563$ ,  $n = 18$ ; Ctx, ns  $P = 0.211$ ,  $n = 23$ . For *Fezf2*, two-tailed paired Student's  $t$  test: Th, ns  $P = 0.2506$ ,  $n = 9$ ; Ctx, ns  $P = 0.3506$ ,  $n = 10$ . For *Slc17a6*, two-tailed Wilcoxon matched pairs test: Th,  $*P = 0.0214$ ,  $n = 16$ ; Ctx,  $***P = 0.0003$ ,  $n = 16$ . For *Pou2f2*, two-tailed Wilcoxon matched pairs test: Th, ns  $P = 0.7819$ ,  $n = 17$ ; Ctx, ns  $P = 0.2121$ ,  $n = 18$ . For *Tbr1*, two-tailed paired Student's  $t$  test: Th,  $***P = 0.0003$ ,  $n = 19$ ; Ctx, ns  $P = 0.1748$ ,  $n = 21$ . For *Ctip2*, two-tailed paired Student's  $t$  test: Th,  $*P = 0.0156$ ,  $n = 17$ ; Ctx, ns  $P = 0.1471$ ,  $n = 18$ . For fig. S10D, *Sp9*, two-tailed paired Student's  $t$  test: dLG,  $**P = 0.0045$ ,  $n = 14$ ; VPM,  $***P = 0.0001$ ,  $n = 14$ ; and MGv,  $***P < 0.0001$ ,  $n = 16$ . *Hs6st2*, two-tailed paired Student's  $t$  test: dLG,  $**P = 0.0031$ ,  $n = 14$ ; VPM,  $***P = 0.0001$ ,  $n = 18$ ; and MGv,  $***P < 0.0001$ ,  $n = 18$ . *Cck*, two-tailed paired Student's  $t$  test: dLG,  $***P < 0.0001$ ,  $n = 15$ ; VPM,  $***P < 0.0001$ ,  $n = 18$ ; and MGv,  $***P < 0.0001$ ,  $n = 18$ . *Crabp2*, two-tailed Wilcoxon matched pairs test: dLG,  $*P = 0.0245$ ,  $n = 14$ ; VPM, ns  $P = 0.0987$ ,  $n = 18$ ; and MGv,  $***P < 0.0001$ ,  $n = 19$ . *Tshz1*, two-tailed Wilcoxon matched pairs test: dLG,  $***P < 0.0001$ ,  $n = 13$ ; VPM,  $***P = 0.0001$ ,  $n = 14$ ; and MGv,  $***P < 0.0001$ ,  $n = 16$ .

## SUPPLEMENTARY MATERIALS

Supplementary material for this article is available at <http://advances.sciencemag.org/cgi/content/full/7/15/eabe8978/DC1>

[View/request a protocol for this paper from Bio-protocol.](#)

## REFERENCES AND NOTES

1. V. Metzlis, S. Steinhauser, E. Pakanavicius, M. Gouti, D. Stamatakis, K. Ivanovitch, T. Watson, T. Rayon, S. N. M. Gharavy, R. Lovell-Badge, N. M. Luscombe, J. Briscoe, Nervous system regionalization entails axial allocation before neural differentiation. *Cell* **175**, 1105–1118. e17 (2018).
2. D. Mi, Z. Li, L. Lim, M. Li, M. Moissidis, Y. Yang, T. Gao, T. X. Hu, T. Pratt, D. J. Price, N. Sestan, O. Marin, Early emergence of cortical interneuron diversity in the mouse embryo. *Science* **360**, 81–85 (2018).
3. C. Mayer, C. Hafemeister, R. C. Bandler, R. Machold, R. Batista Brito, X. Jaglin, K. Alloway, A. Butler, G. Fishell, R. Satija, Developmental diversification of cortical inhibitory interneurons. *Nature* **555**, 457–462 (2018).
4. L. Telley, G. Agirman, J. Prados, N. Amberg, S. Fièvre, P. Oberst, G. Bartolini, I. Vitali, C. Cadilhac, S. Hippenmeyer, L. Nguyen, A. Dayer, D. Jabaudon, Temporal patterning of apical progenitors and their daughter neurons in the developing neocortex. *Science* **364**, eaav2522 (2019).
5. S. Lodato, P. Arlotta, Generating neuronal diversity in the mammalian cerebral cortex. *Annu. Rev. Cell Dev. Biol.* **31**, 699–720 (2015).
6. T. M. Jessell, Neuronal specification in the spinal cord: Inductive signals and transcriptional codes. *Nat. Rev. Genet.* **1**, 20–29 (2000).
7. L. C. Greig, M. B. Woodworth, M. J. Galazo, H. Padmanabhan, J. D. Macklis, Molecular logic of neocortical projection neuron specification, development and diversity. *Nat. Rev. Neurosci.* **14**, 755–769 (2013).
8. T. J. Nowakowski, A. Bhaduri, A. A. Pollen, B. Alvarado, M. A. Mostajo-Radji, E. di Lullo, M. Haeussler, C. Sandoval-Espinosa, S. J. Liu, D. Velmeshev, J. R. Ounadjela, J. Shuga, X. Wang, D. A. Lim, J. A. West, A. A. Leyrat, W. J. Kent, A. R. Kriegstein, Spatiotemporal gene expression trajectories reveal developmental hierarchies of the human cortex. *Science* **358**, 1318–1323 (2017).
9. D. H. Rowitch, A. R. Kriegstein, Developmental genetics of vertebrate glial-cell specification. *Nature* **468**, 214–222 (2010).
10. C. Hochstim, B. Deneen, A. Lukaszewicz, Q. Zhou, D. J. Anderson, Identification of positionally distinct astrocyte subtypes whose identities are specified by a homeodomain code. *Cell* **133**, 510–522 (2008).
11. A. V. Molofsky, K. W. Kelley, H. H. Tsai, S. A. Redmond, S. M. Chang, L. Madireddy, J. R. Chan, S. E. Baranzini, E. M. Ullian, D. H. Rowitch, Astrocyte-encoded positional cues maintain sensorimotor circuit integrity. *Nature* **509**, 189–194 (2014).
12. J. García-Marqués, L. López-Mascaraque, Clonal identity determines astrocyte cortical heterogeneity. *Cereb. Cortex* **23**, 1463–1472 (2013).
13. O. A. Bayraktar, T. Bartels, S. Holmqvist, V. Kleshchevnikov, A. Martirosyan, D. Polioudakis, L. B. Haim, A. M. H. Young, M. Y. Batiuk, K. Prakash, A. Brown, K. Roberts, M. F. Paredes, R. Kawaguchi, J. H. Stockley, K. Sabour, S. M. Chang, E. Huang, P. Hutchinson, E. M. Ullian, M. Hemberg, G. Coppola, M. G. Holt, D. H. Geschwind, D. H. Rowitch, Astrocyte layers in the mammalian cerebral cortex revealed by a single-cell in situ transcriptomic map. *Nat. Neurosci.* **23**, 500–509 (2020).
14. M. Y. Batiuk, A. Martirosyan, J. Wahis, F. de Vin, C. Marneffe, C. Kusserow, J. Koeppen, J. F. Viana, J. F. Oliveira, T. Voet, C. P. Ponting, T. G. Belgard, M. G. Holt, Identification of region-specific astrocyte subtypes at single cell resolution. *Nat. Commun.* **11**, 1220–1215 (2020).
15. B. S. Khakh, B. Deneen, The emerging nature of astrocyte diversity. *Annu. Rev. Neurosci.* **42**, 187–207 (2019).
16. C. Nolte, M. Matyash, T. Pivneva, C. G. Schipke, C. Ohlemeyer, U. K. Hanisch, F. Kirchhoff, H. Kettenmann, GFAP promoter-controlled EGFP-expressing transgenic mice: A tool to visualize astrocytes and astrogliosis in living brain tissue. *Glia* **33**, 72–86 (2001).
17. W.-P. Ge, A. Miyawaki, F. H. Gage, Y. N. Jan, L. Y. Jan, Local generation of glia is a major astrocyte source in postnatal cortex. *Nature* **484**, 376–380 (2012).
18. L. Chen, Q. Guo, J. Y. H. Li, Transcription factor Gbx2 acts cell-nonautonomously to regulate the formation of lineage-restriction boundaries of the thalamus. *Development* **136**, 1317–1326 (2009).
19. B. Tasic, Z. Yao, L. T. Graybiel, K. A. Smith, T. N. Nguyen, D. Bertagnolli, J. Goldy, E. Garren, M. N. Economou, S. Viswanathan, O. Penn, T. Bakken, V. Menon, J. Miller, O. Fong, K. E. Hirokawa, K. Lathia, C. Rimorin, M. Tieu, R. Larsen, T. Casper, E. Barkan, M. Kroll, S. Parry, N. V. Shapovalova, D. Hirschstein, J. Pendergraft, H. A. Sullivan, T. K. Kim, A. Szafer, N. Dee, P. Groblewski, I. Wickersham, A. Cetin, J. A. Harris, B. P. Levi, S. M. Sunkin, L. Madisen, T. L. Daigle, L. Looger, A. Bernard, J. Phillips, E. Lein, M. Hawrylycz, K. Svoboda, A. R. Jones, C. Koch, H. Zeng, Shared and distinct transcriptomic cell types across neocortical areas. *Nature* **563**, 72–78 (2018).
20. B. J. Molyneaux, L. A. Goff, A. C. Brettler, H.-H. Chen, J. R. Brown, S. Hrvatin, J. L. Rinn, P. Arlotta, DeCoN: Genome-wide analysis of in vivo transcriptional dynamics during pyramidal neuron fate selection in neocortex. *Neuron* **85**, 275–288 (2015).
21. J. D. Cahoy, B. Emery, A. Kaushal, L. C. Foo, J. L. Zamanian, K. S. Christopherson, Y. Xing, J. L. Lubischer, P. A. Krieg, S. A. Krupenko, W. J. Thompson, B. A. Barres, A transcriptome database for astrocytes, neurons, and oligodendrocytes: A new resource for understanding brain development and function. *J. Neurosci.* **28**, 264–278 (2008).
22. H. Gezelius, V. Moreno-Juan, C. Mezzera, S. Thakurela, L. M. Rodríguez-Malmierca, J. Pistollic, V. Benes, V. K. Tiwari, G. López-Bendito, Genetic labeling of nuclei-specific thalamocortical neurons reveals putative sensory-modality specific genes. *Cereb. Cortex* **27**, 5054–5069 (2017).
23. A. Zeisel, H. Hochgerner, P. Lönnerberg, A. Johnsson, F. Memic, J. van der Zwan, M. Häring, E. Braun, L. E. Borm, G. L. Manno, S. Codeluppi, A. Furlan, K. Lee, N. Skene, K. D. Harris, J. Hjerling-Lefler, E. Arenas, P. Ernfors, U. Marklund, S. Linnarsson, Molecular architecture of the mouse nervous system. *Cell* **174**, 999–1014.e22 (2018).
24. A. Baser, M. Skabkin, S. Kleber, Y. Dang, G. S. Gülcüler Balta, G. Kalamakis, M. Göpferich, D. C. Ibañez, R. Schefzik, A. S. Lopez, E. L. Bobadilla, C. Schultz, B. Fischer, A. Martin-Villalba, Onset of differentiation is post-transcriptionally controlled in adult neural stem cells. *Nature* **566**, 100–104 (2019).
25. M. Figueres-Oñate, J. García-Marqués, L. López-Mascaraque, Ubc-*StarTrack*, a clonal method to target the entire progeny of individual progenitors. *Sci. Rep.* **6**, 33896 (2016).
26. W. Shi, A. Xianyu, Z. Han, X. Tang, Z. Li, H. Zhong, T. Mao, K. Huang, S. H. Shi, Ontogenetic establishment of order-specific nuclear organization in the mammalian thalamus. *Nat. Neurosci.* **20**, 516–528 (2017).
27. S. Z. H. Wong, E. P. Scott, W. Mu, X. Guo, E. Borgenheimer, M. Freeman, G. L. Ming, Q. F. Wu, H. Song, Y. Nakagawa, In vivo clonal analysis reveals spatiotemporal regulation of thalamic nucleogenesis. *PLoS Biol.* **16**, e2005211 (2018).
28. S. Gascón, E. Murenu, G. Masserotti, F. Ortega, G. L. Russo, D. Petrik, A. Deshpande, C. Heinrich, M. Karow, S. P. Robertson, T. Schroeder, J. Beckers, M. Irmiler, C. Berndt, J. P. F. Angeli, M. Conrad, B. Berninger, M. Götz, Identification and successful negotiation of a metabolic checkpoint in direct neuronal reprogramming. *Cell Stem Cell* **18**, 396–409 (2016).
29. C. Mallika, Q. Guo, J. Y. H. Li, Gbx2 is essential for maintaining thalamic neuron identity and repressing habenular characters in the developing thalamus. *Dev. Biol.* **407**, 26–39 (2015).
30. N. Mattugini, R. Bocchi, V. Scheuss, G. L. Russo, O. Torper, C. L. Lao, M. Götz, Inducing different neuronal subtypes from astrocytes in the injured mouse cerebral cortex. *Neuron* **103**, 1086–1095.e5 (2019).
31. B. Mahato, K. D. Kaya, Y. Fan, N. Sumien, R. A. Shetty, W. Zhang, D. Davis, T. Mock, S. Batabyal, A. Ni, S. Mohanty, Z. Han, R. Farjo, M. J. Forster, A. Swaroop, S. H. Chavala, Pharmacologic fibroblast reprogramming into photoreceptors restores vision. *Nature* **581**, 83–88 (2020).
32. K. K. Bluske, T. Y. Vue, Y. Kawakami, M. M. Taketo, K. Yoshikawa, J. E. Johnson, Y. Nakagawa,  $\beta$ -Catenin signaling specifies progenitor cell identity in parallel with Shh signaling in the developing mammalian thalamus. *Development* **139**, 2692–2702 (2012).
33. S. Lodato, B. J. Molyneaux, E. Zuccaro, L. A. Goff, H.-H. Chen, W. Yuan, A. Meleski, E. Takahashi, S. Mahony, J. L. Rinn, D. K. Gifford, P. Arlotta, Gene co-regulation by *Fezf2* selects neurotransmitter identity and connectivity of corticospinal neurons. *Nat. Neurosci.* **17**, 1046–1054 (2014).
34. A. B. Mihalas, R. F. Hevner, Control of neuronal development by T-box genes in the brain. *Curr. Top. Dev. Biol.* **122**, 279–312 (2017).
35. A. Y.-S. Huang, J. Woo, D. Sardar, B. Lozzi, N. A. Bosquez Huerta, C.-C. J. Lin, D. Felice, A. Jain, A. Paulucci-Holthausen, B. Deneen, Region-specific transcriptional control of astrocyte function oversees local circuit activities. *Neuron* **106**, 992–1008.e9 (2020).
36. Q. Guo, J. Y. H. Li, Defining developmental diversification of diencephalon neurons through single cell gene expression profiling. *Development* **146**, dev174284 (2019).
37. Y. Hirabayashi, N. Suzuki, M. Tsuboi, T. A. Endo, T. Toyoda, J. Shinga, H. Koseki, M. Vidal, Y. Gotoh, Polycomb limits the neurogenic competence of neural precursor cells to promote astrogenic fate transition. *Neuron* **63**, 600–613 (2009).
38. Y. Hirabayashi, Y. Gotoh, Epigenetic control of neural precursor cell fate during development. *Nat. Rev. Neurosci.* **11**, 377–388 (2010).
39. K. Kim, A. Doi, B. Wen, K. Ng, R. Zhao, P. Cahan, J. Kim, M. J. Aryee, H. Ji, L. I. R. Ehrlich, A. Yabuuchi, A. Takeuchi, K. C. Cunliff, H. Hongguang, S. McKinney-Freeman, O. Naveiras, T. J. Yoon, R. A. Irizarry, N. Jung, J. Seit, J. Hanna, P. Murakami, R. Jaenisch, R. Weissleder, S. H. Orkin, I. L. Weissman, A. P. Feinberg, G. Q. Daley, Epigenetic memory in induced pluripotent stem cells. *Nature* **467**, 285–290 (2010).
40. J. P. Magnusson, C. Goritz, J. Tatarishvili, D. O. Dias, E. M. K. Smith, O. Lindvall, Z. Kokaia, J. Frisen, A latent neurogenic program in astrocytes regulated by Notch signaling in the mouse. *Science* **346**, 237–241 (2014).
41. G. Nato, A. Caramello, S. Trova, V. Avataneo, C. Rolando, V. Taylor, A. Buffo, P. Peretto, F. Luzzati, Striatal astrocytes produce neuroblasts in an excitotoxic model of Huntington's disease. *Development* **142**, 840–845 (2015).

42. H. Qian, X. Kang, J. Hu, D. Zhang, Z. Liang, F. Meng, X. Zhang, Y. Xue, R. Maimon, S. F. Dowdy, N. K. Devaraj, Z. Zhou, W. C. Mobley, D. W. Cleveland, X. D. Fu, Reversing a model of Parkinson's disease with in situ converted nigral neurons. *Nature* **582**, 550–556 (2020).
43. N. Tamamaki, Y. Yanagawa, R. Tomioka, J.-I. Miyazaki, K. Obata, T. Kaneko, Green fluorescent protein expression and colocalization with calretinin, parvalbumin, and somatostatin in the GAD67-GFP knock-in mouse. *J. Comp. Neurol.* **467**, 60–79 (2003).
44. N. Antón-Bolaños, A. Sempere-Ferrández, T. Guillamón-Vivancos, F. J. Martini, L. Pérez-Saiz, H. Gezelius, A. Filipchuk, M. Valdeolillos, G. López-Bendito, Prenatal activity from thalamic neurons governs the emergence of functional cortical maps in mice. *Science* **364**, 987–990 (2019).
45. M. Scandaglia, J. P. Lopez-Atalaya, A. Medrano-Fernandez, M. T. Lopez-Cascales, B. del Blanco, M. Lipinski, E. Benito, R. Olivares, S. Iwase, Y. Shi, A. Barco, Loss of Kdm5c causes spurious transcription and prevents the fine-tuning of activity-regulated enhancers in neurons. *Cell Rep.* **21**, 47–59 (2017).
46. Y. Liao, G. K. Smyth, W. Shi, featureCounts: An efficient general purpose program for assigning sequence reads to genomic features. *Bioinformatics* **30**, 923–930 (2014).
47. A. Zhu, J. G. Ibrahim, M. I. Love, Heavy-tailed prior distributions for sequence count data: Removing the noise and preserving large differences. *Bioinformatics* **35**, 2084–2092 (2019).
48. G. Yu, L.-G. Wang, Y. Han, Q.-Y. He, clusterProfiler: An R package for comparing biological themes among gene clusters. *OMICS* **16**, 284–287 (2012).
49. T. Stuart, A. Butler, P. Hoffman, C. Hafemeister, E. Papalexi, W. M. Mauck III, Y. Hao, M. Stoekius, P. Smibert, R. Satija, Comprehensive integration of single-cell data. *Cell* **177**, 1888–1902.e21 (2019).
50. A. Butler, P. Hoffman, P. Smibert, E. Papalexi, R. Satija, Integrating single-cell transcriptomic data across different conditions, technologies, and species. *Nat. Biotechnol.* **36**, 411–420 (2018).
51. V. Moreno-Juan, A. Filipchuk, N. Antón-Bolaños, C. Mezzera, H. Gezelius, B. Andrés, L. Rodríguez-Malmierca, R. Susín, O. Schaad, T. Iwasato, R. Schüle, M. Rutlin, S. Nelson, S. Ducret, M. Valdeolillos, F. M. Rijli, G. López-Bendito, Prenatal thalamic waves regulate cortical area size prior to sensory processing. *Nat. Commun.* **8**, 14172 (2017).
52. C. Heinrich, S. Gascón, G. Masserdotti, A. Lepier, R. Sanchez, T. Simon-Ebert, T. Schroeder, M. Götz, B. Berninger, Generation of subtype-specific neurons from postnatal astroglia of the mouse cerebral cortex. *Nat. Protoc.* **6**, 214–228 (2011).
53. T. L. Bailey, M. Boden, F. A. Buske, M. Frith, C. E. Grant, L. Clementi, J. Ren, W. W. Li, W. S. Noble, MEME SUITE: Tools for motif discovery and searching. *Nucleic Acids Res.* **37**, W202–W208 (2009).
54. G. Yu, L.-G. Wang, Q.-Y. He, ChIPseeker: An R/Bioconductor package for ChIP peak annotation, comparison and visualization. *Bioinformatics* **31**, 2382–2383 (2015).
55. S. Gillot, F. Guillemot, Micro-chromatin immunoprecipitation ( $\mu$ ChIP) protocol for real-time PCR analysis of a limited amount of cells. *Bio Protoc.* **6**, e1846 (2016).

**Acknowledgments:** We are grateful to L. M. Rodríguez and B. Andrés for excellent technical support to I. Huerga for helping with the collection of tissue for RNA-seq, to S. Péron for establishing the in vivo injection protocol for the reprogramming experiments, to I. Huerga for helping with the collection of tissue for RNA-seq, to V. Borrell for providing the plasmids for

retroviral production, and to the members of G.L.-B.'s laboratory for stimulating discussions. We thank D. Jabaudon and A. Nieto for input into the manuscript. **Funding:** This work was supported by grants from the Spanish Ministry of Science, Innovation, and Universities cofinanced by ERDF (RYC-2015-18056 and RTI2018-102260-B-I00) to J.P.L.-A.; the Wellcome Trust (206410/Z/17/Z) and the German Research Foundation Collaborative Research Center 1080 (INST 161/875-2) to B.B.; and the European Research Council (ERC-2014-CoG-647012), PROMETEO/2017/149, and the Spanish Ministry of Science, Innovation, and Universities (PGC2018-096631-B-I00, BFU2015-64432-R, and Severo Ochoa Grant SEV-2017-0723) to G.L.-B. A.H.-N. held an FPI fellowship from the MINECO. **Author contributions:** A.H.-N. and G.L.-B. designed the experiments. A.H.-N. conducted the astrocyte reprogramming experiments in vitro and the epigenetic analyses. L.P.-A. and J.P.L.-A. conducted all bioinformatic analysis of massively parallel sequencing data. V.M.-J. and A.H.-N. conducted the in vivo clonal studies and performed the in situ hybridization validation of the RNA-seq. A.S.-F. performed the electrophysiological recordings. A.H.-N., V.M.-J., and A.E. collected tissue for RNA-seq. R.S. produced the viruses. L.T.-M. cloned the Bcl2-Neurog2 plasmid for in vivo reprogramming. E.L.-D., M.K., and B.B. performed pioneer reprogramming experiments in vitro and provided the Neurog2 reprogramming construct. M.F.-O. and L.L.-M. provided the StarTrack constructs. G.L.-B. acquired funding. A.H.-N., J.P.L.-A., B.B., and G.L.-B. wrote the paper. **Competing interests:** The authors declare that they have no competing interests. **Data and materials availability:** All data needed to evaluate the conclusions in the paper are present in the paper and/or the Supplementary Materials. The RNA-seq data generated in this study are deposited in the NCBI Gene Expression Omnibus repository under accession GSE135602 (astrocytes of the mouse cortex and thalamic nuclei; URL: [www.ncbi.nlm.nih.gov/geo/query/acc.cgi?acc=GSE135602](http://www.ncbi.nlm.nih.gov/geo/query/acc.cgi?acc=GSE135602)) and GSE138976 (neurons of the mouse thalamic nuclei; URL: [www.ncbi.nlm.nih.gov/geo/query/acc.cgi?acc=GSE138976](http://www.ncbi.nlm.nih.gov/geo/query/acc.cgi?acc=GSE138976)). Transcriptional profiles (RNA-seq) of mouse cortical neurons from (20) were obtained from the NCBI Gene Expression Omnibus repository (accession GSE63482; URL: [www.ncbi.nlm.nih.gov/geo/query/acc.cgi?acc=GSE63482](http://www.ncbi.nlm.nih.gov/geo/query/acc.cgi?acc=GSE63482)). Mouse brain scRNA-seq data from (23) were obtained from the NCBI Sequence Read Archive (accession SRP135960; URL: [www.ncbi.nlm.nih.gov/sra/SRP135960](http://www.ncbi.nlm.nih.gov/sra/SRP135960)). ChIP-seq coverage tracks for in silico Neurog2 binding sites determination were performed based on publicly available datasets from H3K4me3 (accession experiment ENCSR258YWW; URL: [www.encodeproject.org/experiments/ENCSR258YWW/](http://www.encodeproject.org/experiments/ENCSR258YWW/)) and H3K27me3 (accession experiment ENCSR070MOK; URL: [www.encodeproject.org/experiments/ENCSR070MOK/](http://www.encodeproject.org/experiments/ENCSR070MOK/)) histone marks from the ENCODE Project. Additional data related to this paper may be requested from the authors.

Submitted 28 September 2020

Accepted 18 February 2021

Published 7 April 2021

10.1126/sciadv.abe8978

**Citation:** Á. Herrero-Navarro, L. Puche-Aroca, V. Moreno-Juan, A. Sempere-Ferrández, A. Espinosa, R. Susín, L. Torres-Masjoan, E. Leyva-Díaz, M. Karow, M. Figueres-Oñate, L. López-Masaraque, J. P. López-Atalaya, B. Berninger, G. López-Bendito, Astrocytes and neurons share region-specific transcriptional signatures that confer regional identity to neuronal reprogramming. *Sci. Adv.* **7**, eabe8978 (2021).

## Astrocytes and neurons share region-specific transcriptional signatures that confer regional identity to neuronal reprogramming

Álvaro Herrero-Navarro, Lorenzo Puche-Aroca, Verónica Moreno-Juan, Alejandro Sempere-Ferrández, Ana Espinosa, Rafael Susín, Laia Torres-Masjoan, Eduardo Leyva-Díaz, Marisa Karow, María Figueres-Oñate, Laura López-Mascaraque, José P. López-Atalaya, Benedikt Berninger and Guillermina López-Bendito

*Sci Adv* 7 (15), eabe8978.  
DOI: 10.1126/sciadv.abe8978

### ARTICLE TOOLS

<http://advances.sciencemag.org/content/7/15/eabe8978>

### SUPPLEMENTARY MATERIALS

<http://advances.sciencemag.org/content/suppl/2021/04/05/7.15.eabe8978.DC1>

### REFERENCES

This article cites 55 articles, 10 of which you can access for free  
<http://advances.sciencemag.org/content/7/15/eabe8978#BIBL>

### PERMISSIONS

<http://www.sciencemag.org/help/reprints-and-permissions>

Use of this article is subject to the [Terms of Service](#)

---

*Science Advances* (ISSN 2375-2548) is published by the American Association for the Advancement of Science, 1200 New York Avenue NW, Washington, DC 20005. The title *Science Advances* is a registered trademark of AAAS.

Copyright © 2021 The Authors, some rights reserved; exclusive licensee American Association for the Advancement of Science. No claim to original U.S. Government Works. Distributed under a Creative Commons Attribution License 4.0 (CC BY).

## Supplementary Materials for

### **Astrocytes and neurons share region-specific transcriptional signatures that confer regional identity to neuronal reprogramming**

Álvaro Herrero-Navarro, Lorenzo Puche-Aroca, Verónica Moreno-Juan, Alejandro Sempere-Ferrández, Ana Espinosa, Rafael Susín, Laia Torres-Masjoan, Eduardo Leyva-Díaz, Marisa Karow, María Figueres-Oñate, Laura López-Mascaraque, José P. López-Atalaya, Benedikt Berninger, Guillermina López-Bendito\*

\*Corresponding author. Email: [g.lbendito@umh.es](mailto:g.lbendito@umh.es)

Published 7 April 2021, *Sci. Adv.* **7**, eabe8978 (2021)  
DOI: 10.1126/sciadv.abe8978

#### **The PDF file includes:**

Figs. S1 to S10  
Legends for tables S1 to S7

#### **Other Supplementary Material for this manuscript includes the following:**

(available at [advances.sciencemag.org/cgi/content/full/7/15/eabe8978/DC1](https://advances.sciencemag.org/cgi/content/full/7/15/eabe8978/DC1))

Tables S1 to S7

## Supplementary Figures

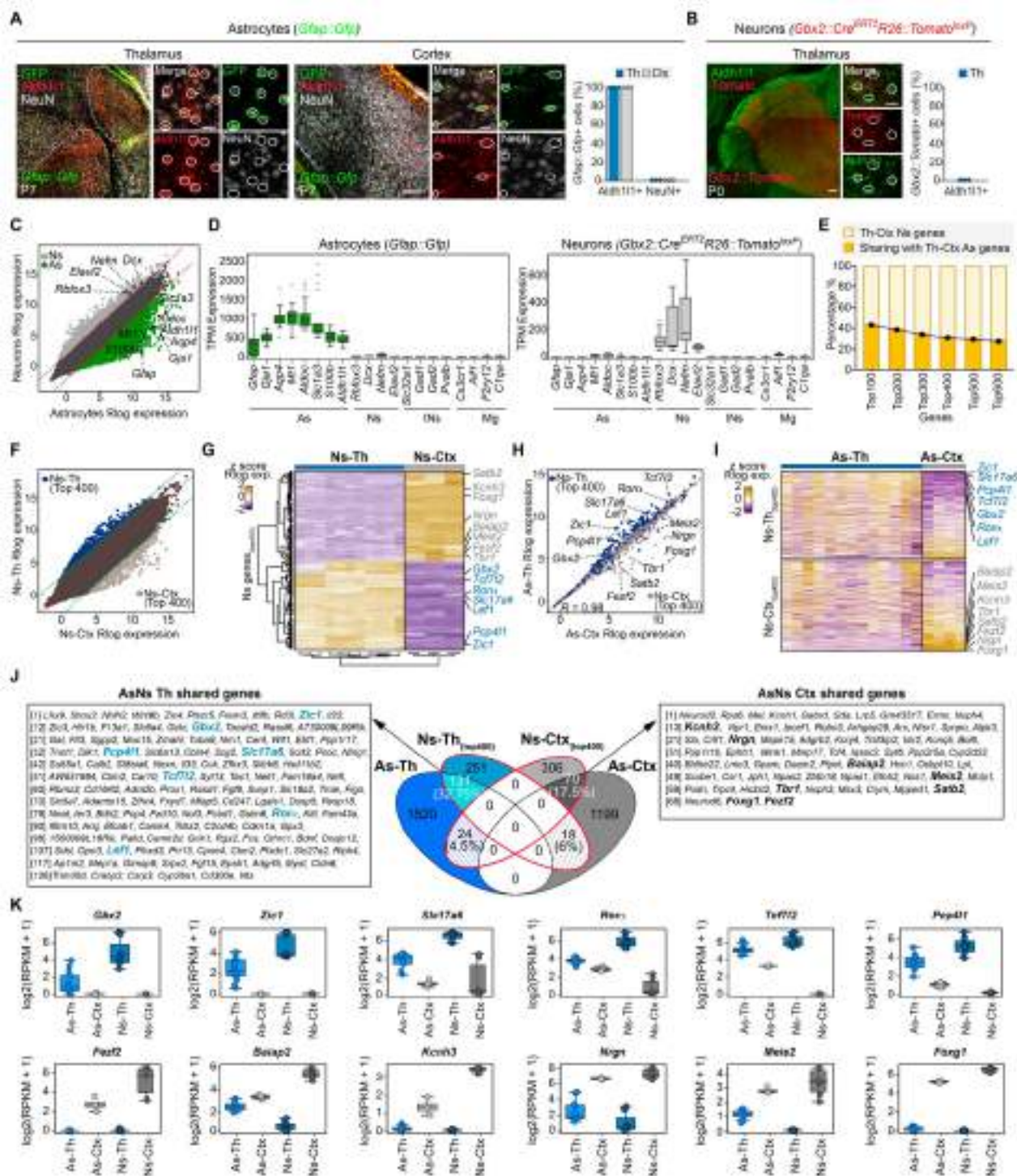


**Fig. S1 | Neuronal genes shared in thalamic and cortical astrocytes. Related to Figures 1 and 2. (A)** Images showing colocalization of GFP<sup>+</sup> cells from a *Gfap::Gfp* mice with the astrocytic marker Aldh111, and the neuronal marker NeuN both in thalamus and cortex of P7 mice ( $n = 150$  GFP<sup>+</sup> cells from 3 different animals). **(B)** Images showing the expression of TdTomato in the *Gbx2::Cre<sup>ERT2</sup>-R26::Tomato<sup>loxP</sup>*. Note the absence of colocalization of TdTomato with the astrocytic marker Aldh111 in P0 mice ( $n = 120$  Tomato<sup>+</sup> cells from 3 different animals). **(C)** Scatterplot of gene expression levels in neurons (Ns) and astrocytes (As) from thalamus and cortex (normalized Rlog expression). Enriched transcripts (|Rlog ratio| > 2) in neurons (light gray) and astrocytes (dark green) are shown. **(D)** Box-and-whisker plots representing the expression levels (Transcripts Per Million, TPM) of known astrocytes (As), neuronal (Ns), interneurons (INs) and

microglia (Mg) genes in the purified astrocytes from a *Gfap::Gfp* mouse and purified thalamic neurons from a *Gbx2-Cre::Tomato-floxed* mouse. **(E)** Percentage of overlapping of significantly DEGs between thalamic or cortical astrocytes and top-ranked DEGs in thalamic or cortical neurons according to the number of neuronal specific genes used for the analysis. **(F)** Scatterplot of normalized Rlog expression showing the 400 top-ranked differentially enriched genes between thalamic and cortical neurons. **(G)** Heatmap of z score of normalized Rlog expression and unbiased clustering of the 400 top-ranked differentially enriched genes between thalamic (Ns-Th) and cortical neurons (Ns-Ctx). **(H)** Scatterplot of normalized Rlog expression in thalamic against cortical astrocytes for 400 top-ranked genes differentially enriched between thalamic and cortical neurons. **(I)** Heatmap of z scores of normalized Rlog expression in thalamic (As-Th) and cortical astrocytes (As-Ctx) for 400 top-ranked differentially enriched genes in thalamic and cortical neurons. In the heatmaps each row represents a gene, the columns are biological replicates and the color-code represents the normalized expression for upregulated genes in yellow versus downregulated genes in purple. **(J)** Venn diagram showing shared genes between the Ns-Th and Ns-Ctx 400 top-ranked differentially enriched genes and the As-Th and As-Ctx significantly DEGs. **(K)** Box plots showing RPKM expression levels of selected region-specific genes shared between neurons and astrocytes of the thalamus (top) or the cortex (bottom). Data in (A) and (B) represent mean  $\pm$  SEM and every dot the single value for each animal. Data in (D) and (K) are plotted with box-and-whisker plots, which give the median, 25th and 75th percentiles, and range. Dots in (D) represent every single value considered an outlier. Scale bars, 100 $\mu$ m and 20 $\mu$ m in insets in (A) and (B).

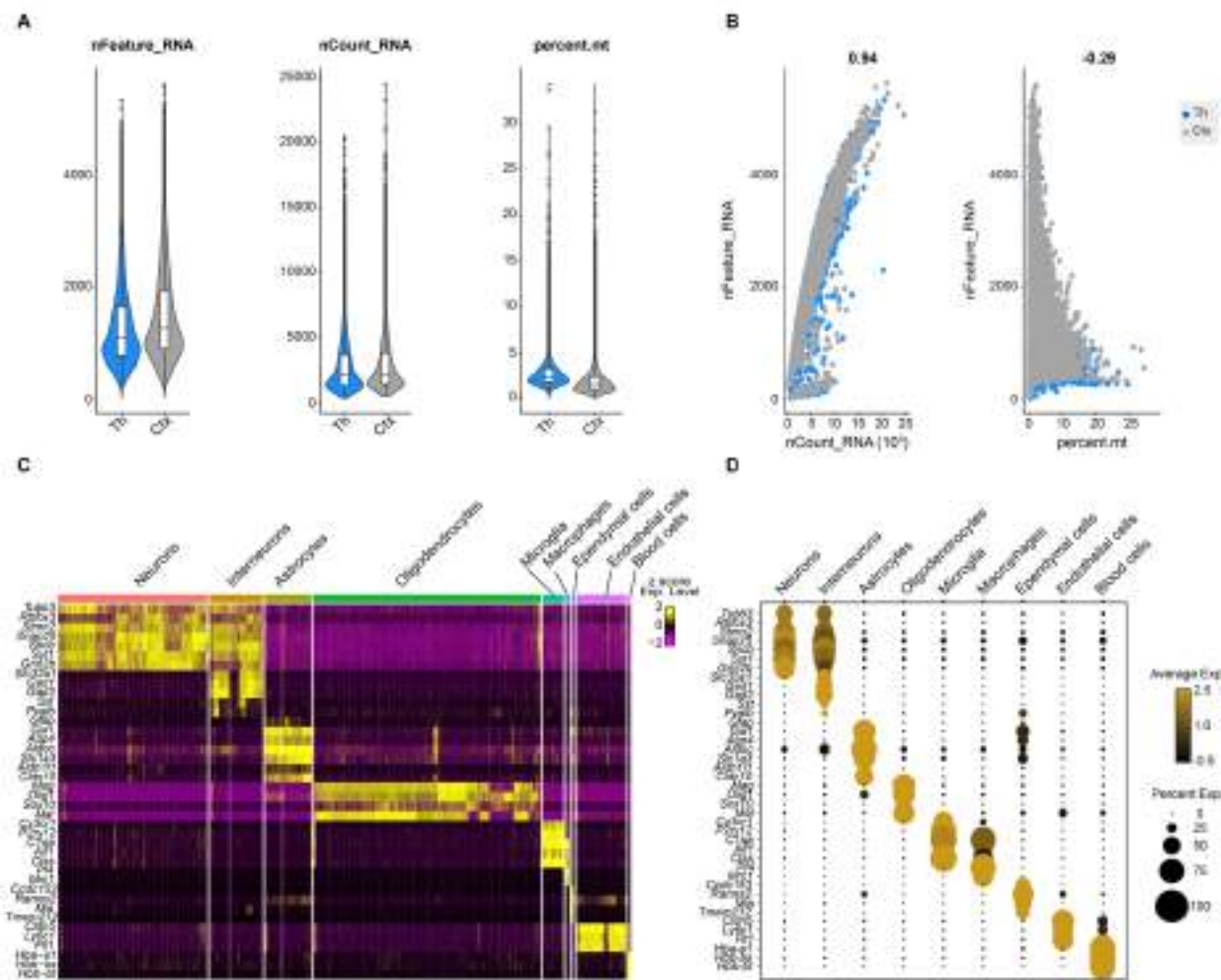


**Fig. S2 | Quality control (QC) and cell-type assignment of the single cell data. Related to Figure 2. (A)** QC metrics of single-cell data from Zeisel *et al.* (2018) (23) between thalamus (blue) and cortex (gray), including the number of unique genes (nFeature\_RNA) (left), the number of total molecules (nCount\_RNA) (middle), and the percentage of reads that map to the mitochondrial genome (percent.mt) (right). **(B)** High correlation of gene expression across cells (left) and low correlation of mitochondrial genes across cells (right) from thalamus (blue) and cortex (gray). **(C)** Heatmap of z score of single cell expression levels of selected bona fide marker genes identified by Wilcoxon Rank Sum test, Bonferroni adjusted (min.pct = 0.1; logfc.threshold = 0.25), over all cell types identified in Zeisel *et al.* (2018) (23), with select genes displayed on y axis and cells on x axis. The bulk of the cells belong to 9 major cell populations. **(D)** Dot plot showing the level of expression of selected bona fide marker genes for each major cell population identified in Zeisel *et al.* (2018) (23), The size of the dot represents the fraction of cells in a given major population in which the gene was detected. The color of the dot represents the average expression z score of the cells within a given major population.

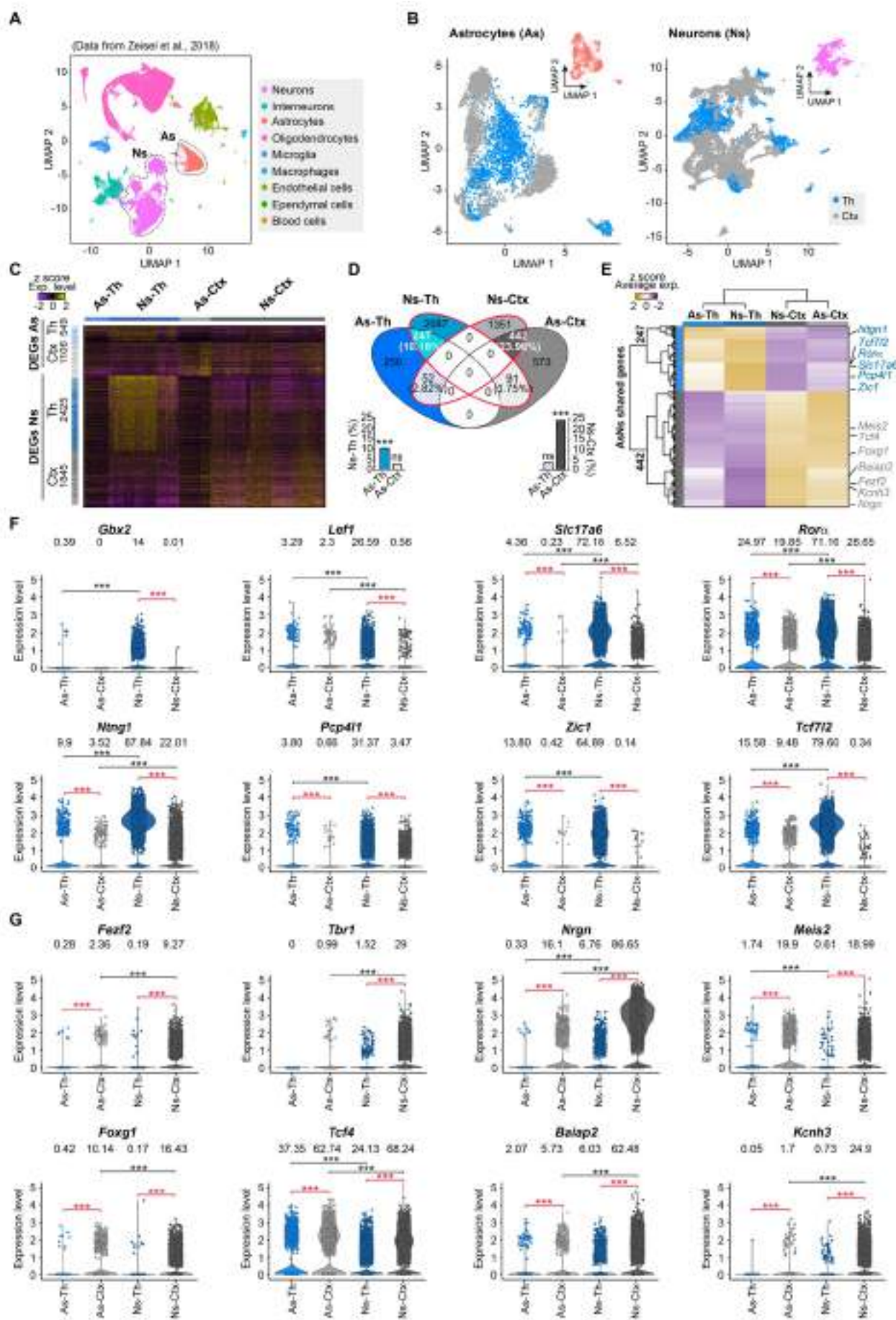


**Fig. S3 | Single-cell sequencing analysis revealed region-specific genes between neurons and astrocytes. Related to Figure 2.** (A) UMAP plot showing the integration of single-cell RNA-seq datasets from mouse thalamus and cortex (23). Astrocytic (As: 4763 cells) and neuronal (Ns: 15391 cells) populations are underlined. (B) UMAP plots displaying differential clustering on astrocytic (blue dots correspond to 2131 thalamic cells and gray dots to 2632 cortical cells) and neuronal populations (dark blue dots correspond to 5856 thalamic cells and dark gray dots to 9535 cortical cells). The insets show the same clusterization but colored by cell type as in (A). (C) Heatmap of z score of single cell expression levels of significantly differentially expressed genes (DEGs) between thalamic (As-Th) and cortical astrocytes (As-Ctx) and thalamic (Ns-Th) and cortical neurons (Ns-Ctx). Each row represents a gene, the columns are cells and the color-code represents the normalized expression for upregulated genes in yellow versus downregulated genes in purple. (D) Venn diagram showing the genes that overlap between As and Ns in both the thalamus and cortex in these single-cell datasets. Bar plots represent the percentage of the enriched genes shared between population. (E) Heatmap of z score of average expression levels and unbiased clustering showing overlapping genes between As and Ns in thalamus and cortex in (D). (F-G), Violin and dot plots showing normalized expression levels in thalamic and cortical astrocytes and neurons of selected genes that are differentially expressed between thalamic and cortical neurons in the bulk RNA-seq (As-Th, thalamic astrocytes; As-Ctx, cortical astrocytes; Ns-Th, thalamic neurons; Ns-Ctx, cortical neurons). Values above every violin plot represent the percentage of cells where the feature or gene is detected in every group. Significant values between both regions in every cell populations are highlighted in red. ns, not significant; \* adj. *P* value < 0.1, \*\* adj. *P* value < 0.01, and \*\*\* adj. *P* value < 0.001.

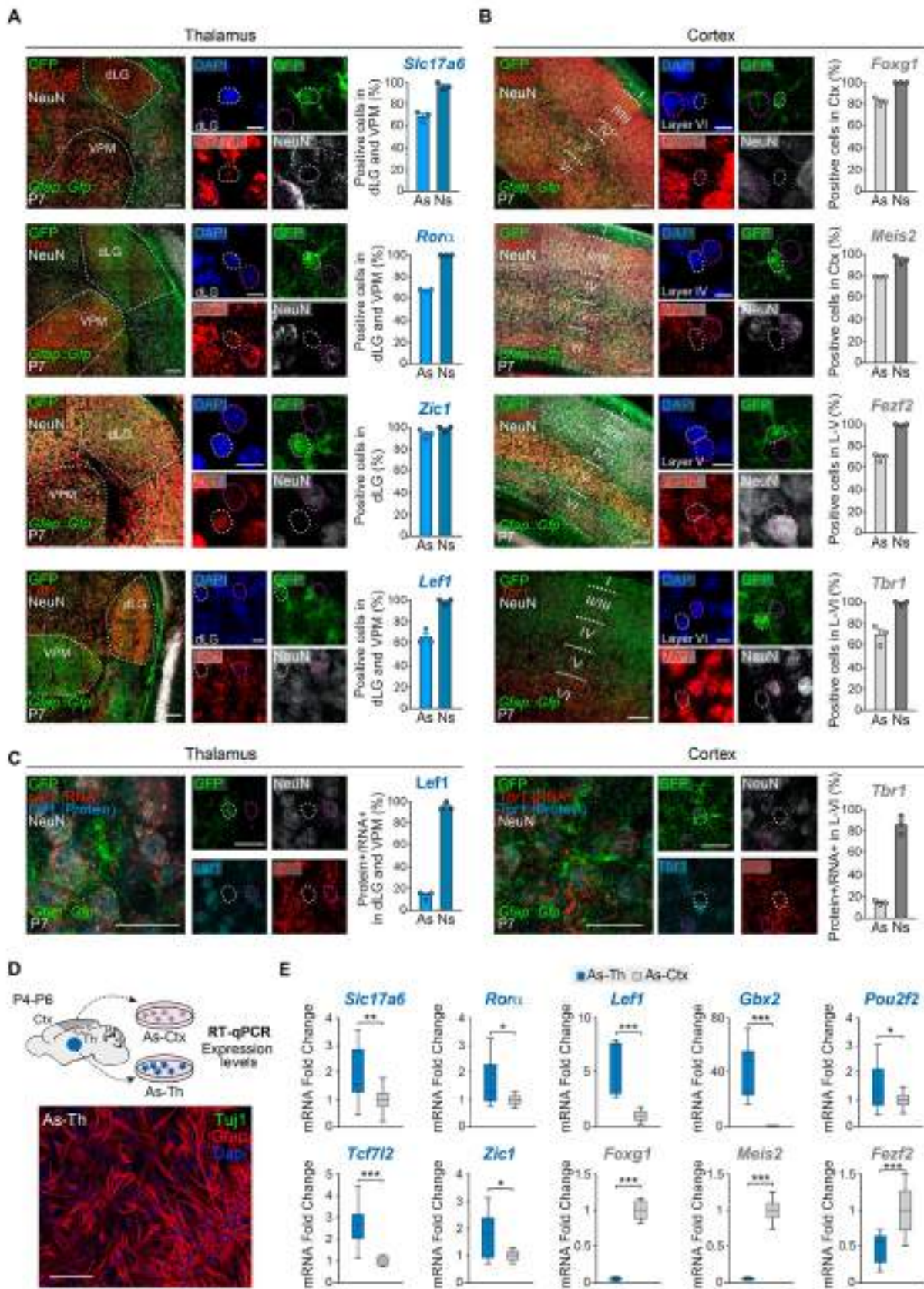


**Fig. S4 | Fluorescent *in situ* hybridization and qPCR of isolated astrocytes validate RNaseq and scRNaseq results. Related to Figures 1 and 2. (A) Images showing the expression of region-specific shared genes in astrocytes and neurons of the thalamus of *Gfap::Gfp* mice. Graphs represent the percentage**

of astrocytes and neurons expressing the analyzed gene in either thalamus or cortex ( $n = 150$  astrocytes and  $n = 150$  neurons from 3 different animals for every gene) **(B)** Images showing the expression of region-specific shared genes in astrocytes and neurons of the cortex of *Gfap::Gfp* mice. Graphs represent the percentage of astrocytes and neurons expressing the analyzed gene in either thalamus or cortex ( $n = 150$  astrocytes and  $n = 150$  neurons from 3 different animals for every gene) **(C)** Images showing the protein and mRNA expression for two region-specific shared genes in astrocytes and neurons from thalamus or cortex. Data shown in **(C)** ( $n = 3$  mice for every gene). In **(A)**, **(B)** and **(C)** white dotted circles label astrocytes and purple dotted circles label neurons. **(D)** Schema of the isolation and purification of thalamic and cortical astrocytes. Example image of cultured thalamic astrocytes. Note that no neurons are present in the cultures. **(E)** Quantification of the differential expression of thalamic and cortical markers in the isolated astrocytes from thalamus and cortex ( $n = 8$  to 15 independent cultures). Data in **(A)**, **(B)** and **(C)** represent mean  $\pm$  SEM and every dot the single value for each animal. Data in **(E)** are plotted with box-and-whisker plots, which give the median, 25th and 75th percentiles, and range. Scale bars, 100 $\mu$ m and 10 $\mu$ m in insets in **(A)** and **(B)** and 25 $\mu$ m in insets in **(C)**. \* $P < 0.05$ , \*\* $P < 0.005$ , and \*\*\* $P < 0.0005$ .

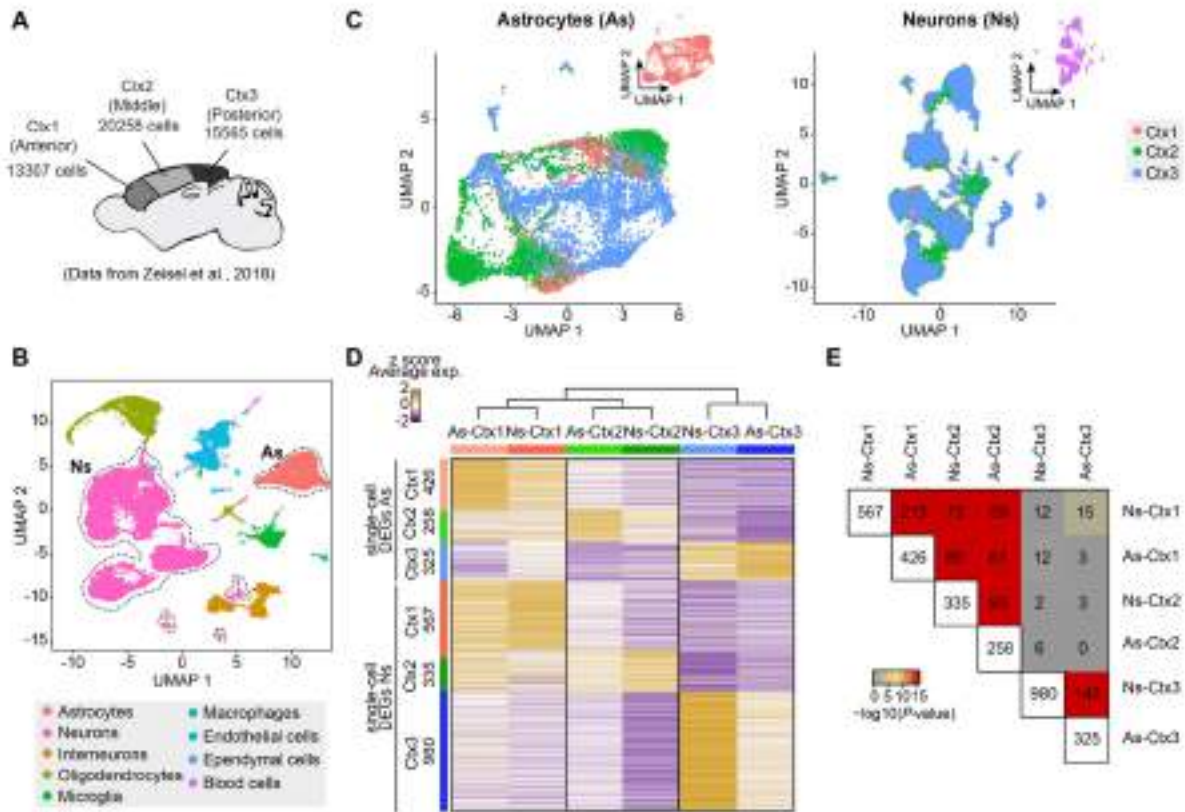


**Fig. S5 | Astrocytes and neurons from the same cortical territory share region-specific genes. Related to Figure 2.** (A) Schema of the three distinct coarse regions sampled along the antero-posterior axis of the mouse cerebral cortex and surveyed by scRNA-seq in Zeisel *et al.* (2018) (23). (B) UMAP plot showing the integration of single-cell RNA-seq datasets from 3 distinct coarse cortical regions. Astrocytic (As: 6743 cells) and neuronal (Ns: 26388 cells) populations are underlined. (C) UMAP plots displaying isolated clustering on astrocytic (Ctx1: 1318 cells, Ctx2: 2671 cells, Ctx3: 2754 cells) and neuronal populations (Ctx1: 8159 cells, Ctx2: 9538 cells, Ctx3: 8691 cells). The insets show the same clusterization but coloured by cell type as in (B). (D) Heatmap of z score of average expression levels of significantly differentially expressed genes (DEGs) ( $P_{Adj} < 0.1$ ,  $|\log_2(\text{fold change})| > 0.1$  using Wilcoxon rank-sum test; Bonferroni adjusted) at the single cell level, between the 3 different cortical regions in astrocytes (As-Ctx) and neurons (Ns-Ctx). Genes (rows) are grouped by anatomical regions and the columns (averaged cell type-cortical region) are arranged by hierarchical clustering. (E) Comparison matrix of the number of shared specific gene list between As and Ns datasets of every specific region. Colour-code according to significance of overlap.

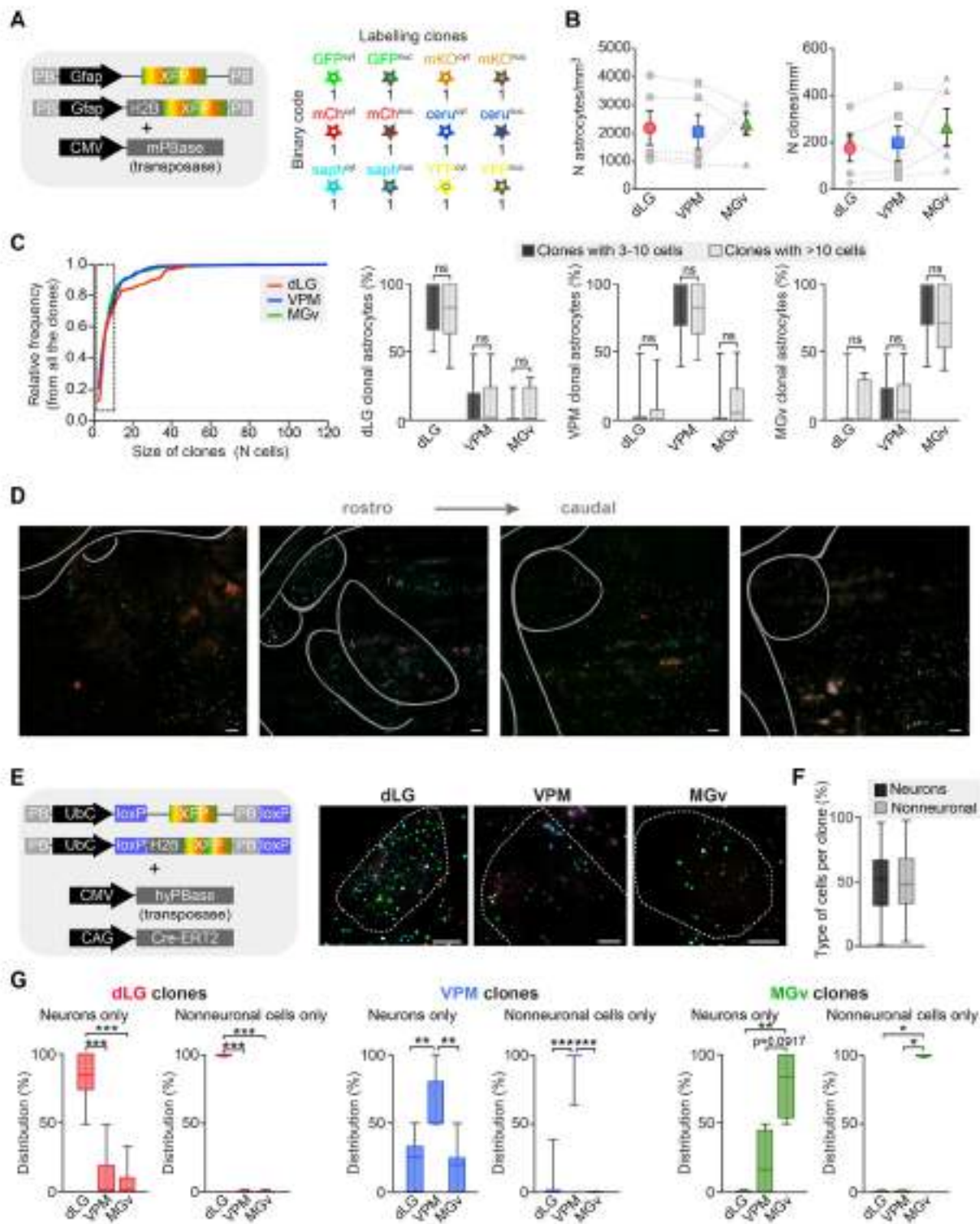


**Fig. S6 | Astrocytes and neurons from the distinct thalamic nuclei are clonally related. Related to Figure 4.** (A) Left, StarTrack plasmid combination used for the study of astrocytic clones. Right, binary code used for labelling the clones based on the presence and location of each fluorophore. (B) Quantification of the distribution of the cells and clones through dLG, VPM and MGv nuclei in every electroporated animal ( $n = 5$ ). Every point linked with a dashed line represents the data in each electroporated animal. Also, mean  $\pm$  SEM of all the points is represented in each column. (C) Left, plot showing the relative frequency to the size of the astrocytic clones. Right, quantification of the distribution of the clones depending on their size ( $n = 320$  clones from 5 electroporated animals). (D) Images showing four different rostro-caudal levels of an

E11.5 electroporated thalamus at P8. (E) Left, StarTrack plasmid combination used for the study of clones including neurons and nonneuronal cells. Right, images showing electroporated cells in dLG, VPM and MGv of the same animal. (F) Percentage of the presence of every cell type in the clones. (G) Quantification of the distribution of the clones containing only neurons or nonneuronal cells across the three thalamic nuclei ( $n = 72$  neuronal clones and  $n = 42$  nonneuronal clones). Data are plotted with box-and-whisker plots, which give the median, 25th and 75th percentiles, and range. Scale bars, 100  $\mu\text{m}$ . ns, not significant,  $*P < 0.05$ ,  $**P < 0.005$ , and  $***P < 0.0005$ .

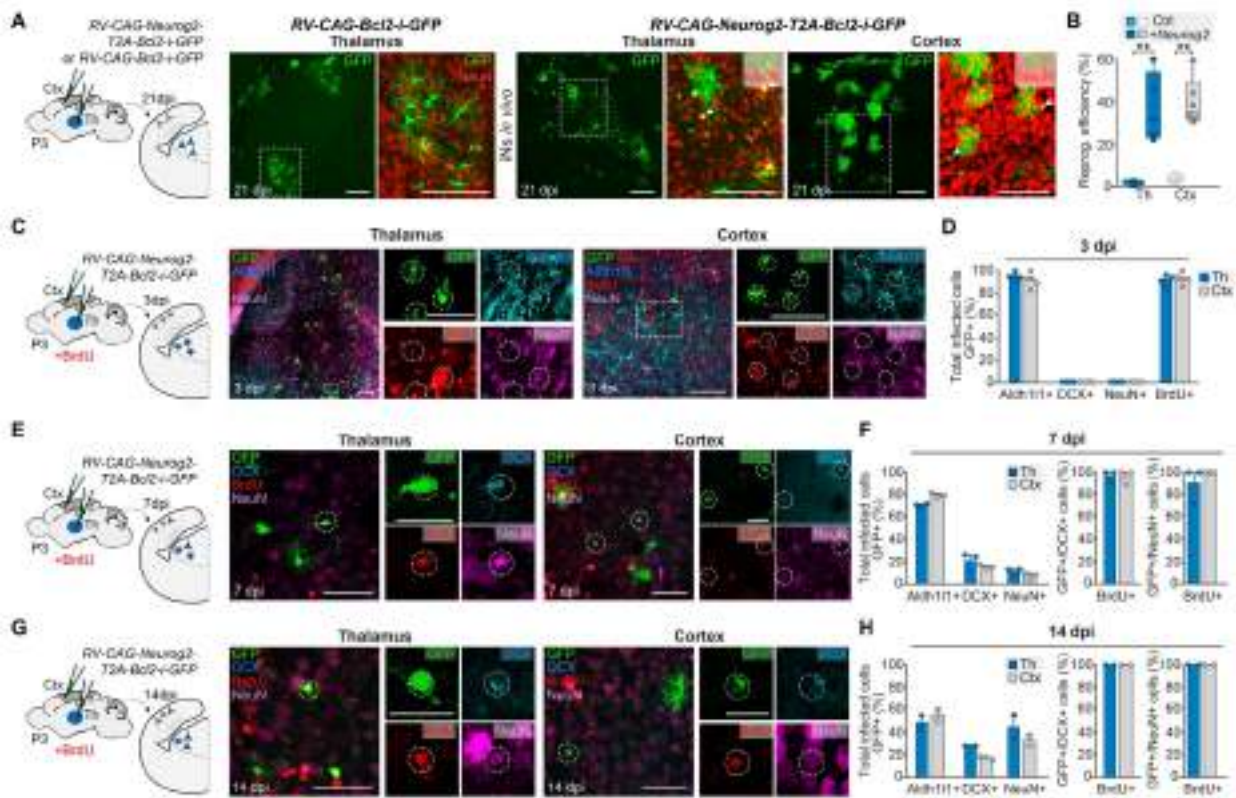


**Fig. S7 | Astrocytes from thalamus and cortex are reprogrammed into neurons *in vivo* by overexpressing *Neurog2* and *Bcl2*. Related to Figure 5.** (A) Immunofluorescence of infected astrocytes *in vivo* with a control virus and a virus with *Neurog2* and *Bcl2* ( $n = 4$  to  $6$  injected animals per condition). (B) Quantification of the reprogramming efficiency *in vivo* in cortex and thalamus, based on the percentage of infected cells (GFP+) that are also positive for the neuronal marker NeuN 21 days after the injection. (C) Left, experimental design. A retrovirus with *Neurog2* and *Bcl2* was injected at P3, and BrdU administered at the same time to label proliferating cells. Right, images showing infected cells in thalamus and cortex at 3 days post-injection (dpi). (D) Quantification of the percentage of infected cells positive for the astrocytic marker Aldh111, for the neuronal markers DCX and NeuN or for BrdU in thalamus and cortex at 3 dpi ( $n = 143$  Th cells and  $95$  Ctx cells from 4 independent mice). (E) Left, experimental design. Right, images showing infected cells in thalamus and cortex at 7 dpi. (F) Quantification of the percentage of infected cells positive for the astrocytic marker Aldh111 or for the neuronal markers DCX and NeuN in thalamus and cortex that at 7 dpi ( $n = 179$  Th cells and  $210$  Ctx cells from 4 independent mice). Percentage of reprogrammed cells (GFP+ and DCX+ or NeuN+) that were positive for BrdU staining. (G) Left, experimental design. Right, images showing infected cells in thalamus and cortex at 14 dpi. (H) Quantification of the percentage of infected cells positive for the astrocytic marker Aldh111 or for the neuronal markers DCX and NeuN in thalamus and cortex 14 dpi ( $n = 114$  Th cells and  $44$  Ctx cells from 2 independent mice). Percentage of reprogrammed cells (GFP+ and DCX+ or NeuN+) that were positive for BrdU staining. Data in (B) are plotted with box-and-whisker plots giving the median, 25th and 75th percentiles, and the range. Data in (D), (F) and (H) are means  $\pm$  SEM. Data in (B), (D), (F) and (H) contain the individual values for every injected mouse. Scale bars,  $100 \mu\text{m}$  in (A) and (C);  $50 \mu\text{m}$  in (E), (G) and insets in (C), and  $25 \mu\text{m}$  in insets in (E) and (G). \* $P < 0.05$ , \*\* $P < 0.005$ , and \*\*\* $P < 0.0005$ .

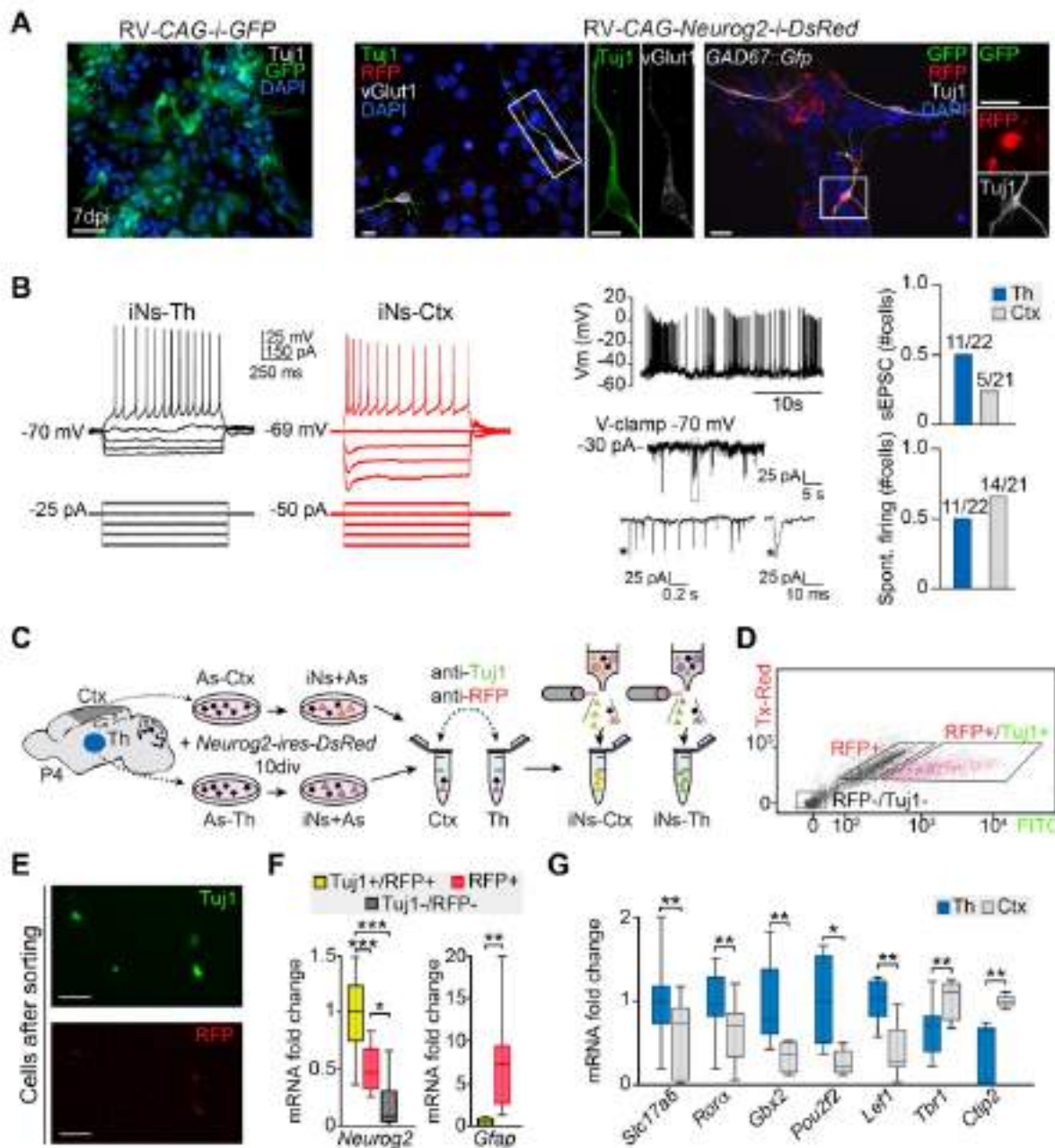


**Fig. S8 | Thalamic astrocytes are reprogrammed into functional glutamatergic neurons *in vitro* by *Neurog2* and express region-specific neuronal genes. Related to Figure 5. (A) Left, expression of Tuj1 in thalamic astrocytes infected with a control retrovirus containing *CAG-IRES-Gfp*. Right, immunostaining for vGlut1 and GFP in reprogrammed astrocytes (Tuj1+/RFP+) in thalamic cultures from wild type and *Gad67::Gfp* mouse after 10dpi. (B) Left panel, whole-cell patch-clamp recordings in thalamic (left, black traces) and cortical (right, red traces) induced neurons (iNs). Central panel, whole-cell recording of the membrane potential (Vm) of a thalamic iN. Also, putative spontaneous excitatory postsynaptic currents recorded at -70 mV in a thalamic iN. Right graphs, number of recorded iNs from thalamic ( $n = 22$  cells from 14 cultures;  $28.3 \pm 2.0$  div) and cortical ( $n = 21$  cells from 8 cultures;  $30.8 \pm 2.8$  div) cultures that showed spontaneous excitatory post synaptic currents (sEPSC) or spontaneous firing. (C) Experimental design for isolating induced neurons (iNs) with immunofluorescence followed by FACS sorting. (D) Clouds of cells obtained by FACS sorting 10dpi after *Neurog2* viral induction. (E) Double positive cells collected after sorting. (F) Quantification of the expression of *Neurog2* and *Gfap* in the different sorted populations ( $n = 8$**

to 12 independent cultures). **(G)** Quantification of the differential expression of thalamic and cortical markers in the isolated iNs from thalamus and cortex ( $n = 5$  to 17 independent cultures). Data in are plotted with box-and-whisker plots, which give the median, 25th and 75th percentiles, and range. Scale bars, 50 $\mu$ m in (A) and (G). \* $P < 0.05$ , \*\* $P < 0.005$ , and \*\*\* $P < 0.0005$

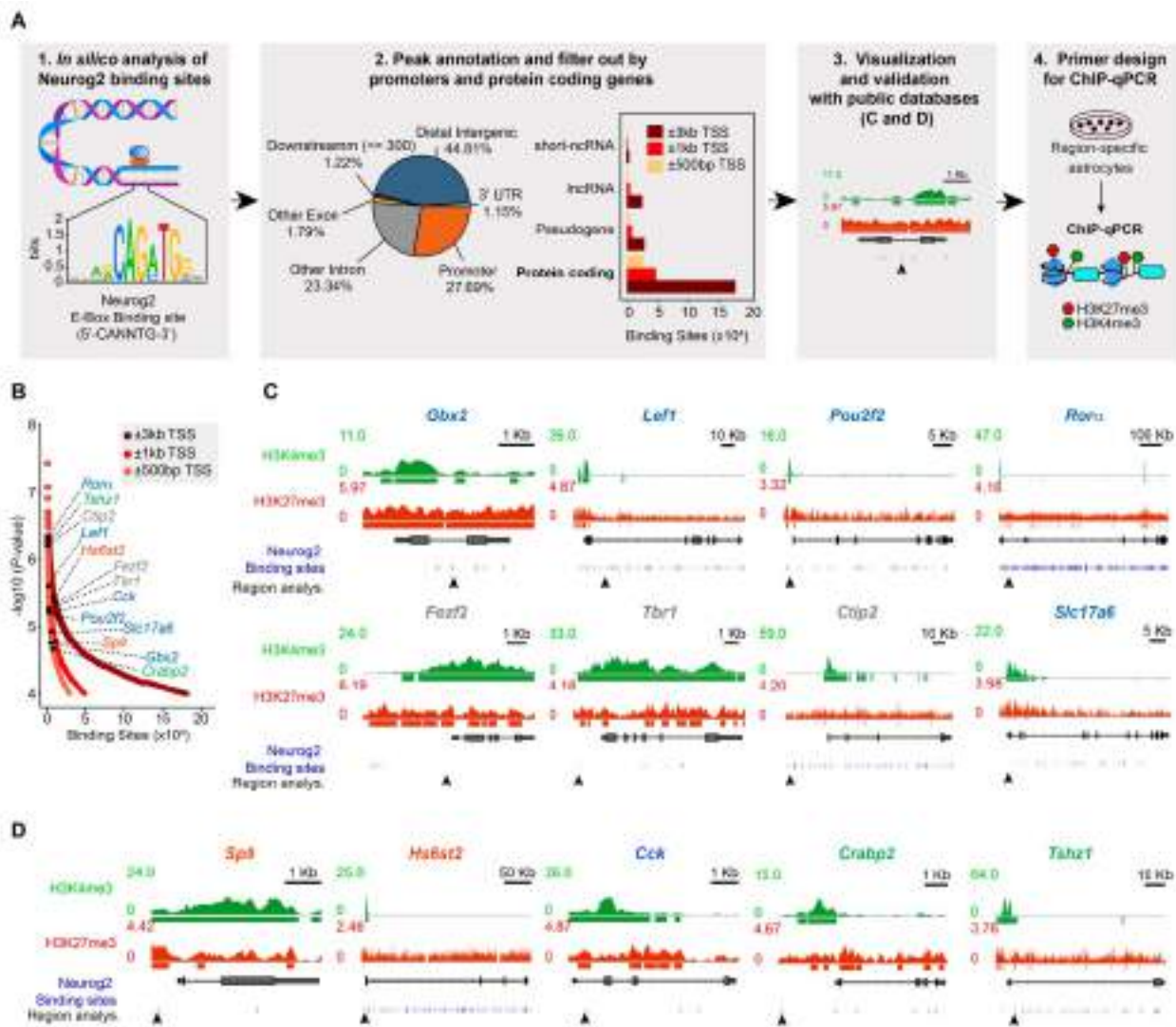


**Fig. S9 | *In silico* analysis of candidate regions for the study of the epigenetic states of tissue-specific genes. Related to Figure 6. (A) *In silico* pipeline analysis of Neurog2 targets binding sites used to design ChIP-qPCR primers. (1) Schema of the consensus binding site of Neurog2. (2) Peak annotation and filter out by promoter region and protein coding genes. Left, pie plot showing the genomic annotation by gene region. Right, number of binding sites of Neurog2 classified by gene biotypes extracted from promoter region and filtered out by genic proximity to transcription start site (TSS) ( $\pm 3$  Kb,  $\pm 1$  Kb,  $\pm 500$  bp from TSS). (3) Visualization and validation with public databases through genomic tracks. (4) Primer design for ChIP-qPCR. (B) High-confidence putative binding sites of specific genes filtered by genic proximity ( $\pm 3$  Kb,  $\pm 1$  Kb,  $\pm 500$  bp) to TSS found for Neurog2 across the whole genome by order of  $-\log_{10}$  ( $P$ -value). (C-D) *In silico* determination of selective promoter regions (black arrows) used to perform ChIP-qPCR analysis for thalamic, cortical and thalamic nuclei-specific genes, based on publicly available datasets of ChIP-seq from H3K4me3 and H3K27me3 histone marks and the putative binding sites for *Neurog2*.**

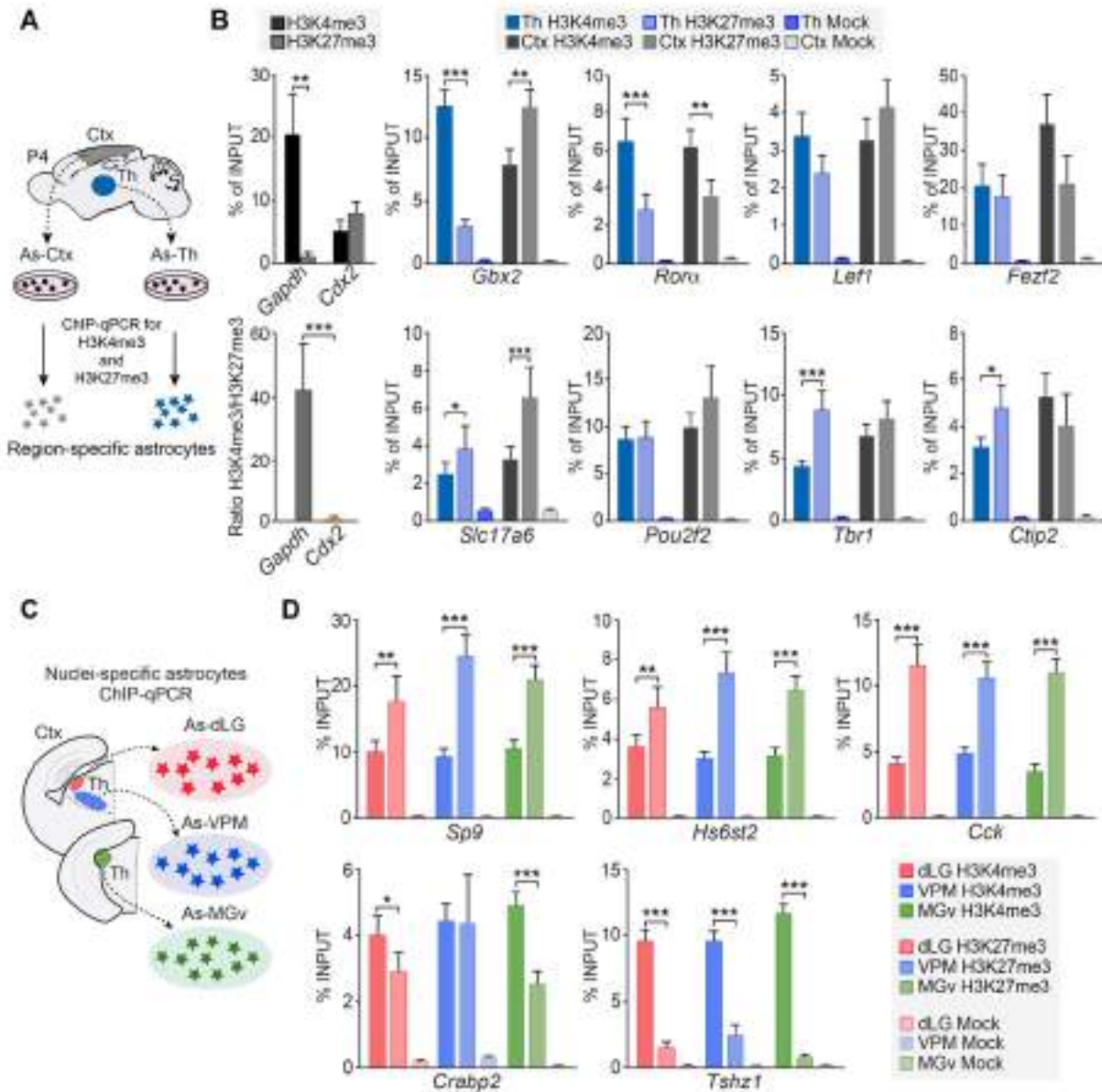


**Fig. S10 | Region-specific genes show less epigenetic repression in the astrocytes in a tissue-dependent manner. Related to Figure 6.** (A) Experimental design in thalamic and cortical astrocytes. (B) Quantification of the percentage of recovered input after the immunoprecipitation with H3K4me3, H3K27me3 and mock antibodies in thalamic and cortical cultured astrocytes ( $n = 8$  to 21 ChIP samples). (C) Experimental design in astrocytes from dLG, VPM and MGv. (D) Quantification of the percentage of recovered input after the immunoprecipitation with H3K4me3, H3K27me3 and mock antibodies in dLG, VPM and MGv cultured astrocytes ( $n = 14$  to 19 ChIP samples). Data are means  $\pm$  SEM \* $P < 0.05$ ; \*\* $P < 0.005$  and \*\*\* $P < 0.0005$ .

## **Supplementary Data 1-7**

**Table S1.** Differential expression analysis of cortical and thalamic astrocytes from bulk RNA-seq. Related to Figures 1 and Figure 2.

**Table S2.** Differential expression analysis of cortical and thalamic astrocytes and neurons from scRNA-seq. Related to Figure 2 and Figure S3.

**Table S3.** Differential expression analysis of astrocytes from sensory-modality thalamic nuclei (bulk RNA-seq). Related to Figure 3.

**Table S4.** Differential expression analysis of neurons from sensory-modality thalamic nuclei (bulk RNA-seq). Related to Figure 3.

**Table S5.** Differential expression analysis of neurons and astrocytes from distinct cortical regions (anterior, middle, posterior) from scRNA-seq. Related to Figure S5.

**Table S6.** List of antibodies and their corresponding concentrations of use for immunohistochemistry. Related to histology section in Methods.

**Table S7.** List of primers used for RNA expression levels and ChIP-qPCR assays. Related to “Purification of total RNA and quantitative real-time PCR” and “Chromatin immunoprecipitation for H3K4me3 and H3K27me3” sections in Methods.